Conference Proceedings

European Telemetry and Test Conference

May 10th - 12th, 2016 in cooperation with
SENSOR+TEST 2016, Nuremberg, Germany

Proceeding

36th European Telemetry and Test Conference – etc2016

Bei diesem Band handelt es sich um den Kongressband der 36th European Telemetry and Test Conference – etc2016.
Dieser Band beinhaltet die Manuskripte zu den jeweiligen Vorträgen.

Für Form und Inhalt der Beiträge zeichnen sich die Autoren verantwortlich. Die AMA Service GmbH übernimmt keine Gewähr für die Richtigkeit, Genauigkeit und Vollständigkeit der Angaben sowie die Beachtung privater Rechte Dritter.

This volume covers the proceedings of the 36th European Telemetry and Test Conference – etc2016.
This volume comprises the manuscripts of the lectures.

The authors are responsible for form and content of the papers.
AMA Service GmbH accepts no responsibility for the correctness and completeness of the details and the consideration of private rights of third parties.

Herausgeber / Publisher:

AMA Service GmbH
Von-Münchhausen-Str. 49 • 31515 Wunstorf / Germany
Tel. +49 5033 9639-0 • Fax +49 5033 1056
info@ama-service.com • www.ama-service.com /
www.sensor-test.com / www.ama-science.org

ISBN 978-3-9816876-2-0

Dear Telemetry Friends,

The European Society of Telemetry was pleased to welcome you back to Nuremberg! The 36th European Telemetry and Test Conference took place in cooperation with SENSOR+TEST, the measurement fair for the innovation dialog.

etc2016 was especially proud to host the 27th Symposium of the Society of Flight Test Engineers – European Chapter. Both our Conference and the Symposium took place in a joined area so that participants of both events could assist all presentations and exchange with each other on the latest telemetry technologies and their application in the newest flight test methods.

As part of the mission of the European Society of Telemetry to support technical growth and education in the fields of telemetry, etc2016 presented outstanding technical papers, short courses in the current telemetry hot topics, an exhibition with product innovations and a continuous interaction with the experts. Special sessions offered a platform for innovation with AIM2016 – Advance In-Flight Measurement –, but also for standardization with the ICTS General Session – International Consortium for Telemetry Spectrum –, the ETSC Open Meeting – European Telemetering Standardisation Committee and the MDL User Meeting – Measurement Description Language.

The technical papers are merged in these Conference Proceedings. Here you can find the latest and most promising hardware and software ideas for the telemetry solutions of tomorrow!

The ultimate success of the conference remains entirely dependent upon your continued patronage. So thank you very much for supporting etc2016!

We are always seeking ways to improve the European Telemetry and Test Conferences. Please contact us with ideas, critiques, suggestions, fill in the feedback forms or visit us on www.telemetry-europe.org.

We're looking forward to meeting you!

Renaud Urli
President of the European Society of Telemetry

1. Positioning & Timing

Chairmen: Pilar Vicaria Torralbo, Airbus Defence and Space, Getafe (Madrid) (Spain)

2. Sensors & AIM2016

Chairmen: Fritz Boden, DLR, Göttingen (Germany)

3. Video & Data Management

Chairmen: Christian Herbepin, Airbus Helicopters, Marignane (France)

4. Remote Data Acquisition

Chairmen: Diarmuid Corry, Continuity Consulting, Lusby (USA)

5. Data Links

Chairmen: Nelson Leite, Instituto de Pesquisas e Ensaios em Voo, Sao Jose dos Campos (Brazil)

6. Ground & Onboard TLM systems

Chairmen: Günter Müller, Airbus Defence and Space, Manching (Germany)

7. Antennas & Tracking

Chairmen: Gilles Fréaud, AIRBUS France, Toulouse (France)

8. Wireless Data Acquisition

Chairmen: Sergio Penna, EMBRAER, Sao Jose dos Campos (Brazil)

9. Data Processing

Chairmen: Pedro Rubio, Airbus Defence and Space, Getafe (Madrid) (Spain)

DOI 10.5162/etc2016/1.1

PTP VERSION 3 IN FTI?

Øyvind Holmeide[1], Markus Schmitzr[2]
[1] OnTime Networks AS, Oslo, Norway,
oeyvind@ontimenet.com
[2] OnTime Networks LLC, Dallas, USA,
markus@ontimenet.com

Abstract:

Time synchronization based on the Precision Time Protocol (PTP) according to the IEEE 1588 standard is a core building block for state-of-the-art high-performance Flight Test Instrumentation (FTI) systems. Two versions of the IEEE 1588 standard have been launched: PTP version 1 according to IEEE 1588™ - 2002 and PTP version 2 according to IEEE 1588™ - 2008. Now a new IEEE 1588™ working group has been established with the goal to launch a new revision of the IEEE 1588™ standard; i.e. PTP version 3.

The FTI industry is using both PTP version 1 and 2. The poor backward compatibility between PTP version 2 and 1 has been a big challenge for the FTI community. Backward compatibility with older PTP versions, new functions and to what extent PTP version 3 is relevant for the FTI industry are described and discussed in this paper.

The IEEE 1588 standards define several PTP profiles for various time synchronization usages in different industries. This paper also describes how PTP is used in FTI and also proposes a PTP profile definition for FTI including special time synchronization parameters/properties taken from the iNET standardization.

Keywords: IEEE 1588, PTP version 3, PTP profile, FTI, iNET.

Introduction

The FTI industry was one of the first industries that started to use PTP. This means that there is a large install base of FTI systems that are based on PTP version 1. The poor backward compatibility between PTP version 2 according to IEEE 1588™ - 2008 and PTP version 1 according to IEEE 1588™ - 2002 represented a major challenge for the FTI community since off-the-shelf PTP version 1 and 2 clocks could not be combined in the same network. A solution to this problem was launched by OnTime Networks in 2013 by the introduction of TC/SC Ethernet switches with PTP version translation support implemented according to the principles described in [1]. These TC/SC switches made it possible to combine PTP version 1 and 2 in the same network.

What about backward compatibility for new revision of the IEEE 1588™ standard?

A PTP version 3 working group, see [2] and [3], has been established and approved by IEEE. The working group shall ensure that the resulting standard has the highest degree of backward compatibility with previous editions of the IEEE 1588™ standard and all new features will be optional.

The scope of this working group is as follows:

- Correct known technical and editorial errors
- Better accuracy
- Definition of an SNMP MIB
- Security
- Clarify the layering, interfaces and protocol of the standard

Several IEEE 1588 PTP profiles for different industries such as profiles for telecom, power systems (C37.238), PROFINET, etc. are defined. These PTP implementations are very different and should not be combined in the same network. The de-facto PTP implementation used in FTI is to a large extent based on the default PTP profile of the IEEE 1588™ - 2002 or IEEE 1588™ - 2008 standards, but also the evolving iNET standard specifies time synchronization properties that should be considered for such a PTP profile. This means first of all support for SNMP management of the network clocks and the possibility for generating alarms, i.e. SNMP trap, in case of synchronization loss and GMC hold-over capability in case of GPS loss.

The main PTP properties that are relevant for a FTI PTP profile for both IEEE 1588™ - 2002 or IEEE 1588™ - 2008 are as follows:

- Clock modes
- One-step vs. two step clocks
- Media
- Delay mechanism
- Transport mechanism
- Domain
- Selection of Best Master Clock
- PTP EPOCH
- Sync interval
- Delay_Req interval
- Announce interval
- PPS output
- IRIG-B 002/122
- Management
- SNMP traps
- GMC holdover
- SC accuracy
- SC time to synchronization

Abbreviations

BC	Boundary Clock
BMCA	Best Master Clock Algorithm
DST	Daylight Saving Time
E2E	End-to-End
FCS	Frame Check Sequence
FTI	Flight Test Instrumentation
GMC	Grand Master Clock
GUI	Graphical User Interface
IED	Intelligent Electronic Device
IP	Internet Protocol
IRIG	Inter-Range Instrumentation Group time codes
MAC	Medium Access Control
MC	Master Clock
OC	Ordinary Clock
P2P	Peer-two-Peer
PPM	Parts per Million
PPS	Pulse Per Second
RTOS	Real Time Operating System
SC	Slave Clock
SyncE	Synchronous Ethernet
TAI	Temps Atomique International
TC	Transparent Clock
TCP	Transmission Control Protocol
ToS	Type of Service
TZ	Time Zone
UDP	User Datagram Protocol
UTC	Coordinated Universal Time

PTP version 3

The working group formed to revise the IEEE 1588™ has established five sub-committees:

- Architecture
- High Accuracy
- Upkeep
- Management
- Security

Architecture

The charter of the Architecture sub-committee is as follows:

- "..clarify the layering, interfaces, and protocols of the standard, including the behaviour of systems that deploy different protocol options."

Relevant topics for this sub-committee are:

State reduction

The FAULTY, PRE-MASTER and UNCALIBARTED states would become optional. This means that IEEE 802.1AS becomes a complaint profile and faster re-configuration/synchronization can be achieved.

This change is first of all an implementation requirement that will not impact the observed node's PTP protocol behaviour.

State reduction might be convenient for FTI SC if fast synchronization is required, see SC accuracy and time to synchronization section below.

Profile isolation

Multiple PTP profiles may exist on the same network with different BMCAs. The sub-committee suggests to use a transport specific attribute in the PTP header in order to define the PTP profile that the PTP packet belongs to in order to isolate the PTP profiles available on the network.

Only one PTP profile should be used in an FTI system. This function is not considered for FTI.

Port State Configuration

Port State Configuration means that a PTP port can be BMCA capable, SC only or GMC/MC only, where manual configuration is possible.

This is not considered to be relevant for FTI. FTI should allow SC only clock modes (DAUs), while all GMC candidates should support BMCA.

PTP domains

PTP domains in IEEE 1588™ - 2002 or IEEE 1588™ - 2008 do not interact. The sub-committee suggests that domains can share the same timing data in order to offer support for multiple simultaneous GMCs and multipath PTP for time synchronization redundancy purpose.

This is not considered to be relevant for FTI. FTI should only allow one PTP domain (i.e.: 0 – default).

High Accuracy

The charter of the High Accuracy sub-committee is as follows:

- “The protocol enhances support for synchronization to better than 1 nanosecond.”

A proposal including support for SyncE for frequency synchronization at physical layer will be proposed. Frequency synchronization may be achieved through a different spanning tree than the spanning tree used for PTP. Calibration of each SC including compensation for all asymmetric components and cable delays will be part of the proposal. A “Golden Calibrator” for a given system may be required.

Data acquisition with sub-nanosecond or single digit nanoseconds accuracy in future FTI systems may be relevant. The High Accuracy section of PTP version 3 standard can then be relevant.

Upkeep

The charter of the Upkeep sub-committee is as follows:

- “Incorporate official IEEE interpretations and other known errors or needed clarification into 1588-2008 in order to provide clean version as a basis for modifications of the current P1588 working group.”

- “Once this is done serve as a “quality control” function for any modifications proposed by other committees to ensure freedom from inconsistencies and backward compatibility issues.”

This work includes clarification of the TC source address topic.

No major impact from the Upkeep section is expected for FTI.

Management

The charter of the Management sub-committee is as follows:

- “The management sub-committee will consider the management of IEEE 1588 clocks, e.g. MIB, related management protocols (SNMP and native management protocol), and OAM mechanism.”

The Management sub-committee proposal is to create a single IEEE 1588 SNMP MIB. A mechanism to allow in-service monitoring of synchronization quality will also be proposed.

An IEEE 1588 SNMP MIB as well as extended support for monitoring the synchronization quality of the PTP clocks can be convenient for FTI. iNET standardization are targeting some of the same needs, but future FTI system can benefit from this proposal from the Management sub-committee.

Security

The charter of the Security sub-committee is as follows:

DOI 10.5162/etc2016/1.1

- "To specify a security capability for PTP. This capability is expected to be optional.

The Security sub-committee considers technologies such as IPSec and MACSec. The requirements are based on IETF document: "draft-ietf-tictoc-security-requirements".

FTI systems are in most cases considered as closed systems. Security related to PTP synchronization has not been an issue for FTI up to now.

PTP profile for FTI

The main PTP properties/parameters that are relevant for FTI are as follows:

Clock modes

IEEE 1588 defines the following PTP clock modes:

- Grand Master Clock (GMC)
- Ordinary Clock (OC)
- Boundary Clock (BC)
- Transparent Clock (TC)
- Slave Clock (SC) only

An OC can either act as a GMC or a SC. If the OC wins the BMCA for the network, then the clock will be the GMC for the network. If not, then the clock may be passive or run as a SC. If the OC enters SC mode then the clock will discipline its local clock based on time updates from the chosen GMC of the network, while the clock will discipline its local clock based on its local time base (e.g. GPS) if the clock enters passive mode. More than one GMC or OC in the same network means better redundancy and robustness.

Ethernet switches and routers in a network can either support BC, TC, TC/SC or GMC clock modes. BC means that one port is in SC mode and the remaining ports are in MC mode. TC clock mode means that the local switch/router clock is used for calculating the switch/router residence time for each PTP event packet forwarded through the network element. This local clock may or may not be symphonized with the GMC clock of the network. The clock drift of a SC compared to the GMC in the network is calculated and compensated is the clock is synthonized, while both the clock drift and offset is calculated and compensated if the SC is synchronized with the GMC. A TC/SC switch contains also SC support. This means that the network element is both synthonized and synchronized with the GMC. A synthonized TC offers better accuracy compared to a TC with free running clock.

A SC only implementation means that the device only supports SC mode. This clock will discipline its local clock based on time updates from the chosen GMC of the network.

BCs are not used in today's FTI systems. Only TC and TC/SC implementation are used. This is also valid for FTI systems based on the IEEE 1588™ - 2002 standard even though this standard does not specify TCs. The TC implementations used in FTI systems that are based on IEEE 1588™ - 2002 follows the proprietary principles presented and demonstrated by OnTime Networks at the IEEE 1588 conference in 2004, [4].

1-step vs. 2-step clock

IEEE 1588 specifies two types of clocks:

- 1-step clock
- 2-step clock

Figure 3 below shows the PTP packets used for performing time updates on a SC either based on 1-step clock or 2-step clock principles. The Sync and Delay_Req packets are PTP event packets, while the Follow_Up and Delay_Resp packets are general packets.

A one-step clock implementation is based on including the precise egress timestamp, t1, from the GMC into the Sync packet payload, while a corresponding two-step clock implementation is based on sending this timestamp in a Follow_Up packet that follows the Sync packet.

A one-step clock implementation must generate and update the Sync packet with the precise egress timestamp and perform and update the packet FCS in hardware. No Follow_up packet is required if one-step clocks are used.

Only 2-step clock implementations are used in FTI for both IEEE 1588™ - 2002 and in IEEE 1588™ - 2008.

DOI 10.5162/etc2016/1.1

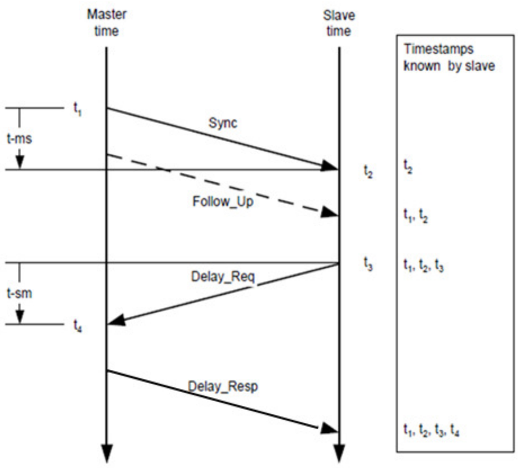

Figure 3, 1-step vs- 2-step clock

Media

IEEE 1588 can be used for several media. Wired Ethernet is by far the most used communication technology used for IEEE 1588, where both copper and fiber and any Ethernet speeds can be used. The IEEE 1588™ - 2002 or in IEEE 1588™ - 2008 standards do not specify that the duplex connectivity must be full duplex, but most PTP profiles do specify this. Note that half duplex connectivity and Ethernet PHYs/MACs supporting IEEE 1588 might not work properly.

Only full duplex connectivity is used in FTI.

Delay mechanism

The delay mechanism defined in IEEE 1588™ - 2002 is used to calculate the propagation delay between a given SC and the GMC. This principle is shown in Figure 3 above. A normal time update is based on the egress timestamp generated by the GMC when the Sync is sent from the GMC, t1, and the ingress timestamp of the same packet is generated by the SC when this packet is received on the SC, t2. The SC can also send event packets. The Delay_Req packet originates from a SC and this packet is used for the purpose of calculating the propagation delay between the GMC and the given SC. An egress timestamp is generated when this packet is sent from the SC, t3, and a corresponding ingress timestamp, t4, is generated on the GMC when the packet is received on this PTP clock.

The propagation delay is calculated based on the following formula:

$t_{pd} = ((t4-t1) – (t3-t2))/2$

The above delay mechanism technique is in IEEE 1588™ - 2008 standard referred to as End-to-End (E2E).

The IEEE 1588™ - 2008 standard also introduced a new delay mechanism technique called Peer-to-Peer (P2P). P2P is based on the same principle as E2E except the propagation delay calculation performed by a PTP clock is only performed for the link partners of the PTP clock. A set of three new PTP packets are defined for P2P:

- PATH_DELAY_REQUEST
- PATH_DELAY_RESP
- PATH_DELAY_RESP_FOLLOW_UP (in case of two-step clock)

A P2P clock must update the PTP packet (Sync packets in case of one-step and Follow_Up packets in case of two-step) with the peer-delay to the PTP clock the packet is sent to. For a TC switch this means that the switch must update the PTP packet with both the switch residence time and the propagation delay of the link where the SYNC packet is received if the switch is enabled for P2P.

Only E2E is used as delay mechanism in FTI for both IEEE 1588™ - 2002 and in IEEE 1588™ - 2008.

Transport mechanism

IEEE 1588 defines several transport mechanisms for PTP. PTP can be based on unicast communication (telecom) or multicast (most other PTP profiles), PTP above layer 2 (power stations) or UDP/IP (default profile).

FTI is based on:

- PTP over UDP/IP
- Multicast with destination IP address: 224.0.1.129
- UDP destination port number 319 (event packets) and 320 (general packets)

This is valid for both IEEE 1588™ - 2002 and IEEE 1588™ - 2008.

PTP domain

IEEE 1588 defines several domains for PTP. This means that several time domains can exist in the same network. Separate MC selections will be done in a network where two or more time domains exist. Default domain is 0.

FTI only uses the default domain for both IEEE 1588™ - 2002 and in IEEE 1588™ - 2008.

Selection of Best Master Clock

The default BMCA as defined in IEEE 1588™ - 2002 or IEEE 1588™ - 2008, are used in today's FTI systems. Simpler FTI systems that are based on a single GMC without any BMCA support do also exits, but this is not recommendable since such solutions do not offer redundancy and may also represent IEEE 1588 interoperability issues when GMC and BMCA capable clocks later are installed.

PTP EPOCH

PTP is based on using TAI as its epoch. That means the number of seconds elapsed since January 1st 1970. The difference between this epoch and UTC is the accumulated number of leap seconds introduced since January 1st 1970. The current number of leap seconds is provided by the PTP GMC by the value of the currentUTCOffset parameter.

26 leap seconds have been inserted since 1970, the most recent on June 30, 2015 at 23:59:60 UTC.

The SCs in the network are responsible for converting TAI to UTC if such time representation is required and/or to compensate the time for DST or local TZ. This is valid for all for all PTP profiles.

Sync interval

The minimum interval between Sync packets was reduced in IEEE 1588™ - 2008 standard compared to IEEE 1588™ - 2002 standard. Legal range for the Sync interval is typical defined in the given PTP profile. The accuracy can be improved if the Sync interval is small, depending on the oscillator choice and the temperature variation at the SCs.

Most FTI systems are based on one (1) second Sync interval. A Sync interval range of [1, 2] seconds for IEEE 1588™ - 2002 and [0.125 .. 2] seconds for IEEE 1588™ - 2008 with one (1) second as default Sync interval for IEEE 1588™ - 2002 and 0.125ms for IEEE 1588™ - 2008 are proposed for FTI.

Delay_Req interval

The minimum Delay_Req interval for IEEE 1588™ - 2002 is 60 seconds with randomization. Randomization is introduced in order to avoid that the SCs send Delay_Reqs at the same time. This interval is controlled by two parameters on the SC: PTP_DELAY_REQ_INTERVAL (30 seconds) and PTP_SYNC_INTERVAL_TIMEOUT (2^(Sync interval)).

This parameter is controlled by the GMC and not each SC in the IEEE 1588™ - 2008 standard. The Delay_Req interval parameter is propagated to the SCs in the Delay_Resp packets originating from the GMC. The legal range for this parameter for IEEE 1588™ - 2008 is [Sync interval, 32 x Sync_interval] seconds with randomization.

Announce interval

The Announce packet was introduced in IEEE 1588™ - 2008 standard. Announce packets are used for BMCA. Similar parameters found in the Sync packets are used for the BMCA for IEEE 1588™ - 2002 systems. The Announce interval is typical two times the Sync interval, and this principle should also be used for FTI systems.

PPS output

The IEEE 1588 standards do not specify that a PTP clock shall have a PPS output interface, but this is highly recommended for time synchronization systems. FTI is not an exception. A PPS output is therefore proposed as a mandatory requirement for a PTP profile for FTI for both IEEE 1588™ - 2002 and IEEE 1588™ - 2008.

IRIG-B output

IRIG-B, both IRIG-B 002 (DC) and IRIG-B 122 (AM), has traditionally been used in FTI context. Compatibility between PTP and IRIG-B can be achieved if some of the PTP clocks in an FTI system can provide IRIG-B output signals. IRIG-B should be defined as a mandatory function for FTI for both IEEE 1588™ - 2002 and IEEE 1588™ - 2008 for GMC and optional for TC/SC.

Management

Chapter 15 of IEEE 1588™ - 2008 specifies IEEE 1588 management. IEEE1588 management packets are used for reading all

DOI 10.5162/etc2016/1.1

possible PTP parameters and also for setting all writeable PTP parameters.

The same PTP data set parameters may also be available via SNMP private MIBs.

The PTP management protocol is particular useful for verification of synchronization lock of SCs in the PTP network. The OffsetFromMaster parameter can be monitored in order to verify that a given SC is synchronized with GMC of the network and how accurate the SC is. The PTPv2Browser MS Windows tool from OnTime Networks that supports the PTP management protocol. Figure 2 shows the PTPv2Browser GUI of the OffsetFromMaster variable for two SCs in a PTP network. Monitoring the OffsetFromMaster parameter is an alternative technique to comparing PPS output signals from the GMC and SC on an oscilloscope.

The iNET standard specifies a set of time synchronization parameters available via MDL or the iNET SNMP MIB, where e.g. PTP version can be set and PTP state can be read

PTP management according IEEE 1588™ - 2008 should be defined as an optional management protocol for FTI, while management via iNET MDL and SMNP according to the iNET TmNS MIB is mandatory.

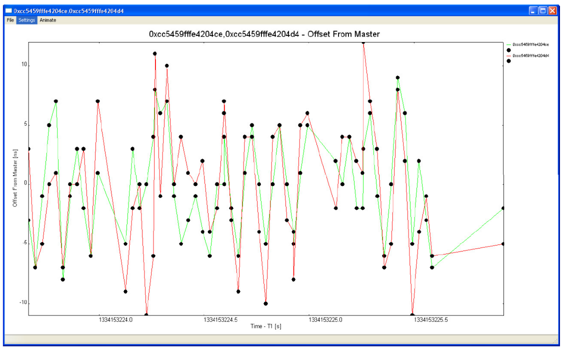

Figure 2, PTP Browser GUI, monitoring the OffsetFromMaster parameter of two SCs

SNMP traps

The iNET TmNS MIB specifies several SNMP traps that can be sent to an SNMP host station in order to immediately detect any time synchronization problems. The following traps are defined:

- timeLockLostNotificationBranch
  Trap is sent from the PTP GMC if synchronization lock from its time base is lost

- ieee1588MaxOffsetFromMasterNotificationBranch
  Trap is sent from SC if the OffsetFromMaster parameter exceeds pre-defined thresholds

- ieee1588MaxJitterNotificationBranch
  Trap is sent from the PTP clock if the measured jitter of the local clock exceeds pre-defined thresholds

GMC hold-over

The iNET standard specifies that an iNET GMC must offer a clock hold-over capability of minimum 0.1ppm in order to ensure that clock synchronization for the whole FTI system is kept when GPS lock is lost or when GPC lock is established after a period of no GPS lock.

0.1ppm means 100ns drift over one seconds or a maximum of 360us during one hour. This worst case drift is, however, calculated over the whole temperature range that the FTI GMC must support: i.e.: [-40 ..185]˚F / [-40 ..85]˚C.

Figure 3 shows that the clock drift for the CM1608F0 GMC with OCXO as oscillator from OnTime Networks after GPS lock is lost, is less than 320µs over a time period of 60 minutes when the temperature is cycled from: -40˚F/-40˚C to 203˚F/95˚C. This means clock hold-over capability better than 0.1ppm.

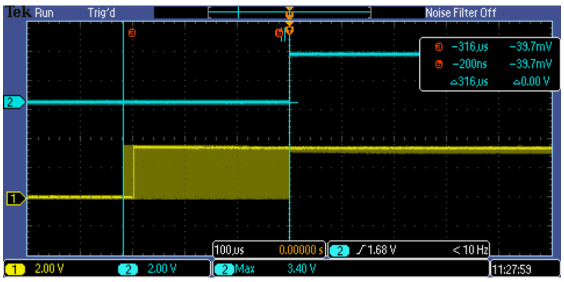

Figure 3, CM1608F0-AERO-GMC, clock drift

Clock drift of an oscillator when the temperature variation is less than e.g. 18˚F / 10˚C for a one hour period will only be a few percentage of the clock drift of the whole temperature range. That means less than 10us drift during one hour.

The GMC is supposed to stay in MASTER state when GPS lock again is found. The GMC will then start to discipline its local clock based on the new PPS input from the GPS based on its clock servo algorithm. The SCs will correspondingly discipline their local clocks based on clock updates from the GMC that gradually will be based on GPS clock. How fast the PTP clocks are disciplined to GPS time after a GPS lock period depends on the drift amount and clock servo implementations on the GMC and SCs.

SC accuracy and time to synchronization

iNET specifies that a SC shall not drift more than 1ppm from the GMC of the network, and that time to synchronization must be less than 1 seconds for airborne systems and 3 seconds for ground installations after the GMC becomes available.

This iNET requirement requires that the Sync interval is as small as possible This is why the proposed Sync interval is 1s for IEEE 1588™ - 2002 and 0.125ms for IEEE 1588™ - 2008.

PTP profile for FTI

Table 1 below summarizes the proposed PTP profile for FTI:

DOI 10.5162/etc2016/1.1

	IEEE 1588™ - 2002 FTI PTP profile	**IEEE 1588™ - 2008 FTI PTP profile**
Clock modes	OC (GMC), TC(*), Slave only	OC (GMC), TC, Slave only
One-step or two step clocks	Two-step	Two-step
Media	Ethernet, full duplex according to IEEE802.3	Ethernet, full duplex according to IEEE802.3
Delay mechanism	E2E	E2E
Transport mechanism	PTP above UDP/IP, multicast with destination IP address: 224.0.1.129 and UDP destination port number 319 (event packets) and 320 (general packets)	PTP above UDP/IP, multicast with destination IP address: 224.0.1.129 and UDP destination port number 319 (event packets) and 320 (general packets)
Domain	Only default domain (0x00) is used	Only default domain (0x00) is used
Selection of Best Master Clock	Default BMCA algorithm	Default BMCA algorithm
PTP EPOCH	Time representation based in TAI, offset to UTC time (accumulated number of leap seconds) is defined in the currentUTCOffset parameter.	Time representation based in TAI, offset to UTC time (accumulated number of leap seconds) is defined in the currentUTCOffset parameter.
Sync interval	[1, 2]s, default = 1s	[0.125 .. 2]s, default = 0.125s
Delay_Req interval	60s, randomized	[Sync interval .. 32]s, default = 32s, randomized; controlled by GMC
Announce interval	NA	[1, 2, 4, 8, 16]s, default = 2s
PPS output	Mandatory	Mandatory
IRIG-B 002/122	Mandatory for GMC Optional for TC/SC	Mandatory for GMC Optional for TC/SC
Management	iNET SNMP/MDL	iNET SNMP/MDL Optional: PTP management according to IEEE 1588™ - 2008
SNMP traps	iNET MIB	iNET MIB
GMC holdover	0.1ppm, iNET requirement	0.1ppm, iNET requirement
SC accuracy	1ppm, iNET requirement	1ppm, iNET requirement
SC time to synchronization	1s/3s (airborne/ground), iNET requirement	1s/3s (airborne/ground), iNET requirement

(*) Proprietary TC implementation

Table 1

Conclusion

Backward compatibility between the new emerging PTP revision, PTP version 3, and PTP version 2 will be kept. This means that PTP version 2 and 3 can be combined in the same network. The new functions that are planned in PTP version 3 will be optional. These new functions are not expected to be crucial for the FTI industry. PTP version 2 is expected to be the preferred PTP version for FTI for the foreseeable future, but new PTP version 3 functions can be considered for FTI application with high accuracy and/or security requirements.

This paper also describes the main PTP properties/parameters that are relevant for FTI and proposes a PTP profile definition for FTI based on the PTP default profile for both IEEE 1588™ - 2002 and IEEE 1588™ - 2008 in addition to time synchronization requirements defined in the iNET standard.

Reference

[1] D. Lefevre1, N. Cranley, Ø. Holmeide, “PTPv1 and PTPv2 translation in FTI systems”, ITC2013 Las Vegas - USA.

[2] Silvana Rodrigues, “New IEEE 1588 Revision”, WSTS 2014, San Jose

[3] Doug Arnold, “IEEE 1588 Working Group Update”, WSTS 2015, San Jose

[4] S. Nylund and Ø. Holmeide, “IEEE1588 Ethernet switch transparency – No need for Boundary Clocks!”, IEEE1588 conference, 2004.

DOI 10.5162/etc2016/1.2

Nanosecond Synchronous Analog Data Acquisition over Precision Time Protocol

Matthias Braun, Milan Juranek, András Széll, Péter Szántó, Dr. Cruz Marín
Zodiac Data Systems GmbH, Friedrich-Ebert-Str. 75, 51429 Bergisch Gladbach, Germany
matthias.braun@zodiacaerospace.com
milan.juranek@zodiacaerospace.com
szell@fpgart.hu
szanto@fpgart.hu
cruz.marin@zodiacaerospace.com

Abstract

This paper describes an implementation of the Precision Time Protocol – IEEE™1588-2002 and IEEE™1588-2008 – in order to reach maximum accuracy in time synchronization as a requirement for simultaneous analog data sampling.

Exact cross-correlation calculation between various measurements calls for a very small phase error margin between the sampled signals. Besides, there is an increasing need to synchronize the analog sampling carried out at different places without utilizing additional synchronization connections between different devices.

Nowadays, Ethernet is universally used and therefore present almost everywhere. Data acquisition systems typically deliver their data via networks. For time synchronization, the Precision Time Protocol (IEEE1588™) is basically a mandate. This protocol provides the high accuracy required for synchronous and simultaneous analog sampling.

The performance evaluation of the present implementation shows that an absolute time synchronization better than 10 nanoseconds can be achieved between two given data acquisition systems. Furthermore, this paper elaborates on how the analog sampling can be synchronized to the absolute time with this same accuracy.

Key words: IEEE1588, Time Synchronization, Analog Data Acquisition, Synchronous and Simultaneous Analog Sampling

Introduction

In flight test instrumentation, reducing and simplifying wiring is a continuous effort. One way to achieve this goal is to use distributed data acquisition systems, where connecting only power and some serial digital communication lines (most commonly Ethernet technology) obviates the need of long cabling for all sensors over long distances. Beyond data transfer, Ethernet is used for the distribution of absolute time for coherent time stamping, enabling more and more accepted methods to guarantee synchronous analog sampling between multiple data acquisition units. Because no additional hardware or software components are required, the method described in the following, which is based on the standard Precision Time Protocol (PTP), is data acquisition hardware manufacturer independent.

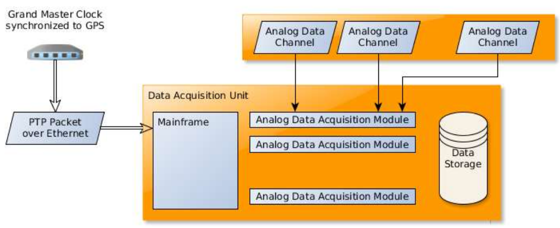

Fig.1 Data Acquisition Unit

Analog Synchronization

In order to be able to correlate analog data from different acquisition systems it is necessary to synchronize the time and the analog sampling points in multiple systems to each other. Using the PTP protocol is one approach conducive to synchronizing the acquisition systems to a GPS based PTP time server. To avoid the need of a digital resampling of the analog data the target is to ensure that the real analog samples are taken at the same time by means of synchronizing both the frequency and phase of the sampling clocks.

The first step is to establish a precise absolute time base for the Data Acquisition Devices based on the PTP Synchronization Protocol. To synchronize the sampling clock frequency of all analog to digital converters (ADCs) to this absolute time base, the digital frequency generator devices have to be tuned in a second step. This tuning can only be done in very small steps in order to avoid jitter in the analog sampling – so the generated absolute time from the first step must be jitter-free as much as possible. In the last step the same phase of the sampling has to be guaranteed. To be able to sample the analog signals simultaneously in multiple systems it is necessary to take into account the delays effective along the entire signal path, on which a signal propagates from the input connector to the place where digital sampling takes place, including the pass through amplifiers and filters – the analog sampling needs to be delayed accordingly.

On one hand it is possible to design digital filters with arbitrary delays so that the total propagation delay of the ADCs and digital filters is typically an integer number of samples. But on the other hand, when it is not possible, the sampling signals shall be adjusted to compensate also fractions of the delays.

With this method it is theoretically feasible to phase correlate the acquired signals even if different types of acquisition hardware components are used. To simplify the analysis process of finding corresponding samples based on the timestamps included in data streams, the start of the data packets can be synchronized to the second's change, which is only doable when using integer sampling rates.

The accuracy of sampling synchronization depends on the following factors:

- The stability of the reference clock.
- The accuracy of the absolute time synchronization in the data acquisition unit.
- The resolution of the sampling frequency control.
- The accuracy of the compensation of the analog and digital delays of the digitalization process.
- The jitter of the sampling clock.

Recording Format

This implementation uses the IRIG106 Chapter 10 data format [1] for its recordings. In this data format (see Fig. 2) all acquired data is timestamped with a free running relative time counter. While every data acquisition unit has its own relative time counter and their values don't necessarily equal each other, it is necessary to convert all timestamps to one time domain to correlate two analog channels from different systems. The following steps are mandatory to convert the time domain of recording 2 to the time domain of recording 1:

1. Calculate the time offset between analog channel 1 and time channel from recording 2. In this case 1480-1478=2. The unit is 100 ns.
2. Calculate the time offset between analog channel 1 and time channel from recording 1. In this case 1236 – 1234 = 2.
3. Calculate the time offset of the relative time counters between the two time channels at time packets containing the same absolute time.1478 – 1234 = 244.
4. Analog channel 1 from recording 2 gets its new relative time by TS - offset1 + offset2 + offset3 = 1480 – 2 – 244 + 2 = 1236.

In this example the analog data was created simultaneously.

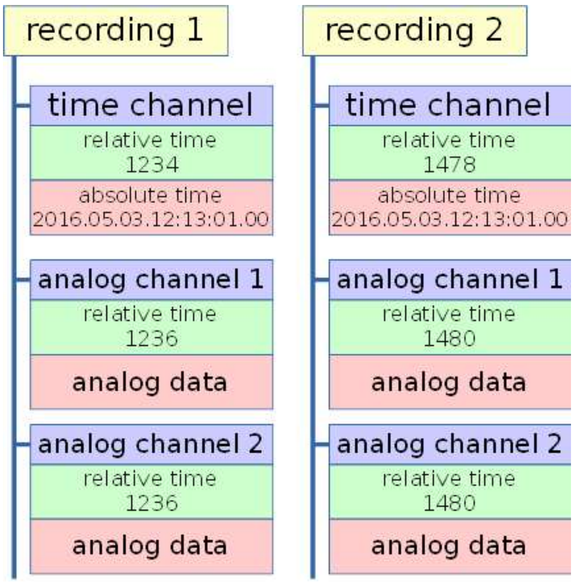

Fig. 2 Packet structure of two IRIG106 CHAPTER 10 recordings.

Precision Time Synchronization Protocol

To synchronize computer clocks over a given network, a protocol called 'Precision Time Synchronization Protocol' exists. Today two versions are available. The first version was published in 2002, and therefore it is named

'IEEE Std 1588™-2002, IEEE Standard for a Precision Clock Synchronization Protocol for Networked Measurement and Control Systems'. Version 2 was introduced in 2008, and it is known as 'IEEE Std 1588™-2008, IEEE Standard for a Precision Clock Synchronization Protocol for Networked Measurement and Control Systems'. It is not backwards compatible and is designed to improve the precision and robustness of the time synchronization while achieving an accuracy better than 1 nanosecond.

In a PTP network domain, different types of clocks can coexist. They are called 'Ordinary Clocks', 'Boundary Clocks' and 'Transparent Clocks'. An 'Ordinary Clock' is a device that uses a single network connection for time synchronization. It can act as a master or as a slave clock. A 'Master Clock' sends out timing information for a 'Slave Clock' to get in sync with it. A 'Boundary Clock' uses multiple network connections and is used to synchronize several network segments. The third type of clock is called 'Transparent Clock'. This one is introduced in IEEE™1588-2008. 'Transparent Clocks' convey PTP messages and modify the timing information with the time slice the PTP messages need to pass through the network node. This allows better compensation of message delays.

In a PTP domain, more than one master clock can be present. By evaluating the 'Announce Messages' every master clock generates, a 'Grand Master Clock' also known as GMC, is elected by the 'Best Master Clock Algorithm' (BMC). The GMC is the root timing reference which transmits synchronization information for all other clocks in the PTP network. The slave clocks synchronize to this 'Grand Master Clock' by exchanging different timing messages.

The GMC periodically broadcasts 'Sync Messages' over the network to let the slave clocks know about its timing information. Therefore, the instant of time when the 'Sync Message' leaves the GMC hardware has to be embedded into this message. This is called a one-step synchronization and requires hardware processing for highest accuracy. Master clocks without such hardware follow a two-step synchronization protocol. Here the 'Sync Message' contains an estimated timestamp, but in addition, a separate 'Follow_Up Message' is broadcasted with the accurate timestamp of the instant the 'Sync Message' leaves the GMC. For the implementation of the delay compensation, the calculation of the predicted propagation time of the PTP message transfer over the wire ('Mean Path Delay') is required. Two more PTP messages have to be sent over the network: The slave clock sends out a 'Delay_Req Message' for which the GMC notes the timestamp when it arrives and after that sends back a 'Delay_Resp Message' containing this timestamp. For an exact description of how this message exchange happens please have a look at: 'IEEE1588™-2008, 11.3 Delay request-response mechanism' [3].

The PTP messages are divided into 'General Messages' and 'Event Messages'. 'General Messages' provide more general information whereas 'Event Messages' are time critical and provide timing information for calculations in the PTP stack. Therefore they have to be timestamped. This can be done in software or in hardware. While software timestamping is not deterministic, hardware timestamping allows a much more precise accuracy in timing information for the offset calculations in the PTP stack.

In order to timestamp arriving and departing 'Event Messages', the hardware layer needs to detect these as close as possible to the physical wire using the physical interface chip also known as PHY. Once a PTP Ethernet packet is identified as an 'Event Message', the PHY core stores the value of the PHY internal global counter and the ID of the PTP packet into specific registers. Also, it informs the CPU respectively the kernel PHY driver that such an event happened. As shown in figure 3, a '100MHz Relative Time Counter' (rtc100) is implemented in every Data Acquisition Unit which is driven by a ‘Controlled Oscillator’ (CXO). To allow correct calculations of the value of the timestamp in nanoseconds when an 'Event Message' arrives or departs, the PHY of the given hardware is programmed to continuously trigger an impulse to the FPGA to capture the actual '100MHz Relative Time Counter' value and match them against the PHY internal global time counter. The PTP stack can now grab the timestamp information from the PHY driver for further calculations. In order to sync a Slave Clock to a given Grand Master Clock, the Time Processing Unit has to be informed by the PTP stack of the elapsed nanoseconds since the start of the PTP epoch (January, 1st 1970 00:00:00 UTC) at a given rtc100 counter value. This timestamp is the instant of time when the 'Sync Message' leaves the GMC (also known as the 'Precise Origin Timestamp'), compensated with the 'Mean Path Delay'. For further details refer to 'IEEE1588™-2008, 11.3 Delay request-response mechanism' [3].

DOI 10.5162/etc2016/1.2

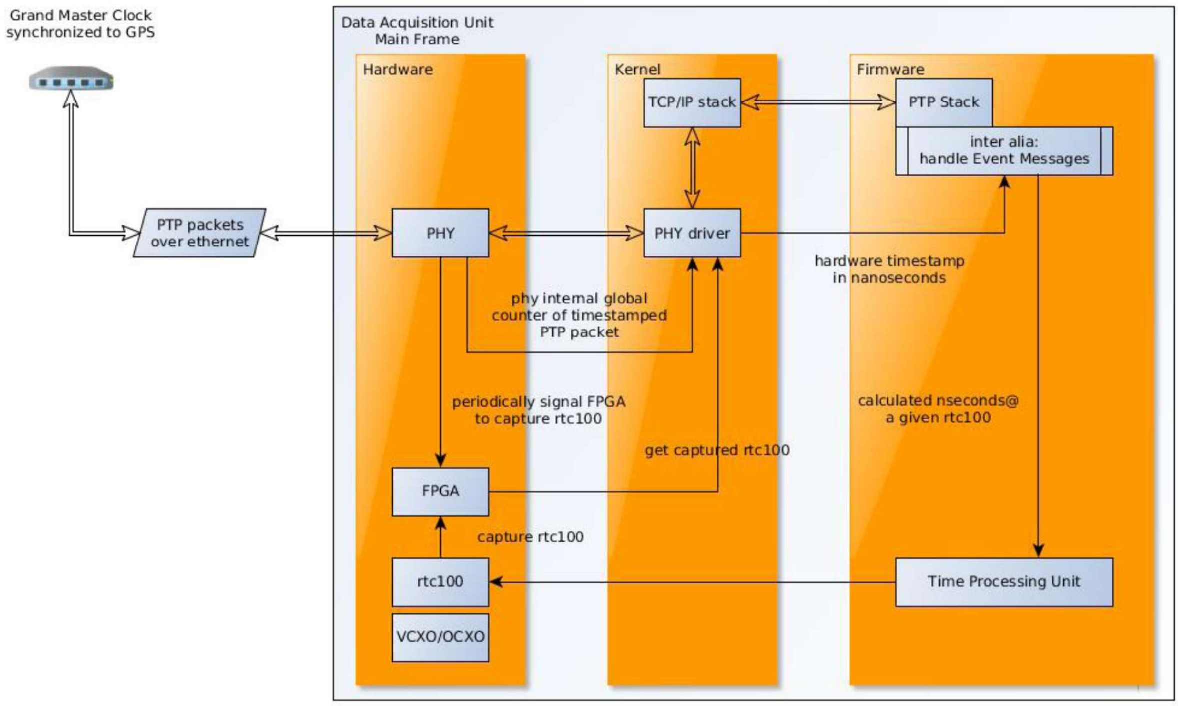

Fig. 3 PTP Message Flow and Timestamping in a Data Acquisition Unit

Time Processing Unit

The time synchronization subsystem or Time Processing Unit (TPU) supports synchronization to several source types including PTP. For any of these time sources, pulse-per-second (PPS) may also be connected to increase time precision. High precision (better than 100 ns) time synchronization to most sources is possible either with the PPS pulses or using long-term filtering in order to reduce measurement noise. Longer filtering (in the range of minutes, up to half an hour) is sensible only if proper time keeping is possible by means of using a stable oscillator. Otherwise, even though measurement noise is reduced by long-term averages or filtered values, temperature changes and other factors affecting the internal clock will introduce mid-term and long-term frequency deviations, degrading the performance of any filters applied to the input source.

The TPU is a time source itself. There is a trade-off between the filtering/tuning parameters: By applying strong filters on the input time source, the clock output will appear more stable and less jittery (assuming an oscillator with good short-term stability), but it will lock in and follow frequency drifts more slowly, resulting in large temporary offset errors against the source.

Due to the different characteristics of the external clock sources, the TPU uses clock source specific filtering. For some sources it is possible to record the raw, unfiltered input timestamps (for error detection) or filtered ones. Filtering, outlier detection and averaging of the input signals is necessary to reduce noise and sampling errors.

Even the best algorithms fail to perform well if the underlying hardware architecture doesn`t allow to properly sample the incoming timestamps and to keep the internal clock in sync with the external source. The base clock used in the TPU is either a voltage controlled oscillator (VCXO) or an oven controlled oscillator (OCXO) with better than 10 ppb stability. The VCXO has frequency fluctuations in the range of 50 ns/sec (50 ppb) even under stable temperature conditions. This is partly due to the imprecision of the crystal and partly due to the higher tuning range of the VCXO, thus it is more susceptible to minor tuning voltage noises (of mV level). In order to synchronize within 30 ns to the master clock, the presented synchronization method uses an OCXO. Under stable ideal conditions this setup can be fine-tuned to be within 1-2 nanoseconds from the reference clock.

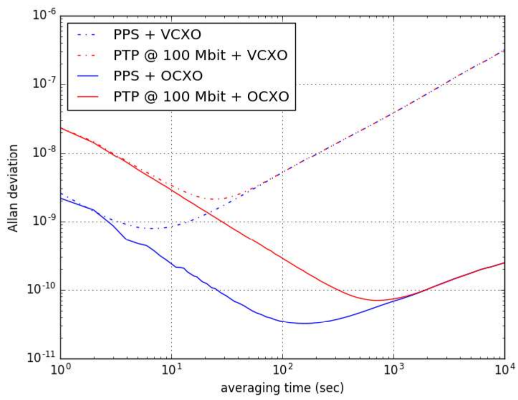

Fig. 4 Oscillators compared: Allan deviation of a TPU synchronized over PTP or PPS featuring an OCXO (solid lines) or VCXO (dashed)

Time stamps in the TPU are generated at 200 MHz resolution for PPS source and at 100 MHz for PTP sources (the rtc100 counter), meaning an inherent time stamping jitter of 5-10 ns. In case of PTP, the actual timing inaccuracy resulting from the finite resolution of the Ethernet PHY's time stamps is larger if the clock source is connected via 100 Mbit Ethernet, as the 25 MHz frequency used for data transmission means 40 ns resolution at best (in contrast to the 1 Gbit Ethernet's 125 MHz clock and 8 ns resolution). To reach the best analog synchronization performance, a Gbit Ethernet was used for the present work

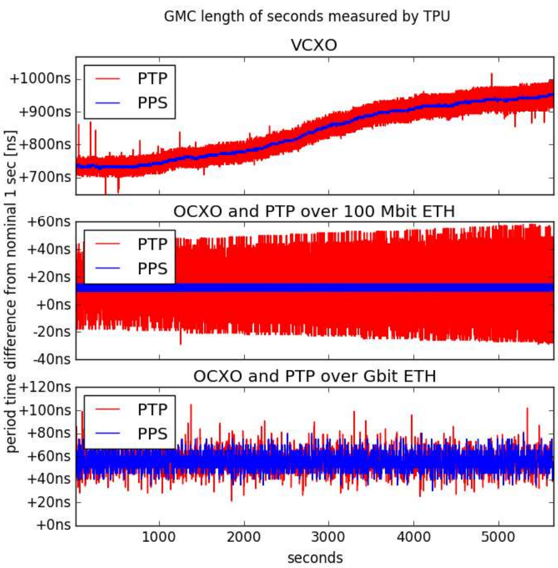

Fig. 5 Effect of Ethernet speed and oscillator type on PPS/PTP timestamping jitter and frequency drift

In Figure 4 the performance of the voltage controlled oscillator is compared to the oven controlled, temperature-stabilized oscillator. In this Allan deviation plot it is apparent that the short-term PTP precision is below the accuracy of PPS input due to the 40 ns resolution, but for longer averages (in the range of 10^3 seconds) their variances match, and the OCXO based solution is one order of magnitude better than the other system utilizing a VCXO. The VCXO frequency stability already deteriorates in the range of 100 seconds mostly due to temperature changes, as seen in Figure 5.

During the initial phase of the synchronization the oscillator is tuned to match the short-term averaged frequency of the GMC (3-5 seconds) and the offset is compensated with period time modification (as if the seconds are a few extra microseconds longer or shorter than 10^6). Once the oscillator frequency and offset errors are within bounds, only oscillator frequency tuning is applied afterwards. Synchronous analog sampling begins only in this second phase. The filter coefficients gradually change to reduce tuning the jitter as the observed offset and frequency error gets smaller. Offset errors are reduced by dithering (temporarily mistuning the frequency similarly to how one car keeps distance from the other just by minor accelerations and decelerations).

After successful synchronization the synchronized internal RTC clock is recorded into IRIG 106-09 Chapter 10 time packets and sent out to all other modules taking part in the data acquisition. The time packets contain the UTC time recorded at the given relative recording time, which is by default time stamped with 100 ns resolution. Later Chapter 10 extensions will increase the precision to nanoseconds.

Sampling Clock Generation

In a distributed system it is often not possible for the analog data acquisition units to communicate with each other, only their clocks can be synchronized. A 1 Hz 'analog frame signal' populated from the time synchronization subsystem via a dedicated clock pulse distribution network to the analog sub-systems is used to ensure simultaneous sampling.

The analog sampling clock is derived from the time subsystem's 100 MHz clock with a digital synthesizer. This clock value is an integer multiple of the analog sampling clock rate only in a limited set of frequencies, so in most cases it is necessary to fine-tune the synthesizer by means of a PI controller (proportional-integral controller) to ensure that the 1 Hz analog frame signals match the PPS signal of the TPU. The regulation of the PI controller can be seen in Figure 6. In this case an Analog Master Clock of 19.1979 MHz will result in a standard deviation of 3.519 ns. The time offset is measured between the falling edge of the analog frame signal C3 (which is an active low signal) and the rising edge of the PPS out signal C1.

DOI 10.5162/etc2016/1.2

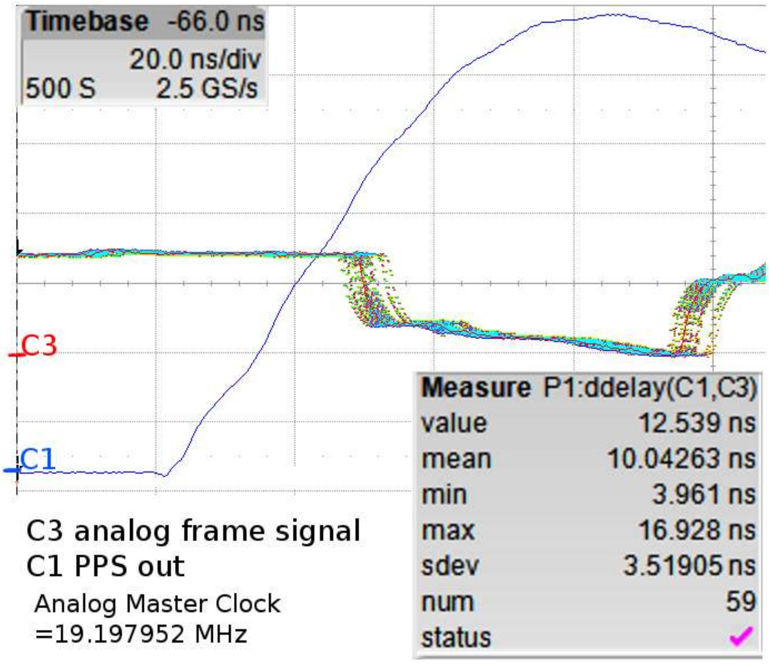

Fig. 6 Deviation measurement between the PPS output and the low active Analog Frame

Properly compensating signal delays in each input channel will allow a correlation between the latter even if their sampling rates are different.

Evaluation of Results

Figure 7 shows the Data Acquisition Unit's synchronization to a Grand Master Clock. The synchronization was carried out via a dedicated 100 Mbit network connection, the recorded data was transferred over a separate Ethernet interface.

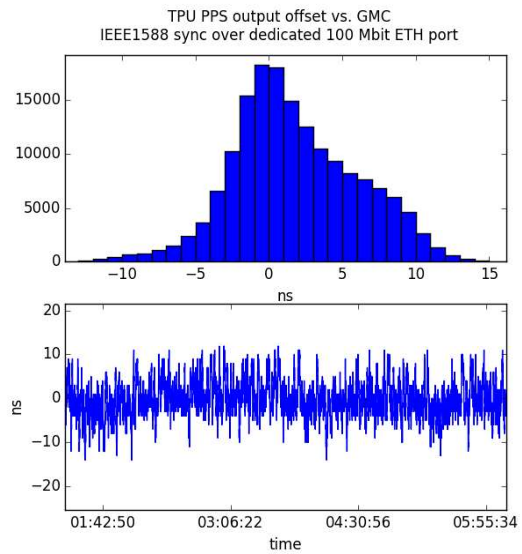

Fig. 7 IEEE1588-2008 direct synchronization against Grand Master Clock: offset error distribution

There are a multitude of possible error/jitter sources, among others:

- Frequency drifts due to temperature changes
- Noise/jitter in the signal (on PTP the network traffic, the carrier/PHY buffering jitter and performance of other network components; delay measurement issues)
- Time stamping inaccuracies caused by finite time stamping resolution ('time domain quantization errors')
- Analog sampling clock synchronization against internal (synchronized) clock

In suboptimal cases a lot depends on the input filtering. It is necessary to filter PTP Sync message timestamps and delay measurements for outliers; the tuning coefficients are modified if incoming timestamp jitter/offset is above threshold. Under ideal real world conditions (proper PTP-aware network devices, analog recorders are on the same subnode/switch) some of the described effects are marginal, and others are mitigated by the filtering capabilities of the tuning algorithm. This way, a 30 ns synchronization precision can be achieved against the GMC. In case of a direct connection an even better 5-10 ns precision was measured between two modules synchronizing against the same GMC.

Figure 8 shows the measurement picture of an oscilloscope sampling the 1 PPS signals of the two Data Acquisition Units (C2 and C3) and the Grand Master Clock (C1). The trend-line F1 shows the delta delay of C2 against C3 with 100 measurements per division in the direction of the x axis. The time base in y axis is 5 nanoseconds per division. A jitter of the delta delay of ±5 ns is measured. For this measurement 3711 samples were taken at a measurement rate of 1 Hz. Within this one hour of measurement a mean delta delay of the 1 PPS signals of the two acquisition units of 7.65871 ns is achieved with a standard deviation of 2.17535 ns.

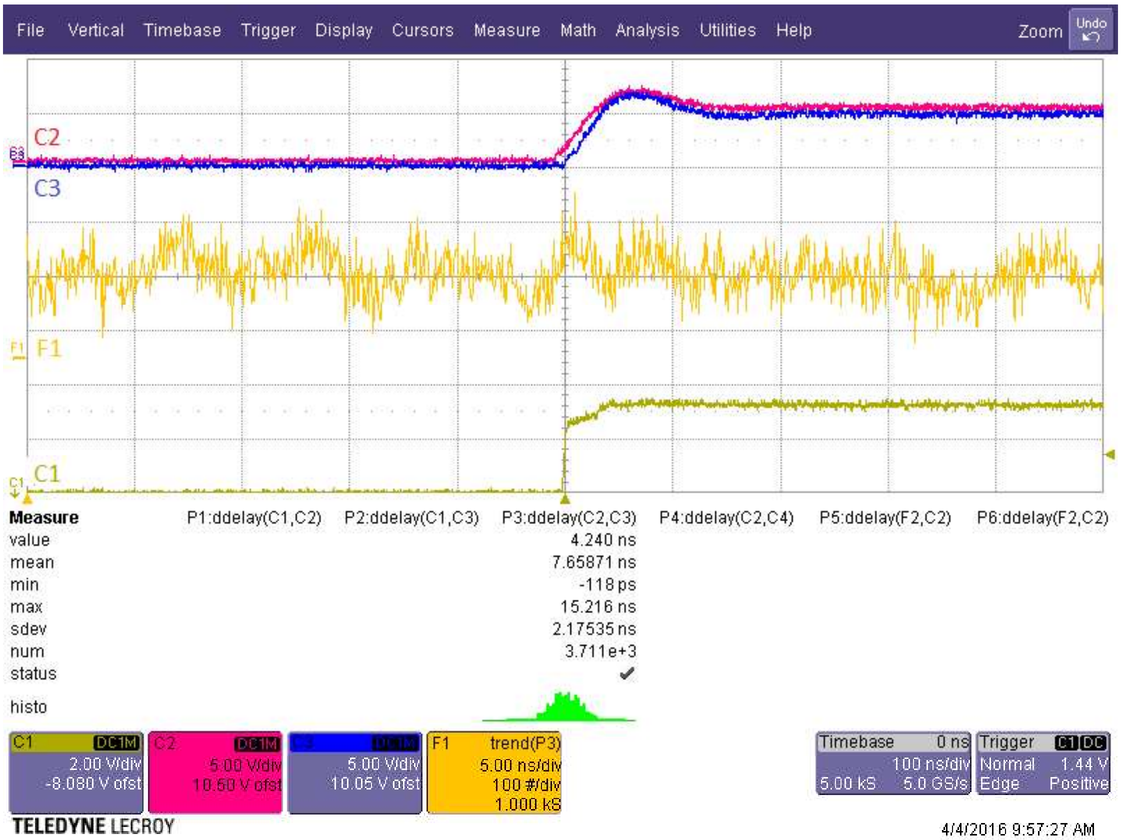

Fig. 8 1 PPS Offset between GMC and two synchronized Data Acquisition Units

Conclusion

It was demonstrated that with precise onboard oscillators and a good quality time source a distributed data acquisition system can achieve synchronous analog sampling accuracy of the 10 ns range by the means of the IEEE^{TM}1588-2008 Precision Clock Synchronization Protocol.

The precise synchronization is not instantaneous. In the current implementation it takes up to 5 minutes to achieve stable sync but there are several possibilities to reduce the time the different filters need for settling.

It should be noted that even though module-to-module the analog sampling can be extremely synchronous, this remains so only as long as the same algorithm with same parameters is used for synchronization. E.g. if one of the modules uses PID controller for PTP synchronization and the other uses a Kalman filter based approach [4] or a very simple FIR filter (e.g. present in the earlier IEEE^{TM}1588-2002 implementation), these will result in very different responses to the GMC clock changes and a 10 ns analog sampling precision as shown in Fig. 9, may become impossible in a heterogeneous recording environment.

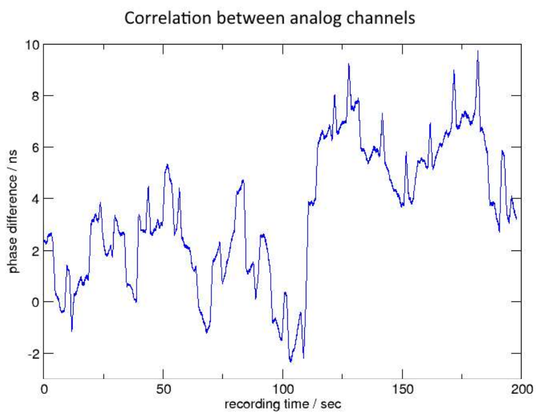

Fig. 9 Phase correlated PTP synchronized analog channels of two Data Acquisition Units

There are possible improvements over the basic implementations of the PTP utilizing Synchronous Ethernet (e.g. White Rabbit [5]) that target the sub-nanosecond synchronization range. These systems use expensive hardware and guarantee that the Ethernet clock frequency is the same throughout the network, removing some noise sources.

References

[1] Telemetry Standards, IRIG Standard 106-13 (Part1), Chapter10, http://irig106.org/docs/106-13/chapter10.pdf

[2] IEEE Std 1588™-2002, IEEE Standard for a Precision Clock Synchronization Protocol for Networked Measurement and Control Systems, Print: ISBN 0-7381-3369-8, SH95023; PDF: ISBN 0-7381-3370-1, SS95023

[3] IEEE Std 1588™-2008, IEEE Standard for a Precision Clock Synchronization Protocol for Networked Measurement and Control Systems, Print: ISBN 978-0-7381-5401-5, STDPD95773; PDF: ISBN 978-0-7381-5400-8, STD95773

[4] G. Giorgi, C. Narduzzi, Performance analysis of Kalman filter-based clock synchronization in IEEE 1588 networks, *International IEEE Symposium on Precision Clock Synchronization for Measurement, Control and Communication* 2009, doi: 10.1109/ISPCS.2009.5340221

[5] P. Moreira, J. Serrano, T. Wlostowski, P. Loschmidt, G. Gaderer, White Rabbit: Sub-Nanosecond Timing Distribution over Ethernet, *International IEEE Symposium on Precision Clock Synchronization for Measurement, Control and Communication* 2009, doi: 10.1109/ISPCS.2009.5340196

DOI 10.5162/etc2016/1.3

Evaluation of Radio Communication System for sharing location information between traffic objects

M. Kraetzig[1], T. Speth[2], K. Theuerkauf[1], L. Rauchhaupt[1]

[1]Institut für Automation und Kommunikation e.V. Magdeburg, Werner-Heisenberg-Str. 1, 39106 Magdeburg, Germany, marko.kraetzig@ifak.eu
[2]Technische Hochschule Ingolstadt, CARISSMA, Paradeplatz 13, 85049 Ingolstadt, Germany, Thomas.Speth@thi.de

Abstract:

Dedicated short range communication (DSRC) or radio systems for intelligent transport systems (ITS) should be used for transmission of position information between dynamic traffic objects. The position information shall be used to improve the accuracy of localisation of traffic objects. Therefore the safety in road traffic is increased by avoiding dangerous situations and accidents. Due to relative movement of traffic objects the position data becomes outdated, the longer it takes to transmit the information via ITS radio system. For that reason, the transmission time of ITS radio system shall provide an input to correct the transmitted position data at the receiver.

Keywords: Intelligent Transport Systems, System analysis, Transmission characteristics, Timing analysis, Performance analysis, Performance characteristics, Reliability analysis, Reliability evaluation

1. INTRODUCTION

This paper starts with a description of the application scenario of time critical communication between intelligent transport systems (ITS). Thereafter a model is introduced from which relevant characteristic parameters are derived which are used to assess reliability. The test method to evaluate the performance of ITS radio system is also part of the report. The main part of the paper is the performance assessment of radio system for intelligent transport systems (ITS). The focus is the assessment of time and error behaviour. Furthermore, the effects of influencing parameters will be shown by measurements results. At the end of the paper the results of evaluation will be discussed.

2. APPLICATION SCENARIO

Applications for integral vehicle safety as well as some advanced driver assistance systems (ADASs) benefit from precisely determination of relative positions between dynamic traffic objects. Especially the inter-vehicular exchange of position and dynamic data offers a new potential for these systems, e.g. vehicle-interactive applications [1]. Compared to conventional environmental sensors like Radar or Lidar, there are two major benefits: there is no limitation of angle of beam spread, i.e. vehicle-to-vehicle (V2V) communication acts like a 360° field of view sensor. Second, it works in non-line-of-sight conditions and thus an autonomous safety system can react earlier. For this purpose, a vehicle’s self-positioning has to better than lane-level accuracy [2].

However, with conventional global navigations satellite system (GNSS) measurements, e.g. using Global Positioning System (GPS), the required accuracy cannot be achieved [3]. Known methods for improved positioning are Differential GNSS (DGNSS) or Real-Time Kinematic (RTK). Both techniques lean on GNSS observation data of a nearby reference station.

Focusing on RTK, the typical accuracy is below 0.1 m RMS. To achieve this accuracy, a moving GNSS receiver, called rover, calculates double differences out of its own carrier phase measurements and the received one from a reference station. The result of this calculation is a base line vector between both receivers. With the well-known position of the reference station, it is trivial to get a high accurate position of the rover in global reference frame. [4]

However, the reference station operator often charges for these observation data and also the data link, often established by cellular mobile communication, causes costs. For this reason, we propose, instead of a stationary reference station, a moving base, which can be any other vehicle in the vicinity of the ego-vehicle. By this reduced RTK method, no absolute positioning is possible anymore, thus it is not necessary for the moving base sending their position information. Sending the GNSS observation suffices to calculate a base line vector. Future vehicle safety system might benefit from this cooperative relative positioning method. Similar approaches can be found in [5], [6], [7].

With growing transmission time, however, the accuracy is decreasing, because the base line vector is calculated between the two points of moving base and rover at that the observation were taken. Thus, with larger differential age between both observation data, the calculated relative position becomes obsolete and inaccurate. In this paper we analyse this error source so it can be considered and corrected in further works.

3. MODEL

3.1 Requirements

First we would like to clarify what reliability means in context of wireless communication for intelligent transport systems. A user of a wireless communication system expects a certain value, e.g. position or velocity, at a certain interface within a defined time frame without any errors under defined conditions. This is an informal definition. In order to be able to assess the degree of fulfilment of this requirement by means of simulation or measurement, a formal model is required.

First of all this model has to take into account the application field - the wireless communication for ITSs. The parameters to be investigated have to be in line with the design criteria of wireless communication systems. Parameters such as Data Throughput or Bit Error Rate are normally not useful to design a particular wireless application which e.g. shall transmit time, critical localisation and motion data information.

Furthermore, the model has to consider that there is no standard interface between communication and application available. Last but not least the model should represent the conditions of reality as accurate and complete as possible and necessary. The following section introduces an approach which fulfils the mentioned requirements.

3.2 Approach

The abstraction of a localisation application using wireless communication for ITSs is shown in Fig. 1. The wireless communication modules are seen as an internal or external part of localisation devices. The localisation devices have to fulfil certain functions in distributed moving traffic objects and therefore they have to communicate via wireless communication media. From the point of view of the ITSs, the communication characteristics at the interface provided by the wireless solution are important. These communication characteristics have to fit to the time and error categories.

The communication interface must be clearly defined, upon which the characteristics are related to. This interface consists of a hardware part such as Ethernet and a software part such as a communication protocol or an application interface. Besides a clear statement concerning the communication interface and the communication characteristics, the conditions have to be described under which the characteristic values are valid. The conditions can be described by a number of influencing values which have different origins. It is obvious that the communication system itself affects the characteristics concerning e.g. data rate. It is also evident that the communication media has influence because of other users of the spectrum or because of the effects of fading effects. Furthermore, the characteristics depend on the options chosen in the devices, which means on its configuration. It is sometimes forgotten that also the application affects the characteristic values in the sense of the size of a packet or the cycle of requests on the communication system.

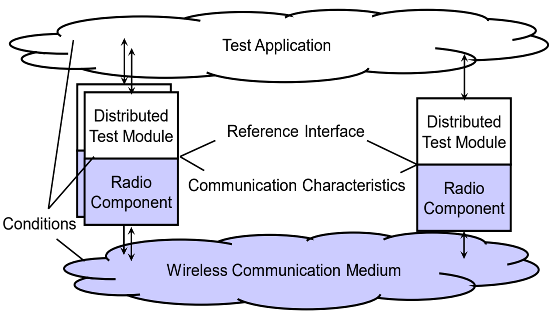

Fig. 1: Model approach for the assessment of wireless communication systems.

4. CHARACTERISTIC PARAMETERS

4.1 Definitions

Reliability

Now we can define the term reliability more specific and we can describe how to assess reliability. In line with the definition of chapter 2.1, reliability can be seen as the degree in which you can expect that a wireless communication solution meets the limits of relevant characteristic parameters. With this definition it is obvious that the assessment of reliability requires stochastic methods. The characteristic parameters are random variables. Their behaviour follows probability density functions. The reliability is the probability that a value of a characteristic parameter is less or equal to the limit defined by the application.

The reliability according VDI 4001 [8] is a comprehensive term to describe the availability with corresponding influencing parameters functionality, maintainability and supportability capabilities.

DOI 10.5162/etc2016/1.3

Therefore, the reliability is no measurable characteristic parameter.

Availability

The availability according VDI 4001 [8] is the ability of a unit to perform a required function at a given time or during a given time interval. The meaning in the context of wireless communication for intelligent transport systems is that the wireless device transfer application relevant user data from the producer to the consumer and the opposite direction. The required functions are an unchanged content of user data and a user data transfer within a prescribed period of time or at a required point of time.

Maintainability

The maintainability according VDI 4001 [8] is the ability of a unit under the given conditions may be left in a state or restore to the state in which it can perform the required functions. The meaning in the context of wireless communication for intelligent transport systems is that the wireless device provides procedures to observe system condition and to detect incipient deviations from that condition. Furthermore the wireless devices provide mechanisms to restore the previous status automatically. Wireless solutions use mechanisms like forward error correction, cyclic redundancy check, transmission repetition or multiple transmissions.

4.2 Characteristic parameters to assess the time behaviour

The characteristic parameters to assess the time behaviour of wireless systems are set out in this subsection. VDI 2185 [9] define characteristic parameters for the assessment of radio based communication in industrial automation. The characteristic parameters “Transmission Time” and “Packet Lost Rate” according to [9] are adequate for the assessment of time and error behaviour of wireless devices for intelligent transport systems.

Transmission Time

The transmission time according to [9] is a very important characteristic parameter, because:

- Real-time location applications are difficult or impossible with unforeseeable deviations of transmission time
- High values of transmission time are a problem for high-precision localisation algorithms

The definition of the transmission time according to [9] is based on a producer-consumer-model (see Fig. 2). It is the time duration from the handing over of the first user data byte of a packet at the reference interface in the test producer, up to the handing over of the last user data byte of the same packet at the reference interface at the test consumer.

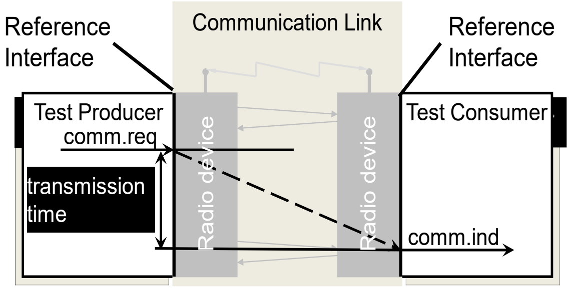

Fig. 2: Definition of the transmission time. [9]

Packet Loss Rate

The packet loss rate (PLR) is ascertained according to the producer-consumer-model. It reveals, how many of the packets, transferred from the application to the communication interface within the producer, are transmitted from the communication interface to the application within the consumer. The packet loss rate is determined as follows in equation (1):

$$\mathrm{PLR} = \frac{\mathrm{N_{Tx}} - \mathrm{N_{Rx}}}{\mathrm{N_{Tx}}} = \frac{\mathrm{N_{PL}}}{\mathrm{N_{Tx}}} = 1 - \mathrm{A} \tag{1}$$

Whereby:

- N_{Tx} means transmitted packets
- N_{Rx} means received packets
- $\mathrm{N_{PL}}$ means number of lost packets

The number of lost packets (NPL) is determined by three cases. The first case of packet loss is that a transmitted packet was not received. The second case of packet loss is that a packet was received after an application related maximum of transmission time (t_{TTmax}). Moreover a packet received in an incorrect sequence is classified as packet loss. The three cases of lost packets are summarized in equation (2).

$$N_{PL} = \sum_{i=1}^{N_{Tx}} l(p_{Rxi}) \;\; with \;\; \begin{cases} l(p_{Rxi}) = 0, \; other \\ l(p_{Rxi}) = 1, t_{TT}(p_{Rxi}) > t_{TT\max} \\ l(p_{Rxi}) = 1, \sum_{j=1}^{i} t_{TI}(p_{Rxj}) < \sum_{k=1}^{i-1} t_{TI}(p_{Rxk}) \end{cases} \tag{2}$$

Availability

The availability (A) is the ability of a unit to perform a required function at a given time or during a given time interval. The availability is the ratio of correct data transmission time (uptime: t_U) to observation time (t_O).

$$A = \frac{t_U}{t_O} \tag{3}$$

Under the assumption that the producer or client transmits cyclic user date frames with a fixed transmission interval (t_{TI}) during the observation period (t_O) and each received frame consider as correct for the transmission interval (t_{TI}). The availability can be calculated as follows in equation (4):

$$A = \frac{N_{Rx} t_{TI}}{N_{TX} t_{TI}} = \frac{N_{Rx}}{N_{TX}} \qquad (4)$$

The availability (a_i) depends on the number of lost frames for any observation period (t_{Oi}) and can be calculated as in the following equation (5):

$$a_i(t_O) = \frac{\Delta N_{Rxi}}{\Delta N_{TXi}} = 1 - \frac{\Delta N_{PLi} t_{TI}}{\Delta N_{TXi} t_{TI}} = 1 - \Delta N_{PLi} \frac{t_{TI}}{\Delta t_{oi}} \qquad (5)$$

The ration between transmission interval (t_{TI}) and observation period (t_O) according to equation (5) is particularly important. If the observation period approaches the transmission interval, the number of single lost packets has a much greater effect on availability. But in the opposite direction the influence of lost packets at availability can't recognise with longer observation periods.

5. TEST ARCHITECTURE

5.1 System under test

The system under test (SUT) consists of two devices under test. The devices under test (DUT) are on-board units (OBU) MK5 from Cohda Wireless (see Fig. 3).

Fig. 3: DUT: On-board Unit MK5

The frequency band for intelligent transport systems (ITS) range from 5.875 GHz to 5.905 GHz (ITS-G5). The ITS-G5B frequency band is specified for ITS non-safety road traffic applications and the ITS-G5A frequency band is specified for ITS road traffic safety applications and it is only allowed to be used by ITS-G5 compliant stations [10], [11].

Tab. 1: ITS channel allocation

ITS Frequency Band	Channel type	Centre frequency [MHz]	IEEE channel number	E.I.R.P. limit [dBm]
ITS-G5B	G5-SCH4	5860	172	0
	G5-SCH3	5870	174	23
ITS-G5A	G5-SCH1	5880	176	33
	G5-SCH2	5890	178	23
	G5-CCH	5900	180	33

The SUT use the service channels G5SC1, which is dedicated for ITS road traffic safety applications and allow an equivalent isotropically radiated power (E.I.R.P.) of 33 dBm. Detail of ITS channel allocation can be found Tab. 1. The basic topology of SUT is a point to point topology with two end points. Two physical links are established between the end points, because the DUT use a 2x2 MIMO. The DUT hardware interfaces, RS232 and Ethernet, are considered as reference interface and all determined characteristic parameters a valid according to the used reference interfaces.

5.2 Measurement Setup

The test architecture and measurement setup is depicted in Fig. 4. All testing shall be conducted in a reproducible, shielded area. Therefore the DUT's are placed in a radio frequency (RF) shielded box and the RF signal is connected via coaxial cable. The radio transmission channel is emulated by a channel emulator and the physical endpoints (PEP_C, PEP_P) of DUT's are connected with this channel emulator. The type of test application depends on the reference interface. An Ethernet quality analyser is used for the measurement of time and error characteristics at the reference interface Ethernet. Therefore the Ethernet quality analyser analyses the Ethernet traffic simultaneously at the reference interface at producer and consumer site. The test data traffic is generated by a PC. A different test application is used for the reference interface RS232. The test data traffic is generated by an embedded device with RS232 interface. The time and error characteristics are measured via a software application within the DUT's. For this purpose the GPS signal is used for time synchronisation between DUT's. But for measurement on the reference interface RS232 only the wireless communication is considered. The serial communication from the embedded device to the DUT is neglected in assessing the SUT. The measured values of characteristic parameters are transferred via Ethernet to a PC and saved in a result file.

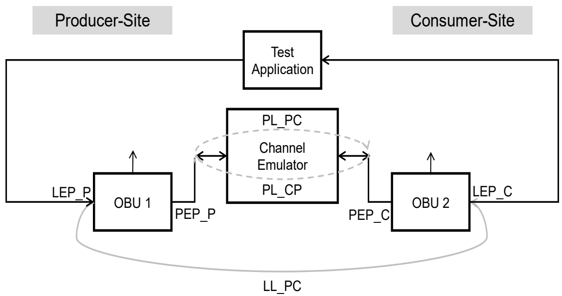

Fig. 4: Measurement setup

The channel emulator emulates the radio transmission channel for a static and an application-related scenario. The static scenario considers a fixed attenuation without moving effects between the DUT's. The application-related scenario considers two cars, each with an OBU. The cars go straight on a street until a crossing with traffic light. The cars must reduce speed and stop in front of a red traffic light for a period of 10 s. Thereafter both cars accelerate and the same procedure takes place in reverse order. The application-related scenario is designated as movement scenario below.

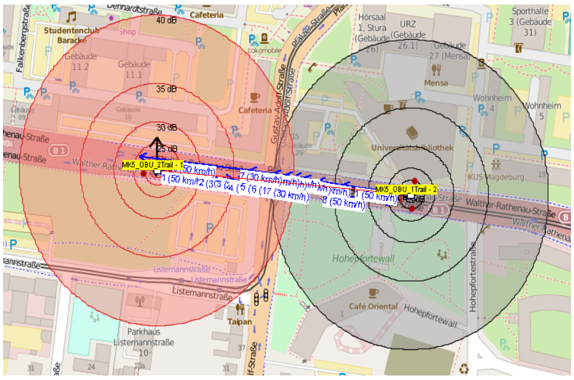

Fig. 5: Measurement setup 2

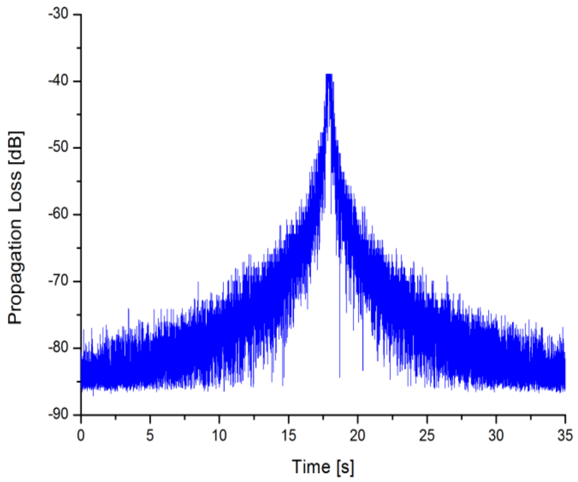

Fig. 6: Propagation loss

The propagation loss between the DUT's (OBU's) is depicted in Fig. 6. The statistical model for the effects of real propagation environment is emulated with a Rician distribution, as we are assuming that the dominant path is available between the two DUT's.

6. MEASURMENT RESULTS

To assess the time behaviour of a wireless systems for ITS, the well-known statistical parameters for extreme values (e.g. minimum and maximum value), the most commonly occurring value (e.g. Mode) and other values for the measures of location (e.g. Percentile 95% or 99 %) can be used. The maximum value is not qualified for assessment, since it is a single value of a series of measurements and it is not sure that the real maximum value is captured. An infinite measurement of the transmission time would be necessary or an inference to a larger population using methods of interferential statistics. However, the maximum value is considered so far as it influences the percentile value.

The results of transmission time measurements for reference interface Ethernet are depicted in Fig. 7 and Fig. 8.

Tab. 2: Statistical parameters for measurement results with reference interface Ethernet

Scenario	Transmission Time [ms]				PLR [%]
	Min	P95	P99	Max	
Static	2,2	4,4	6,3	25,5	0,0
Movement	2,2	4,1	6,0	60,8	4,4

Tab. 2 lists the statistical parameters for the measurement results with the reference interface Ethernet for the scenario static and movement. There is a minor difference between the measurement results of transmission time in scenario static and movement. But, the number of lost packets is growing for scenario movement. The reason for the lost packets is the random signal attenuation at the maximum distance between the SUT transceiver and receiver. If the constellation is particularly disadvantageous, the link budget (signal level above receiver sensitivity) is too small and packets can`t be received.

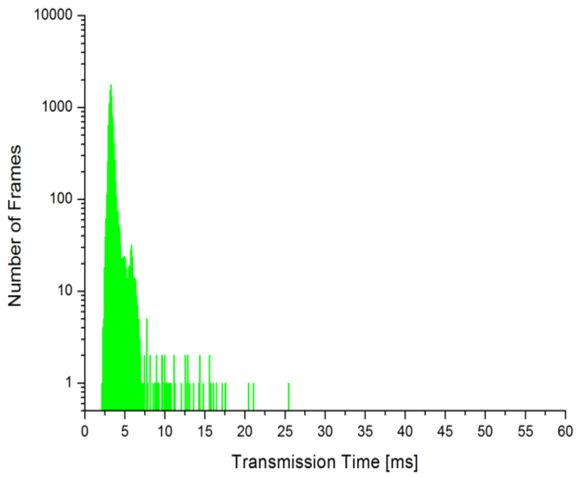

Fig. 7: Static scenario, Reference Interface: Ethernet

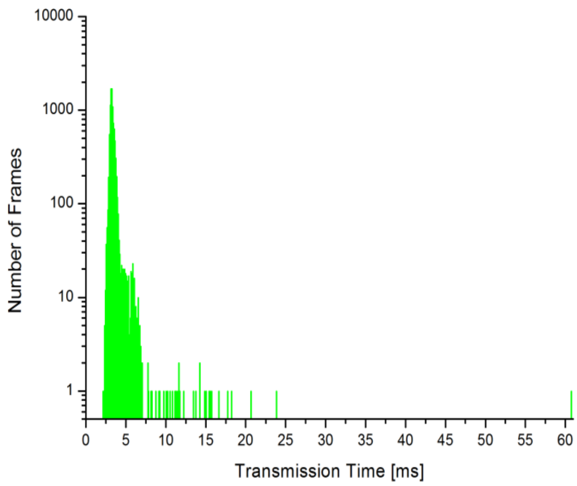

Fig. 8: Moving scenario, Reference Interface: Ethernet

Tab. 3 lists the statistical parameters for the measurement results with the reference interface RS232. There is also a minor difference between the test results of transmission time in scenario static and movement. The number of lost packets of scenario static with reference interface RS232 is with 5.5 % lost packets relative high in contrast to the measurement results with reference interface Ethernet. The number of lost packets is doubling for scenario movement. The reason for the high number of lost packets of scenario movement is once again the random signal attenuation at a maximum distance between DUT transceiver and receiver. The reason for the lost packets of test case static was not clarified.

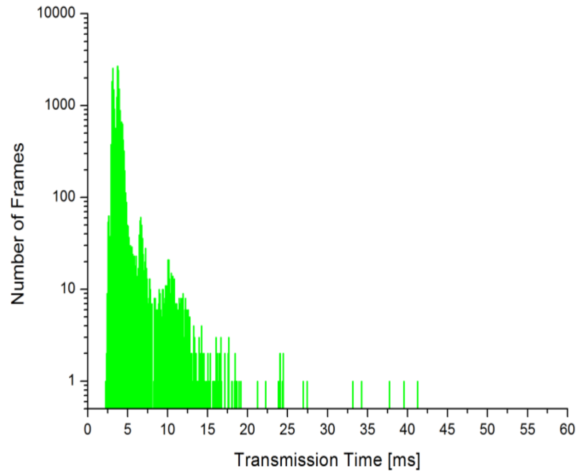

Figure 9: Static scenario, Reference Interface: Ethernet

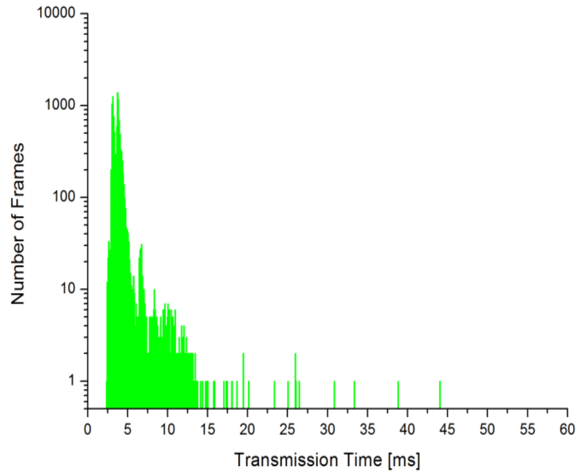

Fig. 10: Static scenario, Reference Interface: Ethernet

Tab. 3: Statistical parameters for measurement results with reference interface RS232

Scenario	Transmission Time [ms]				PLR [%]
	Min	P95	P99	Max	
Static	2,3	5,4	10,8	41,3	5,5
Movement	2,4	5,1	10,2	44,0	10,9

The results of transmission time measurements for reference interface RS232 are depicted in Figure 9 and Fig. 10.

7. CONCLUSIONS

In the paper we presented a proposal on how to assess the time and error behaviour of wireless solutions for intelligent transport systems. A fundamental requirement for such a method is the focus on the application. That is why characteristic values such as transmission time and packet loss are used in the way defined in this paper. It was pointed out that these parameters are random variables, which means that the statistical parameters have to be considered. The approach can be used for analytical studies, simulations and tests.

Furthermore the results can be used for the assessment of wireless systems from the point of view of vehicle to vehicle communication for time critical localisation applications. The measurement results can help to estimate the usage of the considered wireless communication system for high-accurate position applications. The random time behaviour with lost packets errors must be considered in the design of localisation algorithms.

8. Acknowledgement

The results presented in this paper were developed as part of a study commissioned by Audi AG. The authors would like to thank AUDI AG for supporting their research.

9. REFERENCES

[1] J. Huang and H. S. Tan, “Error Analysis and Performance Evaluation of a Future-Trajectory-Based Cooperative Collision Warning System,” IEEE Trans. Intell. Transp. Syst., vol. 10, no. 1, pp. 175–180, Mar. 2009.

[2] S. Shladover and S.-K. Tan, “Analysis of Vehicle Positioning Accuracy Requirements for Communication-Based Cooperative Collision Warning,” J. Intell. Transp. Syst. Technol. Plan. Oper., vol. 10, no. 3, pp. 131–140, Sep. 2006.

[3] J. G. Grimes, “Global Positioning System - Standard Positioning Service - Performance Standard,” 2008.

[4] P. Misra and P. Enge, Global Positioning System: Signals, Measurements, and Performance. Lincoln, Mass: Ganga-Jamuna Press, 2010.

[5] K. Ansari, C. Wang, L. Wang, and Y. Feng, “Vehicle-to-Vehicle Real-Time Relative Positioning Using 5.9 GHz DSRC Media,” in Vehicular Technology Conference (VTC Fall), 2013 IEEE 78th, 2013, pp. 1–7.

[6] N. Alam, A. Tabatabaei Balaei, and A. G. Dempster, “Relative Positioning Enhancement in VANETs: A Tight Integration Approach,” IEEE Trans. Intell. Transp. Syst., vol. 14, no. 1, pp. 47–55, Mar. 2013.

[7] W. Travis and D. M. Bevly, “Trajectory duplication using relative position information for automated ground vehicle convoys,” in Position, Location and Navigation Symposium, 2008 IEEE/ION, 2008, pp. 1022–1032.

[8] VDI/VDE 4000 (1998). General guide to the VDI-Handbook reliability engineering. VDI 4001 Blatt 1, The Association of German Engineers (VDI)

[9] VDI/VDE 2185 (2007). Radio based communication in industrial automation. VDI/VDE 2185, The Association of German Engineers (VDI)

[10] ETSI EN 302 571 (V1.1.1): "Intelligent Transport Systems (ITS); Radio communication equipment operating in the 5 855 MHz to 5 925 MHz frequency band; Harmonized EN covering the essential requirements of article 3.2 of the R&TTE Directive".

[11] ETSI EN 302 663 (V1.2.0): Intelligent Transport Systems (ITS); Access layer specification for Intelligent Transport Systems operating in the 5 GHz frequency band

DOI 10.5162/etc2016/1.4

Testing GNSS Receivers Robustness Against Spoofing Attempts

L. Perdue[1], G. Boime[2], H. Sasaki[1], E. Sicsik-Paré[2]
[1] Spectracom Corp., 1565 Jefferson Road, Rochester 14623 NY, USA,
lisa.perdue@spectracom.orolia.com
hiro.sasaki@spectracom.orolia.com
[2] Spectracom SAS, 3 avenue du Canada 91974 Les Ulis FRANCE,
gilles.boime@spectracom.orolia.com
emmanuel.sicsik-pare@spectracom.orolia.com

Abstract:
Spoofing as it applies to GNSS/GPS is an attempt to deceive the GNSS/GPS receiver by broadcasting signals that the receiver will use instead of the live sky signals. A test system for spoofing allows testing the three major factors to consider in a spoofing attack, time synchronization to the signals to be spoofed, power level of the spoofing signal compared to the live sky signals, and accuracy of the position obtained by the spoofing signal to that of the actual position of the device being spoofed.
Receivers can provide some indications that something out of the ordinary is happening during a spoofing attack. But if the system the receiver is integrated into does not monitor or attempt to use these indications, it is difficult to identify a spoofing attack. Understanding how a receiver will respond in a spoofing attack is the key to detecting spoofing. For example, using multiple GNSS systems will prevent a spoofing attack consisting of only GPS. This is only true if the receiver is set up to monitor this type of information.
The spoofing test system allows full control over key parameters in a completely closed system that will not interfere with actual GNSS signals. Each of these variables is described in detail and a sample of three popular, widely-used GNSS receivers test presented. Test results include variations of time, power, and position. Tests are performed using GPS only and also a combination of GPS and GLONASS systems to understand if multi-GNSS is an effective method to overcome spoofing attacks. Using a spoofing test system will allow a user to better understand the GNSS receiver behavior and harden the system against spoofing attacks.

Key words: GNSS, Positioning, Spoofing, Hardening, Simulation.

1. Introduction

Spoofing as it applies to GNSS/GPS is an attempt to deceive the GNSS/GPS receiver by broadcasting signals that the receiver will use instead of the live sky signals. Spoofing is different than jamming. Jamming is easier for a receiver to detect, and while it can disrupt the receiver, it cannot re-locate it. A spoofing system can be used as an attack on systems that use GNSS for precise timing or navigation. A spoofing system can also be used for defensive research. Research ongoing in the defense area on spoofing can be used to control an unmanned autonomous vehicle and re-direct it. A spoofing test system can be used to understand how the receiver reacts in a spoofing situation and monitor and react to prevent the spoofing from occurring. This paper describes the spoofing test system and how it is used to test receivers. Understanding the behavior of the receiver when faced with a spoofing attack is key to hardening the receiver against spoofing attacks.

2. Spoofing Test System

A spoofing test system can have two different configurations. The first configuration is a live sky antenna used with one simulator and one synchronization system. The simulator is used to spoofing the live sky signals in a controlled environment but this test system gets very complicated quickly. It is hard to determine power levels and difficult to track a moving vehicle. The second configuration is a full laboratory test system and consists of two simulators and one synchronization system. One simulator acts as the live sky signal and

DOI 10.5162/etc2016/1.4

the other as the spoofer. It provides full control over time synchronization, power levels, and both positions. Using two Spectracom GSG units and a Spectracom SecureSync is the preferred method to understand the receiver in order to harden against spoofing attacks.

The test system used for the testing in this paper consists of two Spectracom GSG simulators, one Spectracom SecureSync, an RF switch, and an RF combiner. A PC is used to control the individual units, the RF switch and to monitor the receiver under test. Figure 1 illustrates this test system.

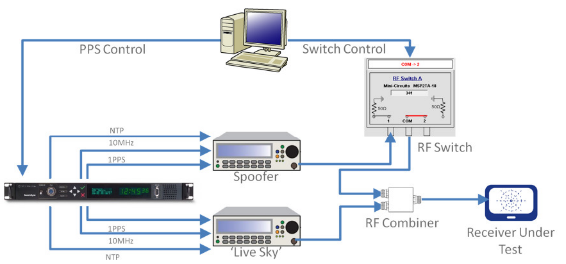

Fig.1.Spoofing test system.

3. Parameters

There are several parameters that can be varied to help understand how vulnerable a specific receiver is to the spoofing threat. Each of these parameters can be varied independently of the other parameters allowing design of a comprehensive test plan. These parameters are Time, Position, and Power level. Figure 2 shows these parameters.

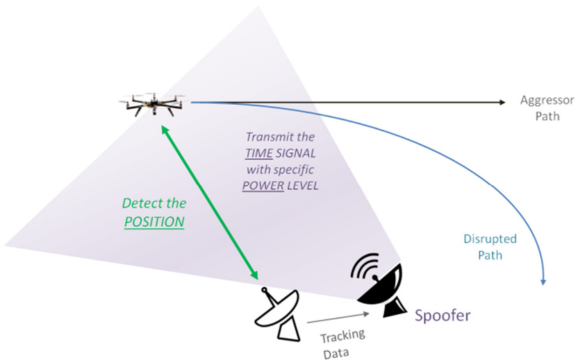

Fig. 2 Important Parameters.

3.1 Time

The timing accuracy of the spoofing signals to the live signals. Utilizing separate outputs from the SecureSync clock system, the PPS offset can be varied. These PPS signals are used as triggers to the GSG Simulator units and therefore cause an offset in time between the two RF signals. This offset is controllable to the nanosecond level.

Another time to consider in the test design is the capture time. This is how long the spoofing signal is applied before attempting to re-direct the receiver. Figure 3 shows the interface in the SecureSync for applying the offset.

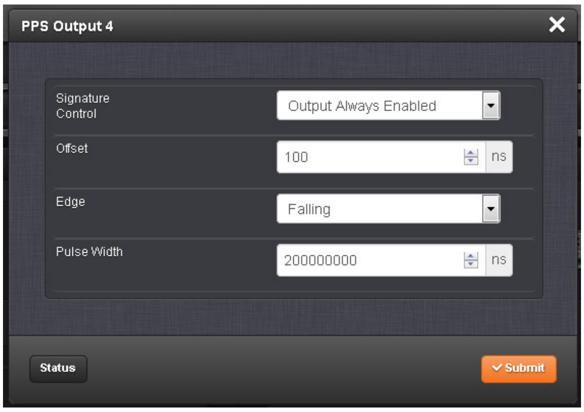

Fig. 3 SecureSync PPS Offset Interface.

3.2 Position

The position provided by the spoofer must be accurate to that of the receiver to be spoofed. Exactly how close the spoofer must be to the receiver position is a variable parameter and can be different based on receiver settings, receiver manufacturer, and initial conditions (moving vs. stationary). Using two simulators allows full control of the two positions so many different test cases can be designed and executed to understand the receiver limitations. The more accurate the spoofer must be to successfully take control of the receiver, the more difficult it will be for an attacker to spoof the receiver. Figure 4 shows an example of the two different positions with a 500m offset.

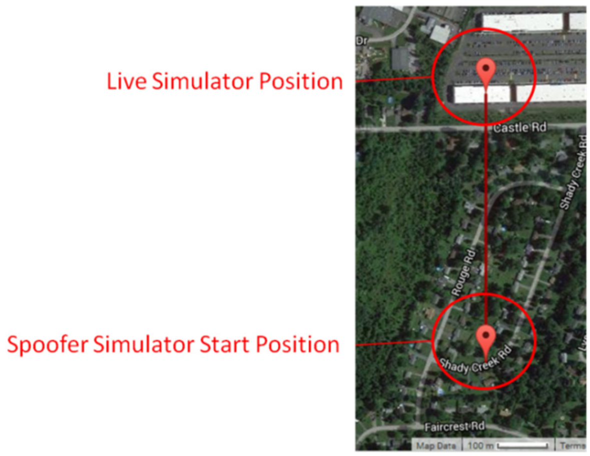

Fig. 4 500m Position Offset.

3.3 Power

The spoofing signal should be greater than the live signal in order to capture the receiver. The

DOI 10.5162/etc2016/1.4

spoofing test system allows full control of the power levels to determine how much greater the power should be. Too much power will jam the receiver. The test system allows testing of the receiver to try and determine if there are any indicators given by the receiver when a signal only a few dB higher than the transmitted signal is received.

4. Test Cases

Several test cases were designed to observe the effects of varying the critical parameters and attempting to spoof the receiver.

Four TIME offset test cases were created. For these cases the position offset was 0 meters and the power level of the spoofer was 2dB higher than the live sky simulator. Offsets of 1 nanosecond, 100 nanoseconds, 500 nanoseconds, and 1.5 microseconds were tested.

Three POSITION offset test cases were created. For these test cases the time offset was set to 1 nanosecond and the power level of the spoofer was 2dB higher than the live sky simulator. Offsets of 50 meters, 250 meters, and 500 meters were tested.

Three POWER offset test cases were created. For these test cases the time offset was set to 1 nanosecond and the position offset is set to 0 meters. Offsets of 2dB, 1dB, and 0dB were tested.

Finally there was a test created for multi-GNSS. In this case the live sky simulator was set to simulate GPS and GLONASS. The spoofer was set to GPS-only. The position offset was set to 0 meters, the time offset was set to 1 nanosecond, and the power level of the spoofer was 2dB higher than the live sky simulator.

Figure 5 summarizes the test cases.

Fig. 5 Test Cases.

5. Test Implementation

The test set up was configured to execute the following sequence:

- **T=0 Start Automated Test Scenario**
  - Live Sky Only (static position)
  - Spoofer is not switched in
- **∆T=3min Enable Spoofer**
  - Combine Live Sky with the Spoofer set to the starting position
  - Spoofer is automatically switched in
- **∆T=5sec Initiate Spoofer Trajectory**
  - Spoofer position begins to change via GSG Simulator predefined scenario:
    - 90 degree heading; 10m/s speed
    - Allows a 5 second capture time
- **∆T=30sec and ∆T=60sec Automated Data Measurement**
  - Results from receiver's reported position are logged for analysis

Using this sequence tests can be performed in a repeatable and consistent manner, helping to understand the receiver and how its performance is affected when a spoofing attack is attempted.

6. Test Results

Three receivers were used to perform the test cases.

- Septentrio AsteRx3 OEM Receiver (R1)
- Ublox NEO-M8N (R2)
- Inventek USB-GPS / SiRFstarIII (R3)

It is important to note that receiver should perform a cold start at the beginning of each test sequence to maintain consistent behavior from test to test. Otherwise recently accumulated data and position/time solutions will influence the dynamic response of the navigation solution.

The test results can be analyzed by comparing the logged positions from the receiver at 30 seconds and 60 seconds after the movement has started. The results summary for 2D position is shown in Table 1. Each case is categorized as not spoofed, partially spoofed, or fully spoofed. Not spoofed (No) means the position did not changed from the live sky position. Partially spoofed (P) means the position was changed but was not that of the live sky simulator or the spoofer. Fully spoofed (Yes) means the receiver position was that of the spoofer. N/A indicates mode not available in the receiver.

We can see R1 and R2 receivers are more robust to spoofing signals since they request a lower positioning and time offset error to be captured by the fake signal.

Full test results are given in Appendix A. At 30 seconds the spoofer 2D position is 300 meters away from the live sky position. At 60 seconds, it is 600 meters away. The altitude of live sky and spoofer position remains the same, so any deviation from 0m is due to the spoofing signals.

Tab. 1: Test Results Summary

		R1	R2	R3
TIME	1ns	Yes	Yes	Yes
	100ns	Yes	Yes	Yes
	500ns	P	P	Yes
	1.5us	No	No	No
POSITION	50m	Yes	Yes	Yes
	250m	Yes	P	P
	500m	P	P	P
POWER	2dB	Yes	Yes	Yes
	1dB	Yes	Yes	P
	0dB	P	No	P
MULTI-GNSS	Multi-GNSS with GPS Spoof	No	No	N/A

7. Conclusion

The Spoofing Test System allows for better characterization through systematic repeatable tests of receiver performance in the presence of a spoofer. By monitoring the available parameters given by the receiver it may be possible to identify and even overcome a spoofing attack. Monitoring loss of lock, receiver noise, IMU system, and estimated position error are possible parameters to observe but each receiver may report different indications. Receivers may also have different modes of operation to test and observe the results.

Observed results provide insight into how different receivers respond to the same threat. More test cases can be created and performed using the features of the spoofing test system in order to fully characterize a receiver and how it responds to a spoofing attack.

Biographies

Lisa Perdue is an applications engineer at Spectracom and a specialist in GNSS simulation. She has more than 15 years of navigation and RF systems experience, including 10 years of US Naval Service.

Gilles Boime is Chief Scientist at Spectracom. He has more than 34 years of signal intelligence and GNSS signal management experience. He is leading technology advisory and partnership for Spectracom. He contributes to the early standardization activities for Galileo European GNSS. He holds an engineer graduate from Institut Supérieur d'Electronique de Paris with Telecommunication option.

Hironori Sasaki – Director of Solutions Architecture at Spectracom. Hiro has over 11 years of experience designing, selling and implementing communication systems for Government and Military organizations around the World. Hiro joined Spectracom in 2014 with a focus on leading the organization in expanding the system solutions and program business. Hiro holds a BS in Computer and Systems Engineering from Rensselaer Polytechnic Institute and an MBA from the University of Rochester's NY Simon School of Business.

Emmanuel Sicsik-Pare is Strategic Product Manager at Spectracom. Following a first position in radar / optronics program management in French Ministry of Defense, Emmanuel held various positions in Spectracom, focusing on new products and solutions in the Positionning, Navigation and Timing domain. Emmanuel holds a MSc in Telecommunications from Telecom Bretagne.

References

B. Parkinson, J. Spilker, GPS Theory and Applications, *American Institute of Aeronautics and Astronautics*

E. Kaplan, C. Hegarty, Understanding GPS: Principles and Applications, *Artech House*

P. Misra, P. Enge, Global Positionning System: Signals, Measurements and Performance, *Ganga-Jamuna Press*

F. Dovis, GNSS Interference Threats and Countermeasures, *Artech House*

T. Humphreys and Allied, Assessing the Spoofing Threat: Development of a Portable GPS Civilian Spoofer, *Proceedings of the 21st International Technical Meeting of the Satellite Division of The Institute of Navigation (ION GNSS 2008)*, Savannah, GA, September 2008, pp. 2314-2325

H. Kuusniemi, Effects of GNSS Jammer and Potential Mitigation Approaches, *UN/Latvia Workshop on the Applications of GNSS 2012*

Annex A: Test Results

Time Offset Results

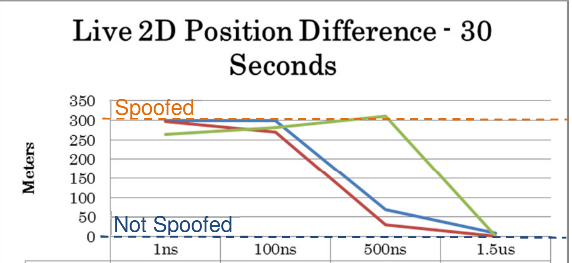

	1ns	100ns	500ns	1.5us
R1/30	299,8	299,8	70	8,2
R2/30	297,8	269,4	30,9	0,9
R3/30	263,1	280,6	310,3	0,6

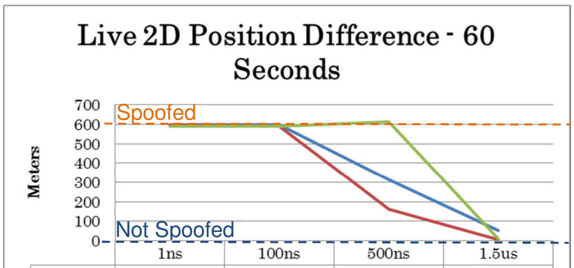

	1ns	100ns	500ns	1.5us
R1/60	597,1	598,5	314,7	50,6
R2/60	599,2	590	160,5	5,6
R3/60	588,8	591,8	613,9	10,7

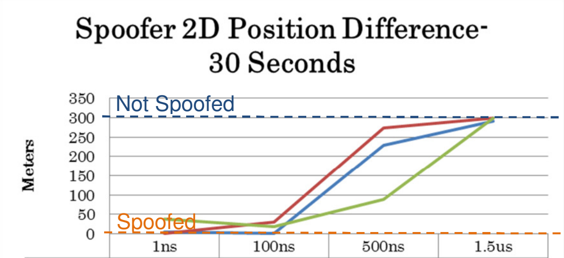

	1ns	100ns	500ns	1.5us
R1/30	5,7	1,2	228,7	291
R2/30	1,9	29,7	272,8	299,6
R3/30	37,1	18,6	88,5	298,9

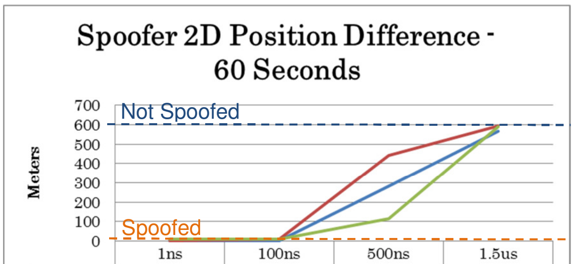

	1ns	100ns	500ns	1.5us
R1/60	1,6	0,4	284,2	568,1
R2/60	1	8,8	441	593,4
R3/60	11,1	9,1	115,2	588,6

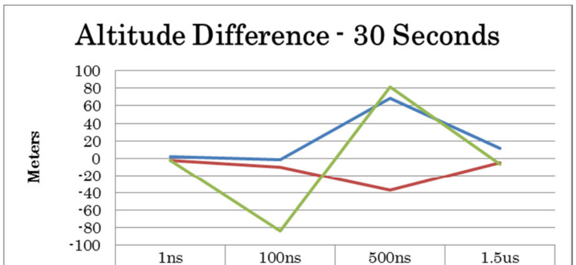

	1ns	100ns	500ns	1.5us
R1/30	1,57	-1,09	68,21	11,72
R2/30	-2,5	-9,789	-36,6	-4,7
R3/30	-2,4	-83,9	81,2	-7

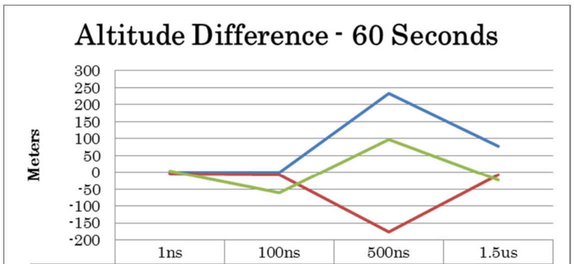

	1ns	100ns	500ns	1.5us
R1/60	-0,42	-0,02	232,3	76,1
R2/60	-4,3	-8,354	-177,3	-7,557
R3/60	4,5	-60,5	97,6	-23,6

Position Offset Results

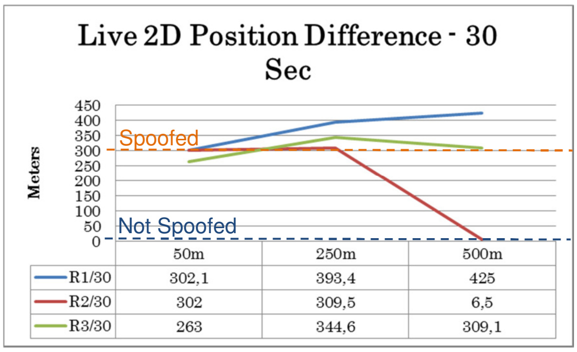

	50m	250m	500m
R1/30	302,1	393,4	425
R2/30	302	309,5	6,5
R3/30	263	344,6	309,1

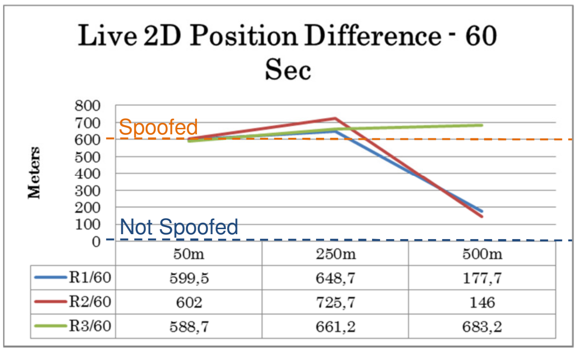

	50m	250m	500m
R1/60	599,5	648,7	177,7
R2/60	602	725,7	146
R3/60	588,7	661,2	683,2

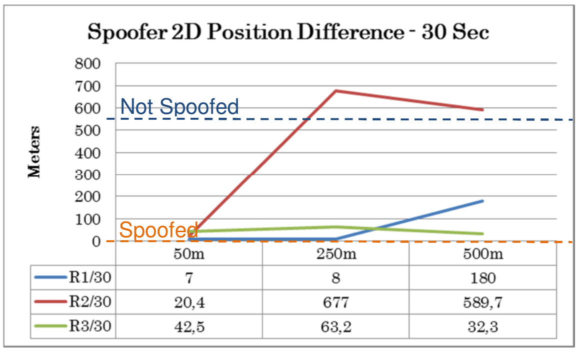

	50m	250m	500m
R1/30	7	8	180
R2/30	20,4	677	589,7
R3/30	42,5	63,2	32,3

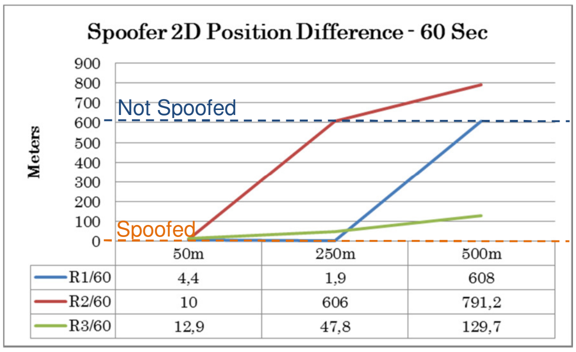

	50m	250m	500m
R1/60	4,4	1,9	608
R2/60	10	606	791,2
R3/60	12,9	47,8	129,7

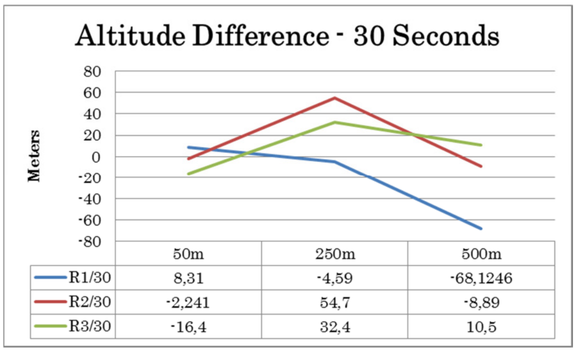

	50m	250m	500m
R1/30	8,31	-4,59	-68,1246
R2/30	-2,241	54,7	-8,89
R3/30	-16,4	32,4	10,5

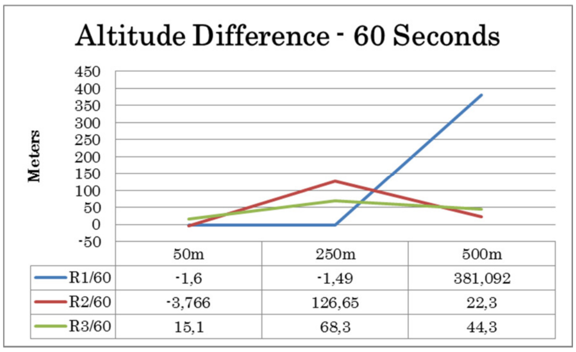

	50m	250m	500m
R1/60	-1,6	-1,49	381,092
R2/60	-3,766	126,65	22,3
R3/60	15,1	68,3	44,3

DOI 10.5162/etc2016/1.4

Power Offset Results

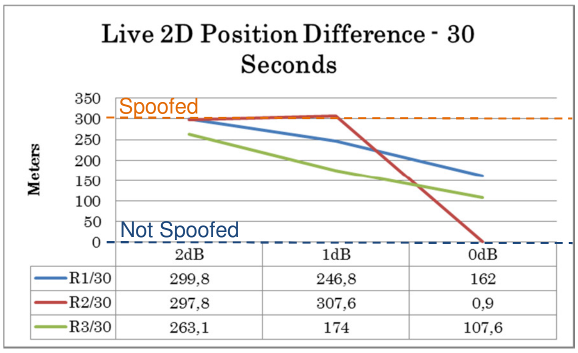

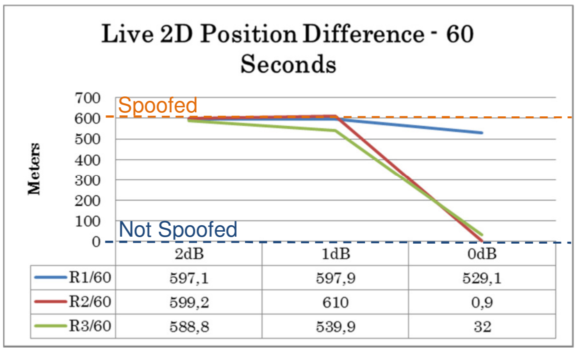

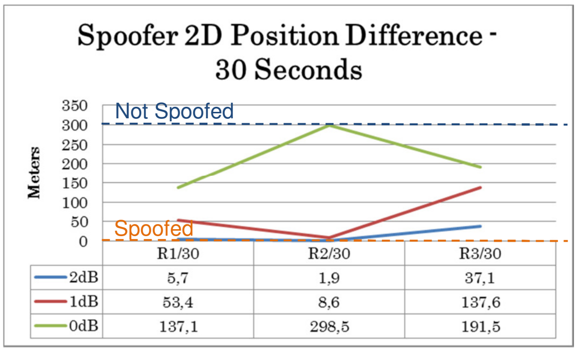

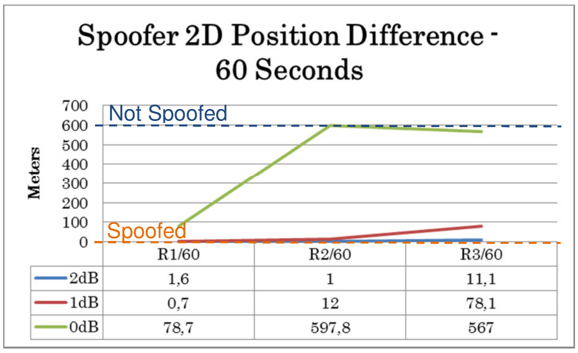

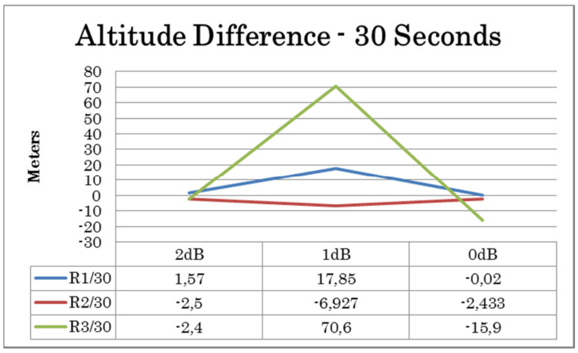

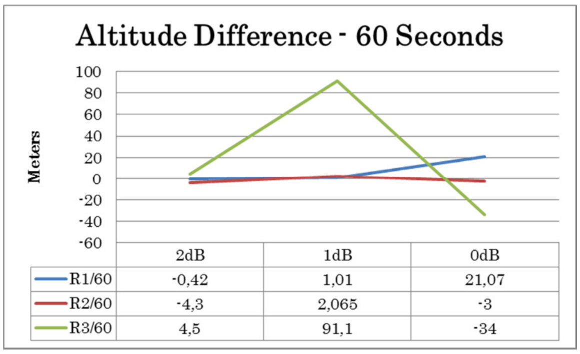

DOI 10.5162/etc2016/1.5

Testing Telemetry Systems, which use GNSS Satellite Navigation Systems

Achieving Reliable and accurate Results with RF Simulation of GNSS Signals

Karen von Hünerbein[1], *Werner Lange*[2]
Lange-Electronic GmbH
Rudolf-Diesel-Str. 29 a
D-82216 Gernlinden
kvhuenerbein@lange-electronic.de

Abstract Text:

Positioning, timing and navigation (PNT) with Satellite Navigation Systems like GPS, GLONASS, Beidou and Galileo are more and more widespread and used in very different types of applications including core telemetry applications. Global Navigation Satellite Systems (GNSS) receivers in Safety Critical Applications such as landing airplanes, Critical Infrastructure or Remote Sensing missions e.g. Earth Observing Satellites need to be very robust and reliable under a variety of environmental conditions, sometimes very harsh ones outside the atmosphere. Timing is critical in communication between satellite ground stations and the satellites, e.g. telemetry tracking and command, or communication protocols using Time Division Multiple Access.

Thus, it is crucial to test GNSS receivers thoroughly under a variety of different conditions, also extreme conditions like very high dynamics or unhealthy GNSS satellites.

For this purpose GNSS RF signal simulators are a versatile and flexible tool. The tests can be repeated as many times as necessary with identical conditions. Besides this a simulator offers complete control across the scenario, every single detail can be controlled and changed. In RF simulators comprehensive error models are available for satellite signals and clocks, satellite orbits and health flags, obscuration and multipath, atmospheric conditions, antenna characteristics, vehicle dynamics, leap seconds, jamming and aiding Inertial sensors. Each of them can be controlled individually. For some tests, like unhealthy satellites or future constellations RF, simulators are the only way for testing, as future signals, for example, are not available in live sky test.

In this paper, we will introduce the capabilities of GNSS simulators with a wide range of different error conditions and show several telemetry use cases.

Key words: GNSS RF simulation, timing, telemetry systems, GNSS system errors, GNSS vulnerabilities

Introduction:

GPS has revolutionized accurate worldwide 3D positioning, navigation and timing during the last 20 years and more global satellite navigation systems (GNSS) and satellite based augmentation systems (SBAS) are being developed continuously, like IRNSS (Indian Regional Navigation Satellite System) and SDCM (System for Differential Corrections and Monitoring, the Russian SBAS) [1]. GPS is used in thousands of applications worldwide, among them many telemetry systems transmitting GPS data remotely.

Telemetry applications of GPS / GNSS are for example:

- Earth observation satellites with GPS timing and attitude control
- computer terminals in banking with GPS timing
- Galileo pseudolite synchronization with GPS timing
- tele communication base stations with GPS timing

- Communication between satellite and ground station via TDMA (Time Division Multiple Access)
- power grids with GPS timing
- precision approach of a tanker vessel to an oil platform exchanging GPS position information
- automatic broadcasting of GPS positions, velocity and altitude by aircraft (ADS-B Automatic Dependent Surveillance Broadcast) to improve air traffic control
- automatic broadcasting of GPS/GNSS positions by ships (AIS – Automatic Identification System) to avoid collision in narrow sea straits,
- fleet management of trucks,
- emergency beacons for people, boats, e.g. (GPS enabled EPIRBS Emergency Position Indicating Radio Beacon), and cars (European e-call system),
- tracking of birds, e.g. white storks in Eastern Germany, re-broadcasting of GPS positions via the ARGOS satellite system for migration research

  only to name a few.

GNSS and telemetry applications

On the one hand, GPS is a telemetry and tele-command system (TT&C) in its own right, since remote signals from satellites more than 20.000 km away enable calculation of accurate positions, velocity and time, anywhere on or above the surface of the Earth. GPS space vehicles are controlled and maintained with telecommands and receive navigation messages uploads by the ground segment. This is true for all GNSS.

On the other hand, there is an ever increasing number of GPS/GNSS application in telemetry. GPS time serves in many ways to synchronize transmission and communication, between remotely located transmitter stations and mobile phone base stations.

In the aviation GATE, the Galileo Testbed around the research airport of Braunschweig, the transmitter stations, acting as Galileo pseudolites, are located in an inner ring of five pseudolites around the runways and an outer ring of 4 pseudolites with distances up to 50 km from the airport, and up to 100 km diameter. Each transmitter station is equipped with a GPS timing receiver. The transmitter stations of the outer ring are connected to a central control server via VPN, WiFi and the internet, the stations of the inner ring have an additional connection via Ethernet. In this setup, the GPS timing receivers manage to synchronize the transmitted Galileo signals to an accuracy of better than 1.5 nsec [2].

GPS based timing is also crucial for base-stations with coordinated transmissions of radio and television programs and mobile phone calls. They depend on precise timing, because they are using Time Division Multiple Access (TDMA), which allows several users to use the same channel, each with a different time slot. Time slots are 0.577 msec long and need to be timed precisely, or else they will interfere with each other [3]. This also applies to all other communication systems using TDMA, e.g. satellite ground control stations communicating with the satellite in orbit.

Generally, GPS and GPS/GLONASS navigation systems are widespread in all sorts of vehicles for positioning and navigation, and more recently also for new safety procedures.

In aviation, the ADS-B Automatic Dependent Surveillance Broadcast is being deployed to improve visibility of airplanes for air-traffic control and other aircrafts. This allows more efficient route planning and situational awareness improving overall safety. The ADS-B onboard unit determines the position, altitude and velocity of the airplane with GPS/GNSS and broadcasts the airplane data and identification via radio transmission. ADS-B becomes mandatory in Australia this year [5]. The ground infrastructure was introduced in the USA in 2014 and it is mandatory for all airplanes to carry the necessary on-board equipment by 2020 [6].

For ships, a similar system has been deployed, since 2000, the AIS – Automatic Identification System allows tracking ships, which are obliged to send their GPS position and identification to satellites, in order to help to avoid collision between sea vessels, e.g. ships in the British channel. A second goal is to inform neighbouring countries, which ships are present in their coastal areas. [7]

Low Earth Orbit satellites (LEOs) monitoring the Earth, need precise GPS positions together with other sensors in orbit to correctly geo-reference the image. GNSS data are part of this orthorectification process. [18]

Vulnerability of GPS signals

"GPS and GNSS signals are easy to interfere with, as they transmit very weak signals below the noise floor. The signals can be attenuated, delayed or disrupted by GNSS system errors, atmospheric disturbances, multipath reflections, jamming, which is intentional or unintentional, RF interference and by spoofing, deception signals or other replicate GPS/GNSS signals potentially misleading the GPS/GNSS receiver." [8,10]. The rebroadcast of GPS positions and timing can also be falsified or prevented by cyber attacks. "Until a few years ago, jamming and spoofing have been more of a theoretical problem, with little practical relevance. Recently, more and more evidence of real-life situations of the different types of disruptive factors have been detected." [8,9].

GNSS system errors include operation failure of satellites, orbit errors, timing errors, incorrect orbit data in the navigation message, or unhealthy satellites whose status is not correctly declared in the navigation message. All these events have occurred in real life in the last few years. In April 2014, most satellites of the GLONASS constellation were uploaded with the wrong ephemerides and the whole GLONASS constellation was unusable for more than 10 hours [13].

Why is Multipath a problem? The reflected GPS/GNSS signals take a longer path to the receiver. The receiver needs to decide which signals to use for the position fix, if choosing multipath signals for the calculation, the accuracy of the position calculation is reduced. [10].

In order to identify problems of GPS receivers with these error effects before they occur in the field and in order to solve issues with controlled procedures before a network of base stations fails to operate or before an airplane crashes, verification of GPS/GNSS devices is crucial, with thorough, controlled and repeatable test conditions.

Field tests versus simulation:

Testing equipment in the field with live sky signals is not repeatable, as the satellites move in orbit and the constellation, and thus the signal environment changes constantly.

"Verification of aviation GPS receiver equipment with real live sky signals can be very time consuming and expensive requiring many test flights, when field tests are the primary test method. Field tests are not always possible, for example for unusual vehicle motion or dangerous situations, like a pilot deviating from the route in low visibility conditions and coming close to a mountain slope." [11] .

Field tests are impossible for LEO Earth observation satellites, or any other space vehicle. Earth Observation satellites use GPS as an AOCS sensor (attitude and orbit control system) and for timing relative to UTC: Extensive, thorough testing must be performed on the ground before launch, or else the satellite could become useless in orbit.

"Field tests are not possible for special conditions required by the test standard **DO-229** for aircraft GPS receiver qualification and by the maritime test standard **IEC 61-108-1** for GPS shipborne receiver equipment, which require tests with unhealthy satellites to validate RAIM algorithms. In the field a test engineer, pilot, or seaman cannot call USNO and ask to switch off satellites, set them unhealthy, or corrupt a satellite's navigation data or "simply" set a time error." [11].

Recently in January 2016, a real life timing error has occurred with GPS satellites during decommissioning of SV-23, where several satellites transmitted a UTC timing offset of -13.7 µsec in the navigation message. This was too much for timing receivers in telecommunication base stations in central Europe, which went out of operation due to this error [14]. This is a typical case, where the error conditions can be best tested and repeated with a GNSS signal simulator.

"For aviation, one test in DO-229 prescribes a) an airplane to statically hover in one position 5000 m above the South Atlantic Ocean b) one satellite (out of the 4 satellites used to calculate DOP) to deviate from its orbit by a large distance. Both conditions cannot be met in a field test." [11].

"The number of operational scenarios that can be evaluated in field tests is typically severely limited by time and cost constraints [12]", especially when testing needs to take place in remote locations. When adding GLONASS, Beidou or Galileo "capability to a GPS receiver, receivers need to be revalidated to guarantee functionality under a variety of environmental conditions and to meet strict performance criteria of national and international aviation administrations" [11].

Strengths of RF simulators

The performance of a GPS or a Multi-GNSS navigation system can be evaluated in the laboratory using a GPS/GNSS RF Constellation simulator, such as a Spirent GSS9000 [11]. "These signal generators precisely emulate the RF signals of the navigation satellites as would be received by the device under test at a defined time and location. Simulation offers unlimited repeatability of tests, full control over all relevant error sources, the possibility to test as many locations as needed, without having to move the device under test. Simulation offers the possibility, to limit the number of satellites in view, to switch off one or several satellites, define deviations of a satellite's orbit," introduce pseudorange errors, set one or several satellites unhealthy, set time errors or corrupt satellites' navigation data. [11].

In addition, it is possible to recreate a historic GPS or GLONASS constellation. This allows the user to analyze the influence of past signal environments and identify algorithmic errors in GPS/GNSS equipment, which only occurred once under one specific constellation condition. At the same time, future signals and constellations can be simulated, e.g. a full GALILEO constellation, enabling receiver development ahead of the full operational phase of a GNSS. Both types of tests are only possible with a GNSS RF simulator.

Excellent simulators can be controlled remotely via an API interface by applying a powerful set of remote commands to control virtually all aspects of the test scenarios including antenna patterns, signal power, signal control, navigation data and by providing vehicle motion in real-time from an external source [11]. This, in turn, enables advanced test cases, like complex, realistic multipath generation calculated in real-time with respect to an external 3-D environment by an external software simulation tool, which then switches on the appropriate multipath and Line of Sight signals by sending remote commands to the RF simulator, as described in [15]. The latest high-end simulator supports complex multi-path rich test cases by providing up to 160 channels in one box [16].

Remote control also allows to inject highly dynamic, real-time, realistic aircraft or spacecraft motion into a GNSS RF simulator Hardware in the loop setup via a flight simulator,e.g. X-Plane. [11], where "the user can emulate a drive or a flight in the lab with a simulator as if flying or driving in the real world. At the same time, this flight or driving simulation controls the vehicle motion of the GNSS simulator. The GNSS simulator then adapts the GPS, GLONASS or Galileo signals accordingly to precisely suit the vehicle motion with high fidelity. The main advantages are the ease of use and the very small time delay between the flight (driving) simulator motion and the RF output of the simulation" [11]. Motion models are available for space, air, land vehicles and sea vessels together with static scenarios and simple motion models in the control software of the RF simulator.

Very high dynamics of air and space vehicles can be represented best with the help of a very high Hardware and software simulation update rate, e.g. 1000 Hz in the GSS9000, resulting in real-time remote control and trajectory delivery with very low latency. Signal accuracy is 0.3 mm RMS for pseudorange, in a range of 120,000 m/sec relative velocity, with a very low phase noise. Signal accuracy and signal quality of simulated signals need to be much better than the performance of the device being tested, else the user measurements do not truly reflect the performance of the device under test, but are degraded by the lacking signal quality [16].

Advanced signal generators are capable of simulating all frequencies and signals from all GNSS and regional systems in the L-bands specified in ICDs, thus enabling true Multi-GNSS tests for research and development [16].

DOI 10.5162/etc2016/1.5

Examples of simulator test setups relevant for telemetry applications

GNSS system errors:

The above mentioned timing error in January 2016 can be simulated with a full constellation GPS/GLONASS simulator with a special scenario, where the timing parameters in the navigation message are set to reflect a timing offset of -13 µsec in 15 GPS satellites, which represent about half of the visible satellites at each location. In the navigation message, every single parameter and each bit can be modified individually inside the control software SimGEN. Subsequently these changes appear in the simulated RF.

Low orbits of Galileo:

After two Galileo satellites were launched in a too low orbit in August 2014, "ESA asked Spirent to develop a special extended message algorithm in SimGEN to calculate the minimum useable orbit and determine if the SVs had enough fuel to reach those orbits

After rigorous analysis it was determined the orbit could be reached with an acceptable compromise on performance and operational life." [17]. Thus simulation helped to find a workaround in a difficult situation, where satellites were thought to be unuseable initially [personal communication Stuart Smith].

Jamming Test Setup:

Jamming by Personal Privacy Devices disrupted the operation of a Ground Based Augmentation system at an airport in the US in 2012, when a truck with a jamming device drove by.

Real jamming events can be recreated in the laboratory, by first monitoring the signal environment in the field, for instance with a DETECTOR, and then storing snapshot spectrograms of the interference events. In a third step, these snapshots are converted to test cases, which are simulated by a combination of a GNSS RF simulator and an RF interference generator. The simulator setup consists of a RF GNSS simulator, up to four Vector Signal generators, a combiner unit and the control software SimGEN that controls all the signal sources either in a coherent or a non-coherent way and is adapted to the vehicle motion with relation to the jammer.

Different types of interference can be added: CW, swept CW, stepped CW, pulsed CW, AM, FM, Gaussian Noise and real waveforms, as seen and recorded in the field. Jammer signal power is automatically adapted depending on the distance between the vehicle and the jamming source. Each interference source can operate independently with either fixed or modelled signal power level. The interference generator can be controlled via an interference file, interactively, or via remote commands.

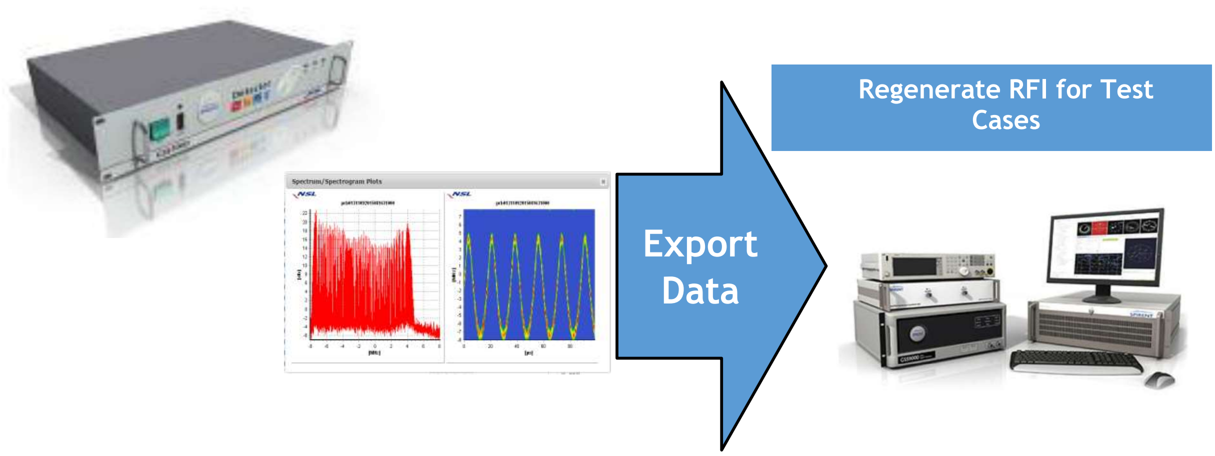

Figure 1 Detector samples jamming snapshots, then they are simulated by an interference simulator

E-call

There are different emergency call systems for land vehicles, e.g. e-call for the European Union and ERA-GLONASS for the Russian Federation, with the aim that an in-vehicle system calls for help automatically in case of an emergency. ERA-GLONASS is already mandatory, e-call is still under development. The In Vehicle System (IVS) for emergency calls for land vehicles consists of several components, mainly one determining the GPS/GNSS position, and a GSM part transmitting the emergency call including the position data to a public safety answering point (PSAP). The GSM communication with the PSAP needs to be tested in addition to the GPS/GLONASS position fix. A complete test solution for verifying the functionality and conformance of the ERA GLONASS system by Spirent consists of an eCall IVS/PSAP simulator, a GPS/GLONASS positioning simulator and a GSM-wireless network emulator.

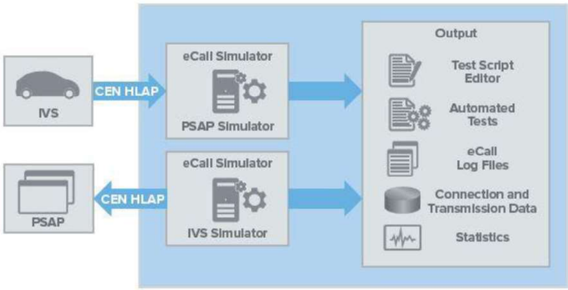

Figure 2 Schematic overview of E-Call Test Setup

This allows testing of the PSAP, the GSM and the GPS/GLONASS simulation, including all officially prescribed test scripts by CEN/ETSI [19].

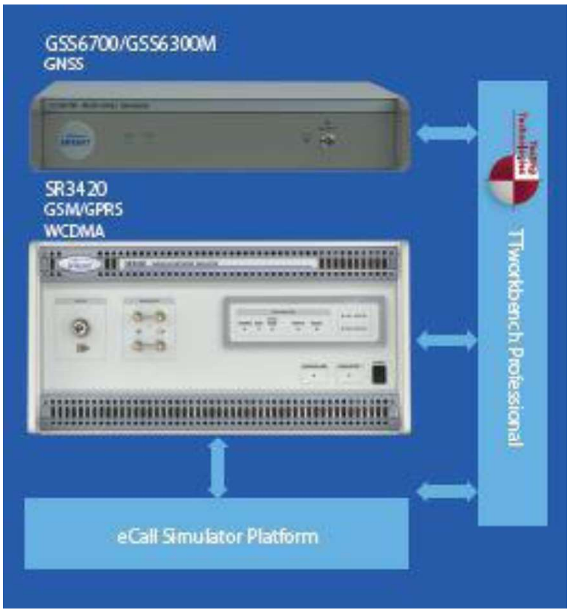

Figure 3 Example of hardware in an E-Call Setup

Accuracy and reliability of Spirent RF signal simulators have been verified in cooperation with major Research Institutions: ESA and DLR [20,21] and have been certified by national authorities of the US, e.g. GPS JPO and GPS Wing and the Russian Federation for GLONASS simulators.

Conclusion:

In this paper, we have shown that the operation of telemetry applications with GPS/GNSS is likely to be compromised by various errors and external events, from time to time. Proper testing is mandatory to improve robustness and continuous, uninterrupted operation.

Simulators allow testing of a wide range of errors, some of which cannot be tested in the field, for example GNSS system errors.

Simulators provide a level of repeatability and control in the lab that are often unattainable in real-world environments. The ability to control test conditions and dynamics repeatedly with ease is extremely effective for system testing and evaluation throughout the system development lifecycle. Using a simulator-based test solution allows fine – tuning and evaluation of navigation algorithms and system performance across a range of operational test scenarios unattainable from field trials [11].

Specialized simulation systems are available for a wide range of applications, covering all major required test cases.

References:

[1] K. Hünerbein,Global Satellite Navigation: new trends, highlights and risks, Conference Proceedings of European Telemetry Conference, Munich, 12th-14th, June, 2012: 370-384.

[2] U. Bestmann, B. von Wulfen, P. Hecker, F. Kneissl, V. Kropp, Aviation Applications: Hybrid Navigation Techniques and Safety-of-Life Requirements Part 2, Inside GNSS, July/August 2010: 62-68.

[3] R. Freeman. Radio System Design for Telecommunication, 2007, 3rd Edition, 524.

[4] K. Hünerbein, Benefits of Multiple GNSS in Aircraft Navigation, Conference Proceedings European Telemetry Conference, Hamburg, 17th-20th May 2010, 361-366.

[5] GPS World, Australia enacts new GNSS requirements for aviation. February 18, 2016, online, http://gpsworld.com/australia-enacts-new-gnss-requirements-for-aviation/

[6] FAA Frequently Asked Questions about ADS-B, online, 2016, https://www.faa.gov/nextgen/programs/adsb/faq/#1

[7] ESA, AIS, 2016, online, http://www.esa.int/Our_Activities/Telecommunications_Integrated_Applications/Satellite_-_Automatic_Identification_System_SAT-AIS

[8] K. Hünerbein, W. Lange, Real Life Evidence for Spoofing and Jamming of GNSS Receivers, Conference Proceedings of CERGAL, 7th-8th July, Darmstadt, Germany, 2015.

[9] A. Rügamer, D. Kowalewski, Jamming and Spoofing of GNSS Signals – An Underestimated Risk?!, 2015, FIG Working Week 2015, From the Wisdom of the Ages to the Challenges of the Modern World, Sofia, Bulgaria, 17-21 May 2015.

[10] Spirent Communications. Fundamentals of GNSS Threats, 2015, White Paper.

[11] K. Hünerbein, W. Lange, User friendly, real time remote control of satellite navigation signal simulation by emulating realistic flight trajectories and driving routes with a standard flight simulator, European Navigation Conference 25th-27th of April 2012, Gdansk, Poland
and European Journal of Navigation, Aug 2012.

[12] N. Fedora, C. Ford, P. Boulton, A Versatile Solution for Testing GPS/Inertial Navigation Systems, Proceedings of the 21st International Technical Meeting of the Satellite Division of The Institute of Navigation, September 16 - 19, 2008, Savannah International Convention Center.

[13] GPS World System News, GLONASS Fumbles forward: Two April Disruptions Furnish Fodder for Multi-GNSS Receivers and Alternative PNT, 2014, GPS World May 2014, 16,17.

[14] GPS World: System of System, Microseconds go Missing in GPS Ground Control Glitch. GPS World March 2016, 12.

[15] K. Hünerbein, G. Moura. A new tool for simulation of geospecific multipath and obscuration of GPS/GNSS signals with relation to realistic 3 D city models, 2014, Conference Proceedings of the European Telemetry Conference, Nürnberg, 3rd-5th June, 2014.

[16] Spirent Communications, Datasheet for GSS9000, 2014

[17] Stuart Smith, Constellation status of GNSS, 2015, Spirent internal presentation.

[18] DLR, Orthorectification, online, http://www.dlr.de/eoc/en/desktopdefault.aspx/tabid-6144/10056_read-20918/

[19] Spirent Communications, Spirent eCall/ERA-GLONASS IVS Test Solution, 2015, Datasheet

[20] P Boulton, R Wong, A Read, Galileo RF Constellation Simulator Design Verification and Testing, 2007, Conference Proceedings of Frequency Control Symposium joint with the European Frequency and Time Forum, Geneva, 29th May – 1st June 2007, 511-516.

[21] A Hornbostel et al, “Simulation of Multi-Element Antenna Systems for Navigation Applications”, IEEE Systems Journal, March 2008, Vol. 2, No. 1, pp. 7-19

DOI 10.5162/etc2016/1.6

Research on the Realization of Passive TDOA in PCM/FM System

DAI Tao XIE Nan FENG Lei WANG Yuan Dong
Institute of Electronic Engineering, China Academy Engineering Physics,
Mian yang, Sichuan, China,daitao8484@163.com

Abstract:
A kind of PCM/FM telemetry system which can realize the passive time difference of arrival (TDOA) position is introduced in this paper. The positioning principle is hyperbolic algorithm based on least squares method, and the method of system time-measurement is a timing synchronization algorithm based on data transformation tracking loop (DTTL). In this paper, the structure and hardware implementation platform of the positioning system are introduced, and the random error of the system is analyzed. In order to improve the positioning accuracy, the pre filtering method is adopted to reduce the random error caused by noise. The test results show that the positioning error is 18 meter when the SNR is 8.5dB and the source rate is 2Mbps.Therefore, this system can realize the precise positioning of the target signal in PCM/FM system.

Key words: TDOA, timing synchronization, cubic interpolation, random error

Introduction

The passive location techniques estimate the geometric position of the target by detecting the characteristic parameters (such as the electric field intensity, propagation time or time difference, incidence angle, etc.) of the signal which transmitted between the source and multiple receiving stations. The time difference of arrival (TDOA) position technology has the advantages of high precision, high stability and low complexity of equipment, and it has become an important method in the field of reentry telemetry. The PCM/FM has been mainly used in the reentry telemetry transmission system. Therefore, it is necessary to study the multi station passive time difference location of PCM/FM system.

The Positioning Principle

TDOA positioning, also known as the hyperbolic positioning, by measuring the time difference between the radio signal to reach the different measurement stations to locate the source of the signal. A hyperbolic surface can be obtained by a time difference, when determining the position of the radiation source in the three-dimensional space, three hyperbolic surfaces are required. This will need four or more stations to measure the arrival time of the signal for the source positioning [1]. The sketch map of multi station time difference location system is shown in Fig. 1.

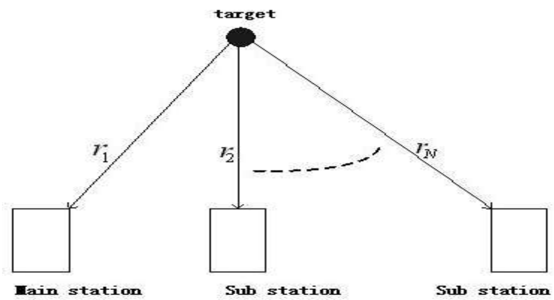

Fig. 1. Sketch map of TDOA

Set the position of the measuring station is

$[x_i\ y_i\ z_i]^T$(i=1,2,…,N), where i=1 means the main station, and the rest are sub stations. Set the position of the target is $[x_T\ y_T\ z_T]^T$. The distance between the target and the stations are r_i, and the distance difference of the target to the main station and the sub stations is r_{1i}.

$$\begin{cases} r_1^2 = (x_T - x_1)^2 + (y_T - y_1)^2 + (z_T - z_1)^2 \\ r_i^2 = (x_T - x_i)^2 + (y_T - y_i)^2 + (z_T - z_i)^2 \\ r_{1i} = r_1 - r_i = ct_{1i} \end{cases} \tag{1}$$

In (1), t_{1i} is the target signal arrival time difference of the main station and sub stations, c is the signal transmission speed.

According to the error transmission principle, differential on the third equation of (1), the estimation error of target location can be obtained as (2).

$$dX = (C^T C)^{-1} C^T [d\Delta R - dX_s] \tag{2}$$

where,

$$c_{ix} = \frac{x_T - x_i}{r_i}, c_{iy} = \frac{y_T - y_i}{r_i}, c_{iz} = \frac{z_T - z_i}{r_i} \tag{3}$$

$$k_i = c_{ix} dx_i + c_{iy} dy_i + c_{iz} dz_i \tag{4}$$

$$C = \begin{bmatrix} c_{2x} - c_{1x} & c_{2y} - c_{1y} & c_{2z} - c_{1z} \\ c_{3x} - c_{1x} & c_{3y} - c_{1y} & c_{3z} - c_{1z} \\ c_{4x} - c_{1x} & c_{4y} - c_{1y} & c_{4z} - c_{1z} \end{bmatrix} \tag{5}$$

It represents the relationship between target location and station location;

$$d\Delta R = [d(\Delta r_{12}), d(\Delta r_{13}), d(\Delta r_{14})] \tag{6}$$

It represents the error introduced by the time difference measurement of each station;

$$dX_s = [\Delta k_{12}, \Delta k_{13}, \Delta k_{14}] \tag{7}$$

Where $\Delta k_{1i} = k_1 - k_i$. It represents the error introduced by site measurement of each station; dX is the measurement error of target location.

So that, the calculation of target position depends on the measurement of the station location and the target signal arrival time difference to each station. Site measurement can be completed through the self localization by each station. Therefore, the basis of TDOA is the accurately record of the arrival time of the signal, the symbol clock recovery of PCM/FM signal is completed by the timing synchronization, so the timing synchronization is the key point of the system.

Timing Scheme

In PCM/FM all digital receiver, the timing estimation is usually performed after the completion of the frequency discrimination. But due to the threshold effect of FM demodulation, the performance of PCM code stream can be deteriorated sharply when the SNR of input signal is lower than the threshold value. Therefore, in this paper, the timing synchronization is directly carried out after DDC, so as to avoid the influence of the threshold effect. The system structure diagram is as follows.

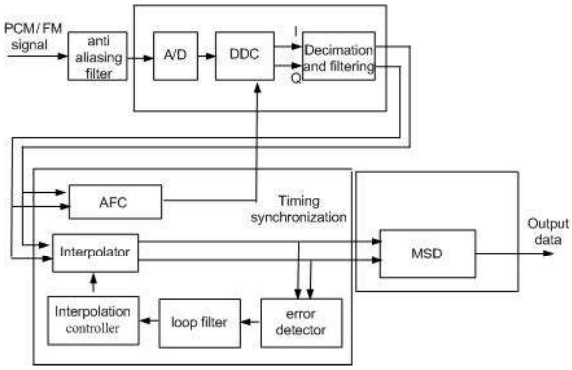

Fig. 2. Elements of all digital receiver.

Because the timing synchronization is carried out prior to the carrier synchronization, we choose the data conversion tracking loop (DTTL) algorithm which is not sensitive to the carrier phase [2].

In order to facilitate the realization of the subsequent signal processing, the I/Q data is decimated and filtered to reduce the signal rate. The I/Q signals are performed the same operation to detect the timing error. The process is divided into two branches, each branch has integrator, the integration period is equal to the symbol width, but the two branches staggered half symbol width. The up Branch is used to detect the data conversion and direction, the down branch is used to determine the size of the timing error, multiplying the output of the two branches. Finally, the calculation results of I /Q signals are summed up to yield the final timing error.

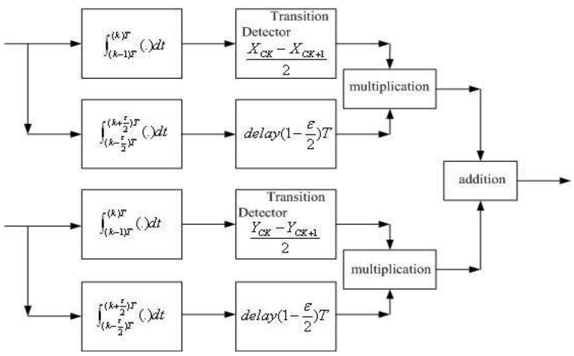

Fig. 3. Block diagram of DTTL.

The obtained error signal pass through the loop filter, and the two-order filter is usually adopted. It also consists of two branches: proportional and integral branches, according to the control theory, we can know that the proportion of branch can track the phase error, but cannot track the frequency error. The coefficients of the two branches determine the bandwidth of the loop and the damping coefficient, which affect the acquisition ability and convergence speed of the timing error, so they are important parameters in the debugging process.

Due to the sampling clock of the system is independent; the ideal sampling point cannot be got directly. It needs to be calculated by interpolation [3]. The filtered timing error is fed into the interpolation controller to obtain the interpolation point and interpolation interval, and the interpolator completes the calculation to get the ideal sampling point.

It applies polynomial interpolation to correct timing error in the system. Polynomial interpolation can be regarded as low pass filtering, the frequency response of the request is: in the frequency range $0\sim1/(2T_s)$ with a flat response and linear phase, and the high frequency component of the signal can be suppressed as much as possible. Usually there are three kind of interpolator: linear, parabolic and cubic interpolation. Because of the efficient farrow structure and better interpolation performance, the choice is cubic interpolation; the cost is the increase of computation amount.

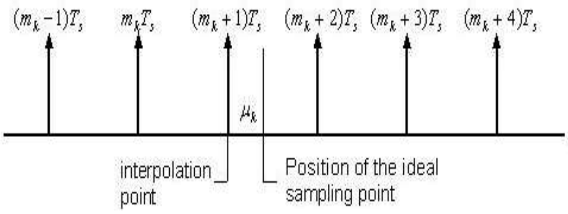

Fig. 4. Timing relation of interpolation

In Fig. 4, $(m_k+n)T_s$ (n=-1,…,4) are the sample times of the digital sequence that is send into the interpolation filter. The sample period is T_S, $(m_k+1)T_s$ is the interpolation point, which is selected by the enable signal that output from the interpolation controller. μ_k is the interpolation interval, which is the timing error, also output from the controller. It shows that $(m_k+1)T_s$ and μ_k reflect the actual position of the ideal sampling point, which is the real arrival time of the signal.

When recording the arrival time of the signal, it is necessary to record $(m_k+1)T_s$ and the value of μ_k. $(m_k+1)T_s$ can be recorded by high-precision 200MHz clock and 1PPS signal which output from GPS receiver. μ_k is used as a correction value to compensate for $(m_k+1)T_s$ to ensure the accuracy of the measurement. The structure of time measurement is shown below in Fig. 5.

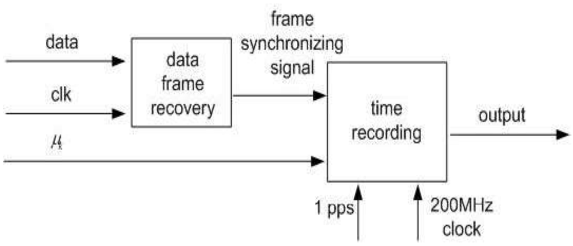

Fig. 5. Structure of time measurement

Error analysis and improvement

Compare with the site measurement error of each station, the time measurement error ε is the main measurement error in multi station passive location.

$$\varepsilon = \sqrt{2\varepsilon_c^2 + 2\varepsilon_q^2 + \varepsilon_s^2 + \varepsilon_d^2 + \varepsilon_f^2} \quad (8)$$

In (8), ε_c is the signal transmission error, it caused by atmospheric delay, when the altitude of the target is low, it is mainly troposphere delay. In engineering applications, it is generally thought to be 5ns; ε_q is measurement station clock error, it caused by the local clock oscillator inaccuracy and instability, it is considered to be 5ns In this system; ε_s is synchronization error between measurement stations, when using GPS Common-view approach，it generated by the GPS receiver of each station, and it is usually about 10 ns; ε_f is doppler error, it produced by High speed movement of the target, it is usually about 15 ns; ε_d is random error which reflects the timing error jitter[1].

ε_d is mainly affected by noise and timing loop bandwidth. If only the loop filter is used to reduce the timing error jitter, the loop bandwidth will be reduced, thereby increasing the acquisition time and making the loop stability worse. The noise includes signal noise and timing synchronization self-noise, so the self-noise can be reduced by using the pre filtering method, and then the timing jitter is reduced. Its structure is shown in Fig. 6.

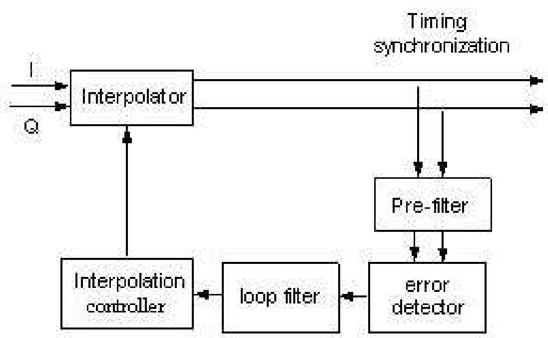

Fig. 6 Elements of timing synchronization with pre-filter

When the even symmetrical bandpass signal which frequency spectrum range in (1/4T, 3/4T) and take 1/2T as the center reaches the steady state, the timing jitter is approximately 0 [4]. Therefore, the pre filter should meet the requirements of the spectral characteristics of the signal. Its amplitude frequency characteristic is expressed in (9).

$$H_0(f) = \begin{cases} G(f-\frac{1}{T}), 0 \leq f < \frac{1}{T} \\ G(f+\frac{1}{T}), \ -\frac{1}{T} \leq f < 0 \end{cases} \quad (9)$$

Where G(f) is the spectral characteristic expression of the shape filter. So the pre-filter is a symbol rate of the shaped filter in the frequency domain. After adding this filter, the synchronization performance is significantly improved, and the results are as follows.

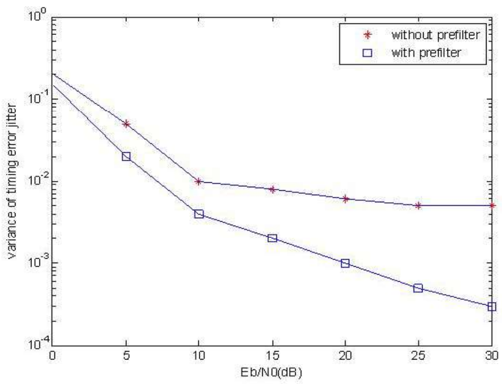

Fig. 7 Restult of matlab simulation

After adding the pre-filter, the timing error jitter ε_d is about 1/120 of the symbol period. When the symbol rate is 2Mbps, ε_d is about 4ns, so the time measurement error ε is 21ns. The position error is 6.3m introduced by time measurement.

Testing results

Block diagram of the system testing is shown in Fig. 8, signal source generates radio frequency signal transmitted by antenna, A, B, C, D four receivers receive the signal at the same time. By comparing the time scale information in the demodulation data, and combined with the station's own coordinates, positioning the coordinate of the signal source.

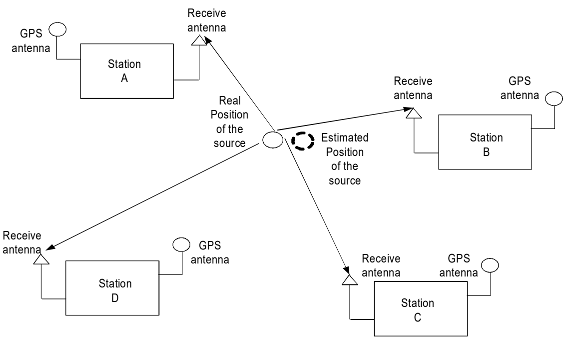

Fig. 8 Sketch map of system test

Where the rate of the test signal is 2Mbps, signal to noise ratio is 8.5 dB, and the distance between the calculated location of the signal source and the actual location is 18 m. So it realize the accurate location of the target.

Conclusions

This paper introduces the basic principle of multi station TDOA location on PCM/FM signal. According to the principle of positioning, using digital transformation tracking loop estimate timing error, coupled with the time measurement module to complete high precision calibration records. The testing results show that the system can achieve precise positioning of PCM/FM signal source.

References

[1] Xie Nan. *Precision Analysis of Time Difference Locating Technology Base on Multi-ground Stations*. Information and Electronic Engineering,2003,1(3):38-42

[2] Marvin K. Simon, Andre Tkacenko. *Noncoherent Data Transiton Tracking Loops for Symbol Synchronization in Digital Communication Receivers*. IEEE Trans. Communications,2006,54(5):889-899

[3] GARDNER F M. *Interpolation in digital modems—part I: fundamentals*. IEEE Trans.Communications,1993,41(3):501—508.

[4] Franks L E, Bubrouski J P. *Statistical properties of timing jitter in a PAM timing recovery Scheme*. IEEE Trans. Communications,1974,22(7):913-920

DOI 10.5162/etc2016/2.1

Adaption of Fibre Optic Sensors and Data Processing Systems for Flight Test on a Bulldog Light Aircraft

N.J. Lawson, R.N.G. Correia, M. Partridge, S.E. Staines, S.W. James, J.E. Gautrey, R.P. Tatam
Cranfield University, Cranfield, Beds. MK43 0AL, U.K.
n.lawson@cranfield.ac.uk

Abstract:
Fibre optic sensors for pressure and strain measurement offer significant advances in a flight test environment as they have no local electromagnetic compatibility (EMC) restrictions, offer high spatial and temporal resolution and have a minimal footprint on surfaces or through aircraft structures. Sensors can also be distributed over large distances. Through the previous FP7 research program Advanced In-Flight Measurement 2 (AIM^2), Cranfield University successfully flight tested fibre optic sensors for unsteady static pressure and surface strain measurement. An extrinsic fibre Fabry-Perot interferometer (EFFPI) was used as a pressure sensor and fibre Bragg gratings (FBGs) were used for surface strain measurement on a wing. This paper outlines the approaches taken in adapting and deploying the sensors onto a flight test platform, in this case a Scottish Aviation Bulldog light aerobatic aircraft. The nature of the certification process required the development of bespoke software and sensor packages to accommodate certifiable hardware. These systems and approaches will be outlined and data presented from flight tests in the Bulldog over a range of dynamic manoeuvres with a normal g-range of-1g to +4g, which has been extended to 6g in more recent tests.

Key words: fibre optic sensors, flight test, pressure sensor, fibre Bragg grating strain sensor.

Introduction

The certification process of aircraft requires a significant program of flight tests where parameters including strain, acceleration, pressure, sideslip, angle of attack and wing shape are measured to validate the design processes and to ensure that the design meets the certification standard [1]-[3]. Recent advances in optical measurement methods have provided new opportunities for the flight test community to implement novel measurement techniques to streamline and improve the flight test process [4],[5]. More specifically, a two-part research program funded under EU FP6 and FP7, called 'Advanced In-Flight Measurement' (AIM and AIM2), recently completed a significant number of flight tests demonstrating the use of optical methods to measure parameters ranging from wing shape, measured using Image Pattern Correlation Technique (IPCT), to the measurement of pressure and strain ofn a wing using fibre optic based methods [4],[5]. In the latter case, fibre optic methods offer significant advantages as they have a minimal footprint (the diameter of an optical fibre is typically around 120μm), no electromagnetic compatibility (EMC) considerations and, for strain and pressure, they offer measurement resolution equivalent or better than standard instrumentation.

This paper presents recently obtained results from one of the flight test programs in AIM2, where a fibre optic strain measurement system, based on fibre Bragg gratings (FBGs), and a unsteady pressure system, based on an extrinsic fibre Fabry Perot interferometer (EFFPI), were certified on an aerobatic light aircraft and tested under steady state and dynamic conditions over a g-range of -1g to +6g.

Fibre Optic Strain Measurement

A fibre optic sensing system was developed for the measurement strain on wings using fibre Bragg grating (FBG) technology [6]. An FBG is a periodic modulation of the refractive index of the core of an optical fibre. This modulation acts to reflect a specific wavelength back along the optical fibre. The reflected wavelength is sensitive to perturbations such as temperature and strain, and thus interrogation of such strain sensors relies on measurement of the reflected wavelength. The wavelength encoded nature of FBGs facilitates the multiplexing of an array of sensors fabricated in a single optical fibre, where each reflects a distinct wavelength under quiescent conditions.

The use of this method for the measurement of strain is relatively mature, with FBGs finding application in areas including structural health monitoring [7],[8], temperature sensing [9] and in the oil and gas industry. In addition, the technique is now seeing increasing use in aerospace applications [10] including for the measurement of the shape of wings [11].

In the work reported in this paper, 5 FBG's, with different Bragg wavelengths were fabricated in SMF-28 optical fibre to enable the multi-point measurement of strain. Prior to exposure of the optical fibre to the output from a frequency quadrupled pulsed Nd:YAG laser operating at 266 nm, the polyacrylate buffer jacket was removed from the sections of fibre to be written. Each FBG had a length of 4mm with a typical reflectivity of 50% and 3dB bandwidth of 0.5nm. The FBGs were not recoated.

To prepare the FBG's for the wind tunnel tests and flight tests, the sensors were calibrated in the laboratory. FBGs were adhered to a number of samples of aluminum aircraft skins (size 25 mm by 200 mm). In addition to bare aluminum surfaces, some of the FBGs were attached to samples with coatings representative of paint used on light aircraft. A number of adhesives were trialed, including epoxy resin and cyanoacrylate. For comparison with the strain measured by the FBGs, conventional resistive foil strain gauges (RFSGs), RS Components model 632-124, were mounted adjacent to the FBGs. The FBGs were interrogated by coupling the output from a Tunics Plus – 3642 HECL tunable laser (tuning range 1520 nm -1620 nm) into the optical fibre, and monitoring the reflected light using a photodiode. The complete spectral output was processed by fitting polynomial functions to the Bragg peaks and differentiating the polynomials to find zero crossing points and thus determine the central wavelengths.

The calibration experiments showed no significant differences between the strain sensitivity of FBGs mounted on painted or bare samples, with the FBG repeatability better than 0.29% of full scale over a range of 600$\mu\varepsilon$, compared with 0.41% from the conventional resistive foil strain gauges. FBG sensors attached using cynoacrylate glue offered the best performance. The RFSG calibration closely matched the FBG measurements, yielding 0.8296 $\mu\varepsilon$/N compared to 0.8321 $\mu\varepsilon$/N for the RFSG. A single optical fibre containing an in-house fabricated wavelength division multiplexed array of 5 FBGs was used for the flight test.

Fibre Optic Pressure Measurement

The fibre optic pressure sensor was based on an extrinsic fibre Fabry Perot interferometer (EFFPI) [12]. In its simplest form, an EFFPI consists of an optical cavity formed at the end of an optical fibre by using a mounting sheath and a reflective diaphragm.

The use of EFFPI's to measure pressure in aerospace applications appears to be limited [13],[14]. At the time of writing, there are no reports of the use of EFFPI's for aircraft flight test. Here, a bespoke EFFPI sensor was fabricated by mounting a single mode fibre into a zirconia ferrule. The ferrule was inserted into a zirconia sleeve and an electret metallised Mylar film microphone membrane was attached to the end of the sleeve to create an optical cavity. This diaphragm was expected to have good frequency characteristics up to 20kHz. The ferrule was also machined on the side to create a 'D' profile to permit the fitting of a vent tube into the sleeve to allow the sensor to be configured as a relative pressure sensor. A general schematic of the EFFPI sensor is shown in *Fig 1*.

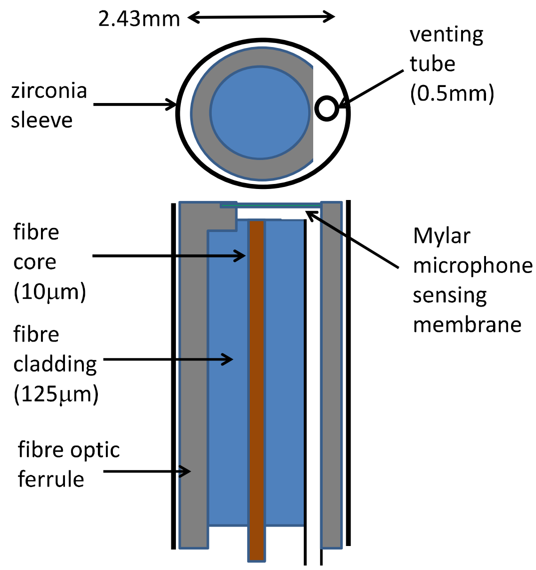

Fig. 1. Schematic of the EFFPI relative pressure sensor.

The channeled optical spectrum reflected from the EFFPI was monitored using the tunable laser and photodiode described previously. As the ferrule was pushed into the sleeve, and the separation between the end of the fibre and the diaophragm decreased, the period of the sinusoidal channeled spectrum increased. The ferrules was glued in position when the 10 periods of the channeled spectrum were observed over a wavelength range of 27.45nm, which corresponded to a cavity length of 387μm. The ferrule was glued into the sleeve using an epoxy resin.

EFFPI System Calibration and Data Processing for Wind Tunnels

The EFFPI was calibrated under laboratory conditions prior to the wind tunnel tests. This calibration involved recording the complete spectral output of the EFFPI during interrogation with a Santec HSL 2000 tunable laser. This laser was coupled to the fibre and a Druck DPI610 pressure calibrator connected to the reference port of the sensor. The output from the laser was tuned through the optical spectrum (1262.5-1311.5nm) at a frequency of 2.5 kHz with a 3dB bandwidth of 1.6nm. The pressure was varied over a range up to 400 Pa, which was the pressure range expected for the wind tunnel tests and flight tests. This calibration showed the EFFPI resolution to be better than 0.33% of full scale. Comparisons to a conventional Kulite pressure sensor, calibrated over a similar pressure range using the Druck DPI610, showed the Kulite to have acceptable linearity and a resolution better than 0.15% of full scale. The Kulite sensor was mounted adjacent to the EFFPI sensor during both the wind tunnel and flight tests as a benchmark for the performance of the EFFPI.

EFFPI System Calibration and Data Processing for Wind Tunnels

Due to the certification requirements for the aircraft modification, defined through Certification Standard CS-23, the systems used to interrogate the FBG and EFFPI sensors in the laboratory could not be used in the aircraft. For the flight testes, both types of sensor were interrogated using a SmartScan Aero FBG interrogator. This system met CS-23 standards and simplified the aircraft modification. The SmartScan interrogator is optimized for FBG sensors, providing a data stream that comprises the central wavelengths of intensity peaks observed in the reflection spectrum, determined using a centroid based algorithm. There is no direct access to the spectral output of the interrogator. This meant that it was not possible to employ phase analysis approaches, and thus the EFFPI was interrogated by tracking the central wavelength of the peaks in the channeled spectrum. If the change in pressure was sufficient to move one of the channeled spectrum peaks out of the spectral window of the interrogator, “jumps were observed within the data, which were removed using the approach detailed in figure 2, and implemented in Labview [16].

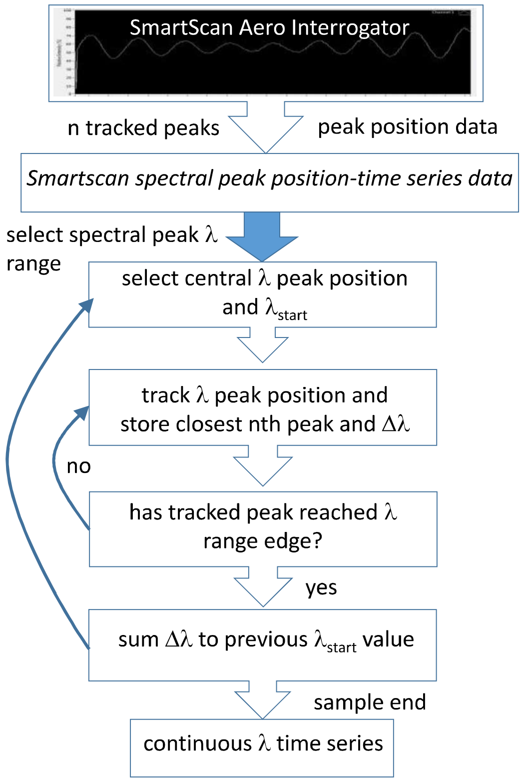

Fig. 2. Schematic of the EFFPI post-processing method for the SmartScan spectral peak data.

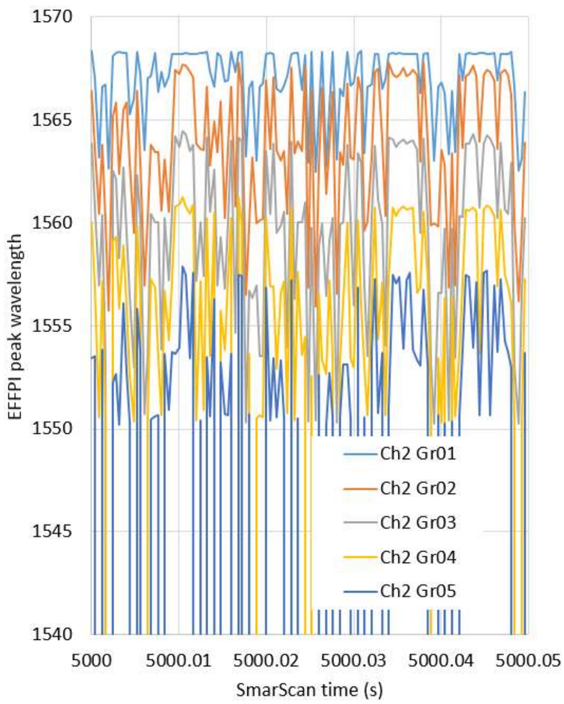

Fig. 3. Raw data from the interrogator. Gr01, Gr02…Gr05 refer to 1st to 5th peak wavelengths returned by the interrogator.

DOI 10.5162/etc2016/2.1

A typical set of SmartScan peak raw data is shown in *Fig. 3*, illustrating the problem associated with the jumps in the data

The Labview post-processing code was tested by analysing data obtained when the Druck DPI610 was used to change the reference port pressure. This process ensured repeatability and checked for sensor hysteresis. In these tests, the sensor was also tested to significantly higher pressures to check for non-linearity, with the tests repeated at three different temperatures, 22°C, 9.2°C and -13.5°C, representative of typical ambient temperatures found during the flight test. The raw spectral peak wavelength data was then post-processed into a wavelength vs. time series plots as shown in *Fig* 4. In this case, the temperature dependency of the sensor is clearly visible.

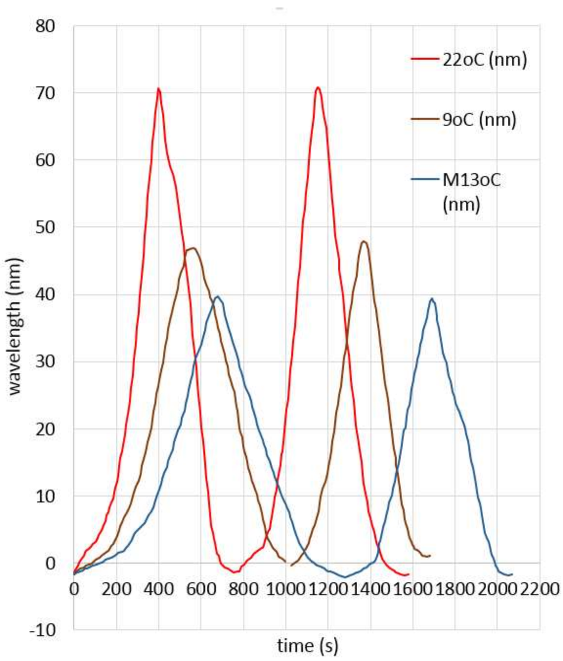

Fig. 4. Pressure response of the EFFPI sensor, measured at different temperatures (22°C, 9.2°C and -13.5°C). The raw data from the interrogator was post-processed using the algorithm shown in figure 2

The time series of peak wavelengths was used to generate calibration curves and a temperature calibration coefficient 2-exponent relationship was determined from the three calibration curves as shown in *Fig 5,* taking the form:

$$C_{FP} = 0.4458e^{-0.01933T} + 6.35 \times 10^{-9}e^{0.04642T} \tag{1}$$

where C_{FP} is the EFFPI calibration coefficient and T is the temperature in Kelvin. The response of the sensor to pressure over the tested range was linear at all temperatures, although the repeatability of the measurements was an order of magnitude lower than that observed in the initial laboratory calibration of the sensor. In this case the calibration data indicated 95% confidence intervals ranging from +/-2.15% at 22°C, +/-4.17% at 9.2°C, increasing to +/-4.92% at -13.5°C.

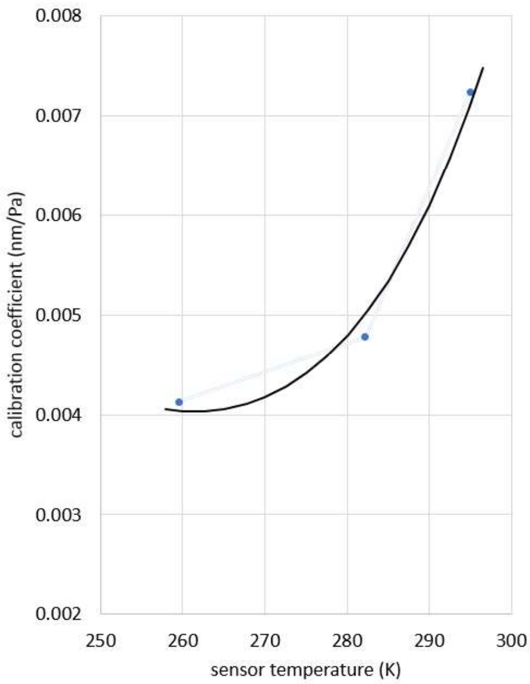

Fig. 5. EFFPI temperature-calibration coefficient relationship

The r significant reduction in the resolution of the sensor was a result of the non-optimal peak-fitting and tracking algorithm that was set in the SmartScan Aero firmware. Solutions to this issue is the subject of further work.

Preliminary Wind Tunnel Tests

Initial tests of the EFFPI sensor in a wind tunnel were performed by mounting the sensor in a test plate on a 30% model of the Bulldog aircraft fuselage, The test plate contained both the EFFPI and Kulite sensors. Details of these tests can be found in previous work [17], [18]. These tests showed the sensor to be robust and to have the repeatability and characteristics expected from the initial calibration. The high level of repeatability was possible as, in this case, the interrogation system used the initial calibration of the sensor could be used. The wind tunnel tests also confirmed that the Kulite and EFFPI sensors could be used over the range of pressures expected to be measured during the the flight test.

DOI 10.5162/etc2016/2.1

Bulldog Flight Test Platform

In order to complete the flight tests, a Scottish Aviation Bulldog aerobatic light aircraft was modified to carry the FBG strain sensors and EFFPI pressure sensor. The Bulldog aircraft was chosen as it has adequate payload and space available for the instrumentation. Its use permits testing of the sensors up to 10,000 feet and the aircraft has a certified g-range of -4g to +6g, allowing the testing of the dynamic response of the sensors.

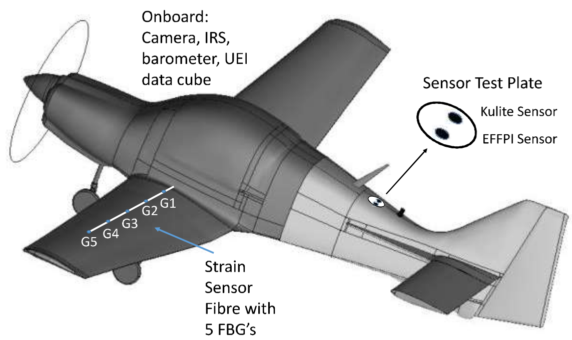

Fig. 6. General schematic of the modifications to the Bulldog aircraft.

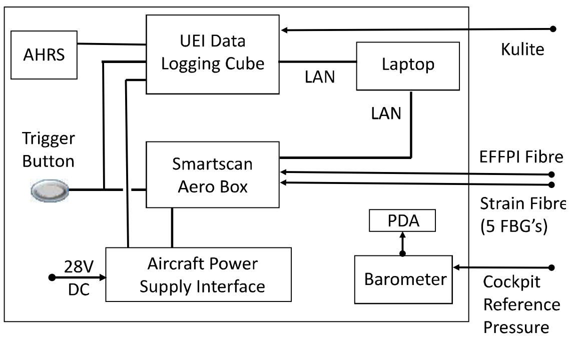

Fig. 7. Schematic of Bulldog aircraft flight test instrumentation

The modification to the aircraft, classed as 'Minor' under CS-23, included the addition of a power supply box, the SmartScan Aero interrogator, a trigger box, an UEI data acquisition cube, an SBG Systems SBG Systems IG-500A-G4A2P1-B AHRS, a pressure sensor mounting plate positioned just behind the cockpit and other carry-on instruments including a handheld barometer to monitor reference pressure and a camera system to record a view from the cockpit during the flight.

The power supply and the SmartScan Aero interrogator were mounted onto a honeycomb floor plate just behind the pilots seat. The honeycomb srcture was used to reduce weight, such that the total increase in weight following the modification was less than 13kg. Schematics of the aircraft and instrumentation are shown in *Fig 6* and *Fig 7*. The cockpit view from the on-board camera is shown in *Fig 8.* This allowed a number of cockpit instruments including the altimeter and airspeed indicator, to be monitored and it also permitted the use of external visual references during dynamic manoeuves such as the spin.

Fig. 8. View from the Bulldog on-board cockpit camera

The 5 FBGs in the sensor array attached to the wing skin using a cyanoacrylate adhesive. The entire length of fibre was covered with 3M 425-50 speed tape. The 5th FBG (the furthest way from the fuselage) was placed inside a hypodermic needle in order to float during the test, such that it measured only the temperature and could be used to compensate for the temperature response of the other 4 FBGs. Prior to the flight test, an additional set of RFSG's were attached adjacent to the FBGs and static tests were performed to check the performance of the FBG's. These tests confirmed acceptable agreement with the RFSGs. The wires connecting the RFSGs to the instrumentation were then removed.

The pressure sensor test plate was positioned behind the cockpit, between the aerial and beacon. The EFFPI and XCQ-093 Kulite sensors were mounted in the plate as indicated in *Fig 6*. The Kulite sensor wiring and optical fibre connected to the EFFPI were loomed and mounted down the fuselage and through the cockpit rear bulkhead, where they were connected to the UEI cube and to the SmartScan interrogator, respectively. The sensor reference pressure ports were also connected onto the same loom using a single pitot tube with a t-joint next to the sensors and sensor test plate. The pitot tube was then left open to cockpit ambient pressure, which was monitored by the DPI 740 barometer connected to a data logging personal digital assistant (PDA).

A trigger box was used to provide trigger signals to the UEI data logger during test flights. The SmartScan interrogator could not be synchronized to the UEI or AHRS data. Therefore manual synchronization was employed, using a dynamic manoeuvre during the during the flight test where all the recorded parameters contained a significant change at the start of the manoeuvre. During the test flights, the acquisition rates varied from several Hz for the barometer data logger to 2.5kHz for the EFFPI, the FBG and the Kulite sensor.

Flight Test Results and Discussion

For the initial flight test program, seven flights were completed to test the sensors and systems. The first six flights were concerned with troubleshooting issues with the equipment, including data-acquisition issues and an earthing problem with the Kulite sensor, which made the data from the first 6 flights void.

Flight 7, however, allowed a complete set of data from all the sensors to be recorded. The flight consisted of a climb out to 8400 feet based on a standard altimeter pressure setting of 1013 mbar, with two straight and level conditions. A series of dynamic manoeuvres were then completed including a spin, a stall turn, a loop, a slow roll and a barrel range with g-load ranges from -1g to +4g. Subsequent flight tests have successfully extended this g-range to +6g. Data from flight 7 is shown in *Fig 9* to *Fig.11*.

The barometer data shows the change in ambient pressure and is analogous to the altitude profile of the flight. The different stages of the flight are visible including the dynamic manoeuvres. Of interest is a comparison to the EFFPI corrected and uncorrected data. Both data sets follow similar profiles to the barometer, which suggests the sensor is behaving as absolute pressure sensor and not a relative pressure sensor. However, the magnitude in the change in pressure from the temperature corrected EFFPI data is still only half the barometric range, which suggests a partially blocked reference port for the sensor. The Kulite sensor behaves as expected for a relative pressure sensor and the manoeuvres and power changes are visible during the profile. The FBG data shows clearly the wing loading changes throughout the flight profile with the maximum load changes evident during the high-g manoeuvres, as would be expected. Further analysis, yet to be published, has found a good correlation of the FBG strain with the bending behaviour of the wing, considered as a cantilever system.

Further more detailed plots of the dynamic manoeuvres are shown in *Fig.10* and *Fig.11*. In this case, all the sensors capture the significant features of the manoeuvres. In particular spectral analysis of the data recoded by the EFFPI, Kulite and FBG data during the spin yielded a spin frequency of around 0.4 Hertz which matches to within 1%, the spin frequency estimated from the on-board camera movie. For the loop manoeuvre, the AHRS data also matched expected load characteristics seen in the FBG data.

Conclusions

Two types of fibre optic sensor have been developed and flight tested on a Bulldog aerobatic light aircraft over a g-range of -1g to +6g. An FBG system has been used to measure wing strain at 4 points on the aircraft wing and an EFFPI sensor has been developed to measure dynamic pressure on a selected point on the aircraft fuselage. The resolution of the strain system was shown to be 0.29% of full scale, i.e. equivalent to conventional RFSG's. Laboratory tests of the EFFPI pressure sensor suggested a resolution of 0.33% of full scale. However, due to the requirement to use a certified interrogator on-board the aircraft, use of non-optimal peak-tracking methods in the interrogator firmware reduced the EFFPI resolution by a factor of 10. The flight tests though still provided sufficient resolution from both fibre optic sensors to allow analysis of a series of 5 dynamic high-g manouevres. Further aircraft modifications and flight tests are planned in the near future and it is hoped the EFFPI resolution issues can addressed through either firmware changes to the SmartScan Aero box, or the carriage of more bespoke EFFPI interrogator equipment. This will then provide an unsteady fibre optic pressure sensor with an equivalent resolution to conventional Kulite, but without the EMC limitations.

Acknowledgements

The authors would like to acknowledge European Framework 7 funding, contract number 266107 'Advanced In-Flight Measurement 2' and EPSRC Grant number EP/H02252X/1. For enquiries relating to access to the research data or other materials referred to in this article, please contact Cranfield University Library and Information Services– library@cranfield.ac.uk.

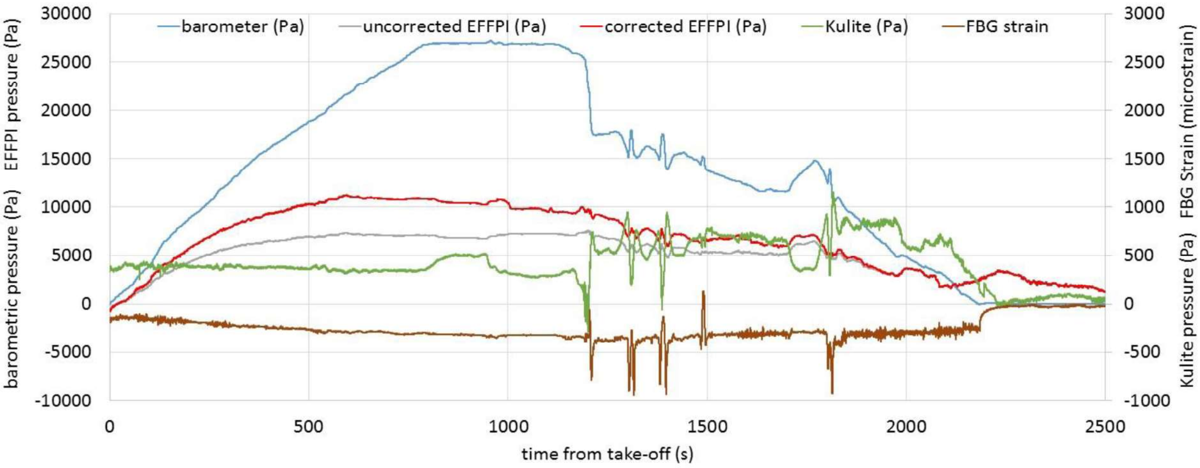

Fig.9. Bulldog flight test profile showing data from the FBG, EFFPI, Kulite and barometer sensors.

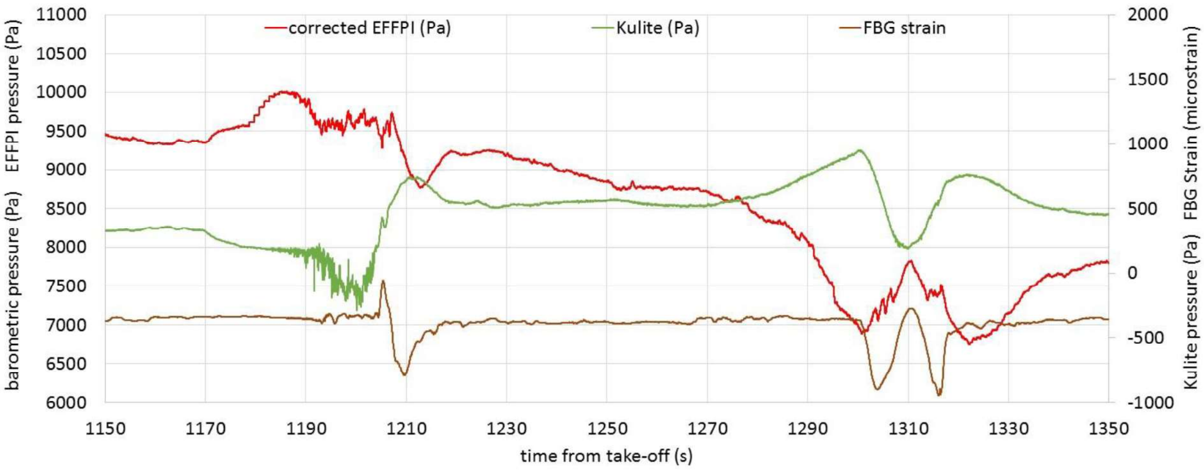

Fig.10. Bulldog flight test profile showing selected data from the FBG, EFFPI and Kulite sensors during the spin and loop manouevre.

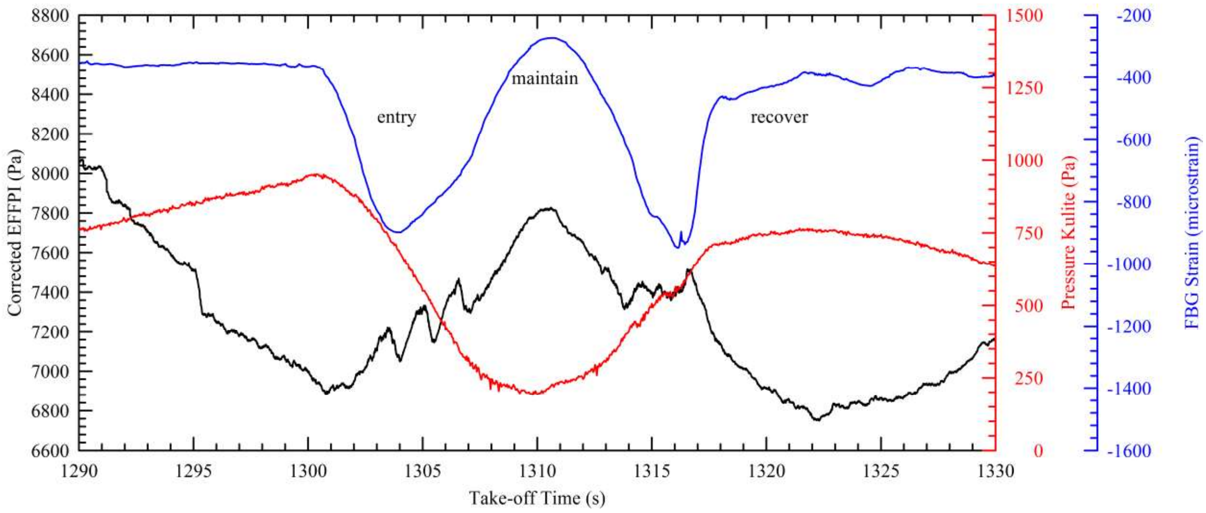

Fig.11. Bulldog flight data from the loop manouevre indicating the stages of the manoeuvre.

References

[1] Kottcamp E., Wilhelm H. and Kohl D. “Strain Gauge Measurements on Aircraft”, AGARD and RTO Flight Test Instrumentation Series AGARDograph 160 (AG 160), Volume 7 (1976)

[2] van der Linden J.C. and Mensink H.A., “Linear and Angular Measurement of Aircraft Components”, AGARD and RTO Flight Test Instrumentation Series AGARDograph 160 (AG 160), Volume 8 (1977)

[3] Borek R. and Pool A., “Basic Principles of Flight Test Instrumentation Engineering (Issue 2)”, AGARD and RTO Flight Test Instrumentation Series AGARDograph 160 (AG 160), Volume 1 (1994)

[4] Boden F., Lawson N., Jentik H.W. Kompenhams J., “Advanced In-Flight Measurement Techniques”, Springer-Verlag, Berlin, 2013

[5] Boden F. “AIM2 Advanced Flight Test Workshop – Handbook of Advanced In-Flight Measurement Techniques”, Eds – Boden F., Books on Demand, Norderstedt, Germany ISBN 978-3-7322-3740-1 (2013)

[6] Rao Y.-J. “In-fibre Bragg grating sensors” Meas. Sci. Tech. 8, 355-375 (1997)

[7] Measures R.M. “Structural Monitoring with Fiber Optic Technology”, London, Academic Press (2001)

[8] C. Barbosa, N. Costa, L.A. Ferreira, F.M. Araujo, H. Varum, A. Costa, C. Fernandes and H. Rodrigues, “Weldable fibre Bragg grating sensors for steel bridge monitoring” Meas. Sci. Tech. 19, 125305 (10pp) (2008)

[9] A. Azhari, R. Liang and E. Toyserkani, “A novel fibre Bragg grating sensor packaging design for ultra-high temperature sensing in harsh environments”, Meas. Sci. Technol. 25 075104 (11pp) (2014)

[10] Trutzel M N, Wauer K, Betz D, Staudigel L, Krumpholz O, Muehlmann H-C, Muellert T, Gleine W, “Smart sensing of aviation structures with fiber-optic Bragg grating sensors”, Proc. SPIE 3986, pp. 134-143 (2000)

[11] Jutte, C.V., Ko, W.L., Stephens, C.A., Bakalyar, J.A., Richards, W.L. and Parker, A.R., “Deformed Shape Calculation of a Full-Scale Wing Using Fiber Optic Strain Data from a Ground Loads Test”, NASA/TP-2011-215975 (2011)

[12] Rao, Y.J. Recent progress in fibre-optic extrinsic Fabry-Perot interferometric sensors, Optical Fibre Tech., 12,227-237, (2006)

[13] Pulliam W J, Russler P M and Fielder R S “High-temperature high-bandwidth fiber optic MEMS pressure-sensor technology for turbine engine component testing”. Proc. SPIE 4578, 229-238 (2001)

[14] Gander M J, MacPherson W N, Barton J S, Reuben R L, Jones J D C, Stevens R, Chana K S, Anderson S J and Jones T V “Embedded Micromachined Fiber-Optic Fabry–Perot Pressure Sensors in Aerodynamics Applications” IEEE Sens. J. 3 102-107 (2003)

[15] Jiang Y. and Ding W., “Recent Developments in Fiber Optical Spectral White-Light Interferometry” Photonic Sensors 1(1), 62-71 (2011)

[16] Qi B., Pickrell G.R, Xu J., Zhang P, Duan Y., Peng W., Huang Z., Huo W., Xiao H., May R.G., Wang A., “Novel data processing techniques for dispersive white light interferometer”, Opt Eng 42(11), p3165-3171 (2003)

[17] Lawson N.J., Gautrey J.E., Salmon N., Garry K.P., Pintiau A., “Modelling of a Scottish Aviation Bulldog using Reverse Engineering, Wind Tunnel and Numerical Methods“ IMechE Part G, Journal of Aerospace 228, 2736-2742 (2014)

[18] Lawson N.J., Salmon N., Gautrey J.E., Bailey R. “Comparison of Flight Test Data with a Computational Fluid Dynamics Model of a Scottish Aviation Bulldog Aircraft” The Aeronautical Journal 117, 1273-1291 (2013)

DOI 10.5162/etc2016/2.2

Coupling of MEMS gyroscope application with wavelet analysis for detection of airframe oscillations in flight conditions

Jerzy Bakunowicz[1] Paweł Rzucidło[1]
[1] Rzeszów University of Technology, al. Powstancow Warszawy 12, 35-959 Rzeszów, Poland
bakun@prz.edu.pl

Abstract:
The gyroscopes established one of the fundamental reference for attitude and heading in aerospace applications. The information about angular velocity gives input not only for autopilot, but also damping devices, as yaw or pitch dampers for example. The MEMS gyroscopes (Micro Electro Mechanical Systems) are much less reliable than their laser or fibre optic cousins. Nevertheless, availability and low price of MEMS components cause growing area of application in avionics for General Aviation aeroplanes. This paper presents certain results of flight data analysis registered during flight testing campaign of the new class aeroplane – experimental low power single engine turbo-prop utility I-31T. The researches were focused on identification of oscillation modes, distinctive for the new aircraft, such as engine precession, whirl or shimmy. The data came from three-axis MEMS gyroscope recorder, placed near to the aircraft centre of gravity. Wavelet transformation gives better precision in time domain than Fourier transformation, especially for signals of low frequency.

Key words: Flight-test, MEMS, load-spectrum, wavelet analysis, I-31T.

1. Introduction

The development in the field of aeronautical engineering is always connected with research activities of high-risk. The incessant rush in improving of introduced solutions is entailing desire for their immediate implementation from one side, on the other, however, we are dealing with the quite natural conservatism firstly putting the protection of human life. The awareness of the great responsibility accompanied designers from the very beginning – Wright brothers, while manufacturing their aeroplane, known later as No.1, considered strength of each element to cope with the weight 5 times greater than mass of the pilot [18]. The methodology of research has been established and proven starting from ground static and stiffness tests to testing in flight. Within the decades, they were supplemented by many other, today inevitable, tests, such as flutter, vibration, fatigue to mention only few, most important. The whole array of tests and trials before putting a new aeroplane to the market has the only one goal – to eliminate all unwelcome features, may affect badly on her future career. In the course of the technological progress, the metrologies advance, giving wider cognitive abilities through more accurate and more extensive registration abilities, as well as practically any form of processing and presenting results. On the other hand, however the benefit of progress is giving rise to negative side effects in the form of extending the time of research works, and hence their cost, the number of different systems and the need for their mutual harmonizing. As a result, the number of new aerospace vehicles is decreasing constantly, comparing to the rising costs of development. So called 14th Augustine's law gives an excellent illustration [2], telling in subversive manner about the escalation of U.S. Air Force airborne research programs: *In the year 2054, the entire defence budget will purchase just one aircraft. The aircraft will have to be shared by the Air Force and Navy, 3.5 days each per week except for leap year, when it will be made available to the Marines for the extra day*. The simplification of metrologies, measurement software and hardware and the tests at large would seem reasonable in the light of budget optimizing. Nevertheless, one may be wrong, forcing the simple „back to the roots" solution. Although, whenever paper and pencil should lay on the desk. Test planning should follow towards the search for new applications of advanced but simple in general metrologies in unexplored areas. A significant indicator for the new application would be a number of parameters and number of samples measured during the test. The methods utilizing a reduced number of entry parameters become crucial for total time of the test program, especially in-flight. As an example one may recall a group of “bootstrap” methods [16].

One of the most important information recorded during the flight, furthermore not only in the development phase, but also during the entire life of the structure, is flight loads spectrum of the whole airframe and individual parts as well [21]. Early attempts of flight loads recording in organized manner are dated as soon as the dawn of modern aviation [7]. Familiarity with aeroplane accelerations gives not only information about the load factor the structure is exposed to during sustained or instantaneous manoeuvres. The coupling of the load magnitude and exact aeroplane attitude in the time history enables to find a load spectrum, inevitable for preparation of long-term ground fatigue tests. The essence of such data might be underlined by the fact that their importance does not terminate when the fatigue durability tests of the new structures were completed successfully. There may come time for revisiting the data when the aeroplane would serve for many years and problems of ageing will appear [11].

Increasing the sampling frequency of the measurement device gives ability to register not only low-cycle flight loads, but also faster spectra, such as vibrations originated by propulsion or turbulence, also aeroelastic response of the structure. Proper comparison of this data with the results of Ground Vibration Tests (GVT) makes ground for identification of resonance.

The gyroscopes belong to the group of sensors widely utilized for low and high cycle loads recording. MEMS accelerometers in 1990s found their application to air-bags activation systems in automotive. But they become widespread in household and hobbycraft electronics due to their small size and relatively low price. The aerospace industry absorbed them as well, especially in avionics for General Aviation light aeroplanes [14], [24] or systems onboard of RPAS [10], [19].

This paper presents a preliminary study of acceleration spectrum flight data analysis with continuous wavelet transformation [1]. The airborne measurement device based on MEMS gyroscopes and was placed on board of a light turboprop utility aeroplane. Several examples with unique frequency representations of different flight states have been presented to illustrate the method.

2. Aeroplane and flight testing

The measurements took place on the I-31T aeroplane (Fig. 1), the advanced modification of the I-23 *Manager* aeroplane [5]. Both crafts were designed in Institute of Aviation, Warsaw, Poland. The origins of the aeroplane reach back to early 1990s. The light, piston engine powered, high performance, equipped with advanced avionics aeroplane belonged to the chain of Small Air Transport System. Following worldwide crisis in General Aviation sector caused that only sole prototype has been built. But the idea to build a transportation system in Europe with door-to-door operation time less than four hours left in minds and became one of the core directions in the aviation development today [23], being focused on personal aeroplanes propelled by small engine units [17]. Introduction of low power, below 200kW, turbine engines for propeller propulsion gave opportunity to create a prototype of a new aeroplane class, reconciling handling and performance of a light General Aviation aeroplane with economy and simplicity of turbopropeller engine.

Fig. 1. I-31T aeroplane during one of the test flights.

The I-31T aeroplane has been designed and manufactured as one of several technology demonstrators in large, international, collaborative European project ESPOSA (Efficient Systems and Propulsion for Small Aircraft) co-funded by European Commission with the 7th Framework Program [9]. The concept of a new aeroplane class has been proven during the flight test campaign led by Institute of Aviation, Warsaw together with Rzeszów University of Technology. But the fundamental remark for similar future initiatives says that this class of aeroplanes must not be developed by ordinary conversion of previously piston driven aeroplanes into turbine. The design should be dedicated for the propulsion exclusively to share all benefits of the new propulsion.

Flight test campaign of the new I-31T aeroplane covered all items described in CS-23 requirements, inevitable to prove conformity [6].

Certification test flights were organized in rather classic, conservative manner, bearing in mind the simplicity of the aeroplane. The main recording of the flight parameters has been left for the eye and hand of the Flight Test Engineer (FTE), who was accompanying the test pilot side-by-side during the flight. Independent recording devices were used supplementary for certain measurements of rather scientific nature, e.g. temperature distribution.

The measurement data analysed in this paper came from the flight data recorder (FDR) installed on board, inside the cabin, close to the centre of gravity, which enables to record following parameters with sampling frequency of 50Hz [15]:

- accelerations a_x, a_y, a_z;
- angular velocities p, q, r;
- orientation angles;
- static pressure;
- GPS navigation data (10Hz).

The recorder is an advanced modification of the device designed and manufactured in Rzeszów University of Technology for flying laboratory based on PW-6U glider [3] used in second edition of Advanced In-Flight Measurement Techniques (AIM2) project.

The FDR was put into operation before the flight by FTE and switched off after landing. The data set recorded on SD memory card, was transferred on PC hard disk and processed in dedicated software commercial as well as created in house.

Besides the independent, impartial data recording by the FTE and FDR, the opinions of the test pilots about the handling and other feelings were collected in the disciplined manner [12].

3. Measurements results and discussion

This paragraph deals with several examples of cycle load spectrum analysis recorded during test flights. The emphasis has been laid on the movement of the aeroplane on the ground, due to the fact that these recordings initiated presented research.

Landing and ground manoeuvres

The I-31T aeroplane operated from concrete runway surfaces. Her approach and landing qualities were assessed at the 4 to 5 grade in the Cooper-Harper scale [12]. The aeroplane has a wing loading of 115kg/m^2, which locates her in the upper range in the class. This implies a high approach and landing speeds. Additionally, high effectiveness of elevator and marginal longitudal stability, decreased by a long nose of the new propulsion, require higher pilot's concentration. The flare phase is rather figurative. To summarize, the aeroplane is characterized by short landings in a "carrier-like" style.

One of many landings, at three points and quite "hard", on wet runway with centreline lamps touched by the front wheel during roll-off finished with *shimmy* vibrations of the front undercarriage, which ceased when the aeroplane came to a halt completely.

Shimmy occurs when a wheel oscillates at often large amplitudes about its vertical axis about which the wheel rotates. For light aeroplanes it is common for front gears with one wheel and manifests itself as a limit cycle oscillation with a frequency range typically 10-30 Hz. The most common reasons are inadequate torsional stiffness, torsional freeplay, wheel imbalance, etc. It is normally countered by careful design or use of dampers. The I-23 aeroplane, progenitor of I-31T, has been equipped with shimmy damper during her flight test campaign, but it was removed and no complaints has been recorded so far. Indeed, a quick maintenance after this particular shimmy incident revealed an excessive freeplay in front steering mechanism.

The FDR on board of the aeroplane recorded data on attitude of the aeroplane, navigational parameters and information from the accelerometers and MEMS gyroscopes. The sampling frequency reached 50Hz and it allows for detection and analysis of phenomena at 25Hz or less.

The vibration of the aeroplane during roll-off, caused by shimmy of the front gear, were clearly recognizable by the plane crew and felt on the background of other motions of the aeroplane. Therefore, it might be assumed, the FDR should also register them in a certain manner, e.g. oscillations of angular velocities or linear accelerations.

In the first step, several recordings of different landings including final approach, flare, touch down and roll-off were investigated. The crucial moment to distinguish the moment, the aeroplane leaves the air and starts to ride on the ground is identification of wheel contact with the pavement. The main gear contact was identified by analysis of n_z change in comparison to change of altitude and ground speed (Fig. 2 A-B, G). The touch of the front gear is better visible after continuous wavelet transformation (CWT) of all three components of acceleration n_x, n_y *i* n_z (Fig. 2 D, F, H). But the most repeatable results, regardless of the landing quality were obtained for the n_x component.

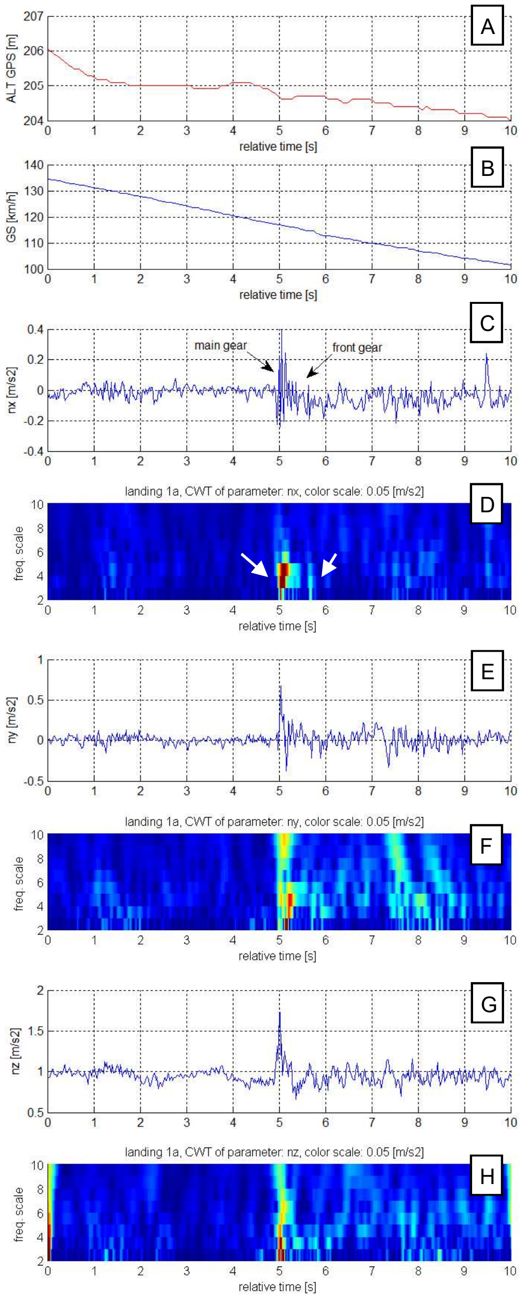

Fig. 2. CWT analysis graphs for main and front gear touch down moment detection (landing No.1a). Charts present respectively: A – altitude [m], B – ground speed [km/h], C – n_x [m/s^2], D – CWT analysis of C, E – n_y [m/s^2], F – CWT analysis of E, G – n_z [m/s^2], H – CWT analysis of G, in time domain span 10 [s].

There is always short term vibration along the longitudinal axis (Fig. 2 D), which concentrates close to the value of 5 on frequency scale (that means 10Hz, according to Fig. 3). The frequency as well as amplitude of n_x oscillations are not correlated with n_z component, which denotes the “hardness” of the landing. Therefore CWT analysis of n_x may be sufficient for effective touch-down identification with accuracy of 50ms. The colour shade in Fig. 2 D, F and H denotes vibration amplitude. Dark blue is equal to “zero” and purple – limit amplitude, defined as colour scale in CWT charts.

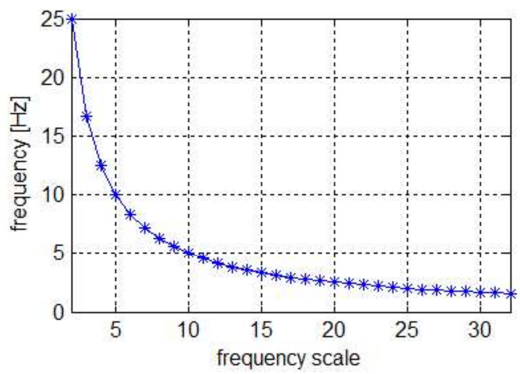

Fig. 3. Complex Morlet wavelet dependency between central frequency and frequency scale.

The landing analysed in the Fig.1 (landing no.1a) may be assumed as regular one with smooth touch-down. During roll-off there were no disturbing phenomena. Shimmy vibrations appeared during the roll-off recorded in landing no.2a. This kind of oscillatory movement is hard to identify in acceleration and angular velocity time plots, however they manifest as high frequency occurrence (frequency scale 2 to 10) from 2nd to 7th second in CWT chart of n_y. In the 4th second there is short braking action of the pilot (Figs. 4 B-C, 5 C-D), that caused unexpected increasing of amplitude. When the aeroplane groundspeed was below 75kph (Fig. 4A), the vibrations of high amplitude occurred, clearly visible as change in acceleration along *y* axis (Fig. 4D-E). Resembling characteristics may be found on time plots as well as on CWT charts of n_z (Fig. 4F-G) and velocities *p* and *r* (Fig. 5A-B and E-F). The analysis of n_x load and angular velocity *p* reveals two attempts of braking action initiated by the pilot between 11.5s to 13s, and following from 18.5s to 24s. Each breaking increased the amplitude with maximums recorded in 12.5s, 19s and 23s respectively. In the second 23 vibrations of n_y reached 1m/s^2, remaining n_x and n_z had amplitudes lower by half.

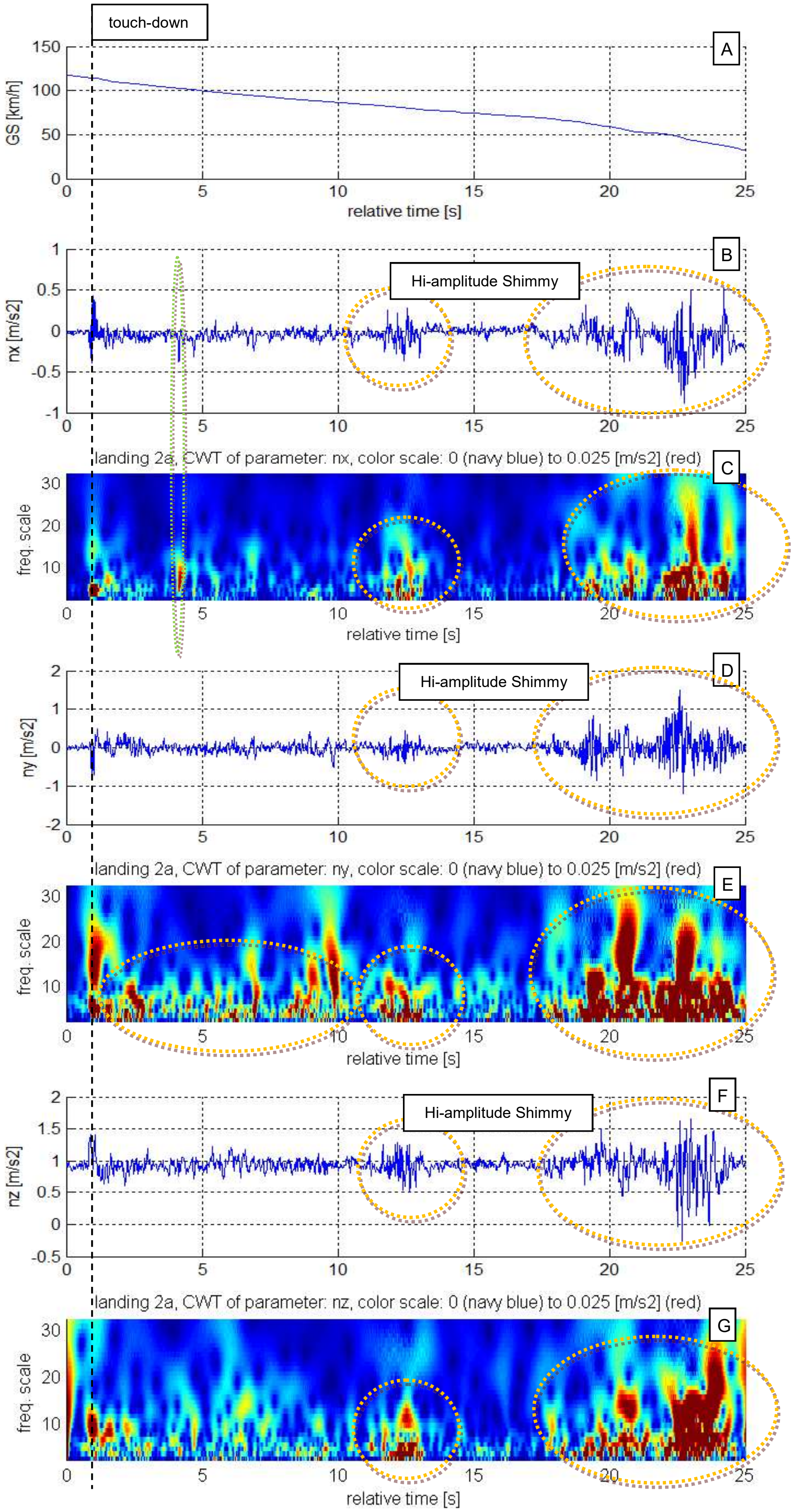

Fig. 4. Load factors analysis, recorded during the roll-off with shimmy vibrations of the front gear (CWT analysis with amplitude normalised), landing no. 2a.

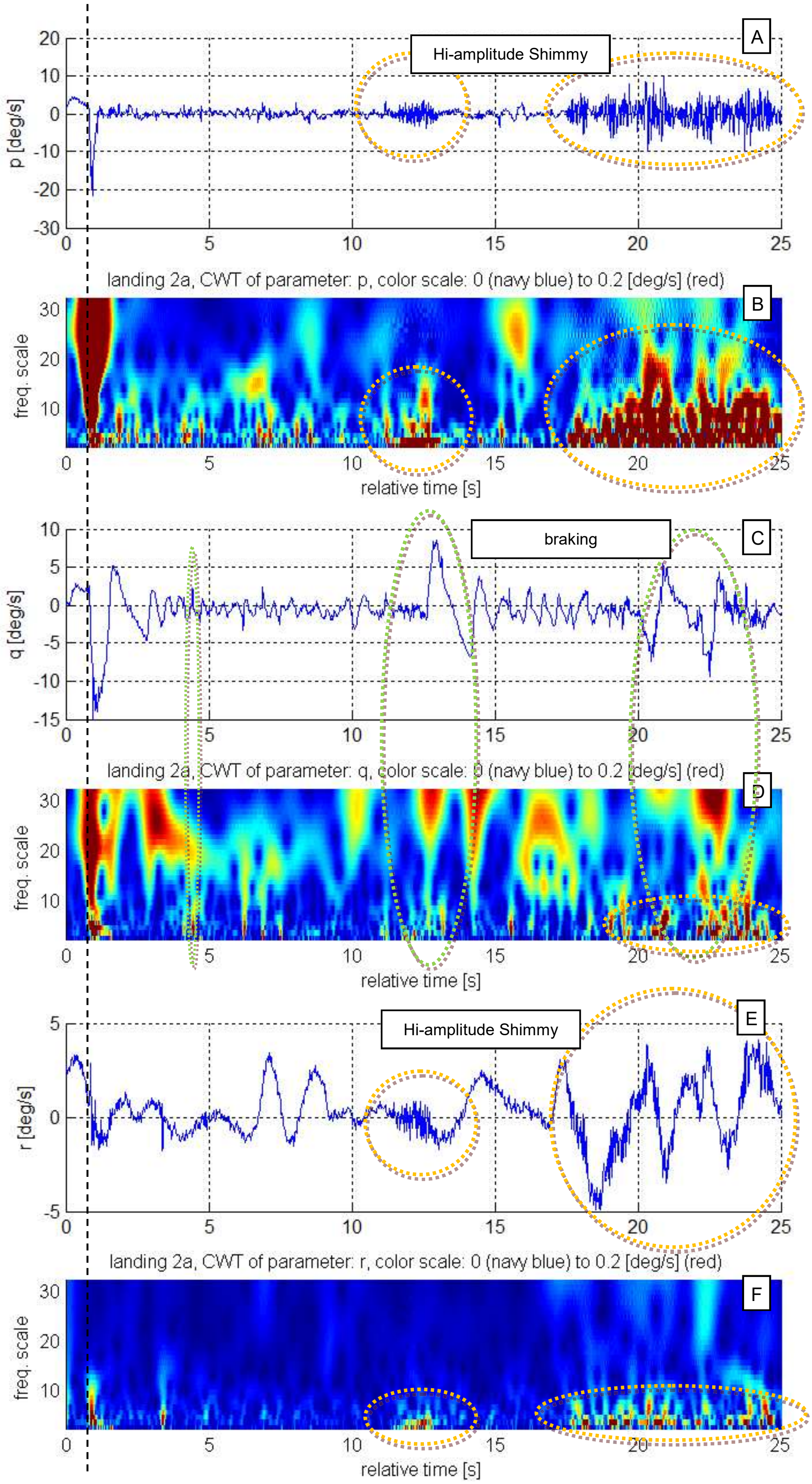

Fig. 5. Angular velocities analysis recorded during the roll-off with shimmy vibrations of the front gear (CWT analysis with amplitude normalised), landing no. 2a.

One may notice, analysing CWT charts of n_y and p in Fig. 4 E, 5 B, that between seconds 2 and 14 the spectrum is dominated by vibrations with frequencies 3 to 4 (normalised). According to the Fig.3, it represents frequencies between 12 and 17Hz. In second 17 and further, when the aeroplane groundspeed decreased below 60kph, high amplitude vibrations of n_y and p arouse gradually, having frequencies in middle of the scale between 10 and 20, that represents frequencies of 5Hz and 2.5Hz (Fig. 4E, 5B). The other accelerations and angular velocities were affected similarly, but with mush less effect (Fig. 4-5). After second 24, when the aeroplane groundspeed decreased below 40kph, the vibrations ceased. The pilot claimed, that the only possible solution to damp the vibration was to halt the aeroplane. Rolling with the groundspeed higher than 40kph caused increasing of the amplitude.

It should be underlined, any other landing in the set of 20 recorded did not contain similar characteristics during roll-off.

The vibrations described above and recorded by FDR represent the effect of interaction between shimmy oscillatory movement of the front gear and the rest of the airframe, an finally the FDR itself. Therefore this spectrum (frequencies and amplitudes) does not represent the behaviour of the undercarriage, and cannot be applied directly. Moreover, the shimmy vibrations belong to the oscillatory movements with more than one degree of freedom. But concerning the effects of shimmy vibrations on the rest of the airframe, the spectrum in this form would give useful information about frequencies and “severity” of the vibrations.

The Fig.6 presents the whole recording from the short “hoop” flight between two parallel runways. There are angular velocities *p, q, r* in the time domain (Fig. 6 B, E and H) starting from the short holding time before take-off and terminating at taxing to the apron (Fig. 6 A). This analysis does not present accelerations, due to troublesome interpretation of a vast number of oscillations.

In the Fig.6 take-off and touch-down were identified. It might be noticed in the CWT chart of p angular velocity (Fig. 6 C-D), when aeroplane is on the ground the spectrum is dominated by high frequencies from the engine. During roll on and roll off they are close to 3Hz, but there is no distinction between the engine itself and rolling. After lift off this band ceased and frequencies of 5Hz and higher are still visible (especially p, Fig. 6C), moreover, there is also band of 10Hz (for q and r, Fig. 6F, I). We presume the main source of the vibrations mentioned in flight is the engine and variation in *N1* revolutions. Unfortunately, at this level, further analysis seems to be rather complicated, due to the fact that sampling frequency of the FDR is only 50Hz, that means the highest vibration frequency possible to detect is 25Hz.

The frequencies below 3Hz contain a wide set of natural frequencies of weathercock and longitudal motions. In the Fig.6 G one may notice oscillations in pitch with mean frequency of 1.25Hz (velocity q). Their amplitude is increasing in moments of levelling off or when descent starts, but also during the approach to land. They may be explained as short period pitch oscillations. Similarly, dutch roll motion may be identified. In the Fig.6 J, there is a constant directional motion with mean frequency of 0.7Hz motion (velocity r), which is correlated with p oscillations of the same frequency (Fig. 6 D).

In the Fig. 6J there may be noticed also short period oscillations of r with mean frequency of 1.25Hz. We presume, the source would lay in gyroscopic moments caused by longitudal oscillations with similar frequency.

The aeroplane control may also have form of oscillations, especially when man-machine feedback loop is cauterised by short time constants [13]. Such behaviour may occur when pilot is focused on precise flight parameters, e.g. during precision approach and landing or following certain trajectory defined by dedicated flight instruments in both examples. While the aeroplane approaches the runway, the closer the threshold, the shorter the time constant, therefore the higher control frequencies. Although all landings during the flight test campaign were performed with reference to the external objects (not instrumental), the analysis revealed similar behaviour. In the Fig. 6D the roll frequency during take-off and final approach is close to 1Hz, but in the entire flight is much lower, about 0.3Hz.

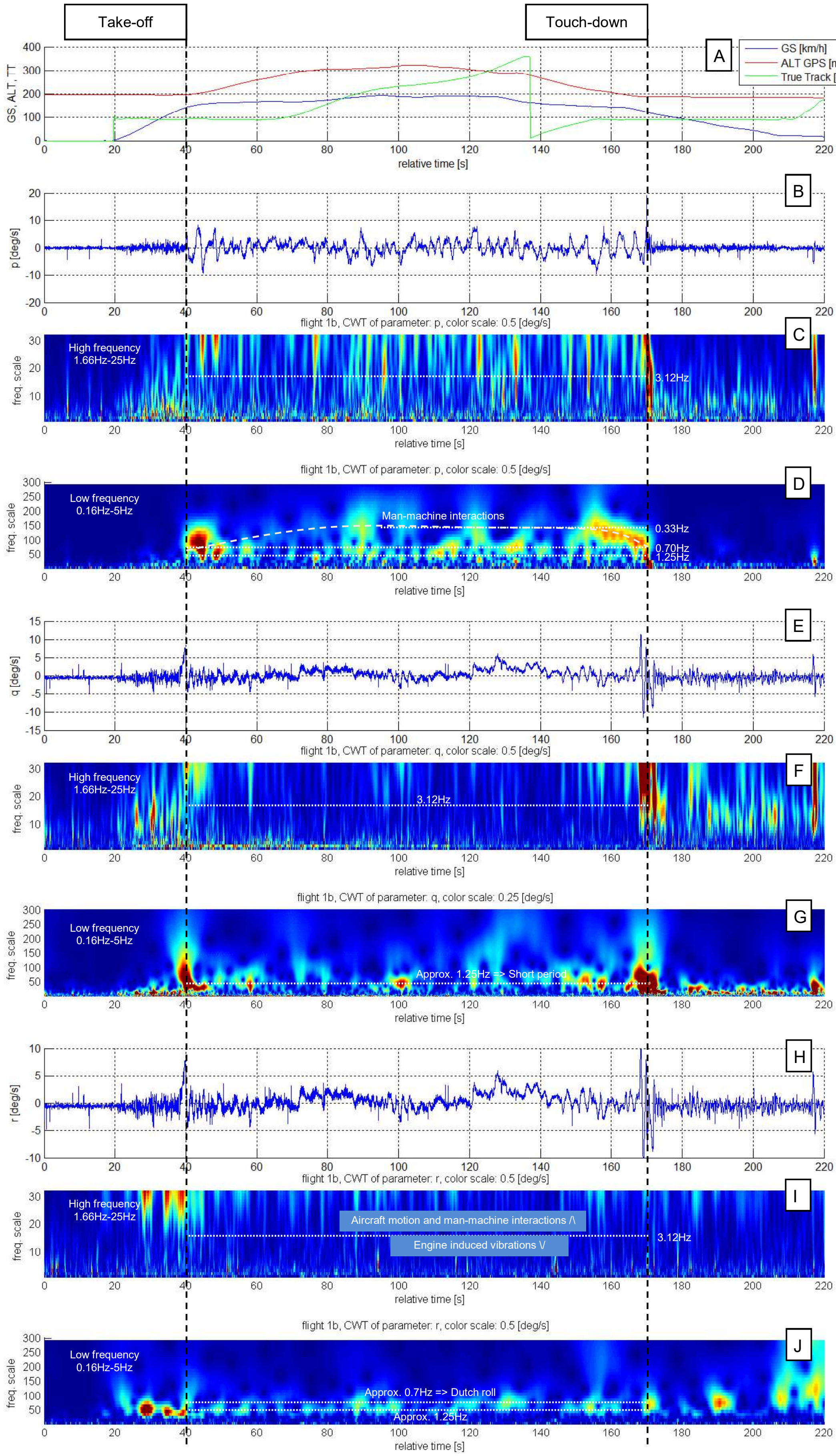

Fig. 6. Angular velocities analysis recorded during a short „hoop" between two parallel runways (CWT analysis with amplitude normalised) Flight no. 1b.

4. Summary

In the presented paper authors introduced examples of wavelet analysis of load spectra recorded with MEMS gyroscopes during the flight testing.

The wavelet analysis of accelerations and angular velocities supplemented with time plots of several other parameters, when appropriate, and having description of flight provided by the pilot, could be applied for aeroplane load analysis during the flight based on data from simple recorder unit.

The continuous wavelet analysis method makes easier the interpretation of high frequency vibrations of airframe induced by propulsion, undercarriage and the airframe itself, as well as the phenomena which take place in flight, such as dutch roll, short period oscillations, gyroscopic torques, but also man-machine interactions. There is also possibility to identify several longperiod phenomena, such as phugoids or gusts.

This paper introduces the method, which seems to be worthwhile for further development, especially towards higher frequencies. Regarding such phenomena, as flutter or comparison with Ground Vibration Tests (GVT) the recording device with at least 200Hz sampling frequency should be applied. The lowest eigenvalues for the I-31T aeroplane start from 8 – 9Hz and concern less probable modes. The eigenvalues connected with airframe deformation which may result in flutter start from 25Hz [7].

The results of analysis allow to identify also flight characteristics of the aeroplane. At this level we may not consider them as full handling qualities analysis due to the fact that several other parameters are still missing.

The other potential application of this method would be academic education. The courses of data analysis, handling qualities or flight testing seem to be still uncommon in aerospace engineering studies [22]. Rzeszów University of Technology has a flying laboratory based on Piper Seneca V aeroplane, equipped with additional devices on board, including FDR, similar to the described one [4], giving the opportunity to incorporate such analysis into study programme.

Acknowledgements

The paper presents results of research done within the project **ESPOSA – Efficient Systems and Propulsion for Small Aircraft**, co-funded by European Commission in 7th Framework Program, Grant Agreement 284859.

References

[1] Abbate A., DeCusatis C., Das P., Wavelets and subbands : fundamentals and applications, Springer Science + Business Media, LLC, New York, 2002.

[2] Augustine N.R. Augustine's Laws. Penguin Books, New York 1987.

[3] Bakunowicz J., Meyer R. In-Flight IPCT Wing Deformation Measurements on a Glider. Presented on Research Aircraft Operations Conference. London 2014. Aeronautical Journal (unpublished).

[4] Bakunowicz J., Tomczyk A., Wałek Ł. Simplified Total in Flight Simulator as a Tool in the Aeronautics Students' Education. 8th World Conference on Educational Sciences. University of Alcala, Spain 2016.

[5] Baron A. Samolot Osobowy I-23 "Manager". Wybrane problemy badawcze. Instytut Lotnictwa, Warszawa 2012. ISBN 978-83-63539-01-6.

[6] Certification Specifications for Normal, Utility, Aerobatic and Commuter Category Aeroplanes CS-23. Amendment 1, EASA 2009.

[7] Cieślak S., Krzymień W., Lorenz Z. Próby rezonansowe samolotu I-31T. Raport z badań. Instytut Lotnictwa w Warszawie, 2015 (unpublished).

[8] Doolitle J.H. Accelerations in flight. NACA TR-203, Washington 1923.

[9] ESPOSA – Efficient Systems and Propulsion for Small Aircraft. Description of Work. Grant agreement no: 284859.

[10] Gosiewski Z., Kulesza Z. [red], Mechatronic Systems and Materials IV, Kopecki G., Tomczyk A., Rzucidło P., Algorithms of Measurement System for a Micro UAV, Solid State Phenomena, Vol. 198, Trans Tech Publications Inc., Zurich 2013, pp. 165-170.

[11] Guillaume M., Uebersax A., Mandanis G., et al. Structural Integrity – Yesterday – Today – Tomorrow. 11th International Fatigue Congress, Melbourne, 2014 Book Series: Advanced Materials Research Vol. 891-892, pp.1053-1058.

[12] Harper R.P., Cooper G.E. Handling Qualities and Pilot Evaluation. Wright Brothers Lectureship in Aeronautics, 1984.

[13] Kitkowski Z. [red], Mechatronic Systems, Mechanics and Materials, Rzucidlo P., Chudy P., Analysis of Interactions between Pilot-Operator and Advanced Flight Control System, Solid State Phenomena, Vol. 180, Trans Tech Publications Ltd, Zurich 2012, pp. 101-108.

[14] G. Kopecki, T. Rogalski, Aircraft attitude calculation with the use of aerodynamic flight data as correction signals, Aerospace Science and Technology, vol. 32, 2013, pp. 267-273.

[15] Kopecki,G., Rzucidło,P. Integrated modular measurement system for in-flight tests. Polskie

Towarzystwo Diagnostyki Technicznej, Diagnostyka, 15(1), pp. 53-60, 2014.

[16] Lowry J.T. Performance of Light Aircraft. AIAA, Reston 1999.

[17] Majka, A. Multiple objective optimisation of the power unit for a very light jet. Aircraft Engineering and Aerospace Technology, Emerald Group Publishing Limited, Volume 86, Number 3, pp. 234-241, 2014.

[18] McFarland M.W. The Papers of Wilbur and Orville Wright. McGraw-Hill, New York 1953.

[19] Naruoka M., Hino T., Nakagawa R., Tsuchiya T., Suzuki S. System Identification of Small UAVs with MEMS-Based Avionics, AIAA Infotech@Aerospace Conference, 6-9 April 2009, Seattle, Washington.

[20] Naruoka M., Hino T., Tsuchiya T., Application of Wavelet Transform to System Identification of Small UAVs Flight Characteristic , AIAA 2010-3536 paper, AIAA Infotech@Aerospace 2010, 20 - 22 April 2010, Atlanta, Georgia.

[21] Norton W.J. Structures Flight Test Handbook. AFFTC-TIH-90-001. Edwards Air Force Base 1990.

[22] Padfield G.D. Flight Handling Qualities. A Problem-Based-Learning Module for Final Year Aerospace Engineering Students. 1st Annual CDIO Conference. Queen's University, Ontario 2005.

[23] Piwek K., Wiśniowski W. Small air transport aircraft entry requirements evoked by FlightPath 2050. Aircraft Engineering and Aerospace Technology: An International Journal, vol.88(2), pp.341-347. DOI: 10.1108/AEAT-02-2015-0065.

[24] Rydlo, K., Rzucidlo, P., Chudy, P. (2013), Simulation and prototyping of FCS for sport aircraft, Aircraft Engineering and Aerospace Technology, Volume 85, Issue 6, pp. 475-486.

[25] Smitha C., Akujuobia C. M., Hamoryb P., Kloeselb K., An approach to vibration analysis using wavelets in an application of aircraft health monitoring, Mechanical Systems and Signal Processing, Volume 21, Issue 3, April 2007, Pages 1255–1272.

[26] Wright, J.R., Cooper J.E. Introduction to Aircraft Aeroelasticity and Loads, Second Edition. John Wiley & Sons, Ltd 2015.

DOI 10.5162/etc2016/2.3

Developing a Novel Contactless Sensor for Helicopter Rotor State Measurements

Potito Cordisco[1], Rui Liu[2], Matteo Redaelli[3], Luca Riviello[3], Alberto Rolando[4], Federico Rossi[4], Lorenzo Trainelli[4], Edoardo Vigoni[1], Emanuele Zappa[2]
[1] Vicoter, Via Stoppani, Calolziocorte, 23801 Italy
[2] Politecnico di Milano, Department of Mechanical Engineering, Via G. La Masa 1, 20156 Milano, Italy
[3] Finmeccanica Helicopter Division, Via G. Agusta 520, Cascina Costa di Samarate, Varese, Italy
[4] Politecnico di Milano, Department of Aerospace Science and Engineering, Via G. La Masa 34, 20156 Milano, Italy
lorenzo.trainelli@polimi.it

Abstract

The present contribution concerns the development of an innovative measurement system for rotorcraft applications. This system aims at the real-time acquisition of the motion of a rotor blade in flight, for applications in emitted noise prediction and monitoring, and in rotor state feedback control augmentation. A structured approach to the system design, implementation and testing has been pursued starting from a survey of applicable technologies. Contactless solutions were targeted, in view of maximum compatibility with a wide class of vehicles. A first development phase saw the selection of three concepts, all conceived to be mounted on the rotor head and pointing the blade root area, based either on 2-D laser transducers or on vision-based sensors. These were implemented in full scale and laboratory tested to choose the most promising for definitive development. The final solution, a stereoscopic vision-based measurement system, was brought to maturity through further development and laboratory testing, up to fully integration on board a prototype helicopter for ground and flight testing. We detail the various stages in this process, motivating the choices made and illustrating the results in terms of measurement accuracy.

Key words: Helicopter blade motion, flapping sensor, blade angle measurement, rotor state feedback, contactless sensing.

Introduction

The ability to acquire on board, in real-time, the motion of a helicopter rotor blade is gaining increasing importance, in view of an improvement of pilot-vehicle capabilities and a widening of the spectrum of rotorcraft flight procedures and operational tasks. In fact, on one hand, rotary-wing vehicles are prone to possibly significant dynamic behaviors impacting on comfort as well as pilot workload, while on the other hand their operations are often limited by the admissible levels of external noise emitted, which inhibits flying terminal procedures over densely inhabited areas. By measuring blade motion on the fly, this information could be processed in order to derive specific quantities used in the estimation of rotor (and hence vehicle) dynamics, with multiple applications, such as noise estimation, vehicle closed-loop control laws, vehicle monitoring, or parameter identification.

In spite of the potential advantages, to date no operational rotorcraft is permanently fitted with equipment devoted to the real-time acquisition of blade motion, of either the main or tail rotor.

Temporary provisions are sometimes employed by rotorcraft manufacturers in the development of new rotorcraft models or versions, as elements of the installed Flight Test Instrumentation. Examples of these kind of sensor systems are given in [1,2]. The former is based on a combination of accelerometer sensors and an observation algorithm for the retrieval of blade motion and load data, while the latter relies on direct mechanical probing through LVDT-fitted rods. These experimental devices are subject to different requirements than production equipment, reflected in

DOI 10.5162/etc2016/2.3

specialized setups with low degrees of integration and portability, and relatively low levels of reliability and endurance.

The present contribution synthetically illustrates a structured approach to the design, implementation and testing of a new rotor state measurement system for rotorcraft applications, conceived as potentially integratable on board current and future production helicopters. This effort has been recently carried out in the framework of a Clean Sky collaborative project in which the novel sensor system plays a fundamental role, enabling the setup of an innovative integrated system for rotorcraft in-flight noise monitoring.

The MANOEUVRES Project

The Clean Sky MANOEUVRES (Manoeuvring Noise Evaluation Using Validated Rotor State Estimation Systems) project is focused on novel solutions in support to the implementation of low acoustic impact rotorcraft terminal procedures [3]. In this 32-month program involving two universities, Politecnico di Milano and Università Roma Tre, and two companies, Vicoter and Logic, with the close cooperation of Finmeccanica Helicopter Division (FHD), an articulated agenda of innovative research activities has been pursued in the attempt to demonstrate the feasibility of an approach to on board, real-time noise monitoring through an estimation of the running acoustic emission based on rotor blade measurements.

To this end, an algorithm providing an estimation of a suitable ‘noise index’ feeds a new instrument, the PAI (Pilot Acoustic Indicator) [4], for graphical presentation in the cockpit. This algorithm retrieves interpolated SPL (Sound Pressure Level) distributions within a database of pre-calculated steady-state acoustic predictions. The input for this process is given by the current values of three parameters, to which noise emission is strongly related: the helicopter advance ratio, the main rotor thrust coefficient, and the main rotor tip-path-plane (TPP) angle of attack, or TPP-AOA [5]. The on-board measurement of these parameters poses some difficulties. In particular, the thrust coefficient and the TPP-AOA are only roughly estimated on the basis of simplified models of the vehicle fed by data extracted from the helicopter avionics (airspeed, altitude, etc.).

However, if a rotor state measurement system is present, the current blade motion (and in particular the cyclic flappings) can be evaluated, leading to a direct estimation of the TPP orientation with respect to the rotor fuselage. This, coupled with an estimation of the fuselage angle of attack and sideslip, may lead to the achievement of the TPP-AOA. Again, this may be difficult, especially in the case of production helicopters, which are not endowed with appropriate sensors for fuselage aerodynamic angles, such as swiveling air data booms. Therefore, for the MANOEUVRES approach, a solution may be found in applying the observation methodology described in [6], by which thrust coefficient and TPP-AOA can be conveniently estimated exploiting the rotor state measurements.

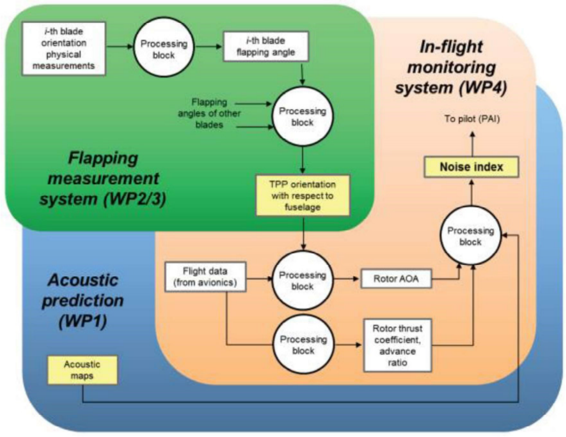

Fig. 1. Schematics of the noise index estimation process within the MANOEUVRES workflow.

Figure 1 depicts the general process in which acoustic predictions produced in the MANOEUVRES Work Package 1 contribute, together with the rotor state measurements provided by the sensor system developed in Work Packages 2 and 3, to the input for the PAI algorithm, developed in Work Package 4.

In addition to this process, in the technical Work Packages (WPs) of the MANOEUVRES project, other activities have been pursued. Indeed, in WP4, the full implementation of the PAI has been carried out, with the realization fo a stand-alone prototype that has been integrated within a FHD research flight simulator for a thorough trial campaign with professional test pilots.

In an effort to assess the capability to accurately predict the noise footprint of a maneuvering rotorcraft, in WP1 two variants of a quasi-steady computational approach have been compared to fully unsteady calculations in relation to typical and low-noise terminal trajectories [7,8]. The highly accurate, but inevitably burdensome, unsteady aeroacoustic solver, coupled with a sophisticated propagation model, has been used to correlate predictions with actual flight test data. Also, the sensitivity of the predictions with respect to perturbations in the nominal trajectory have been studied.

In WP2 and 3, the availability of a rotor state measurement system on board was seen as a motivation to investigate an innovative approach to Rotor State Feedback (RSF) attitude control augmentation. Structured controllers have been applied to a reduced, linearized rotor/fuselage model (2^{nd} order in hover and 5^{th} order in forward flight up to intermediate airspeeds), taking into account a realistic model of the rotor state measurement system, including related values of the sampling frequency and time delay. This activity demonstrated significant potential benefits in pilot/vehicle performance, easing pilot workload and enhancing rotorcraft stability [9,10].

A detailed overview of the results obtained in WP1 and WP4 at 24 months from the project inception is offered in [11]. Here, we delve on the process accomplished in WP2 and WP3, concerning the full-scale development of a novel contactless measurement system mounted on the main rotor head, from preliminary studies to the final integration on board a prototype helicopter for ground and flight testing.

Design Requirements and Technology Survey

For the development of a new rotor sensor system capable of accurate measurements of coupled lead-lag, flap and pitch blade motions, contactless technologies were considered, in an effort to improve system durability and exploit a higher intrinsic flexibility of application. In fact, we targeted a product-oriented prototypal application showing the potential to be fitted on main and tail rotors mounted on operational rotorcraft of different size and configuration.

Appropriate requests, constraints and limitations for the rotor state measurement system to be developed were defined, in view of such an ambitious goal, before carrying out a thorough technology survey. Among these requirements, we identified functional characteristics, physical characteristics, and environmental characteristics.

Functional characteristics involve metrological performance, needed to permit the use of the system in noise prediction, as well as in other promising applications. The analysis led to identify the values shown in Table 1 for measurement bandwidth, accuracy, and range.

Tab. 1: Measurement system performance requirements

Bandwidth	0 – 10 Hz (minimum) 0 – 25 Hz (desired)
Accuracy	0.5 deg (minimum) 0.1 deg (required)
Range	lead-lag: (-13.5, 10.3) deg flap: (-6.0, 18.0) deg pitch: (-22.0, 20.0) deg

Also, the capability to operate satisfactorily on board a helicopter was considered by identifying the need to achieve the measurement while subjected to the loads induced by the in-service accelerations and vibration levels.

Physical characteristics include elements such as weight, geometry, power consumption, and installation requirements, considering both options of installation on the main rotor or on the fuselage airframe. For environmental characteristics, we considered a maximum altitude up to 6,100 ft, and a temperature range from -40°C to the maximum found on the relevant helicopter area. Numerous other requirements, complying to the applicable requests found in the MIL-STD-704E and RTCA/D0160D standards were also included.

Based on this analysis, we carried out an assessment of candidate technologies, considering the sensor types listed in Table 2.

Tab. 2: Types of sensors considered in the preliminary studies

N.	*Technology*	*Installation*
1	Capacitive	On rotor
2	Ultrasonic	On rotor
3	Eddy current	On rotor
4	Hall effect	On rotor
5	Magneto-inductive	On rotor
6	1-D and 2-D laser triangulation	On rotor On fuselage
7	Time-of-flight laser	On rotor On fuselage
8	Vision systems	On rotor On fuselage

Initially, all sensor types were considered for possible installation on the rotor, while only types 6–8 were deemed to be suitable to a fuselage-mounted solution. This is justified by the limitations in range characteristics of types 1–5, which pose serious problems in targeting the main rotor blade from a location on the fuselage on a typical helicopter. However, a further step in the study led to reduce the number of candidates to only types 6 and 8, in view of a reduced risk in obtaining poor measurement characteristics.

Indeed, types 1–5 may suffer of a marked sensitivity to possibly wide variations in environmental conditions, which is typical of flight applications. For example, capacitive sensor measurements are influenced by dirt, moisture, water and other perturbations to the dielectric media. Ultrasonic sensors can be fairly sensitive too to various environmental variations, including air turbulence. In some cases, these problems add to short measuring ranges and inherent difficulties in measuring a fully tri-dimensional, large amplitude motion, such as with eddy current, Hall effect and magneto-inductive transducers. In these cases, the potentially wide amplitude of the motion to be captured struggles with the need of an accurate, constant alignment with the target. Finally, time-of-flight laser systems were discarded for their relatively low sampling frequency.

This preliminary assessment allowed to choose types 6 (1-D and 2-D laser triangulation) and 8 (vision systems) as the most promising for candidate rotor state measurement system concepts.

Preliminary Concept Selection

Given the potential compliance of laser triangulation-based systems and vision-based systems to the preliminary requirements discussed above, the next phase requested to conceive three competing implementations and to test them on appropriate test benches. Based on measured performance, a final selection was eventually accomplished to determine the definitive rotor state measurement system solution, to be integrated on board a AW139, a 15-seat, 7-ton class, twin-engine helicopter.

The three candidates were sorted out of a set of nine possible solutions, listed in Table 3.

Tab. 3: Possible rotor state measurement system solutions considered in the preliminary studies

N.	*Sensor type*	*Sensor position and target*
F1	Single point laser	Fuselage to blade
F2	2-D laser	Fuselage to blade
F3	Vision-based single camera	Fuselage to blade
R1	Single point laser	Hub top to blade root
R2	2-D laser	Hub top to blade root
R3	Vision-based single camera	Hub top to blade root
R4	Vision-based stereoscopy	Hub top to blade root
R5	Vision-based single camera	Hub top to blade tip
R6	Vision-based single camera	Hub side to blade root

Six rotor-mounted (R*x*) and three fuselage-mounted (F*x*) solutions were considered. An important element in this regard is the fundamental difference in the ability to capture harmonic components in the motion of the target. In fact, for all rotor-mounted solutions, where the target (a part of the blade) virtually stays in the field of view of the transducer at all times, a single sensor with an adequate sampling rate allows to acquire all frequencies of interest. On the contrary, the frequency content sensed by sensors employed in fuselage-mounted solutions is strictly a function of their number, given that they can only acquire at each blade passage.

This played an important role in the choice of the three candidates, which were evaluated by applying the *Analytic Hierarchy Process* (AHP) [12] by defining a number of ranking parameters grouped into the following classes: (a) weight, cost and helicopter requirements; (b) technical challenge; (c) technical capability; (d) road to commercial exploitation. In this way, we contemplated measuring performance along with numerous characteristics that must be taken into account when pointing to a potentially airworthy and product-oriented industrial application. The resulting overall ranking for the concepts is shown in Figure 2.

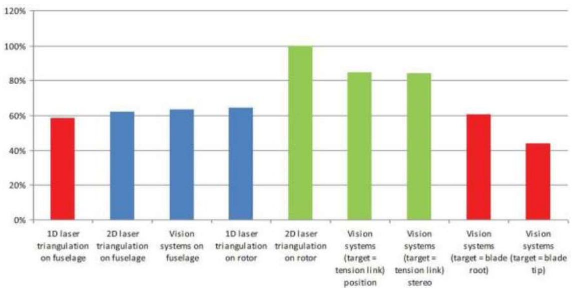

Fig. 2. AHP ranking for the possible rotor state measurement system solutions (from left to right: F1 to F3, followed by R1 to R6).

The three higher-ranked concepts are all rotor-mounted solutions with the transducers installed atop the hub and pointing to some part of the blade root. The winner emerged as solution R2 (2-D laser triangulation), followed by solutions R3 (vision-based single camera) and R4 (vision-based stereoscopy), scoring the same mark.

Preliminary Development and Testing

For each of the three surviving solutions, a prototypal, full-scale implementation was assembled and a thorough test campaign was carried out in order to characterize transducer functionality and measurement performance.

Aiming to assess these characteristics in representative laboratory conditions, we considered three types of experiments:

- Type I tests: the systems were fitted to a shaker and, during the acquisition, subjected to realistic tri-axial vibration levels replicating actual flight data measured on board a AW139.
- Type II tests: the systems were installed on two different non-rotating rigs for accuracy assessment.
- Type III tests: the systems were installed on a rotating rig replicating the actual main rotor speed of a AW139, stressing the equipment with realistic centrifugal loads during the acquisition.

For Type II tests, a pure flapping rig was built at the Politecnico di Milano laboratories (Figure 3). This was achieved assembling specially-produced elements with real helicopter components, to faithfully reproduce the geometry of the installed system. Static flap angles, as well as harmonic flap motion, can be imposed to the blade retention elements.

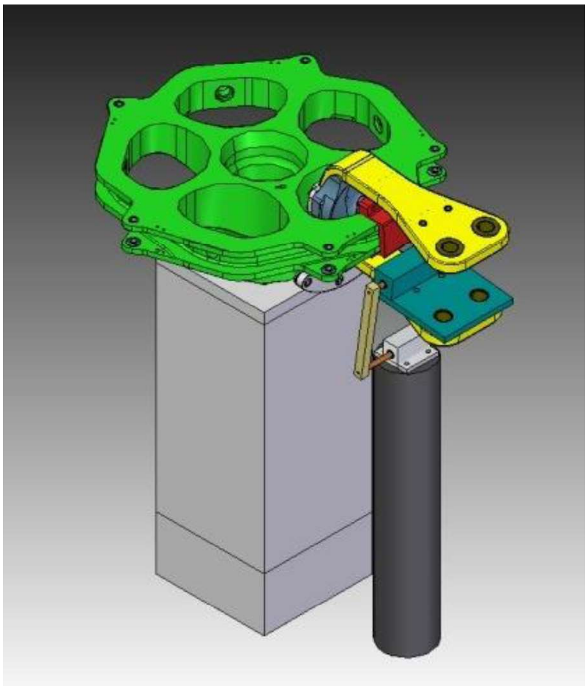

Fig. 3. Pure flapping rig employed for Type II tests.

A second, highly representative rig was also employed in Type II tests: the AW139 endurance testbed available at the FHD premises in Cascina Costa. This is a highly complex device used for main rotor component testing, which allows to impose fully coupled lead-lag/flap/pitch blade motions and simulates the effects of the centrifugal pull on the blade. In some trials, actual blade motion time histories retrieved from AW139 flight test data were reproduced.

Also in Type III tests a special attention was put in achieving a highly representative operating condition. In this case, we employed the A109MKII ironbird available at the Politecnico di Milano laboratories (Figure 4). This test bench is based on a Agusta A109MKII helicopter fuselage, devoid of the tail section, complete with the transmission gearbox and mast. The engines have been replaced by electric motors, the hub assembly is simplified, and the rotor head is fitted with two aerodynamic brakes in place of the blades. With this equipment, real centripetal accelerations and representative vibrations resulting from the gearbox can be reproduced.

Fig. 4. The A109MKI ironbird employed for Type III tests.

All three candidate systems passed Type I and Type III tests, showing continuous operations, with acquisition and data transfer unaffected by sustained vibration and acceleration levels.

In Type II testing, a rich test matrix was put to trial, with numerous single axis and coupled combinations of static and harmonic lead-lag/flap/pitch rotations. During these tests, some differences were detected between the three candidate systems concerning accuracy. Examples are given in Figures 5 and 6, where the errors on the measure of the mean value and the amplitude, respectively, are given in the case of a sinusoidal 1xrev (*i.e.* containing only the first harmonic) pure flapping time history. As apparent, while all three candidate systems exhibit errors below 1 deg about all axes, the 2-D laser solution is characterized by greater inaccuracies. Similar results are obtained when looking at pure lead-lag motions, pure pitch motions, as well as for coupled lead-lag/flap/pitch motions. A case of actual blade motion time histories retrieved from AW139 flight test data is presented in Figure 7 for the error on the mean value. In this specific case, the errors on the 1xrev and 2xrev amplitudes showed similar trends, with maximum values of 0.54 deg (R2) and 0.03 deg (R2) in lead-lag, of 0.35 deg (R3) and 0.07 deg (R3) in flap, and of 0.21 deg (R3) and 0.20 deg (R3) in pitch.

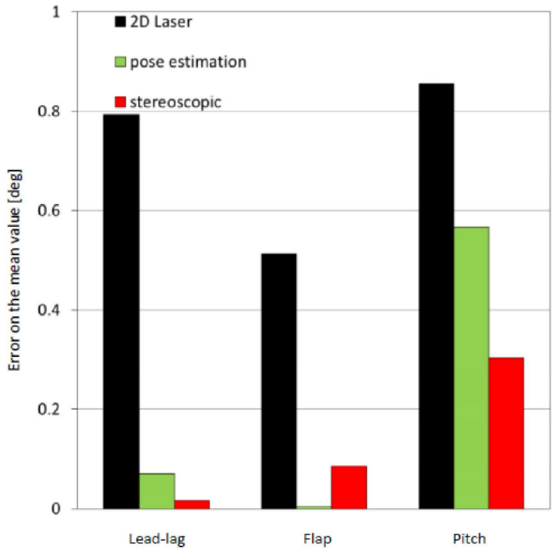

Fig. 5. Error on the mean values for a pure flapping harmonic 1xrev time history.

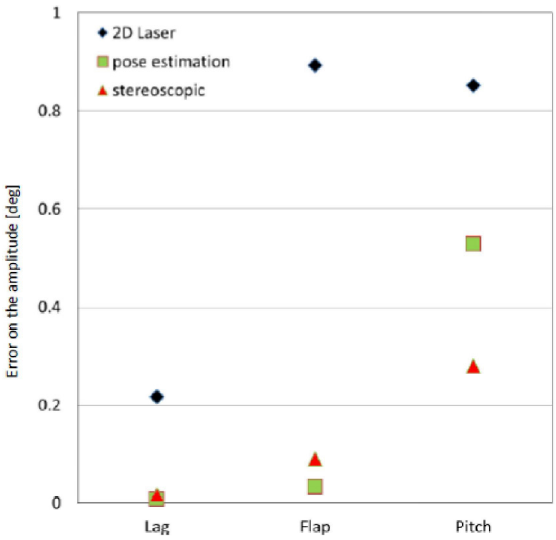

Fig. 6. Error on the amplitude for a pure flapping harmonic 1xrev time history.

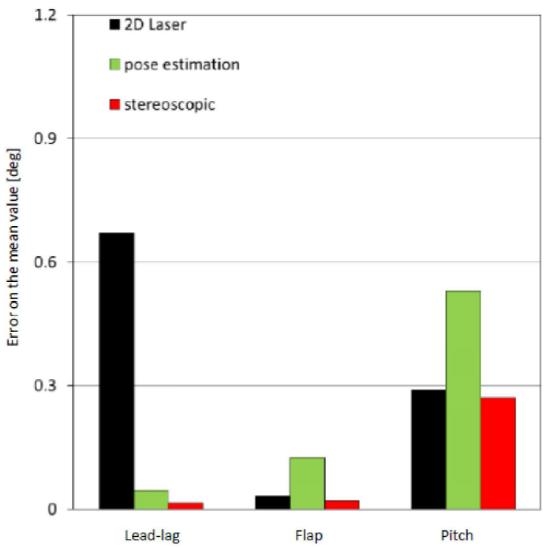

Fig. 7. Error on the mean value for a coupled lead-lag/flap/pitch time history corresponding to flight test data.

Globally, only the vision-based systems R3 and R4 allowed measurements of the mean values and first harmonic components of the three angles in compliance with the mandatory accuracy of 0.5 deg. The highest accuracy is achieved by the stereoscopic vision-based system R4, which achieves the desired accuracy requirement of 0.1 deg when considering the first harmonic.

These results compare favorably to those recently published in [13], where the accuracy of a magnet-based tail-rotor measurement system tested in simplified conditions that did not involve fully coupled blade motions, was achieved as 1.0 deg in lead-lag, 0.3 deg in flap, and over 1.0 deg in pitch.

Final Development and Testing

Based on the demonstrated results, the stereoscopic vision-based system concept was eventually selected to be brought to maturity in the final phase of the project. This process involved the improvement of the concept to obtain a definitive prototype, through further hardware and software development and testing, and the final integration on board an actual AW139 helicopter for ground and flight demonstration and testing.

The additional testing was performed on the definitive system fitted to the AW139 'beanie', a hat-shaped component placed on the top of the main rotor mast, above the hub. Figure 8 shows the installation of the system. The main elements of the rotor state measurement system are the two cameras and a LED lighting device to illuminate the target on the blade root. The necessary balancing masses are also seen. The control unit with its wirings to collect power and transfer data to and fro the airframe systems is housed inside the central cylinder.

Fig. 8. AW139 experimental beanie instrumented with the final rotor state measurement system.

We carried out numerical and experimental structural verifications to clear the design from possible stability problems, and to insure that sufficient structural strength was guaranteed for the elements supporting the sensor system, to prevent potential measurement errors. Subsequently, the final integrated system was tested at Politecnico di Milano laboratories for definitive validation before being installed on board. We considered again three types of test, conceived to assess both safety and performance characteristics:

- Type I tests: the integrated system was fitted to a massive shaker and, during the acquisition, subjected to realistic tri-axial vibration levels replicating actual flight data measured on board a AW139.
- Type II tests: the integrated system was installed on a non-rotating rig for accuracy assessment.
- Type III tests: the integrated system was installed on the A109MKII irondbird for centrifugal load testing during the acquisition, as well as for sunlight sensitivity assessment.

In Type I and Type III tests, sustained conditions up to 5 minutes were experienced, without the occurrence of any structural or functional problem. In Type II testing a novel bench was rigged using a 7-degree-of-freedom robotic arm available at the laboratories of the Politecnico di Milano. In this way, arbitrary static positions and motions to the target, fitted to the end-effector, can be imposed, spanning the full envelope of interest. This trials allowed to refine the acquisition and post-processing algorithms and confirmed the accuracy levels obtained in the preliminary test campaign with the candidate systems. Furthermore, we studied the integrated system sensitivity to sunlight by placing a calibrated light in multiple positions during the rotation, to check its ability in collecting measurements while illuminated by the sun during flight operations. Due to the convenient placement of the sensors below the beanie rim, and of the relatively high sampling frequency, currently set at 7 measurements per rotor revolution, a low influence of sunlight on global measurements was observed.

Following these extensive laboratory trials, the integrated system achieved the necessary clearance for installation on an instrumented AW139 prototype. A power supply unit and a stand-alone data acquisition equipment have been designed and implemented, fully compliant with the prototype helicopter configuration. Furthermore, data acquired from the MANOEUVRES rotor state measurement system are also conveyed to the helicopter Flight Test Instrumentation (FTI) system for on-board storage on mass memories.

Ground tests and flight tests, ongoing at the moment of writing, aim at showing the integrated rotor state measurement system functionality in real conditions. Also, metrological performance will be assessed, in comparison to an independent, contact-based measurement system that will be concurrently installed on board [2].

Concluding Remarks

A novel, vision-based system for the real-time measurement of the motion of a helicopter rotor blade has been designed, developed, and tested within the framework of the Clean Sky GRC5 MANOEUVRES project, in view of noise monitoring and advanced vehicle control applications. The system is currently undergoing the final demonstration trials which involve ground and flight tests on board a AW139 instrumented prototype.

The initial requirements for the system involved metrological performance and airworthiness items, as well as considerations related to a possible product-oriented application, apt to be fitted on current and future rotorcraft models. A structured path was followed in the system development, involving a technology survey, the conception of nine possible architectural solutions, the selection of the three most promising candidates, their full-scale implementation and testing, the final choice of the definitive solution, and its final implementation, testing, and integration on board an actual helicopter.

As a result, a stereoscopic camera system mounted above the rotor hub and pointing towards a target located in the blade root area was devised. Future communications will detail the results of the final demonstration in flight for this promising system which displayed full compliance to applicable requests, constraints and limitations to date.

Acknowledgements

The research leading to these results has received funding from Project MANOEUVRES, financed by the Clean Sky Joint Undertaking Programme under Grant Agreement N. 620068.

References

[1] McKillip R., A Novel Instrumentation System for Measurement of Helicopter Rotor Motions and Loads Data, American Helicopter Society 58th Annual Forum, Montreal, Canada, June 11-13, 2002.

[2] Colombo A., Locatelli A., Measuring Blade Angular Motions: A Kinematical Approach, 30th European Rotorcraft Forum ERF 2004, Marseilles, France, September 14-16, 2004.

[3] Trainelli L., Cordisco P., Gennaretti M., Grassetti R., Lovera M., Redaelli M., Rolando A., Zappa E., Innovative Rotor-State Measurements Enabling Helicopter In-Flight Noise Monitoring and Enhanced Attitude Control, American Helicopter Society 72nd Annual Forum, West Palm Beach, FL, May 17-19, 2016.

[4] Rolando A., Rossi F., Riboldi C. E. D., Trainelli L., Grassetti R., Leonello D., Redaelli M., The Pilot Acoustic Indicator: A Novel Cockpit Instrument for the Greener Helicopter Pilot, 41st European Rotorcraft Forum ERF 2015, Munich, Germany, September 1-4, 2015.

[5] Gennaretti M., Serafini J., Bernardini G., Castorrini A., De Matteis G., Avanzini G., Numerical Characterization of Helicopter Noise Hemispheres, *Aerospace Science and Technology* 52, 18-28 (2016) doi: 10.1016/j.ast.2016.02.013

[6] Trainelli L., Riboldi C. E. D., Bucari M., Observing the Angle of Attack of the Tip-Path Plane from Rotor Blade Measurements, 41st European Rotorcraft Forum ERF 2015, Munich, Germany, September 1-4, 2015.

[7] Bernardini G., Anobile A., Serafini J., Hartjes S., Gennaretti M., Methodologies for Helicopter Noise Footprint Prediction in Manoeuvring Flights, 22nd International Conference on Sound and Vibration Proceedings, Firenze, Italy, July 12-16, 2015.

[8] Gennaretti M., Bernardini G., Anobile A., Serafini J., Trainelli L., Rolando A.,

Scandroglio A., Riviello L., Acoustic Prediction of Helicopter Unsteady Manoeuvres, 41st European Rotorcraft Forum ERF 2015 Proceedings, Munich, Germany, September 1-4, 2015.

[9] Panza S., Lovera M., Rotor State Feedback in the Design of Rotorcraft Attitude Control Laws, *Advances in Aerospace Guidance, Navigation and Control*, edited by J. Bordeneuve-Guibè, A. Drouin and C. Roos, Springer International Publishing, Switzerland, 2015, pp.~205–225; ISBN 978-3-319-17517-1.

[10] Panza S., Bergamasco M., Viganò L., Lovera M., Rotor State Feedback in Rotorcraft Attitude Control, 41st European Rotorcraft Forum ERF 2015, Munich, Germany, September 1-4, 2015.

[11] Trainelli L., Gennaretti M., Bernardini G., Rolando A., Riboldi C. E. D., Redaelli M., Riviello L., Innovative Helicopter In-Flight Noise Monitoring Enabled by Rotor State Measurements, *Noise Mapping* (under review).

[12] Saaty Th. L., Decision Making for Leaders -- *The Analytic Hierarchy Process for Decisions in a Complex World*, RWS Publishing, Pittsburgh, PA, 1990; ISBN 0-9620317-8-X.

[13] Schank T. C., Schulte K. J., Smart Position Sensor for Articulated Rotors, American Helicopter Society 71st Annual Forum, Virginia Beach, VA, May 5-7, 2015.

DOI 10.5162/etc2016/2.4

Non-Intrusive Ice Accretion Detection and Measurement System

Ricardo M. U. Entz[1], Raphael de Andrade Jorge[2]
[1] *Airbus Group Innovations, 81663 Munich, Germany*
ricardo.entz@airbus.com
[2] *University of Sao Paulo, Engineering School of Sao Carlos*

Abstract
Precisely detecting and measuring accreted ice on aircraft requires the overcoming technical challenges posed by the harsh environment outside the aircraft pressure vessel. This work describes a novel ice detection and measurement system based on the principle of light spatial spreading [1]. The main advantages of this method are its robustness and the capability of measuring the target surface directly. Initial results on a proof of concept implementation show that the measurement principle is valid and can also be applied for thickness measurement.

Key words
aircraft ice measurement, light spatial spreading, image processing, optical properties of ice, multiple scattering

Introduction

In-situ measurement of ice accretion is a subject that has been overlooked in flight testing for its difficulty both in the technical and the theoretical aspects. Current icing tests employ indirect measurements such as monitoring of ice accretion on a standard cylinder and recording of atmospheric conditions. While these methods are simple and reliable, they do not substitute for ice accretion measurement on the target surfaces. Test bodies are subject to different flow conditions leading to discrepancies in collection efficiency and in accretion rate[2]. Current methods are especially limited in the development of new anti-ice systems; their validation requires precise detection and measurement of ice accretion where aircraft safety and performance are most affected - wings, elevators and rotors.

This work describes a non-intrusive ice accretion measurement system exploiting the phenomenon of spatial spreading of a light beam [1]. The propagation of light in ice is used for ice thickness measurement by Gagnon [3] and Ikiades *et al.* [4]. Gagnon assumes refraction as the source of spatial spreading, and measures total internal reflection to determine ice layer thickness. His hypothesis assumes in practice a planar, transparent ice layer. Ikiades et al., on the other hand, assume spatial spreading of the light beam from multiple scattering events, but their implementation requires the installation of optical fibres through the wind leading edge and the placement of sensors parallel to the wing spanwise direction. Such limitations demand costly and time consuming modifications if the system is to be applied in flight testing.

Our implementation can be described as a hybrid of both approaches, taking the non-intrusive installation of Gagnon but using spatial spreading as the measurement principle.

Ice accretion

Accreted ice is divided in two categories: rime ice and clear ice.

Rime ice is formed in conditions where supercooled water droplets freeze rapidly, trapping air bubbles in the ice matrix. The bubbles act as light scatterers and causes rime ice to have a white and opaque appearance. Clear ice, on the other hand, is transparent and homogeneous; it is formed in temperatures near the water freezing point, being the result of slower freezing process allowing air bubbles not to be trapped in the ice matrix [5, 6, 7, 8].

Between pure clear and rime ice there are infinitely many possible variations, with relative densities ranging from 0.92 (ice density) to less than 0.4 [9]. There is no clear cut classification to determine whether ice is clear or rime, leaving room for an intermediate category denominated mixed ice.

This work will present results for rime ice, except where indicated, as the general spreading behaviour is similar, and the remaining conclusions of feasibility and technical challenges are the same for both kinds of accretion.

Spatial spreading

Light travelling in non-homogeneous environments is subject to random scattering events, which combine reflection and refraction. The phenomenon can be represented by microscopic models which account for each scattering event in the ice [10]. Their application requires data on ice micro structure, namely size, shape and location of each bubble in the ice; the lack of detailed information precludes the application of microscopic models in our analysis.

On the other end of the model spectrum, macroscopic models based on the radiative transfer equation are capable of predicting some of the spreading behaviour based on average properties of the scattering medium[11]. A major application of such models is in the field of computer graphics, namely for rendering of clouds, smoke or milk.

One example of macroscopic formulation is proposed by Tessendorf [12, 13]. In his model, multiple scattering is assumed to be a stochastic process where light has a probability of being scattered (deflected) by an average (RMS) angle $\langle \theta^2 \rangle$. In cases where $\langle \theta^2 \rangle$is sufficiently small, an analytic point spread function (PSF) is found:

$$I\left(\vec{r}, \vec{n}\right) \propto exp\left(-\frac{\left(\vec{r} - \vec{n} l R(q)\right)^2}{2\left\langle \theta^2 \right\rangle b l^3 h(q)}\right) \qquad (1)$$

Where:

$I\left(\vec{r}, \vec{n}\right)$ is the resulting radiance profile;

$\vec{r}$ and $\vec{n}$ are the direction vectors perpendicular and parallel to the light propagation;

a and b are the absorption and scattering coefficients;

$l = \left(ab\left\langle \theta^2 \right\rangle\right)^{-1/2}$ is a characteristic length relating scattering and absorption phenomena;

q is the propagation length (ice thickness) divided by l;

$R(x) = (cosh(x) - 1)\, sinh^{-1}(x)$; and

$h(x) = (x sinh(x) + 2(1 - cosh(x)))\, sinh^{-1}(x)$.

The coefficients a and b can be estimated using the Mie theory[14, 15, 16].

In the following sections this model will be compared with the obtained results.

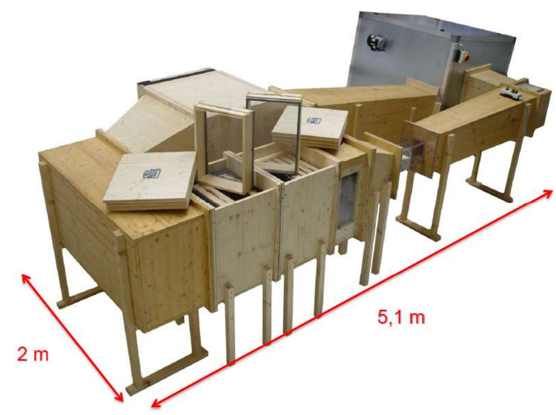

Figure 1: iCORE wind tunnel. Test section dimensions: $150 \times 100 \times 450 mm^3$

Proof of concept measurement

In order to confirm that the physical phenomenon is measurable, a proof of concept experiment was executed.

The test campaign was carried out in the iCORE (Icing and Contamination Research Facility) wind tunnel (Fig. 1)[17]; it is capable of reaching a free stream temperature down to $250K$ at $M0.45$. Water droplets with diameters in the range $10 - 25\mu m$ are created and injected in the free stream before the test section. There is full optical access in the test section, making iCORE ideal for the implementation of our measurement system.

The test model was a NACA0012 wing equipped with a removable insert used for direct measurement of accreted ice and the testing of different ice phobic coatings (cf. Fig. 2). For the reference measurement, instead of manually measuring the ice thickness, we placed a camera along the spanwise direction of the wing. This camera provided direct measurement of the ice accretion; for reference transparent, graduated side plates (baffles) were used (Fig. 3).

The measurement of the spatial spreading was performed by projecting a laser line perpendicular to the wing spanwise direction. The images were recorded with a camera placed on the same plane as the laser sheet, as shown in the diagram of Fig. 2. The spreading phenomenon observed with this configuration is illustrated in Fig. 4.

The acquired images were corrected for camera distortions and projection error, then the intensity profile of the laser line was sampled at several cross sections.

DOI 10.5162/etc2016/2.4

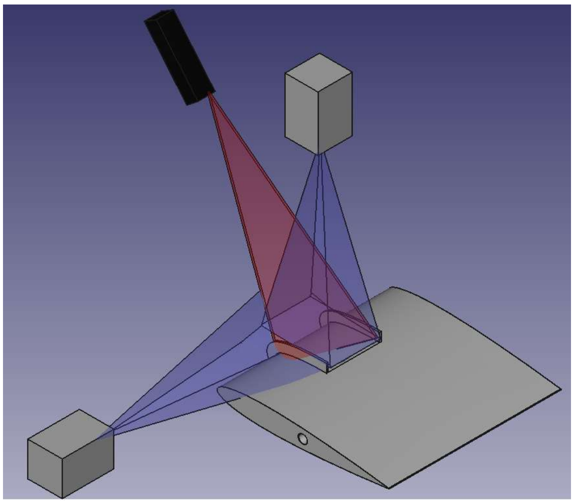

Figure 2: Full experimental set up, including wing with insert, two cameras (parallel to the wing chord for direct ice measurement and perpendicular for beam spreading measurement), and laser sheet (red plane).

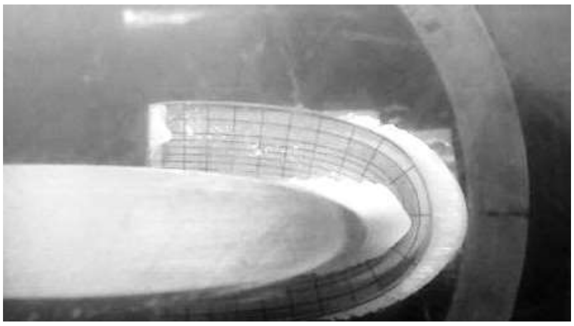

Figure 3: Side camera view with graduated baffle.

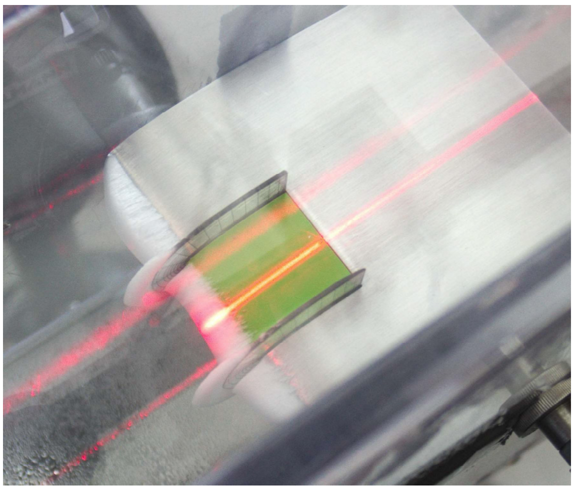

Figure 4: Visualization of the spatial spreading phenomenon on rime ice.

The sampled profiles were normalized to the range $0 \leq I(x) \leq 1$. Following the methodology of spreading measurement proposed by Premože [18], we assumed that the sections had an approximately Gaussian profile reducing the measurement of the line width to a curve fitting problem using the following parametric equation:

$$I(x) = exp\left(-\left(\frac{x-\bar{x}}{\sigma\sqrt{2}}\right)^2\right) \qquad (2)$$

Where the values of $\bar{x}$ and σ were adjusted to obtain the best fitting profile to the measured laser intensities. The value of the coefficient σ is then used to determine the full width at half maximum ($FWHM$) of the profile using the following formula:

$$FWHM = 2\sigma\sqrt{2ln2} \qquad (3)$$

The image processing steps are illustrated in Fig. 5.

Initial results

Initial results show that the spreading phenomenon is measurable using image processing techniques. Fig. 6 shows a time series of the measured laser line width. This series starts with an increase in measured width corresponding to the beginning of the water injection. In two intervals, between images 500-1000 and between images 1500-2000 the water injection was interrupted for the measurement of constant thickness values.

The actual ice thickness could not be measured with the reference camera due to problems in the measurement methodology, namely:

Wing curvature - As the wing chord was small (100mm), the leading edge curvature posed a challenge for the positioning of the laser, as most configurations had a specular reflection point which presented different spreading behaviour as other regions, as shown in Fig. 6.

Erosion of accreted ice - The measurement of stabilized values (without water injection) could not be performed due to erosion of the ice layer by the wind.

Reference camera parallax error - The side camera had to be positioned near the wind tunnel (ca. 200mm) because of limitations with its optics and resolution. This prevented reliable measurement of the accreted ice layer because of parallax error.

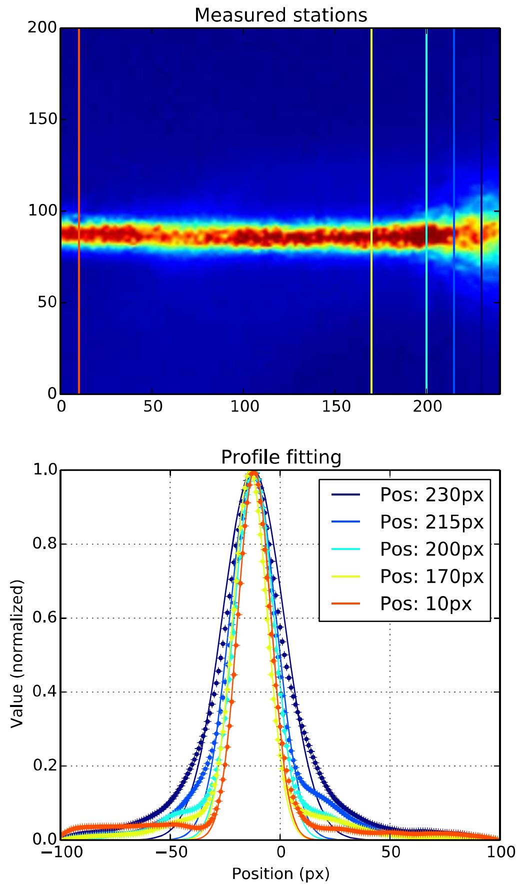

Figure 5: Visualization of the profile fitting methodology. Upper figure shows the laser line with the selected cross-sections for measurement. Lower figure shows normalized intensity profiles (dots) and fitting profiles (lines).

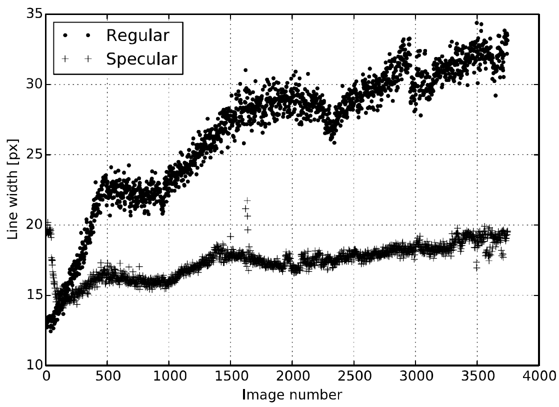

Figure 6: Raw result of first measurements. Results are presented for a regular measurement station (solid dots) and a station on the specular reflection caused by the wing curvature (open dots).

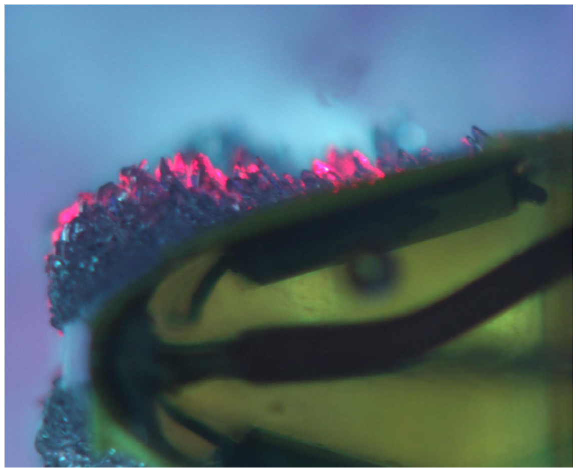

Figure 7: Image of side camera after improvement of experimental setup (cf. Fig. 3 for original images). Clear ice, original resolution - $3000 \times 2000px^2$. The lack of accreted ice on the leading edge is due to the anti-ice system proposed by Strobl[19].

Improvement of the experimental setup

In order to improve the results quality a series of changes was adopted for the second experiment. First, a larger wing with chord of 250mm was used. By correctly choosing the angle of attack, it was possible to have the accretion in a region with less curvature than the leading edge of the previous wing. This gave more flexibility to the positioning the laser-camera group, and also reduced the interference of curvature in the measurements.

The second modification affected the reference camera. A digital single lens reflex (DSLR) camera was used with a long focal length lens (f = 432mm in 35mm equivalent) to allow the positioning of the camera far from the wind tunnel ($>$ 1.5m). This configuration was denominated quasi-telecentric, and it reduced parallax error to less than 0.1mm in the measurement range.

The improvement on the reference images allowed better observation of the accretion structure and a direct measurement with estimated uncertainty of less than 0.5mm. Fig. 7 shows an example of the improved image quality.

In subsequent measurements we made no attempt to measure stabilized ice shapes, as the erosion phenomenon could not be controlled in the icing wind tunnel.

Results of second measurement series

The improvements in the second measurement

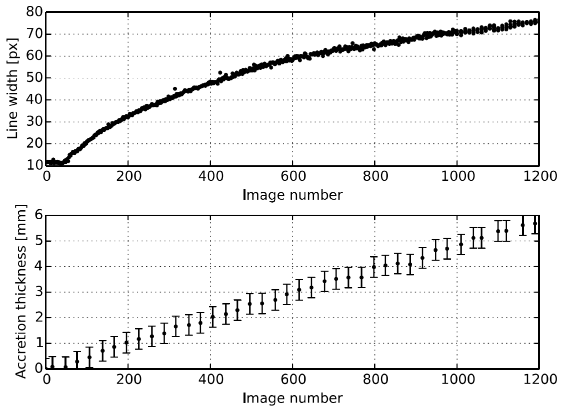

Figure 8: Second measurement results. Maximum spreading width is ca. 10mm.

series allowed comparison between light spreading and ice thickness results, as shown in Fig. 8. Light spreading and ice thickness are strongly correlated, with a Pearson product-moment correlation coefficient of 0.96. However, we found that the relation between variables is non-linear.

Comparison with theory

We assume ice as a solid water matrix with spherical air bubbles, as proposed by Carras and Macklin[6]. This approximation allows the direct application of the Mie theory for the determination of the absorption and scattering coefficients needed for the application of the theoretical model.

Choosing a bubble diameter of $5\mu m$ in rime ice with density $\rho = 400 ^{kg}/_{m^3}$ the following values are obtained:

$$a = 0.047 m^{-1};$$

$$b = 3.11 \times 10^5 m^{-1};$$

$$\langle \theta^2 \rangle = 0.31;$$

$$l = \left(ab \langle \theta^2 \rangle\right)^{-1/2} = 0.015 m$$

Fig. 9 shows the predicted intensity profiles and the measured width for a $1.2mm$ wide laser beam as input. There is no qualitative nor quantitative agreement between the calculated and measured behaviour (cf. Figs. 9 and 8). The predicted width for a $5mm$ ice layer is around $100mm$, an order of magnitude off the measured value. In addition, the curve trend is not the same.

We found that the general behaviour predicted by theory does not change appreciably by varying ice density and bubble mean diameter within

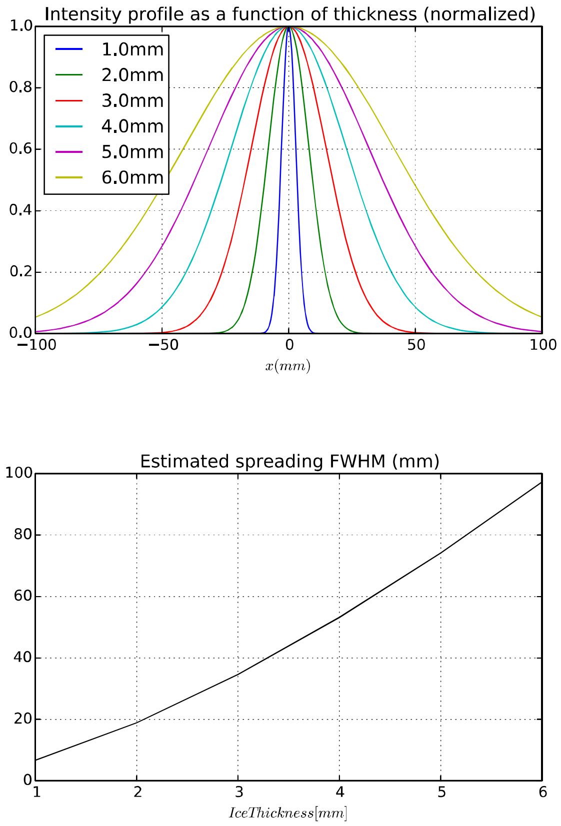

Figure 9: Resulting intensity profiles and FWHM widths as predicted by the theory.

expected values for ice. This indicates that other effects dominate the spreading in this setup.

Application

Despite the disagreement between theory and measurements, the results showed to be repeatable for similar ice types. This allowed us to create a calibration table to determine the ice thickness from light spatial spreading. The system was successfully applied in a measurement campaign in the iCORE facility [19, 20, 21].

Conclusion

This paper presented a novel system for ice accretion measurement. Its main advantage is its simplicity, allowing its implementation using low-cost equipment.

It was shown that measurement using image processing techniques produces measurable results starting from less than $1mm$ in ice thickness. The available theory, however, does not predict the measured behaviour, requiring an empirical calibration for each ice type.

The system, as described in this paper, was applied successfully for measurement campaigns in the iCORE facility. For application in other fields, however, it requires further theoretical development, notably for the extension of the measurement range without the need for exhaustive parameter sweep calibration.

References

[1] F. Olchewsky, M. Weber, and R. M. U. Entz, “Système et procédé de mesure de l’épaisseur de givre sur une surface, notamment d’aéronef, à l’aide d’un motif lumineux généré par diffusion dans le givre,” 2014 (patent to be published).

[2] C. S. Bidwell and M. Papadakis, “Collection efficiency and ice accretion characteristics of two full scale and one 1/4 scale business jet horizontal tails,” in *SAE General Aviation Technology Conference and Exposition sponsored by the Society of Automotive Engineers*, 2000.

[3] R. E. Gagnon, “Method and apparatus for remote detection and thickness measurement of ice or liquid layer,” 1994.

[4] A. Ikiades, G. Howard, D. J. Armstrong, M. Konstantaki, and S. Crossley, “Measurement of optical diffusion properties of ice for direct detection ice accretion sensors,” *Sensors and Actuators, A: Physical*, vol. 140, pp. 24–31, October 2007.

[5] R. Gent, N. Dart, and J. Cansdale, “Aircraft icing,” *Philosophical Transactions of the Royal Society of London. Series A: Mathematical, Physical and Engineering Sciences*, vol. 358, no. 1776, pp. 2873–2911, 2000.

[6] J. N. Carras and W. C. Macklin, “Air bubbles in accreted ice,” *Quarterly Journal of Royal Meteorological Society*, vol. 101, pp. 127–146, 1975.

[7] A. Heinrich, R. Ross, G. Zumwalt, J. Provorse, V. Padmanabhan, J. Thompson, and J. Riley, *Aircraft Icing Handbook*, vol. 1. Federal Aviation Administration, 1991.

[8] T. Ratvasky, B. Barnhart, and S. Lee, “Current methods for modeling and simulating icing effects on aircraft performance, stability and control,” in *AIAA Atmospheric Flight Mechanics Conference and Exhibit*, 2008.

[9] W. C. Macklin, “The density and structure of ice formed by accretion,” *Quarterly Journal of the Royal Meteorological Society*, vol. 88, pp. 30–50, 1962.

[10] W. R. C. Somerville, B. Augui, and E. C. L. Ru, “Accurate and convergent T-matrix calculations of light scattering by spheroids,” *Journal of Quantitative Spectroscopy & Radiative Transfer*, vol. 160, pp. 29–35, 2015.

[11] C. F. Bohren, “Multiple scattering of light and some of its observable consequences,” *Am. J. Phys*, vol. 55, no. 6, pp. 524–533, 1987.

[12] J. Tessendorf, “Radiative transfer as a sum over paths,” *Physical Review A*, vol. 35, 1987.

[13] J. Tessendorf, “Multiple-forward-scattering in volume rendering of participating media,” 2006.

[14] C. Mätzler, “Matlab functions for Mie scattering and absorption,” tech. rep., Institute of Applied Physics, University of Bern, 2002.

[15] R. G. Grainger, J. Lucas, G. E. Thomas, and G. B. L. Ewen, “Calculation of Mie derivatives,” *Applied Optics*, vol. 43, pp. 5386–5393, 2004.

[16] D. W. Hahn, “Light scattering theory,” tech. rep., Department of Mechanical and Aerospace Engineering, University of Florida, 2009.

[17] T. Hauk, T. Strobl, and D. Raps, “Implementation and calibration of the icing and contamination research facility (iCORE),” in *ILASS-Europe, 25th European Conference on Liquid Atomization and Spray Systems*, 2013.

[18] S. Premože, M. Ashikhmin, J. Tessendorf, R. Ramamoorthi, and S. Nayar, “Practical rendering of multiple scattering effects in participating media,” in *Proceedings of the Fifteenth Eurographics conference on Rendering Techniques*, pp. 363–374, 2004.

[19] T. Strobl, S. Storm, D. Thompson, M. Hornung, and F. Thielecke, “Feasibility study of a hybrid ice protection system,” *Journal of Aircraft*, 2015.

[20] T. Strobl, R. Adam, R. M. U. Entz, and M. Hornung, “A hybrid system for ice protection and detection,” in *International Conference on More Electric Aircraft (MEA2015)*, 2015.

[21] T. Strobl, S. Storm, D. Raps, and T. Hauk, “Device and method for deicing and/or preventing ice formation and profile element and aircraft having such a device,” May 14 2015. US Patent App. 14/539,491.

DOI 10.5162/etc2016/2.5

Latest technology in piezoelectric vibration- and pressure sensors and their benefits for measurement

Stefan Meyer

PCB Synotech GmbH
Porschestrasse 20-30
41836 Hückelhoven

Abstract

To measure on turbines, engines and equipment at high temperatures vibrations or pressures, the sensors must meet extremely high demands. Special materials in the sensor design, for sensor housing and cable as well as the sensor element itself, is necessary to achieve extremely high operating temperatures. The new piezoelectric crystal UHT-12™ (Ultra High Temperature 1200°F/650°C) allowed an operating temperature of up to 700°C for sensors with charge output.

In addition, the measurement results are highly accurate, low noise (no popcorn noise) and temperature stable. Using this special synthetic crystal, also ICP® vibration sensors with extremely low temperature coefficients have been developed.

The result is reflected in an improvement in the accuracy of the amplitude response of the entire measurement chain over the entire temperature range from 29% down to 4% .

This is a significant improvement in measurement uncertainty compared with sensors that use ferroelectric ceramics as measuring material.

With a clever choice of materials and manufacturing technologies are now also ICP® vibration sensors up to a working temperature of 180°C possible.

This challenge has been implemented in a miniature triaxial accelerometer with a weight of 1 gram.

Integrated low-pass filter in ICP sensors find increasing popularity because it reduced the chance of amplifier saturation and increase the useable frequency range.

It saves so much trouble in applications where the sensor does not just see periodic signals, but also transient events or strokes.

Against amplifier saturation by acoustic emission we can also integrate mechanically filters.

Key Words

ICP, UHT-12™, Low Temperature Coefficient (LTC), Ferroelectric Ceramics, Piezoelectric Materials, Spurious Noise, Popcorn Noise,

Material Selection

Piezoelectric sensors are made from both naturally piezoelectric crystals and artificially polarized polycrystalline ferroelectric ceramics. The choice of sensing material depends on environmental and performance requirements. Each material has unique features and advantages, which characterize its performance in various applications. Natural crystals tend to provide the highest temperature range and the lowest (or zero) pyroelectric output. However, ferroelectric ceramics offer extended frequency range and smaller size for equivalent charge output. Table 1 organizes material types ranked by temperature and pyroelectric susceptibility.

Natural versus Ceramic Crystals

Material	Natural Piezoelectric Single Crystals	Ferroelectic Ceramic, Piezoceramics	Piezoelectric Coefficient pC/N	Maximum Useable Temp °C	Pyroelectric
UHT-12 shear	X		12	650	No
UHT-12 compression	X		6	650	No
Quartz shear	X		4	250	No
Quartz compression	X		2.2	200	No
Tourmaline shear	X		3.5	650	Yes
Tourmaline compression	X		1.8	650	Yes
Bismuth Titanate		X	21	500	Yes
Bismuth Titanate derivates		X	14	600	Yes

Table 1
Examples of Piezoelectric Material

Single, natural crystals, such as quartz and tourmaline, are inherently piezoelectric. Most natural occurring single crystals that are used for sensors are grown in laboratories rather than mined, resulting in consistent quality with reduced risk of supply. In addition, the man-made aspect of a natural crystal has enabled development of new, higher performance variations. The exception is tourmaline, only available through mining, and thus the supply chain is uncertain and the cost becomes prohibitive for use in sensors.

Ferroelectric ceramic materials are not inherently piezoelectric because upon chemical formulation they are in a random polycrystalline orientation. For the ceramic to become piezoelectric the individual dipoles of each crystalline structure must be aligned. The alignment process involves applying a high voltage to the material to align polar-regions within the ferroelectric ceramic element. After the artificial polarization process is complete, known as poling, the crystal may undergo a pre-aging process and then can be used in a sensor.

Ferroelectric ceramics exhibit significantly higher sensitivity or charge output per imposed unit force. A commonly used high temperature sensor material, BiTi (Bismuth Titanate), has an output three to four times its natural crystal counterpart, quartz. BiTi can be used to temperatures as high as 950 °F (510 °C). Various compounds may be added to the ceramic material to alter sensor characteristics but high temperature ranges come at the expense of sensitivity. Drawbacks of BiTi include the requirement for a carefully controlled environmental condition inside the sensor and for a perpetually stabilized partial pressure level of Oxygen to preserve its operational characteristics.

The new UHT-12™ crystal is quite happy in any atmosphere and these sensors are backfilled with inert gas such as Argon or Nitrogen. UHT-12™ crystal does not exhibit any pyroelectric output and provides for reliable operation at temperatures approaching 1200 °F (650 °C). While the raw charge output of this material is not as high as commonly used BiTi, additional benefits of the material include a relatively low capacitance and higher insulation resistance at operating temperature, which results in a low noise operation when used with a differential charge amplifier.

One often overlooked comparison of BiTi and UHT-12™ is the ability to use the material in a sensing element configuration for use in a shear orientation. Physical and process limitations prevent BiTi from operating in a shear mode and thus legacy high temperature sensors are still manufactured with compression mode sensing elements. On the other hand, UHT-12™ may be used in a shear configuration if properly prepared. The benefits and characteristics of these two sensing element configurations are discussed further.

Insulation Resistance

Very low IR (insulation resistance) may produce signal output drift in a charge amplifier; however, this is not usually a problem in a properly designed accelerometer meeting product specifications and when used with a properly designed charge amplifier. Existing accelerometers with ferroelectric ceramics may have IR values around 100k Ohm at 905 °F (485 °C), whereas the UHT-12™ crystal will have values approximately ten times larger at the same temperature. While the noise in any charge amplified system depends on a number of factors, the larger IR value in UHT-12™ is an important benefit, as the system noise gain is a function of the feedback resistor in the charge amplifier and the input resistance. Larger IR values reduce system noise gain.

It is shown in Figure 1 below that the resolution of the new 10 pC/g sensor is comparable to that of a traditional higher sensitivity 50 pC/g BiTi based sensor for this reason. In addition to being a factor in determining the inherent resolution of the measurement system, the system noise gain also has the characteristic of amplifying externally imposed noise (as with RFI, for example) and therefore is an important characteristic. The new UHT-12™ accelerometers will have a susceptibility to externally imposed noise which is approximately 8 dB (2.5x) less than a comparable system based on ferroelectrics ceramic.

DOI 10.5162/etc2016/2.5

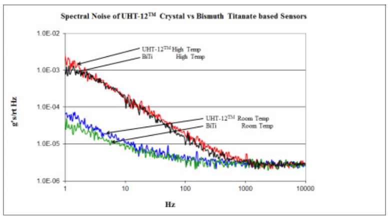

Figure 1
Noise Comparison of UHT-12^{TM} 10 pC/g Accelerometer vs. BiTi 50 pC/g

Spurious Noise Sources

When subjected to temperature gradients, compression element assemblies will experience differential expansions/contractions of the various mating surfaces and the preload bolt. When differential expansion is large enough, the sensor may create a corresponding electrical output as stress is released and the parts instantaneously slip against each other. In addition, ferroelectric ceramic as well as tourmaline elements are pyroelectric, which means charge is created simply due to changes in temperature. In the time domain, the output from these two spurious noise sources may appear as a step output that decays at a rate governed by the signal conditioner's time constant. Example data is shown in Figures 2 for a compression accelerometer design.

The data reveals positive going spike output of approximately 13 g's during the ramp up to 900 °F, at time 1170 minutes. When integrated to velocity the result is 100 in/sec pk-pk. The spiking phenomenon repeats during the cool down phase, in the negative direction with a greater rate, yet at slightly lower amplitude per occurrence.

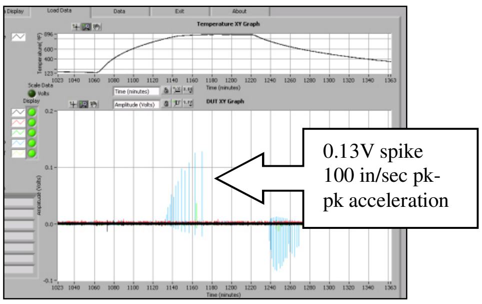

Figure 2
Typical Noise Data from Compression Mode Accelerometer during Temperature Change

The new UHT-12™ shear design, which only responds to shear stress, is significantly more tolerant of thermal changes because those changes occur in the primary axis of the accelerometer, and the sensing element is oriented 90 degrees to the primary axis of vibration. The shear mode UHT-12™ accelerometer consistently shows low amplitude spike levels. The fact that the UHT-12™ also has no pyroelectric output is an additional advantage during thermal transient events. An example data set for the thermal response of the new UHT-12™ shear design is shown in Figure 3.

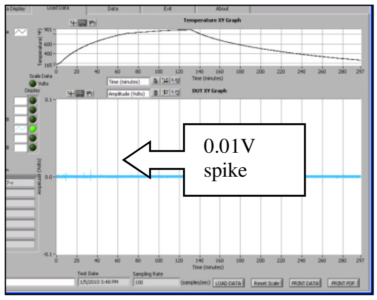

Figure 3
Typical Noise Data from Shear Mode Accelerometer during Temperature Change

To engine balance instrumentation, a step output from an accelerometer will look like a large low frequency signal. The problem occurs during or soon after a change in temperature, such as going from idle to full power for take-off.

Piezoelectric Sensors with new single crystal Material UHT-12™

UHT-12™ is a new crystal designed for more accurate, low noise measurements during temperature variations. UHT-12™ reduces the effect of temperature variation. Pyroelectricity phenomenon may occur during large temperature fluctuations, generating "spikes" and disrupting behavior of the accelerometer and the test results. Accelerometers made with UHT-12™ technology have improved data quality.

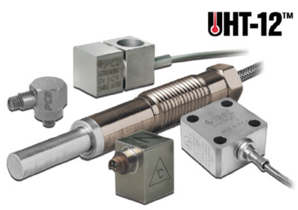

Figure 4
Vibration- and Pressure Sensors with UHT-12™ Technology

Solution to improve measurement uncertainty

For certain applications, it is necessary to know the accuracy of the overall vibration measurement chain. It will be noted that the largest percentage of inaccuracy is supplied by the sensor. The reason is the transformation of the physical quantity in the electric and many other environmental factors including the temperature.

The influence of temperature on a vibration sensor describes the temperature coefficient. The temperature coefficient describes the relative change of a physical property with a given change in temperature, with respect to a specified reference temperature. The quantity of interest is mostly a material property. In piezoelectric sensors is that the sensing material. As discussed, there are a wide range of piezoelectric materials for different applications available.
An outstanding advantage for sensors with ICP technology can be achieved through the use of UHT-12™. The temperature coefficient is improved compared with ferroelectric materials by a factor of 10. Practically this results in an improvement of the amplitude response over the entire temperature range from 29% down to 4% (Figure 5).

The LTC-Series (Low Temperature Coefficient) sensors are designed for wide operating temperature, and good broadband measurement resolution, making ideal for powertrain development and powertrain NVH application, or for any vibration measurement requiring tight control of amplitude sensitivity over wide thermal gradient.

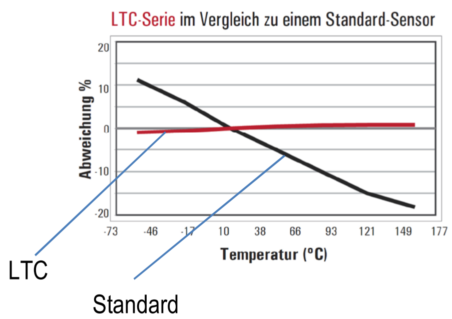

Figure 5
Low Temperature Coefficient (LTC) vs. Standard ICP®-Vibration Sensors

Figure 6
Selection of Accelerometers with LTC (UHT-12™)

Progressive miniaturization and + 180 ° C continuous use for ICP technique.

For most sensors for vibration measurement technology, the advantages of the ICP technique have prevailed. They cannot, however, be used where the ambient temperature exceeds the capability of the built-in circuitry. These are for special versions (HT) + 162°C.
With the model HT456B01 the +180 ° C limit is reached. In addition, extreme miniaturization is achieved.
This triax vibration sensor is unique. The 6,3 mm cube weighs 1 gram only.
A step in the right direction for climate chamber tests and measurements on engines or exhaust system.

Figure 7
Triaxial ICP® Accelerometer Model HT356B01 (+180°C)

What's wrong with my Piezoelectric Accelerometer

A frequently asked question about measurements made with piezoelectric (PE) vibration sensors is related to the measurement parameters. After completing a test and evaluating data, test engineers may observe obvious signs of problems within the data that was collected.
Many factors can affect the data from a PE accelerometer including measurement range, the measurement input amplitude, the measurement input frequency content, and the data acquisition sample rate. For example, input amplitude levels that are greater than the sensor's measurement range will saturate the amplifier. Input frequency content at or near the sensor's resonant frequency may also saturate the amplifier. The high Q-factor at resonance will cause the sensor to enter an overload recovery state and no meaningful data can be acquired (even with post-process filtering in your DAQ). Data of

DOI 10.5162/etc2016/2.5

saturated amplifier will appear as illustrated in Figure 8 and 9.

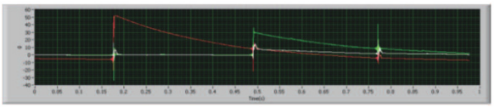

Figure 8
Input amplitude saturate amplifier

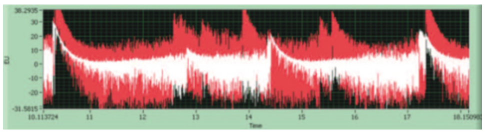

Figure 9
Input frequency near the sensor's resonant frequency saturate amplifier

Sensors with single or two-pole low pass filters will decrease the chance on amplifier saturation and increase the useable frequency range. Low pass filters will attenuate (suppress) signal generation at or near the resonance frequency of the sensor. This counteracts the gain (high-Q) factor caused by the sensor's mechanical resonance. See figure 10.

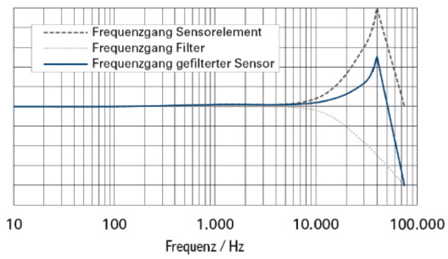

Figure 10
Unfiltered and Filtered Sensor Response

ICP®-Accelerometer with integrated low pass filters (in extracts)

Model 355M102: 10 mV/g, LP-Filter, LTC, isolated, 8 Gram

Model 356A61: 10 mV/g, Triax miniature, LP-Filer, 4 Gram

Models 339A30/A31:10 mV/g, Triax, LP-Filter, LTC, 5,5 / 4 Gram

Conclusion

- High Temerature Sensors with UHT-12™ Sensing Material are Temperature stable, has a low noise output and can used up to 700°C.
- The new crystal shows NO pyroelectric spikes in temperature change (Popcorn Noise).
- ICP®-Sensors with UHT-12™ have an extremely low temperature coefficient. It has a particularly positive effect on the accuracy and temperature stability of the measuring chain.
- UHT-12™ sensors in shear sensing element configuration, limits susceptibility to environmental influence such as temperature transients, base strain and transverse sensitivity errors.
- ICP®-Technology reached +180°C Operation Temperature, sub miniature triax available.
- Integrated low-pass filter protect the sensors for saturation and generate high signal quality.

References

Bob Metz, PCB Piezotronics, Inc "Design and Selection Criteria of High Temperature Accelerometers for Aerospace Propulsion".

DOI 10.5162/etc2016/2.7

Fiber optic acoustic pressure sensor with high dynamic range and low noise

Markus J. Schmid[1], Dr.-Ing. Mathias S. Müller[1], Bernd A. Kuhnle[1],
Dr.rer.nat. Michael W. Bauer[2], Reinhard Pongratz[2],
Dr.-Ing. Andree Altmikus[3]
[1] fos4X GmbH, Thalkirchner Str. 210, 81371 Munich, Germany, www.fos4X.de
Markus.Schmid@fos4X.de
[2] AIRBUS GROUP Innovations, Willy-Messerschmitt-Str. 1, 82024 Taufkirchen, Germany
[3]Wobben Research and Development GmbH, Borsigstr. 26, 26607 Aurich, Germany

Abstract:
Fiber optic sensors for temperature, strain and acceleration are well established and widely available. Here, we present a new all fiber optic acoustic pressure sensor with low noise and high dynamic range and high bandwidth. The sensor is capable of operating in very harsh environment including humidity, water, temporal overpressure, electro-magnetic noise, lightning and environmental impact such as heavy rain and thus applicable in field. Data measured during a laboratory test campaign in a flow channel in cooperation with AIRBUS GROUP Innovations are presented and compared to existing electrical microphones.

Key words: aeroacoustics pressure sensor, fiber optic, static and dynamic pressure sensing, rugged

Motivation

Objects moving through air or overflowed by air generate sound because of unsteady pressures around them. [1] By measuring the acoustic emission in wind tunnels or in the field the sources can be detected and optimized. Furthermore microphones in airfoils enable acoustic pitch control by measuring the transition of boundary layer from laminar to turbulent flow. [2]

State of the art microphones have dis-advantages, which avoid the said applications, like weak and therefore drawn back membrane, unsteady spectral characteristics and resonances, electro-magnetic interference, and corrosion.

Introduction

Here we present the fiber optic pure glass static and acoustic pressure sensor (see Fig. 1). The fos4X GmbH developed the sensor together with Wobben Research and Development GmbH, the research division of ENERCON GmbH, for static and dynamic pressure sensing in rotor blades of wind energy converters.

The sensor with dimensions of 2x3x10 mm³ has a glass membrane with 1.7 mm in diameter. Due to the small size the resonance frequency is above 250 kHz. The sensor is capable of measuring static and acoustic signals with a linear transfer characteristic up to 40 kPa, and tested for nondestructive overpressures of 10 bar. With the flat design the optic microphone can be integrated in surfaces with minimal aerodynamic disturbance to the test specimen. The open membrane at the surface of the sensor enables acoustic measurements without spectral characterization, because of constant frequency response to around 80% of the resonant frequency of 250 kHz.

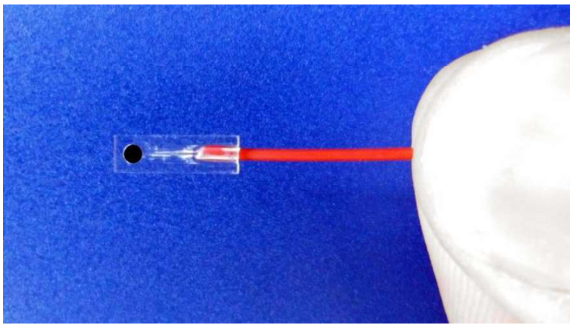

Fig. 1. Fiber optic pressure sensor fos4Pressure by fos4X for static and dynamic pressure sensing.

The fiber microphone is a passive optic sensor without any conductive material, and therefore robust against water, humidity, and corrosion. Due to the absence of conductive material the sensor is inherent immune to electro-magnetic interference, and furthermore to lightning strikes.

DOI 10.5162/etc2016/2.7

The fiber optic sensor is connected to the measurement device via a telecommunication single mode fiber with very low attenuation, so large distances up to several hundred meters between sensor and measurement device can be realized.

Test setup

In cooperation with AIRBUS GROUP Innovations fos4X executed a verification test of the fiber optic pressure sensor in an AIRBUS flow channel. The flow channel is capable of laminar air flow up to 212 m/s.

For the test we integrated two fiber optic pressure sensors (fos4Pressure-1 and -2) by fos4X and one electric reference microphone (electric microphone) by Brüel&Kjær in the surface of the test nozzle's outlet (see figure 2).

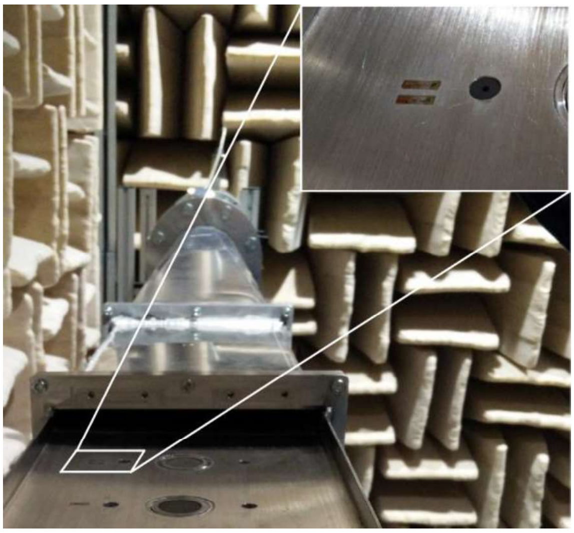

Fig. 2. Flow channel by AIRBUS GROUP Innovations with integrated fiber optic pressure sensors fos4Pressure-1 and fos4Pressure-2 (square objects in detail view), and the electric microphone (round object in detail view).

Before the measurement we calibrated both sensor types using an acoustic calibrator with a single tone at frequency 1 kHz and amplitude 114 dB(SPL). Figure 3 shows the power spectral density of the fiber optic pressure sensor and the electric microphone measuring the calibration signal including the optic sensor noise floor of 0.001 Pa²/Hz and therefore the broadened spectrum compared to the electric microphone. The noise floor of the electric microphone is lower in comparison. Therefore the widening of the spectrum and the noise floor is not illustrated in figure 3.

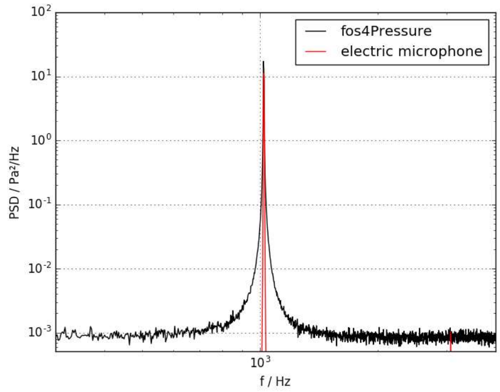

Fig. 3. Power spectral density of the fiber optic pressure sensor fos4Pressure and the electric microphone of the calibration signal 1 kHz, 114 dB(SPL).

In reference to the electric microphone the fiber optic pressure sensor exhibits a deviation of 1 Hz in frequency and 0.2 dB(SPL) in amplitude.

The integration of microphones in surfaces can disturb the air flow of the tunnel and therefore generate undesirable acoustic emission. For the test we applied a high density wire mesh over all sensors to reduce the parasitic flow noise. To compare the influence of the surface integrated microphones and the wire mesh we executed two similar runs with and without wire mesh.

Results

Figure 4 illustrates the power spectral density of electric and fiber optic microphone at flow speed 46 m/s. We executed two runs at that flow speed, one with and one without the high density wire mesh.

The electric microphone – compared to the fiber optic sensor – is strongly influenced by the wire mesh at frequencies greater 2 kHz.

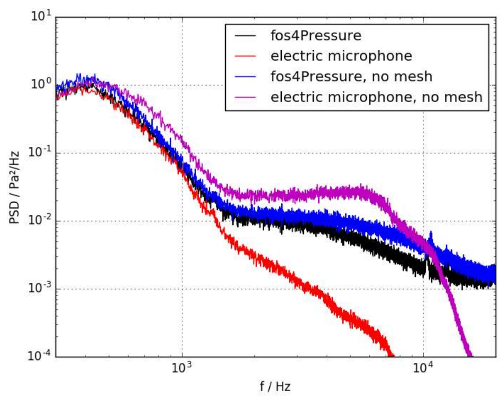

Fig. 4. Power spectral density of the fiber optic pressure sensor fos4Pressure-1 and the electric microphone at wind speed 46 m/s. The plot shows

two runs; with and without high density wire mesh over the sensors.

In figure 5 the power spectral density of electric and fiber optic microphone at flow speed 92 m/s is presented for two runs with and without high density wire mesh.

At around 10 kHz a dominant parasitic acoustic resonance appears for the electric microphone, which is reduced by the applied mesh. The optic sensor shows no significant influence by the mesh.

The colored noise between 1 kHz and 2 kHz appears on both sensors and independent of the mesh, and therefore can be interpreted as background noise of the flow channel due to aerodynamic obstacles.

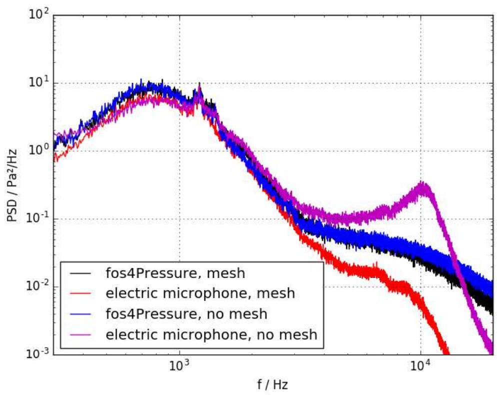

Fig. 5. Power spectral density of the fiber optic pressure sensor fos4Pressure-1 and the electric microphone at wind speed 92 m/s. The plot shows two runs; with and without high density wire mesh over the sensors.

As further benchmark figure 6 illustrates the power spectral density of the two fiber optic pressure sensors fos4Pressure-1 and -2 at 92 m/s flow speed without high density wire mesh. The geometrical distance of the two optic sensors is about 6 mm, therefore sound waves up to approximately 10 kHz appear as pressure equilibrium on both sensors. The illustrated power density plots of the neighboring optic pressure sensors show the expected high spectral correlation.

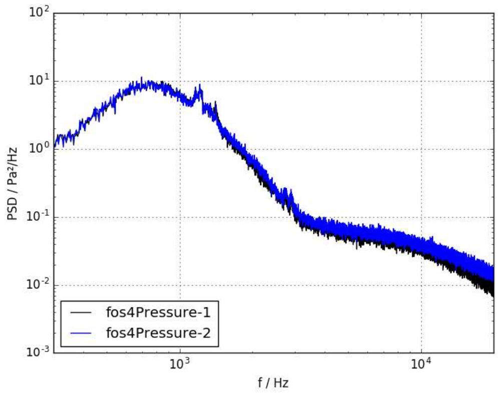

Fig. 7. Power spectral density of the fiber optic pressure sensors fos4Pressure-1 and fos4Pressure-2 at wind speed 92 m/s without high density wire mesh.

Conclusion

We demonstrated a fiber optic pressure sensor with high dynamic and frequency range. Because of all glass construction the sensor can be installed in harsh environments including humidity, water, temporary overpressure, and electro-magnetic noise. Due to the small dimension the sensor is capable of surface integration. Furthermore the real surface membrane enables measurements of noisy boundary layers with minimal aerodynamic and aeroacoustics disturbance.

In cooperation with AIRBUS GROUP Innovations we applied a benchmark test with conventional electric microphones in a flow channel.

The fiber optic pressure sensor shows good performance compared to conventional microphones. Furthermore, due to the open surface membrane of the optic sensor, no parasitic acoustic disturbances occur.

References

[1] T. J. Müller, Aeroacoustic measurements, Springer (2002); doi: 10.1007/978-3-662-05058-3

[2] W. Nitsche, Strömungsmesstchnik, Springer (1994); doi: 10.1007/978-3-662-10111-7

DOI 10.5162/etc2016/3.1

An Adaptable Constraints-based Metadata Description Language (MDL) System for Flight Test Instrumentation Configuration

Michael Neumann[1], Jessica Moore[1], Satyaraj Pantham[2],
Myron Moodie[3], Patrick Noonan[3], Austin Whittington[3]
[1] The Boeing Company, Seattle, Washington, USA
michael.neumann@boeing.com, jessica.d.moore@boeing.com
[2] Consultant, Seattle, Washington, USA
srpantham@gmail.com
[3]Southwest Research Institute®, San Antonio, Texas, USA
mmoodie@swri.org, pnoonan@swri.org, austin.whittington@swri.org

Abstract:

The current telemetry device provider landscape is diverse in approach and capability, and choosing the "best" devices for a particular solution inevitably involves a mix of devices from different vendors. Devices have differing capabilities and limitations. Each vendor offers their own proprietary configuration toolset. In the past it has been possible for the flight test community to build system-wide configurations at very high cost by reverse engineering business rules for existing flight test configuration systems. In addition, technical proficiency was required by the users for every tool in this widely varying set or risk being locked into a single vendor. Historically, the Boeing Flight Test Computing System (FTCS) and similar systems have device rules tightly coupled into the software, and so as device constraints change or new devices are added, significant work is required to update and maintain the software. To solve this problem, Boeing and Southwest Research Institute (SwRI) developed a constraints-based and MDL-centric configuration management approach. Based on this approach, the Boeing Company has developed its own MDL based Modular Instrumentation Setup Tool (MIST) to manage and simplify the configuration of new devices for their users. This paper highlights the success of this approach on the 737 MAX program and discusses how constraints were implemented, how validation occurs, and shows how the system can be rapidly updated with new constraints based on device changes or user insight.

Key words: Flight Test Instrumentation, Constraints, MDL, XForms, XPath.

Introduction

Data acquisition devices used in onboard flight test networks are currently supplied by providers with their respective de facto methods for configuration. In addition, the capabilities and limitations of the devices is widely variable across the spectrum of telemetry device vendors. This often results in a complex and time consuming effort for instrumentation setup as users have to learn and deal with different configuration software and processes.

Recent standardization efforts in flight test networks provide hope for managing this complexity. One example is the Metadata Description Language (MDL) created by the US DOD integrated Network-Enhanced Telemetry project as an interoperable flight test device configuration language and growing in use for both commercial and military flight test applications. An application providing a standardized data transfer medium enables it to interact with multiple applications serving similar business objectives.

In this paper, we will discuss the benefits of using MDL for configuration augmented by multiple levels of constraints in XForms as part of a new system that removes large portions of the complexity and cost for adding new devices and maintaining existing devices. The goal has been to create a system that is vendor agnostic and provides reusability and extensibility. MDL and the constraints representation external to

MDL serve as key components for creating valid device configurations.

We will describe the constraints and MDL backgrounds, followed by description of the chosen constraints format. The final section will explain the implemented Modular Instrumentation Setup Tool (MIST) and its use of constraints and MDL.

Constraints

A constraint is, by definition, a limit or restriction placed on a person or thing, or on an action or behavior. In context of a device within a Flight Test Instrumentation system, a set of constraints defines the limits of how the device may be programmed to perform a specific task. Since each vendor offers their own proprietary configuration toolset and capabilities, the set of constraints for a particular vendor's device must be known in order to build a valid programming file for the device.

A user of this device requires some sort of user interface in which they can define all the necessary inputs to build the programming file. Constraints on these inputs may be simple field validations, such as a set of allowable values or upper and lower limits. There may also be more complex constraints in which values entered in one or more fields affects the constraints on one or more other fields.

In addition to the user interface constraints, there are typically some parameters which the device requires but which the user does not want to explicitly specify. Constraints may be used to limit these parameters to a single value which can be entered into the file with no user interaction. Again these may be simple constraints which limit the parameter to a single value, or they may determine the single value based on the value of other parameters.

For any given system or device, there can be multiple sets of constraints from different sources. The vendor will provide a set of constraints that describe the capabilities and limitations of their device settings. The user of the device may want to add additional constraints based on their own preferences. For a system of devices, there may be additional vendor and/or user constraints describing the capabilities and limitations of the system.

A constraints validation system, then, must be able to describe all of the possible constraints of the device or system, and must be able to validate a configuration against multiple sources of constraints.

Similar to typical flight test systems, Boeing's Flight Test Configuration System has historically embedded all of these constraints in code. Any change or addition to the constraints was costly due to the significant work required to update and maintain the software.

Our many years of building Flight Test Configuration Systems has shown that a *correct-by-construction* approach is needed. The *correct-by-construction* approach prevents invalid configurations being created at any level. Whether by using constraints or hard-coded business rules, you bypass the need to have continual communication with the device being configured as you negotiate and validate the programming file incrementally.

Since input is validated in real-time as the user builds up their configuration, any invalid pieces or new cascading requirements are immediately made known to the user. Additionally, by using *correct-by-construction*, the passing of the completed file to the device for final proofing becomes just a formality. This could otherwise be a step which, stemming from some small value change since the last pass, requires a total rework of the programming file.

By externalizing the constraints into modular XForms files, constraints can be easily modified without changing the code of the configuration system. This paper describes a method by which these constraints files may be used to validate a user-defined MDL configuration for a Flight Test Instrumentation device.

Metadata Description Language (MDL)

Metadata Description Language (MDL) is a common configuration language that describes requirements, design choices, and configuration information for Telemetry Network Systems (TmNS) [1]. MDL encapsulates the setup data of the network nodes and measurement devices, along with their units of measurement. In a typical flight testing computing system, the analog and digital data acquisition units (DAUs) are represented by the network nodes, and various transducers and sensors are represented by devices.

The setup information in MDL is represented in a hierarchical style and is highly readable through any standard XML editor, text editor or even in a browser. Readers can easily walk through the data tree, its nodes and associated data. The data items are defined as elements in terms of tags and attributes. The attributes can lead to utilizing highly efficient search engines or intelligent data mining agents.

Along with simplicity, MDL also comes with all the great advantages of XML which include a wide variety of data types. MDL can also serve as the single-document view for dispersed data across multiple devices, and an MDL instance document supports localization and internationalization.

Except for some trivial cases, an instrumentation setup process for flight testing is cumbersome and may require multiple sessions of interaction with setup systems. A smart client is a preferable choice since it can support the setup data to be saved temporarily into some local data storage. MDL can serve as an XML based data repository for holding device configuration data in one or more offline sessions. When the setup system is online, the MDL configuration can be stored in the flight test database.

MDL has another significant advantage: flight test setup data becomes reusable. A particular flight test setup stored in an MDL instance document contains the content relevant to that test process such as the instrumentation setup and device data. This data may either be utilized in other testing scenarios for the same airplane, or for similar test scenarios of other airplanes, thereby leading to a considerable saving on time and effort.

Flight test systems contain numerous devices that read and format data, and multiplexers that combine and transmit data to other onboard systems. The task of setting up these devices becomes unwieldy if vendors supplying the instrumentation do not conform to a common standard. The flight test instrumentation setup engineers and technicians have to produce multiple data files for each of the vendor device categories. MDL was created and standardized by the integrated Network Enhanced Telemetry (iNET) program to provide a single vendor-neutral standard which promotes interoperability between these systems, devices, and applications which may have been developed by different organizations and vendors [2].

An MDL instance document represents a comprehensive description of a given flight test setup. This kind of a standard configuration language enables flight testing processes to be executed with better portability of setup data among the flight testing systems as well as other enterprise systems that include those that are geographically distributed for other lines of business. The standardization enables reuse of instrumentation setup in other testing scenarios with significantly reduced effort. The standardization of instrumentation setup data can lead to other advantages like reusability of application tools. In the next sections to follow, we will discuss the many advantages in using MDL and the challenges that arise in the development of flight test setup applications.

Constraints Combined with MDL

XML in general uses the common language of XPath to address parts of an XML document [3], and perform calculations and checks upon target elements. This language is used for defining element relationships and schema constraints in XML Schemas, node tests and matching in XSLT, and many other applications along the breadth of the XML ecosystem. For MDL specifically, XPath is used within the schema to define uniqueness on fields and referential constraints checking that elements refer to the correct targets.

For the purposes of vendor and user constraints, XPath is again used. These new layers of constraints go beyond merely checking that the document is valid as an MDL file, which forces their presence external of the MDL schema. For the application of constraints described in this paper, these XPath constraints were built up in XForms, another XML-based technology made for gathering and processing XML data [4]. XForms was chosen for its clear separation of the validation required to check the constraints and the presentation which gives the result of that validation to the user, as well as its direct use of XPath to simplify the application of the constraints to the MDL documents and the availability of a variety of existing tools for processing XForms.

Vendor constraints can exist in many forms, from logic buried deep within compilers to information contained in user manuals to a spreadsheet of requirements. All of these constraints are candidates to be written in XPath and used in a system such as MIST. Due to the set of circumstances present at the beginning of this project, the constraints were not available in XForms directly from the vendor. Consequently, the vendor constraints files were developed by Boeing and SwRI using knowledge of the device capabilities. We were first provided with a list of compiler error messages from the vendor of the device. By consulting with the vendor and through knowledge of the instrumentation field, we were able to translate these error messages into English-language descriptions of the target constraints. From these descriptions, we could create the XPath which checks the description's conditions in a straightforward manner.

There are many industry-standard XML tools that we used for editing, testing, and validating our XML instance documents. However, a custom tool was needed for the XForms and constraints specific functionality we required. As such, we made use of the SwRI-developed XFORGE toolkit to generate several XForms from the MDL schema, each of which contained the presentation layer for the desired elements necessary to constrain the user's input. We then added bindings for the XPath constraints to the XForms model and added descriptive error messages to inform the user of any MDL elements and fields which did not meet the device's requirements discovered by the constraints. These completed XForms were then used by MIST to provide the constraint validation capabilities.

A sample constraint follows in Figure 1. The constraint encodes the English-language sentence "A SignalRange must have two ConditionParameter bounds whose values are not inverted." The constraint therefore checks that the lower bound (the ConditionParameter with a greater-than or greater-than-or-equal sign) is less than the upper bound (the ConditionParameter with a less-than or less-than-or-equal sign).

```
<xf:bind
    ref="mdl:SignalRange"
    constraint="count(mdl:ConditionParameter) ge 2 and
        number(mdl:ConditionParameter[mdl:ConditionOperation
        = ('&gt;=', '&gt;')]/mdl:ConditionValueFloat) lt
        number(mdl:ConditionParameter[mdl:ConditionOperation
        = ('&lt;=', '&lt;')]/mdl:ConditionValueFloat)">
```

Fig. 1. Constraint Example

Modular Instrumentation Setup Tool (MIST)

As part of the 737-MAX flight test program, the Boeing Company has implemented a Modular Instrumentation Setup Tool (MIST) for the configuration of new flight test devices that can be programmed using MDL setup files. The tool works on multiple platforms (Windows, Linux), is scalable for additional modules and provides a vendor agnostic interface where changes to the tool can be limited by having vendors provide business rules in a constraints format using XForms and XPath expressions. Configuration was successfully provided for all new devices for the 737-MAX test airplanes.

MDL was chosen as a vendor interface because the first devices for which MIST provides the programming files are able to accept MDL files. In addition, the Boeing team wanted to conform to the emerging iNET and MDL standards. The tool is capable of interfacing with vendor hardware that can accept different XML schemas, which can also be validated by using the XForms/XPath constraints mechanism.

MIST uses vendor and Boeing specific constraints to validate user input and provide immediate feedback for any values that are not within the constraint specified limitations. Boeing instrumentation users are able to configure a stack of modules through instant feedback for the data they have entered, and save complete or incomplete configurations for later work. If a configuration has been completed with no errors, and successfully compiled by a vendor provided compiler, the resulting MDL file can be sent to the actual devices using the Boeing Flight Test Computing System (FTCS).

Future enhancements will include an onboard version of MIST that will allow users to dynamically configure MDL devices, and a standalone version that will provide users the capability to work on configurations offline and import changes back into the system.

The MIST MDL interface connects the tool to FTCS or any other flight test system that can ingest MDL data. For vendor devices, the tool interfaces using programming files in MDL format based on the vendor and Boeing specific constraints that have been provided and are being used during the validation stage in the process.

DOI 10.5162/etc2016/3.1

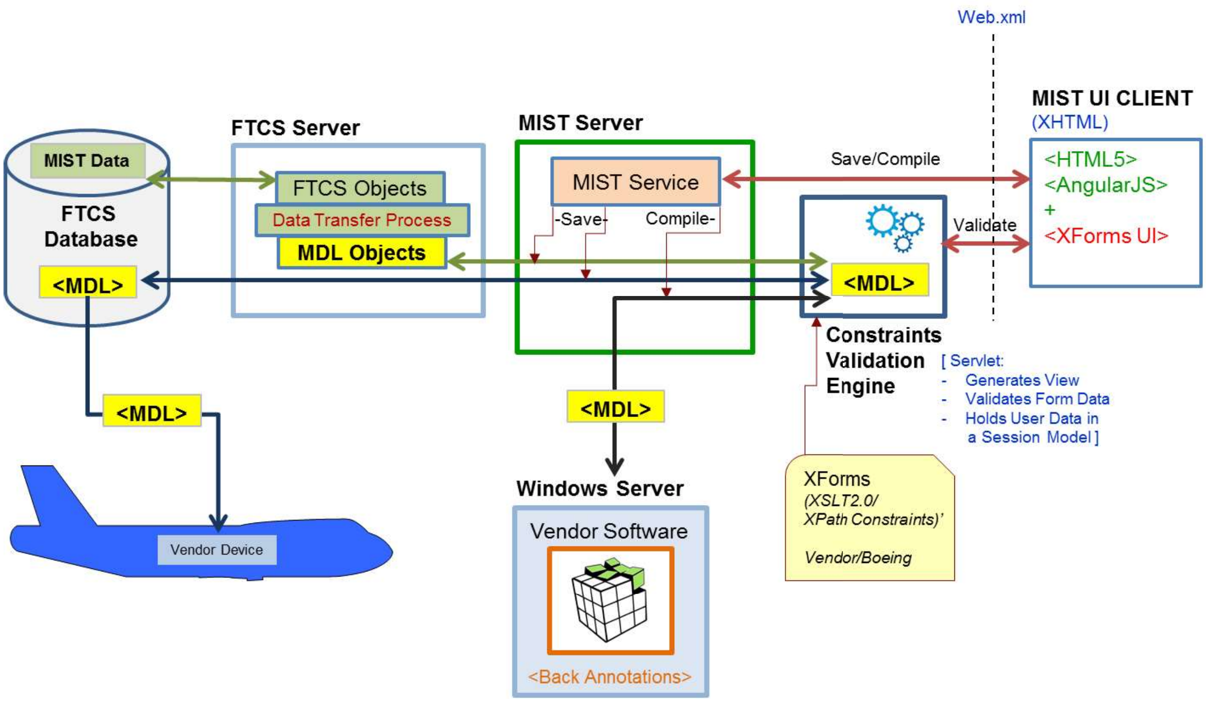

Fig.2. Modular Instrumentation Setup Tool (MIST) Logical Architecture.

Constraints based validation is at the center of the MIST architecture and provides the means for not having to hard-code vendor specific business rules and to reverse engineer vendor provided software that creates the final configuration files for their devices.

MIST accepts constraints in an XForms/XPath standardized format. The constraints are loaded into a third party validation software that will instantly verify user input which can also include additional non-editable vendor constraints and Boeing user and system constraints. An MDL object model for storing the configuration data is internally maintained by the third party validation software, which allows it to instantly verify user input. During the compile and save actions from the MIST tool, the MDL object model will be exported and sent to the vendor software or the FTCS database as a MDL data stream or physical file. Updating any existing constraints will be performed by the vendor or Boeing user in the appropriate constraints file. Only the addition of new constraints that include an update to the MIST user interface will involve new coding.

MIST opens in a Web browser and configures stacks with varying numbers of modules. The user interface contains XForms segments that allow the third party validation software to display components that are constrained in addition to non-constrained components that display information from the FTCS database. Users interactively validate their data using the vendor and Boeing provided constraints and receive instant constraint validation errors in the user interface for their selected input (Figure 3).

Fig. 3. Instant Constraint Validation

Boeing instrumentation users configure a stack by airplane and test number. Measurements can be added to channels for each module, and measurement properties can be modified on different panels with the application providing instant constraint validation. Figure 4 shows an example user interface with proprietary information having been replaced with generic data.

DOI 10.5162/etc2016/3.1

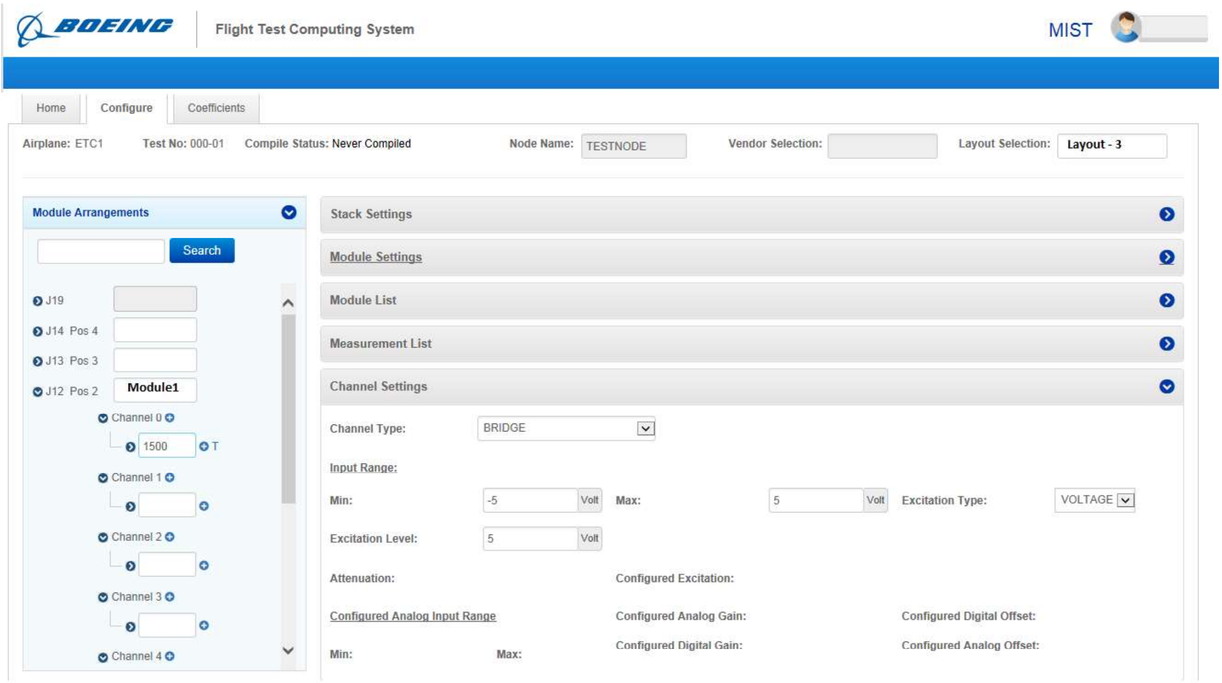

Fig.4. Modular Instrumentation Setup Tool (MIST) Screenshot.

The vendor software is called during the compile process and back-annotates additional vendor specific data to the MDL file that gets returned to MIST and stored in the MDL object model inside the third party validation software. At any time, the current configuration can be saved to the FTCS database as MIST data and the complete MDL file for further loading on a vendor device once the validation process returns no configuration errors.

Conclusion

An adaptable constraints-based MDL system for flight test instrumentation configuration has been successfully implemented by Boeing for the 737-MAX flight test program. Constraints allow for faster integration of new hardware devices since business rules are no longer hard-coded and can be directly provided by the vendor. The end user experiences operational efficiencies through early validation and a process that can guarantee a valid configuration file for the devices in use. The responsive system avoids mistakes and provides an easier learning curve for new instrumentation engineers.

Constraints provide maintenance benefits by allowing engineers and vendors to only modify a constraints file without developers having to write additional code, except in situations where there are new user interface changes required. This also allows Boeing engineers to work their own user constraints and can lead to a future system where engineers can be allowed to directly create programming files for new or modified constraints

The use of XForms to capture the constraints has been shown to provide the flexibility necessary to describe the constraints of complex network flight test instrumentation. When combined with MDL this provided a capable and vendor independent device configuration approach that should scale to a wide variety of future devices.

References

[1] iNET system Management and Configuration, ETC 2010

[2] Metadata Description Language: The iNET Metadata Standard Language ITC 2009

[3] https://www.w3.org/TR/xpath/

[4] https://www.w3.org/TR/xforms/

DOI 10.5162/etc2016/3.2

Heterogeneous Acquisition Systems Managing

José Antonio González Pastrana

Flight Test Instrumentation-TAEVM2

jose.o.gonzalez@airbus.com

Airbus Defence and Space. Getafe. Spain.

Abstract:
When someone coming from the industrial environment arrives to Aerospace Industry suffers a shock because of the very different type of acquisition systems used.
Industrial equipment is usually reliable over the years and cheaper than aerospace equipment.
We will find here why it is very difficult to adapt industrial equipment to FTI environment.

Key words: FTI, Data Acquisition System, SCADAS, Database, PLC(*Programmable Logic Controller*).

Introduction

Automation is a very well known subject in every industry environment. When coming from industry environment to the aerospace industry one wonders why it is not generally used COTS industrial hardware and software. Here we'll find the answer.

Automation equipment shares many features with FT(*Flight Test*) ones, however FT has special characteristics that makes it difficult to use COTS automation software and hardware packets to do the work.

Some reasons have to be with special characteristics that FT projects deal with.

Test/Automation systems are made of hardware for data acquisition and control.

Another part of the system is the display and recording software.

Both hardware and displaying/recording software are configured by databases. We'll find if it is better to use your own database.

A good example would prove the differences between using external tools and your own ones.

Finally, conclusions show the convenience or not for using, FT oriented hardware, your own databases and displaying/recording software. In fact we find that FT oriented hardware is usually the best option. And that SCADAS can't be used in our field.

Industrial/FT projects´ differences

FT projects features are the following:

Some of them last long time, so it makes that requirements, equipment and staff change during the project.

Some others last shorter, so it urges a quick answer.

The aim of a Flight Test is to record the evidences to certificate a system or a whole aircraft.

In the industrial environment, you usually have a project which is developed, installed and will remain there while it is economically feasible or it had an opportunity cost when not updated. The goal in an industrial project is to have the installation payed-back as soon as possible while giving a competitive advantage. Reliability is also a must because the production has to be stable all the time.

Differences between FTI and Industrial Hardware

The industrial hardware for automation is usually the PLC, although there are other systems designed mainly for Process Industries, called DCSs (Distributed Control Systems).

We'll focus on PLCs because they are the most similar to the FT hardware called DAUs (Data Acquisition Units).

In their origins PLCs were aimed to substitute the old relays installations of the industries. Later on, they evolved to be used in many different situations. They usually have a lot of digital I/O (Inputs/Outputs), a certain quantity of analogical I/O, very low amount of control loops (PID) and a small memory to make calculations. They don´t usually have in sum more than 4 Mbytes. These amounts are approximate as they change a lot from low to high-end equipment.

The inputs use to be 4-20 mA or 0-10 V in PLCs. Since sensors can be very far away, up to hundreds of meters from the PLC, they are commonly joined to equipment called transmitters that convert signal levels into 4-20 mA levels.

The rates for pooling inputs can be high, but when the number of I/O increase, the acquisition cycle can increase a lot too. This acquisition cycle can also dramatically vary due to the internal calculations when PIDs or other modern controls are used.

PLCs are aimed to be reprogrammed by the maintenance staff that is used to dealing with electrical equipment and also understand digital logic made from relays. Although every vendor usually has a proprietary language for its PLCs, they commonly have options to program their equipment with languages complying with some industry standard. The most common language is Ladder. Sometimes reprogramming is necessary to be carried out by very skilled engineers due to the complexity of the systems.

In the industrial field temperatures are neither too high nor too low as in aerospace, although in special cases it could happen. The same thing happens with vibrations. Wet environments can be found also in the industry. Placing the hardware in a suitable enclosure controls both the temperature and humidity.

In the vast majority of cases in the industry, the hardware can be installed apart to avoid suffering from harsh conditions.

Synchronization is not a big concern here, but it can be in special situations. i.e. A Net Time Protocol server can be enough for this purpose. The goal of PLCs is to control an installation over time.

In FT one finds DAUs, equipment designed for acquiring data, which have many inputs and a very small number of outputs for some important functions. They can be suitable for the laboratory, the workshop and the field. FTI Data Acquisition Units also have special characteristics due to the environment they are in.

DAUs usually have dedicated inputs for every kind of sensor, such as PT-100 resistors, Bridges, +/- 10 volts, etc. There also can be some adaptors, mainly installed to protect the aircraft installation. A DAU can carry different kinds of inputs by means of different kinds of available cards, such as those for the PLCs.

In DAUs, data acquisition rates have a high variability, from temperatures, needing around 1Hz, to pressures or electrical parameters needing above kHz.

As previously said PLCs can have high rates but the number of I/O signals can change the acquisition cycle. In DAUs the acquisition rate for every signal is defined and maintained forever as long as the requirements are not changed.

The characteristics of Acquisition rates and synchronization are very important in FT but not as demanding in the industries. The usual acquisition rates in FT go from 1Hz to several kHz. The industrial environment usually does not have such high acquisition rates or even synchronization for their purposes.

DAU configuration files usually are based on proprietary languages that each vendor creates for its equipment. Lately, however, there is a tendency to use some kind of standard file (xml) although not necessary.

An additional difference between PLCs and DAUs is that DAUs, specially the airborne ones, are ready to acquire Data Buses, while PLCs simply don't have this possibility. For PLCs, buses are for internal/external communications, but they never are seen as a possible source for acquisition/measurement.

DAUs have to be hardened to support extreme environmental conditions. It is usual to find temperatures from -40ºC to 80ºC and even more. Hardware sometimes has to support very high vibrations due to engine and/or aerodynamic phenomena. The big difference with PLCs is that aircrafts always lack room, so DAUs have to be placed wherever possible.

Displaying Software Differences

Displaying applications are necessary to check the acquired data.

These applications need to take the raw data from any data stream or CVT (Current Value Table), then make all necessary changes, and finally display them in a convenient way. Changes comprise calibration, bit extraction, mask application, etc.

The displays used go from simple numerical objects to moving graphics, representing the real instrumentation of the industry/aircraft.

The software used in the Industry to display data is the SCADA, a software packet aimed at supervising and controlling tasks. Also, it saves data in a database or any type of file.

Because SCADA is software that runs in computers, some hardware, such as a PLC is required to really control the system, to acquire signals and generate the outputs. (See Fig. 1) That data is taken from the PLC and served to the SCADA through some protocol, such as OPC[1], TCP/IP or any other.

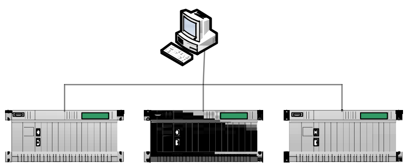

Fig .1.- SCADA-PLC installation

An example of a typical SCADA in the industry could deal with around 2.000.000 Data Tags. Each of them is acquired at 1 Hz or less. So the bandwidth that SCADA can manage is less than 32 Mbit/s. There are more data tags that can be managed by scalability, increasing the budget and the complexity of the system.

The standards used by SCADAs to communicate with the hardware are not compatible with standards used by FT.

In this sense, displaying specialized COTS software is there to help display data in the FT field. This kind of software complies with the standards used by the aerospace environment.

In FT, the GSS (Ground Station Software) takes the role of the SCADA and the DAU does the same with the PLC.

As said before, SCADAS save data into files or databases. The same thing happens with GSS. Each one will do exactly the same on its own. The big difference here is that GSS software will not control the system in any way like SCADAS do.

Databases Similarities

A great similarity between configurations for SCADA-PLC and GSS-DAU is that each one has its own configuration databases. All of them, SCADA, PLC, GSS and DAU have their own separate database.

SCADAs and PLCs need to be configured separately. Nowadays the tendency is to configure any software/equipment through GUIs (Graphical User Interface) that makes things easier. These tools have databases internally that have to be filled in. These databases schemes must represent their corresponding part of the measurement chain. Fig. 2 displays a measurement chain. From the sensor to the multiplexor included they belong to PLC and then, from the multiplexor to the PC they all form part of the SCADA.

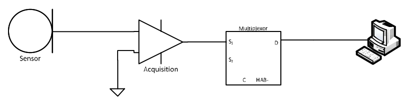

Fig. 2.- Measurement chain

FT Databases have a similar configuration. In this case we are talking about Instrumentation and Display databases. The main characteristic for an Instrumentation database is that it must represent the “Measurement Chain” for every parameter we want to acquire, including the multiplexer. See fig. 2.

Display Databases have to contain all the objects that can be seen on a screen, and they also must contain information for the Displaying Software, so that it can obtain the data from the streams sent by the multiplexor.

Therefore, Databases must have all the information about the configuration of a system.

Example using COTS vs Internal Tools

When someone starts thinking about the tools needed to comply with the customers’ requirements in FT field, many possibilities are found. We will answer a number of questions to show what can be done in FT field.

Industrial Hardware.

PLCs are not suitable for FT requirements, mainly due to the synchronization strategies used in FT. They don't support the standard synchronization buses that FT works with. Besides, their acquisition cycle is not easily predictable.

However there is a type of industrial hardware that is based on DSPs (*Digital Signal Processors*), is highly configurable with standard languages (i.e. C, C#) and can be used for a special purpose. At the same time, some FT DAU makers are offering similar acquisition cards. This shows that DSP based equipment can be very useful under certain situations, if they can bear the environmental conditions.

FTI Hardware.

Due to environmental conditions, electrical and communication standards this is the best solution for hardware.

Industrial Software.

Industrial Software can't be used because, at the present time, the communication standards are incompatible with communication standards used in FT. In addition, the bandwidth supported by SCADAs is not enough for the FT field requirements.

COTS Telemetry Software.

In many situations this solution could be the best. Usually this COTS solution works with the corresponding de-multiplexing hardware. However, if this software needs to be adapted to the client's types of data streams, then the COTS solution would not be the best.

In this case, the best solution would be for the customer to develop its own GSS. This solution will give the customer a great flexibility to expand the software capabilities, and independence at the cost of developing hours. i.e. In Airbus DS-Getafe an internal GSS that can support 65 Mbits/s has been developed. This is much more than the figures shown previously by SCADAs.

Databases.

GSS used to come with their own database. In the case where the customers would choose to develop their own software, a database has to be acquired.

There are a lot of Databases suppliers. There are also Free/open databases available that can do the work exactly as very expensive proprietary ones.

In any case a scheme has to be developed for the database resembling the Instrumentation and Displaying functions. Additionally applications to fill in the tables from the database also have to be developed.

Comparative study.

At this time we have reached to the conclusion that almost always we'll have to use FTI hardware for our solutions.

Now we'll make a comparison to see whether it is more convenient to select internal databases from the hardware and display software or to use our own developed databases and display software.

Let's have a DAU with 30 analog inputs and 12 buses. Each bus it has 30 parameters.

In case A we'll use the GUI supplied by the vendor of the COTS hardware. The display software will be COTS too and we will fill it in by its GUI. We do this because internal databases are configured trough the GUI.

In case B we'll use applications to fill in our own database and the display software will be the one we developed.

We will do the exercise two times to see how much time it takes to do the work. The second time the voltage limits will be changed to analogic parameters and will change the parameters to acquire from the buses.

Tools to convert the output configuration from DAU to input configuration in GSS are supposed to last the same amount of time in case A and B.

In the second part of the exercise we will try to copy all we can from first part.

A)

Fig. 3.- Internal databases

B)

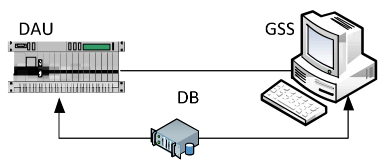

Fig.4.- External database

DOI 10.5162/etc2016/3.2

First part exercise:

Item	A	B
DAU	Time	Time
Place cards	5 min	5 min
Configure analog cards	30 min	30 min (1)
Configure buses cards	6 hour	6 hour (1)
Output	1 hour	1 hour
GSS		
Analog	30 min	30 min
Buses	6 hour	6 hour
Total	14h 5m	13h 5m

Second part exercise:

Item	A	B
DAU	Time	Time
Copy configuration	1 min	1 min
Place cards	0 min	0 min
Configure analog cards	30 min	30 min (1)
Configure buses cards	6 hour	6 hour (1)
Output	1 hour	1 hour
GSS		
Copy configuration	1 min	1 min
Analog	20 min	20 min (1)
Buses	5 hour	5 hour (1)
Total	12:52	12:02

(1) Cards' configuration can be done at the same time for analog and buses in case B, so Total Time is reduced. This can't be done in the GUI internal data base. The same is true for the GSS software.

Looking at the data we can tell that for configuring the DAU and the GSS it is better to use our own Data Base because in this case several people can work in a project at the same time. This is good for big projects but irrelevant for small ones.

Indeed is easier to reuse data for new projects and therefore shortening the configuration time, if we use our own database. This is good when a lot of projects are developed.

Conclusions

Although there are similarities between industrial and FTI applications, the industrial equipment of software hardly ever can be used in FTI.

Hardware.
We'll always have to use Aerospace hardware. Though, there is some cases where DSP based industrial hardware could be used.

Databases.
Internal Databases from GSS or Configuration Software for the Hardware can be used for companies doing small projects or a small number of them. However, if a company has to develop big projects and/or a large number of them, then it is better to adopt a general Database because it permits several people to work at the same time and data can be reused easily.

GSS.
Some of the differences using a GSS COTS or an internally developed one is that an Internal GSS gives:

- Ability to optimize the software for certain capability.

- Flexibility and reaction speed to implement new features as soon as they are required.

List of Acronyms

COTS - Commercial Off The Shelve.

CVT – Current Value Table.

DAU – Data Acquisition Unit.

DB – Data Base.

DSP – Digital Signal Processor.

FTI – Flight Test Instrumentation.

GS – Ground Station.

GSS- Ground Station Software.

I/O – Inputs and Outputs.

OPC – OLE for Process Control.

OLE – Object Linking and Embedding.

PID – Proportional Integral Derivative controller.

PLC – Programmable Logic Controller.

SCADA – Supervisory Control And Data Acquisition.

References

[1] OPC Foundation. https://opcfoundation.org

DOI 10.5162/etc2016/3.3

GUI Simulator for Automated Testing of Embedded Systems

Dipl.-Inform. Andy Walter[1], Dr. rer. nat. Torsten Rupp[2], Dipl.-Inform. (FH) Florian Weber[1]
[1] macio GmbH, Emmy-Noether-Straße 17, 76131 Karlsruhe/Germany
[2] macio GmbH, Am Kiel-Kanal 1, 24106 Kiel/Germany

Abstract:

Software Developers for embedded systems are often confronted with the situation that development tools are less mature than their pendants for desktop systems. During the development process in general, and in particular for automated testing, it can be very helpful to do frequent test-runs on the host rather than on the embedded system. Special care needs to be taken for the GUI and for low-level components like sensors.

This paper summarizes the experiences macio made with simulators in three embedded projects. With relatively little effort, it was possible to port bare-bone GUI applications which are based on low-level graphics engines (bare-metal on a framebuffer devices or simple APIs like emWin) for Linux. The main effort was the implementation of the respective low-level driver layer for the host platform, such that the original source code used on the target could be compiled for the host platform and the resulting binaries can now be executed on the host. Consequently, the screens of the resulting simulator are pixel-identic with those on the target platform.

Another benefit of this approach is that building for a second platform generally improves the robustness of the application, because it increases the probability to trigger timing-related bugs or bugs due to side-effects which may rarely become visible on the original platform.

On the host, the required time for a build-and-run cycle is dramatically reduced compared to cross-compilation and download to the target system. In total, the simulation typically reduces the turnaround time from several minutes down to a few seconds. We measured built time improvements from 6 minutes to 19 seconds on the same host. Also debugging becomes much easier and elaborated tools like Valgrind can be used for finding memory leaks and other runtime errors.

As a benefit for sales and marketing, the simulator can be used for presenting the final application to customers or producing screen shots for the documentation or brochures.

Also, the simulator can easily be integrated in automated test runs. Embedded devices often lack the possibility to generate screen shots or the memory for collecting test data. The automated handling of loading a test-program, executing it and transmitting the test-results back to the test server often is a difficult task.

Two general strategies are possible for the integration of sensors and other components: The communication can be recorded and played back by a simulator. Tools like CANoe provide more comfort and allow the execution of scripts for the simulation of smarter and more complex components. An alternative would be to only run the user interface on the host, while the non-GUI part of the application is executed on the real embedded hardware.

The paper elaborates on the benefits and limitations of the given approaches and gives guidance on the integration of the embedded device with the simulator.

Key words: GUI, simulator, embedded device, automated testing and documentation.

Motivation

Continuous testing is a required measure to ensure that the software works as expected. It improves software quality significantly. It is particularly important for embedded systems, because software failures are usually inacceptable and in some cases disastrous. Some error classes, like memory leaks or performance bottle necks, are much more likely to cause problems on an embedded system than they would on a desktop system. Embedded systems are generally only equipped with the resources which they need for the particular application, and they often run for months or even years without a restart. A memory leak in a desktop application may remain undetected, because the OS can swap and the whole application is likely to be restarted after a couple of days or weeks anyway.

Makers of operating systems and tools for embedded systems typically rather focus on things like footprint and on real-time capabilities than on comfort for software-developers. Also, cross compilation and remote debugging are more difficult to handle and have limitations.

While testing is particularly important for embedded applications, it is often difficult to run the tests on the target device. The limited resources on the target device may prevent the use of remote debuggers or intensive logging which would be comfortable. Standard concepts like the automated comparison of screen shots with a “golden master” are difficult, if there is no comfortable way to communicate with the embedded system and no space on the target device to store those screen shots.

Testing the application on a desktop PC would be more comfortable with this respect, but the target device usually runs a different operating system and even uses a different processor architecture.

Luckily, most parts of an application is usually not specific for the embedded system which is was written for. Often, only very few distinct parts really depend on the device. Especially the GUI and major parts of the business layer usually do not depend on the specific target hardware and may also run on the host system. This has the advantage that more powerful tools may be used, e.g., for code coverage analysis or runtime analyzing tools. Furthermore, testing can more easily be automated and test tools can be used.

This paper presents the experience macio made in three embedded projects with a respective GUI. A simulator framework was developed to execute the software on a standard Linux system including pixel-identic graphics.

Base and Requirements

In order to run an embedded application on a host system, the software must be compiled for the host architecture. If a make generator like cmake is used this is usually simple to do. For hand written make files, the cross-compiler must be replaced by the host standard compiler in the make files.

For the GUI part, a graphics library is needed to simulate the target graphics hardware on the host system. We used for this SDL [1] as a thin and fast graphics layer. SDL is an open-source cross-platform library with basic functions for input devices and graphics including OpenGL. For applications which use no graphics framework at all or some embedded graphics libraries like emWin, SDL is a good base to implement a simulator for the graphics backend hardware.

Concept

In order to run the embedded application with pixel-identic graphics on a host, the application must be adapted at some functional level. A good choice is the level where the graphics data is transferred to the target graphics hardware device. At this level, a system abstraction layer (SAL) is inserted in the application. Usually, this layer is very small and only contains a small number of functions. The layer is responsible for redirecting the graphics output to SDL functions, which draw the GUI on the host system screen. This low-level approach offers the ability to use most of the higher level embedded application graphics functions including testing and give a pixel-identic output on the host system.

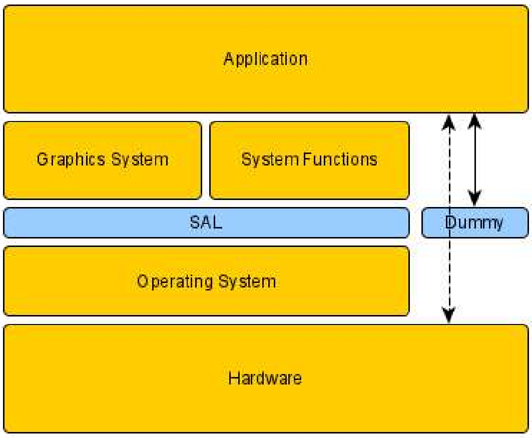

Fig. 1. Target system with application and the level were the SAL was introduced.

All non-graphical functions, e.g., operating system calls, are also redirected in the SAL to an appropriate host function, e.g., opening a file. If the functionality is not required for testing, it may just be implemented as a dummy. This approach results in a partially operating application. E.g., sensor communication may not work, but the correct visualisation of some recorded or otherwise given sensor data may be tested. For development and testing of the GUI and major parts of the business layer, usually none or only a few hardware dependent functions are required. Only this sub-set must be replaced.

Implementation

The approach of building the embedded application for the host system was successfully used in three different projects at macio.

1) Medical emergency respirator system: for this device a graphical user interface was implemented based on an external graphics controller connected to the main system via an SPI bus. For the simulator on the host, the low-level commands for sending and receiving data via the SPI bus were replaced in the SAL by calls to SDL functions. The graphics controller supported different screen buffers and semi-translucent overlay screen buffers, which must be implemented with SDL functions to get a pixel-identic output on the host. The hardware buttons where implemented as software controls in the SDL window, too.

2) Alcohol measurement device: in this project, the graphical user interface of an alcohol measurement handheld system with a monochrome screen of only 128x64 pixels was developed. The application uses emWin [2] for the graphics output. The SAL was inserted at the level were the rendered data from emWin was copied onto the screen buffer. The graphics data was redirected to SDL blit-operations in a window on the host system.

Fig. 2. Simulator window with an example screen of the alcohol measurement handheld application.

3) Embedded system with a complex generic GUI for a large product family on Cortex M-CPUs: this project was based on a domain-specific language, which makes the GUI easily adaptable to other products of the same family, by just replacing the GUI description. The project uses emWin on a frame buffer device for the graphical display. The SAL was inserted at the level were the rendered data from emWin was copied into the frame buffer.

Development benefits

With the major part of the target application running on a Linux host system, most of the further development work could be done one the host including debugging and runtime analysis. The time for an edit-compile-run cycle was dramatically reduced from typical several minutes to a few seconds, both because the standard compilers of the host could be used and the resulting binary could be started immediately without downloading it to the target or copying it to a memory card first. For the largest project, the edit-compile-run cycle was reduced from 6 minutes on the original Windows 7 development environment with a cross-compiler down to 19 seconds on a Linux system on the same desktop hardware.

Besides faster development cycles, runtime analysis is another major benefit when the application can run on a standard Linux x86 system. Especially dangling pointers, buffer overflows, corrupted memory, or lost resources can be tracked and easily identified with tools like Valgrind [3]. On a target system, this is often impossible due to limited system resources (memory and CPU power) or uncooperative processor architectures.

If performance is a critical factor, then a performance analysis may also be done on the host system. The results are not absolutely comparable with the real target system, but measurement values like counters for executed code blocks or functions calls can be used to find platform-independent hot-spots in the application.

Sensor integration

If sensor data is required to execute the embedded application, the data can be injected into the host application on various ways. If a field bus like CAN is used, software tools like CANoe [4] or similar tools may be used in order to simulate a CAN network. With a simulated CAN device, network development of the application can start even before the final CAN backend hardware is available. This approach is particularly convenient for testing product families, when some of the devices would be too big, too expensive or simply not available yet.

If the application has an internal structure like a publish-subscribe pattern for handling sensor data and internal application state information, it is easily possible to extend this by a simulator connector to get and inject sensor and state data from and into this model. The medical respirator system uses a publish-subscribe model and a few additional injection functions to transmit basic sensor data to the host application, too.

Automated testing and documentation

For automated testing, a socket interface was implemented in the simulator framework and the script language Lua [5] was integrated. Lua is used for writing lightweight test scripts. The Lua integration offers the ability to insert user, communication, and simulator events, and for taking and comparing screenshots of the whole screen or regions of interest. Several use cases for the various applications were implemented and the graphical output of the tests was compared with fuzzy rules with the expected screen data. Fuzzy rules were used to limit the overhead and complexity of the comparison function e. g. when text in different languages is rendered. This is sufficient for some general rendering tests. E.g., the automated detection if all text labels fit in the respective space and can be completely drawn in all supported languages.

Based on the Lua integration, a screenwalker script was implemented to be able to instantiate all application screens by an automated menu navigation walk-through. Via this screenwalker functionality, a rendering of all screens can be ensured to test all defined fuzzy rules in one automated test run. Furthermore, the screenwalker can be used to generate a screen map of all screens provided by the application.

When tests can be executed on the host, also a code coverage analysis can be done. On the target system, this is in many cases impossible unless there is a writable storage device available were the coverage analysis results may be stored. With the host simulator, standard coverage tools like GNU gcov can be used to get a detailed code coverage analysis.

Besides automated tests and coverage analysis, creating screen shots with rendered texts in all required languages for the user manual is in many projects a major requirement. Doing this manually on the real target could become a time-consuming task. By using the pixel-identic simulator with the automated screenshot functionality, those screenshots can be created and updated fully automated for all required screens and languages.

Future work and conclusions

Executing the embedded application in a simulated environment on the host is already a major benefit during software development, test and documentation. For detailed testing and for demonstration purposes, some real sensor data may be useful. Implementing simulator functions which supply realistic sensor data is in many cases a very complex task. Alternatively, real sensor data may be collected from a connected target device during the test run and then sent to the simulator software on the host via a network connection. This would also allow remote control of the embedded device for debugging as well as for demonstration purposes.

Using a simulator for the development of an embedded application is a major benefit. The time for an edit-compile-run cycle can dramatically be reduced. Also, collaborate software development with several developers is easier now if there are not enough target devices for the whole team. With a simulator, testing and generating documentation can easily be automated and a simulator is also useful for marketing purposes to give customers an impression of the real system.

Finally, the GUI simulator can be used to decrease the effort and time for text translations of multi-lingual applications. In most cases a translation agency gets authorized to translate

DOI 10.5162/etc2016/3.3

all origin application strings into different languages. This agencies need context information about the text placement to be able to find suitable translations. Often, this context information is provided by screen maps and developer comments, which may lack of expressiveness. The GUI simulator is able to provide this context information by presenting the complete application including the navigation path and the whole screen of the translated text. Additionally, the translation agency can use the GUI simulator for verifying the translated text. The look and feel of the translated text can be displayed directly using a dynamic translator implementation. Therefore the translation agency is able to verify the correctness of text placing concerning newlines and the available space.

In the three presented projects the effort required to develop the simulators was more than compensated by the saved time due to faster development cycles and easier debugging. For future projects, the simulator framework will be used more extensively and building a simulator should become part of the project offer.

References

[1] SDL: Simple Direct media Layer, http://www.libsdl.org/

[2] emWin: https://www.segger.com/emwin.html

[3] Valgrind: http://valgrind.org/

[4] CANoe: http://vector.com/vi_canoe_de.html

[5] Lua: http://www.lua.org/

DOI 10.5162/etc2016/3.4

Achieving Dramatic Increases in T&E Effectiveness and Efficiency Leveraging Dynamic and Flexible M&S Tools

Nathanael McBee[1], Joshua Reicher[2]
[1,2] Analytical Graphics Incorporated, 220 Valley Creek Blvd. Exton, PA 19341 U.S.A,

Abstract:
Much focus has been brought in recent years to the use of statistical methods to “right-size” overall test plan design using design-of-experiments, combinatorial techniques and other rigorous scientific methods. In 2012 a Scientific Test and Analysis Techniques (STAT) Center of Excellence (COE) was initiated to assist programs in developing rigorous and defendable test plans using state-of-the-art methods. These initiatives are meant to produce smarter overall test plans embodied in a given program as well as to produce smarter test plan loading and scheduling in individual test plan blocks. Less attention has been given to the use of smarter methods in the test execution phase for optimum test-card mission design to increase test-point density and to ensure execution effectiveness to reduce re-flight rates.

Modern advances in computer simulation have resulted in tools which enable flexible and interactive virtual environments that can be used to rapidly prototype route designs. Sets of candidate test-point combinations in the assembly of test-cards can be virtually modeled to iteratively arrive at a test mission plan that is more efficient and more robustly designed than by more traditional methods.

Here we will review the application of virtual methods of dynamic planning, execution, and post-flight quick-look that has proven able to increase test-point density and more often ensure test-point objectives achievement. Modeling application and iteration methods used to achieve more optimal test-flight designs will be discussed and contrasted with traditional contemporary methods.

Final consideration and discussion will describe the overall areas of positive T&E execution phase impact including practitioners’ operations efficiency, flight effectiveness & efficiency, post-flight quick-look and forensics analysis and flight safety.

.

Key words: AGI, T&E, COTS, M&S, STK

Introduction

There is significant benefit to using a common modeling and simulation environment for evaluating aircraft performance and measures of mission effectiveness across all portions of the program lifecycle; from concept and engineering, through test and evaluation to training and operations.

Using a commercial modeling and simulation package maintains consistency in asset performance models, environments, and mission goals throughout the various phases of the project or program lifecycle. This ensures reliability and comparability in mission objective assessment. Additional efficiency gains are found through sharing models defined in early stages and passing them along to groups engaged in subsequent phases of product development. This reduces the amount of work to recreate models as well as lowers the risk of introducing errors due to mismatched modeling between applications.

Additionally, having an extendable interface and open API allows for customization of workflows to fit the needs of each phase while continuing to use a consistent toolset.

DOI 10.5162/etc2016/3.4

This paper will emphasize the advantages of using commercially available modeling and simulation packages by highlight the use of the commercial-off-the-shelf software package Systems Tool Kit (STK) produced by Analytical Graphics Incorporated (AGI).

Support of the Aircraft Project Lifecycle

Every project or program progresses through a series of stages to go from concept to implementation. For the purpose of this paper, we will address the following phases: CONOPS and Engineering, Procurement, Training and Simulation, and Test Validation and Operations. Each phase has different requirements for modeling, analysis and visualization but having a single tool capable of participating in all phases will significantly reduce schedule risk and internal tool usage training requirements.
STK provides specific capabilities to evaluate aircraft systems and mission performance across all phases of development ranging from simplified or conceptual aircraft and sensor performance modeling, to detailed modeling in iterative trade study evaluations for engineering and testing of high fidelity mission models for test and evaluation or operational mission planning.

Commercial Modeling and Simulation Software

AGI's commercial off-the-shelf (COTS) software Systems Tool Kit (STK) is a time based 2D and 3D modeling environment for evaluating land, sea, air and space system performance. This environment incorporates terrain data and radio frequency attenuation models, complex vehicle and sensor/payload dynamic behaviors, and the ability to compute relationships between objects based on those dynamics, terrain presence, and RF environment models. Such relationships between objects include (but are not limited to) relative position and orientation, line of sight (including obscuration from terrain), and communication link and radar signal quality.

Engineers, mission analysts, operators and decision makers can model complex aircraft

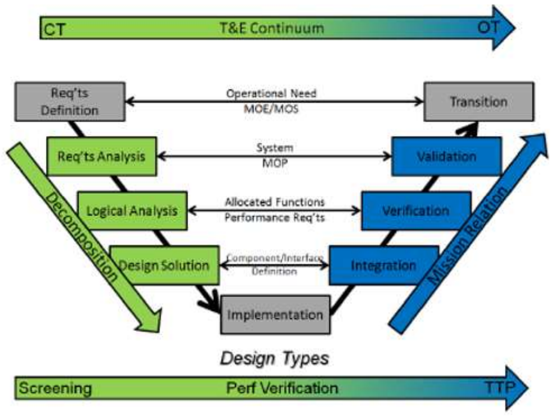

Fig. 1. Illustration of Decomposition and Mission Relation for Test Planning. [2]

and mission systems, from the aircraft performance to the payloads they carry and even the supporting assets on the ground or in space, all within the context of the mission and operating environment. System performance can be evaluated in real or simulated time, with reports, graphs and 3D visualizations to convey easily understandable results.

STK also provides an open API and software development kits for a variety of customization options. This includes analytical plugin points which are provided to allow users to augment any calculation or to compute custom measures of effectiveness in process with STK's other metrics. Alternatively, the engine behind the STK application can be used as an embeddable component in custom application development for desktop and mobile applications as well as server and web-based architectures.

This flexibility makes STK a great choice for customizing solutions for the high-fidelity needs of aircraft system test and evaluation program lifecycles.

CONOPS and Engineering

It is critical to create a realistic depiction of both the conceptual systems in question as well as provide a method for allowing invested engineering development of those systems.

DOI 10.5162/etc2016/3.4

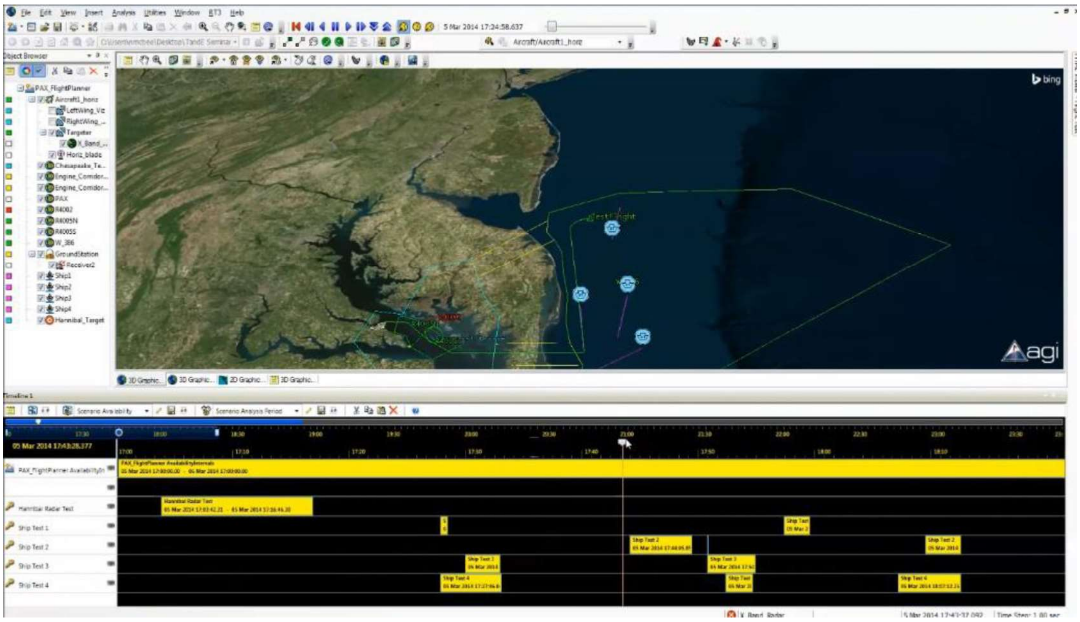

Fig. 2. Systems Tool Kit Example– Timeline of Coordinated Test Events and System Availability Windows

Modeling and simulation environments can provide the capability to simulate flights based on true or conceptual performance parameters in a wide variety of mission profiles. Modeling end to end scenarios for mission threads and vignettes allows users to quickly assess measures of performance/measures of effectiveness (MOP's/MOE's) for missions such as ISR, strike, air defense, close air support (CAS), electronic warfare, and more. This gives analysts the ability to play out a series of concepts to evaluate performance of the design and then make adjustments and reevaluate.

Another critical feature is the basis for aircraft modeling to incorporate a 6 degree of freedom simulator to ensure accurate mission planning and modeling capabilities. This takes in aircraft configuration data (aerodynamic lift and drag curves, propulsion thrust properties, climb, cruise and landing characteristics) and propagates position and attitude through a series of user defined waypoints, holding patterns (circular, racetrack, raster search) and maneuvers (push/pull accelerations, rolls, loops). Missions adhere to the aircraft performance model with realistic bank and flight path angles, turn radii, climb rates and aircraft velocity. This provides the capability to evaluate the design's ability to perform missions and combat maneuvers or to out maneuver and accelerate away from combatants or ground targets.

Utilizing a wide variety of flight profile metrics helps aide in determining design effectiveness such as fuel state over a mission, thrust required to sustain maneuvers (including environmental characteristics like wind speed and direction), load factor and thrust/power remaining throughout maneuvers. Using these data sets, analysts can determine the feasibility of mission profiles and answer questions about the mission such as: 'can the aircraft design achieve the required climb rates?', 'does the proposed aircraft have the required range or endurance?', 'does the selected propulsion system provide the required thrust?'

This provides flight planning relative to other objects in the simulated scenario including the mission environment and the local terrain profile. This allows for easily designing formation flying maneuvers, sensor pointing and weapons drops on stationary or moving targets, low altitude terrain following maneuvers and inflight refueling, just to name a few.

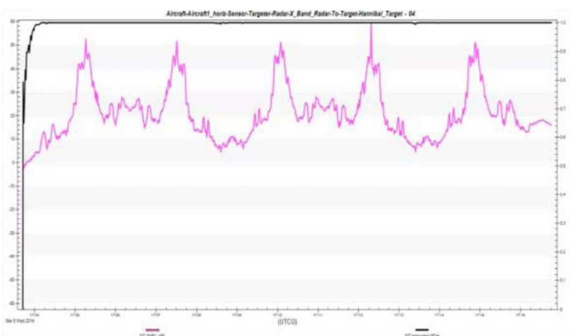

Fig. 3. Calculated Radar Detection of Simulated Target – Showing Probability of Detection (PDET) and Signal to Noise Ratio (SNR)

DOI 10.5162/etc2016/3.4

Incorporating GIS data also provides the ability to establish flight corridors and no fly zones to aid in mission planning.

In addition to flight performance is the need to manage a wide variety of additional mission system models and performance metrics which provides context to the mission plan. Modeling the other subsystems, payloads and objects in the mission (communications, electronic countermeasures, weapons performance, ground based radars, communications packages and refueling capabilities) can help create a full understanding of the aircraft's capabilities such as range and endurance, the ability to avoid detection while closely approaching adversary radars, and kill chain efficiency.
An example of a mission evaluation might be determining how bank angles during fighter maneuvers may exceed sensor gimbal limits or field of regard causing loss of line of sight between sensors and targets or understanding the minimum number of aircraft required to perform ISR coverage of various size regions dependent upon fighter performance and launch/recovery locations.

Taking into account attitude changes in aircraft throughout flight plans provides relative orientation between all other objects and reference frames in the modeled scenario. When an aircraft climbs or banks, the attached payloads rotate appropriately. For example, with a series of receiver antennas mounted about the aircraft, the antenna gain patterns maintain their orientation with respect to the rolling aircraft frame which translates to a reorientation in the Earth fixed reference frame. Knowing how the range and angles between other transmitters and the rolling aircraft change over time, allows software simulations to determine which antenna and what part of its gain pattern is receiving the incoming signal and therefore how the link budget changes during the maneuver. Using information like this, engineers can design or select more appropriate antennae and determine the appropriate number and location of antennae to optimize link availability during expected operations of the aircraft.

With regards to the fighter kill chain (the time to find, fix, track, target, engage and assess), having the ability to model all the various sensors, weapons and timing of events in tandem with the fighter and target performance (stationary or moving) allows for the entire process to be simulated and evaluated early on in the project development. Sensor fields of view can be modeled, detection and tracking

Fig. 4. Flight Plan Editing in Simulation – Systems Tool Kit

algorithms can be integrated, GPS receivers and position accuracy can be evaluated, and even weapon guidance modes can be simulated. Bringing all these together allows for trade studies to be conducted to find weaknesses and assess solutions to improve kill chain effectiveness.

Having these capabilities exist in a simulated software environment provides analysts with the tools to iterate through a series of trials (changing aircraft performance characteristics and sensor details or moving the targets and adversary aircraft) and having the flight path automatically update for the new mission parameters. This makes it possible to efficiently evaluate a large mission deck and determine either how well a specific aircraft design will perform in a series of missions or what the requirements need to be to achieve the goals of each mission, such as wing loading, thrust and sensor/payload requirements.

Fig. 5. Flight Plan Showing Expected Communications Link Quality – Systems Tool Kit

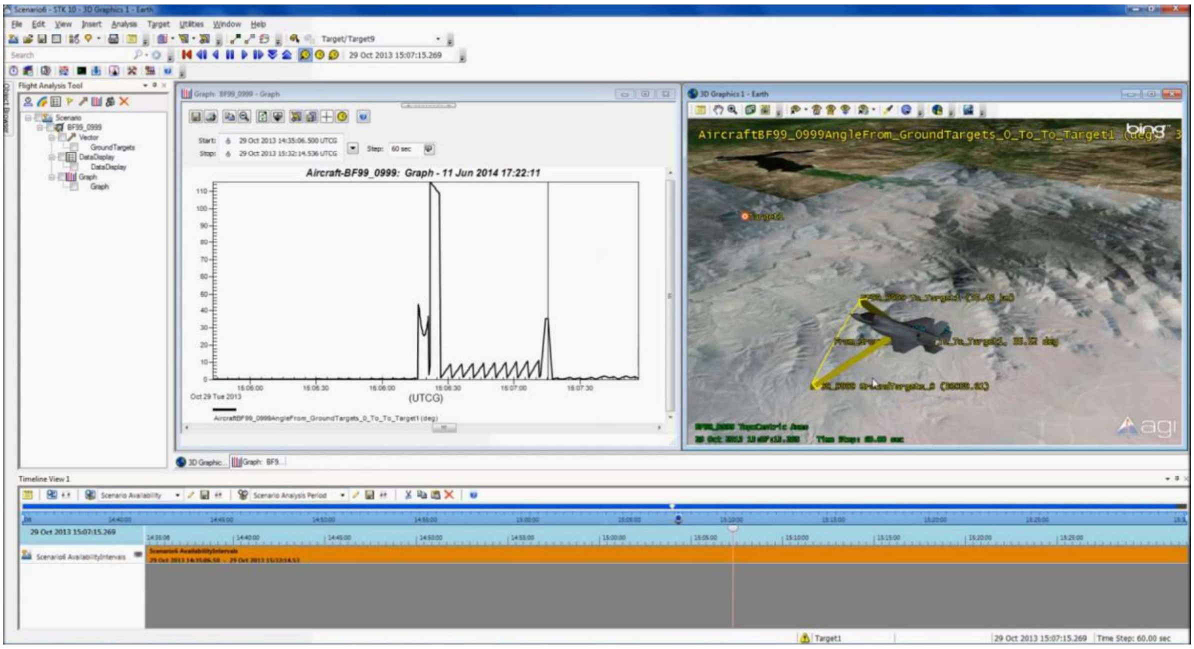

Fig. 6. Vector/Angle Calculations Between Aircraft and Target Locations During Flight

Acquisition

Proposed system designs can be explored within modeling and simulation packages and results can be compared and constrained to requirements, effectively determining whether or not the suggested system is capable of accomplishing the mission goal. For procurement of new systems, there is often the option to trade out various components (sensors/radars, weapons, etc.) and software simulation provides an analytical environment for direct comparison of component choices and their relative performance in current and future missions.

Aircraft performance models can be established for all platform choices such that each platform can be run through the same mission profiles and evaluated. Similar to definitions used during CONOPS and engineering design phases, the aircraft performance can be quantized based on metrics like maneuverability, range/endurance, detectability, and kill efficiency.

Beyond the base platform, the simulated communications and radar capabilities provide ways to evaluate the effectiveness of various payload options and their effect on the overall mission performance of the aircraft and it's systems under consideration. This provides a simple way to investigate the feasibility of different system designs in both measures of performance as well as implementation complexity or even overall system cost. For example, if a weapon has its own radar and is capable of guiding itself to an intended target, how much quicker can the aircraft be retasked rather than the aircraft's radar being required to guide the weapon to its target? Or for electronic countermeasures, which systems significantly improve an aircraft's ability to avoid being tracked by ground radars or incoming missiles?

By employing a robust modeling and simulation environment, these system design options can easily be linked to acquisition decisions and give designers and decision makers a common tool for validating and verifying design decisions.

Test and Evaluation

Modeling aircraft in a simulation environment prior to testing helps maximize the number of tests a vehicle can perform per flight such that fewer flights overall are required and ultimately contributes to saving time and money. The use of an end to end modeling and simulation package such as STK ensures a higher probability of having a successful flight, again reducing the number of required flights to accomplish a full evaluation of aircraft subsystems. The same models used in the design phase can easily be passed along to test and mission planners so that all of the high fidelity design work can be used to optimize flight planning.

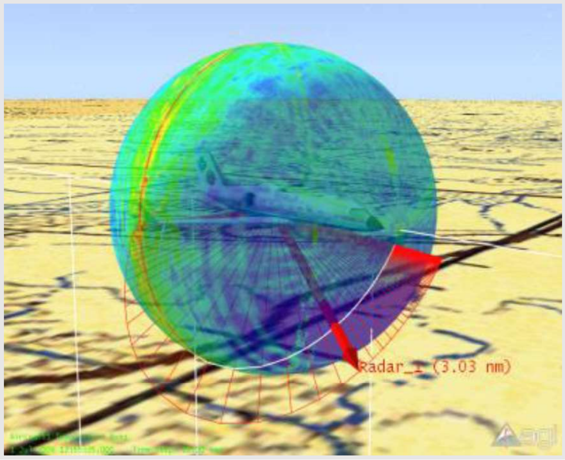

Fig. 7. Aircraft Radar Cross Section Visualized – Systems Tool Kit

These pre-mission simulation activities provide the ability to coordinate many objects and their interactions and intended behaviors. The time dynamic nature of STK provides the tools to synchronize position and orientation of all assets to maximize test efficiency. Simulating the test with supporting assets beforehand can also reveal the potential to fill white space with additional test points. For example, resetting a formation may also result in a flight path that presents an easy opportunity to test a given set of antennas at no extra cost.

Having the test plan plotted in a time-dynamic simulation environment then provides the ability to conduct pretest rehearsals or make quick changes on the day of the test. Rather than putting pilots in a real time simulator and flying the entire mission just to determine whether or not test metrics are collected as expected, operations can be simulated in faster than real time to generate test metrics and evaluate test quality. Moving this process further up the chain also yields significant time savings if test planners can evaluate each test procedure before even constructing the test mission deck, long before test pilots are involved.

On the day of the test, if flight conditions change, for example excessive winds that require the test aircraft to crab into the wind altering the geometry of the plan, a decision can be made as to whether or not adjustments to the flight plan can compensate for the crab angle or if the test is infeasible. This makes for a much more informed go-or-no-go decision, potentially saving both time and operational testing costs.

In addition to pretest planning, STK is also used for post mission playback and test validation. It provides the capability to plot the flight path, playback the mission at faster or slower than real time, visually inspect specific events and add visual indicators for test results such as color contoured flight paths, communication link indicators and dynamic data displays. Test result scenarios can even be shared as images, movies or hosted web based visualizations.

Northrup Grumman Integrated Systems used the STK desktop application to evaluate communications systems for airborne platforms. They were specifically concerned with performance based on antenna placement on the aircraft. After modeling the gain pattern, location and orientation of the antenna multiple flight profiles were evaluated to understand the coverage and blockages they would encounter during the test. By modeling the communications system and selecting optimal flight profiles before their test flights they were able to save millions of dollars in reduced number of flight tests as well as allowing them to deliver on schedule. Bruce MacDougall referred to the process as “valid flight testing at your desk”.

Operations

Moving beyond the test phase and into operations, an end to end modeling and simulation package can continue to provide performance evaluation in mission planning and real time operations. Importing intelligence information into the simulation environment allows planners to construct flight plans that optimize mission plans while minimizing other factors such as radar, acoustic and visual detectability.

Because STK offers a fully documented application programming interface (API), custom applications can be created on the same foundation as the engineering and planning tools. These custom interfaces can provide a simplified workflow which is tailored to the specific operator’s needs, only providing the features required for mission planning with the fewest number of inputs. This allows for individuals to take advantage of all the high fidelity analysis provided by the software, but without the need to learn the workflow for the detailed engineering tools available in the commercial desktop version of the application. This same API makes it possible to embed specific capabilities into existing applications. Since many operational systems cannot be fully replaced due to cost of development and time to retrain all of the operators, plugins can be integrated to augment current capabilities and provide additional functionality without building from scratch or having to change well known workflows.

In areas of real time operations, STK supports live data feeds such as DIS, HLA, and other custom data feeds as necessary to form a complete Common Operational Picture (COP). Entity tracks for all vehicles and resources involved in the operation can be imported into this same environment exposing the ability to compute relationships in real time: who can see who, where communications are available, where the areas of interest are and what assets are closest to them, and other mission critical information. Decision makers can intelligently sift through the vast amounts of data to issue well informed commands.

Summary

The commercial maturity of computer based modeling and simulation software packages provides a depth and breadth of capabilities to engineering activities, and an ease of integration within overall flight test and evaluation efforts. These modeling methods enable the evaluation of systems at reduced risk, and with significantly reduced cost.

Software capabilities are perfectly aligned for concepts development, mission analysis, and engineering design of systems under study while providing an invaluable tool in the study and development of design considerations and requirements in preparation for acquisition activities.

Leveraging commercial off the shelf modeling and simulation software provides unparalleled support across multiple aspects of the operational system program life cycle from system development to operational deployment.

References

[1] U.S. Department of Defense. (2012). SCIENTIFIC TEST AND ANALYSIS TECHNIQUES IN TEST AND EVALUATION IMPLEMENTATION PLAN. Retrieved from http://www.dote.osd.mil/docs/TempGuide3/STAT_TE_Implementation_Plan_30Jan2012.pdf

[2] Scientific Test & Analysis Techniques Center of Excellence. (2013). The Power of STAT. Retrieved from http://www.itea.org/~iteaorg/images/pdf/conferences/2013_Annual/Track_2_Ahner_ThePowerofSTAT.pdf

[3] A. Gill, A. Bellamy, Flight Testing the Nimrod MRA4, Retrieved from http://citeseerx.ist.psu.edu/viewdoc/download?doi=10.1.1.215.2661&rep=rep1&type=pdf

DOI 10.5162/etc2016/3.5

Concept for a modular flight test camera system

Arne Nowak[1], Dr. Michael Schöberl[1], Ingo Bebermeier[2]
[1] Fraunhofer Institute for Integrated Circuits, Am Wolfsmantel 33, 91058 Erlangen, Germany, arne.nowak@iis.fraunhofer.de, michael.schoeberl@iis.fraunhofer.de
[2] SEKAI Europe GmbH, Rissener Str. 102, 22880 Wedel, Germany, ingo.bebermeier@sekai-europe.com

Abstract:
Cameras have been widely in use for in-flight testing and other industrial applications to make observations and record them for later analysis for several years now. With the advent of cheap consumer action cameras like GoPro, this type of cameras became a viable option. However, consumer cameras do not cater for professional needs with regards to functionality, handling and other aspects. The Fraunhofer Institute for Integrated Circuits IIS and SEKAI Europe are working jointly on the development of a modular camera systems that consists of a front-end part with the lens and image sensor and a backend for image processing, control, video encoding and recording as well as streaming over a network interface. The modular approach makes it possible to provide different front-end modules that can be chosen depending on operational needs. One module will be very small and light-weight with an integrated fixed focal length lens while another module will be slightly larger but with a higher quality exchangeable lens and a larger imager chip. The backend can be freely configured regarding image processing and video encoding parameters. New functions can be added in the future by a software upgrade. Fraunhofer IIS and SEKAI Europe would like to present the concept to the audience and gather opinions for further improvement. Fraunhofer IIS and SEKAI Europe would like to present the concept at the etc 2016 (European Telemetry and Test Conference) to the audience and gather opinions for further improvement.

Key words: camera, video, recording, flight test

Introduction

Cameras are a very important tool in flight testing of airplanes and helicopters. They are used to make observation of moving parts of the aircraft in flight and to record them for thorough analysis on the ground after the test flight has been completed or to downlink compressed streams during the flight mission for immediate interaction. Modern digital camera systems offer a plethora of possibilities for this application with different types of image sensors, image post-processing methods and video data compression algorithms. There are many small and light-weight cameras available but most of them do not offer the professional features that are required in flight test applications.

This paper gives an overview on the state of the art and the general requirements and use cases for flight test cameras. Afterwards the general concept of a modular flight test camera system is introduced and the two major components, camera heads and central processing unit, are described in detail. The paper concludes with an outlook on the further possibilities of this approach.

Requirements from the industry and use cases

In flight test applications there are diverse requirements for cameras depending on the actual use case. Where space for installation is limited the size of the camera and also often its weight play an important role. This also simplifies the temporary mounting that is carried out for each flight. For observing fast moving parts a high frame rate and global shutter image sensor is needed. In some situations it is important to simultaneously observe the inside and outside of the aircraft, for example in the cockpit. In these cases, both the flight situation through the window as well as the instrument panel and the pilot’s actions should be visible. Here, a very high intra-frame dynamic range is necessary. For low light situations excellent sensitivity and low image noise are needed. Additionally, the camera system has to be able to cope with adverse environmental conditions: Very high and very low temperatures, low atmospheric pressure, vibration, possibly unstable power supply have to be taken into account. Last but not least the camera system has to provide appropriate electrical and logical interfaces for integration into the flight test and data recording environment and support methods for synchronization and timestamping of the image data to the data from other sensors. There also has to be a solution for later analysis of the image data in conjunction with other collected data often called meta-data.

State of the art

Several years ago, flight test applications where accomplished using analog cameras whose video signals were fed into appropriate, often digital, recording systems. While providing a very simple and universal interface the image quality of these cameras regarding spatial and temporal resolution is very limited. Sometimes, analog cameras are still used today like so-called lipstick cameras that have a very compact camera head [1].

The advent of digital cameras made it possible to more easily make use of higher spatial resolutions and higher frame rates. There are some solutions available especially developed for flight test purposes. Also, consumer grade cameras that became known as action cams are often used [2][3]. While specially developed cameras usually integrate well with the flight test environment this is difficult with consumer grade action cams that do not provide the ruggedness and interfaces necessary for this application. Common industrial digital cameras today use Ethernet as interface to a data recorder or store the video on memory cards. While action cams are often small, they lack professional possibilities for remote control. Furthermore, they mostly employ rolling shutter image sensors that lead to image distortion when observing moving objects. Lenses usually cannot be changed and are often very wide-angled which leads to geometric distortion of the image. Professional cameras are often bigger and heavier than action cams, which makes the temporary installation much more difficult.

Mobile phones and smartphones today employ high-quality camera modules for still images and video. The development and advances in this area have lead to a demise in sales of conventional compact digital cameras because the quality of mobile phone cameras has reached a comparable level [4]. These consumer system are able to deliver an excellent image quality that also sets an expectation and a reference for visual inspection systems. The employed integrated modules are very compact and consist of an image sensor chip with attached lenses. Concurrently, cameras used in industrial applications and machine vision also shrunk in size over the last few years.

For storage and transmission of the video data most solutions use the H.264 compressed video codec that provides a well-proven combination of video quality and low data rates. Hardware and software solutions for compression and decompression are available and make the use of the created files very easy.

A modular concept for a flight test camera system

We propose a modular concept for a flight test camera system that consists of a camera head module and a processing unit. The camera head contains an image sensor and the optics and is built as small and lightweight as possible. The processing unit contains the electronics which is necessary to control the camera head, process the images and create a compressed video stream. Both modules are connected by a cost-effective and light-weight cable that provides power and control to the camera head and transmits the raw video image data signal from the camera head to the processing unit.

Camera heads

The concept includes the possibility to connect different types of camera heads to the processing unit. According to the different requirements of different use cases, each camera head model can be designed for either minimal size and weight, best dynamic range and sensitivity or maximum spatial resolution or frame rate. In order to achieve these goals the different models make use of different image sensor chips and lenses. Typical dimensions of a camera head are 2,5 cm x 2,5 cm x 4 cm (see Fig. 1, Fig. 2). For connecting the camera head to the central processing unit, all heads will use the same cabling and interface. This enables seamless exchange and extensions of the system. The use of cost-effective and light-weight cables with appropriate connectors makes is possible to install the cable in an aircraft and only attach the camera heads when needed for a test flight.

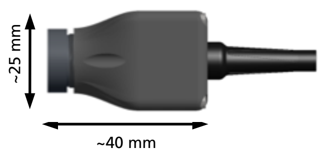

Fig. 1. Rendering of a camera head module

Fig. 2. Camera head and cable of a solution for digital media production

Central processing unit

The central processing unit is typically installed inside the aircraft together with other flight test equipment. Connection to the flight test data recorder or telemetry system is achieved via Ethernet which is used to control the camera system as well as to transmit the compressed video data stream. For video compression the H.264 video coding standard is used with the possibility to output one or more video streams at different data rates. This makes it possible to record a high quality video signal onboard the aircraft and simultaneously transmit a lower data rate video stream to a station on the ground via a telemetry system. By using H.264, the compressed video data stream is compatible with various standard video processing tools, which enables easy viewing, editing and archiving of the recorded video. The processing unit automatically recognizes which type of camera head is connected and adjusts the required image processing automatically.

Outlook

The modular approach of a flight test camera system as described in this paper makes it possible to use a specific camera head which provides the best suited features for that specific application or mission. Additionally, this approach provides the possibility to upgrade the system through the development of new camera heads when improved image sensors become available. Furthermore, it is possible to upgrade the processing unit in regards to hardware and software as well. A new hardware design can provide better performance while using existing camera heads. The functionality of existing camera systems can be improved via firmware upgrades of the processing unit.

The described modular system has a high potential to be deployed also in areas other than flight testing. Additional use cases can be e.g. found in video surveillance, digital media production, general testing applications and many more.

References

[1] http://www.toshiba.ch/ics/cp/products/micro_cams/ik_m51h/detail.html

[2] https://gopro.com/

[3] http://www.sony.com/electronics/action-cam/t/action-cam

[4] P. Cambou, JL. Jaffard, Status of the CMOS Image Sensor Industry report, *Yole Développement*, January 2015

DOI 10.5162/etc2016/4.1

The Challenges of Data Acquisition in Harsh Remote Places

Dave Buckley

Curtiss-Wright
Dublin, Ireland

ABSTRACT

In modern flight test installations there is a continuing trend to move the data acquisition closer to the sensors. As a consequence the data acquisition chassis needs to be mounted in locations that are small, inaccessible and subject to harsh environmental conditions. On top of this there are an increasing number of measurements required for each new flight test campaign. This paper discusses the challenges of designing a small lightweight data acquisition chassis which can provide hundreds of channels of measurement capability while operating in tight spaces which are exposed to fluids, high vibration and extremes of temperature. The paper suggests ways of designing and installing the data acquisition chassis in order to optimize the available installation space while mitigating the effects of the harsh environmental conditions.

Keywords: Data Acquisition, DAU, Modular, Flexible, Remote, Miniature, IEEE 1588, INET

1 INTRODUCTION

In a drive to reduce the wiring of flight test installations there is a continuing trend of moving the data acquisition chassis closer to the sensors. As a consequence the data acquisition chassis needs to be mounted in locations that are small, inaccessible and subject to harsh environmental conditions. This paper discusses the implications of these requirements on the design of the data acquisition chassis. The paper begins with a recap of some of the more important data acquisition design concepts such as reliability and modularity which are so important for flight test equipment. The paper then investigates how small the data acquisition chassis can get while maintaining modularity and flexibility. The paper also presents some solutions to the difficult environmental conditions that are found in remote locations, such as high temperature and exposure to fluids. Finally the paper examines some of the system requirements placed on miniature modular data acquisition chassis.

DOI 10.5162/etc2016/4.1

2 DATA ACQUISITION DESIGN CONCEPTS

Modern data acquisition chassis require a very high degree of flexibility and configurability. Flexibility can be provided on the chassis level by designing each chassis to consist of multiple acquisition cards, with each acquisition card carrying out a different function. Further flexibility can be provided at the card level by allowing the behavior of the acquisition card to be configured. At the chassis level the flight test instrumentation engineer can create almost any configuration with a large catalog of acquisition modules.

Depending on the platform, the size envelope available to install a data acquisition chassis will vary. Therefore it could be argued that the flight test instrumentation engineer requires multiple chassis types, each of which will house different sized data acquisition cards. In this scenario each chassis will come with its own catalog of acquisition cards. However this approach has its disadvantages. Firstly the flight test instrumentation engineer will not be able to mix and match his acquisition cards between different chassis. A card from one chassis will not necessarily fit into a second chassis type. Secondly it is unlikely the vendor of the equipment will support all interfaces in all chassis types. Therefore many possible configurations will not be supported.
In fact it is possible to create many different chassis shapes and sizes using the same sized data acquisition cards. Figure 1 shows many examples of a KAM 500 chassis all of which use the same data acquisition cards. This solution allows you to tailor your chassis for different size envelopes while choosing acquisition cards from a single large catalog.

Figure 1: KAM 500 Chassis Shapes and Sizes

All the chassis in Figure 1 are solid chassis in the sense that the there is a chassis into which data acquisition cards are inserted. Another method of building chassis is to construct the chassis out of the acquisition cards themselves. Using this “slice of bread” method there is no separate chassis. The chassis is formed by connecting several acquisition cards together and securing them via some locking mechanism. This method has the advantage that the flight test engineer can build a chassis with any number of slots up to a maximum value. However the “slice of bread approach” also has a number of disadvantages. Firstly when removing a module from the chassis it is not a simple matter of removing the module that you would like to change. The entire chassis must be disassembled in order to remove any module. Secondly the orientation of the modules in the chassis cannot change. Using the solid chassis approach shown in Figure 1 the orientation of the acquisition cards in the chassis can changed to create a long narrow chassis or even a circular chassis which could be mounted on a rotor. Furthermore it is also possible with the solid chassis approach to create a chassis which is any number of slots in length, up to a maximum value.

Arguably the most important feature of a data acquisition chassis is reliability. If the acquisition chassis malfunctions during flight then the test points will need to be re-flown. This incurs a large expense. It has been shown that designing data acquisition chassis using FPGA based state machines produces extremely reliable data acquisition products. Even if the system gets into an unforeseen state due to power dips during flight it will cycle out of that state within one acquisition cycle and begin operating normally again. It is quite common for processor based systems to not recover fully after such an event. Also in the event of a brief loss of power to the acquisition chassis, a chassis designed using an FPGA based state machine approach will begin acquiring data immediately after resumption of power. This is due to the fact that there are no processors which need to reboot. Acquiring immediately on power up enables test points to be completed even when there is a temporary power interruption to the acquisition system.

3 MOVING CLOSER TO SENSORS

It was noted in section 2 that using a solid chassis approach chassis of many different shapes and sizes can be created, all of which use the same catalog of data acquisition cards. However there is a limitation to how small you can make a data acquisition chassis which houses a particular type of data acquisition card. In order to house at least one card the chassis must be larger than the dimensions of a single card. In practice the chassis needs to be significantly bigger than a single acquisition card as the minimum requirement for a chassis would typically be an acquisition card, a transmitter card (to send data via Ethernet or IRIG 106 chapter 4 PCM) and a power supply.

The amount of wiring required on a flight test installation has always been a concern for flight test instrumentation engineers. The time taken to define and install the wiring, the necessity to drill holes through structures and the sheer weight of the wiring bundle are all reasons why there is a continuing drive to reduce the quantity of wiring on a flight test article. One way to reduce the quantity of wiring is to move the data acquisition chassis closer to the sensors. This has the advantage of replacing a section of the wiring loom with a single Ethernet cable from the chassis. As the data acquisition chassis moves closer and closer to the sensors the available locations where a chassis can be installed get smaller. In some cases the space envelope may be smaller (at least in 2 dimensions) than the dimensions of the data acquisition card that is used in the rest of the configuration.

One solution for these locations could be the creation of a dedicated acquisition box which fits in the required dimensions with a small number of measurements. However a dedicated acquisition box will solve the acquisition needs of only one location on one test article. A new box would need to be defined and created for every other location, which would typically have a different number and different types of measurements. The way to solve this generally would be to create a miniature modular chassis which could be populated with miniature acquisition cards.

However even this approach has its limitations. As noted previously the smallest modular chassis will typically require an acquisition card, a transmitter and a power supply. As data acquisition chassis get smaller the power supply is increasingly becoming a larger percentage of the volume. This is due to the fact that any piece of equipment which is connected to aircraft power must comply with standards such as MIL STD 704 to ensure that it can be used safely on the aircraft.

In order to fit the acquisition into even smaller spaces it may be necessary to mount the acquisition card itself in a separate location to the chassis. This acquisition card would send its acquired data back to the chassis via a serial cable from which it would also be powered. This would ensure that the acquisition card could fit in a space that was just marginally larger than its own dimensions. Multiple of these remote cards could be connected to single chassis to allow a network of miniature acquisition to be placed in the tightest of spaces. The fact that these cards could be used internal or external to the chassis would allow a relatively large catalog of cards to be created.

4 ENVIRONMENTAL CONCERNS

Another consequence of moving the data acquisition chassis closer to the sensors is that the chassis will get placed in more inhospitable places. For example one location for remote chassis is in the engine casing. During some phases of the flight test the ambient temperature of the casing will be in excess of 100 degrees Celsius. The electronics of the acquisition chassis will also add some self-heating. The 2 primary means of removing heat from a chassis are convection via air flow and conduction via the surface that the chassis is installed on. However in some locations there is very little airflow and the surface on which the chassis is installed is not thermally conductive. In this case depending on how much power is being consumed in the chassis, the chassis may be between 20 and 40 degrees hotter than ambient. This can result component temperatures outside the operating range of even military grade components.

One potential solution is to add a large heat sink to the chassis to increase the surface area and allow more heat to be dissipated by convection. However this results in a much bigger chassis, negating the advantage of a small sized chassis, and prevents the chassis from being installed in many of the locations it could have been installed without the heatsink.

Another potential solution is to locate many of the acquisition cards remotely from the chassis. This drastically reduces the heat generated in the chassis itself as most of the power will be consumed by the electronics on the acquisition cards. Also the surface area of each acquisition card would be sufficient to dissipate significantly more heat than if the cards were physically located together in chassis.

Another inhospitable location for a miniature data acquisition chassis is the landing gear of a fixed wing aircraft. While the temperature will be more benign in these locations the chassis may be more exposed to the elements and sprayed with various fluids while on the ground. One of the challenges with a modular chassis is ensuring that the chassis is fully weather sealed. A chassis that is designed to allow modules to be quickly and easily removed may have small gaps between the modules when they are installed in the chassis. These gaps can be filled using form in place gaskets. Form in place gaskets use elastomer to provide sealing between two surfaces. The elastomer is applied to one side of the acquisition module as shown in Figure 2. When the modules are placed in the chassis side by side, the compression and the cohesion of the elastomeric material will then provide sealing. These gaskets can be electrically conductive and also provide an RFI shield.

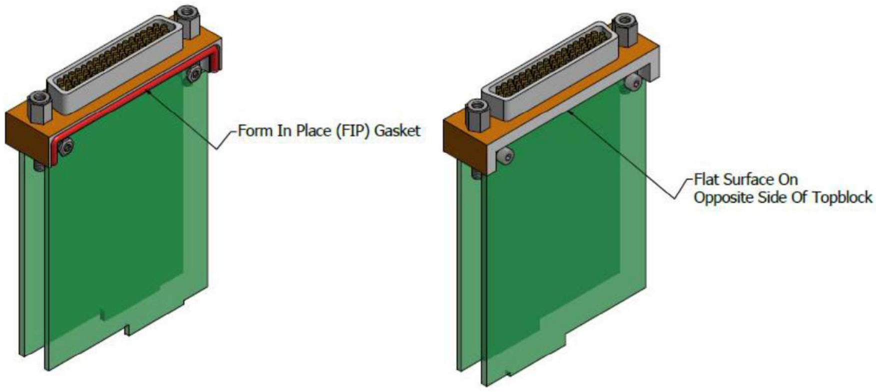

Figure 2: Form in place gaskets

5 SYSTEM SOLUTIONS

In section 3 we discussed how the requirement to move the data acquisition chassis ever closer to the sensors could necessitate a miniature acquisition chassis with its own catalog of acquisition modules. However it is important to note that any miniature chassis would need to be fully compatible with existing data acquisition chassis such that a heterogeneous network of standard and miniature chassis could be created. It should be possible to program both chassis types from the same configuration software. The entire configuration should be stored in a single configuration file, for example XidML [1]. It should be possible to analyze the acquired data from both chassis together in the same analysis software. Moreover in order to correlate the parameters from all channels in a heterogeneous network all channels must sample simultaneously. The network synchronization protocol IEEE 1588 [2] can be used to synchronize each chassis such that each chassis has the correct absolute. However it is equally important that both chassis have the same sampling strategy. For example if each chassis samples at the start of an acquisition cycle and at equal intervals thereafter and if the acquisition cycle is tied to absolute time then once the chassis are synchronized via IEEE 1588 they will also sample data simultaneously.

In fact to provide full flexibility of configuration each miniature chassis should be a

DOI 10.5162/etc2016/4.1

full network node. This would allow any number of the miniature chassis to be added to a network which also included third party equipment. There is a large of number of open standards which can be used on Ethernet networks to ensure interoperability between equipment from different vendors. In particular the INET working group [3] is defining a superset of these standards which should be supported such that there is consistent interface on flight test equipment from all vendors. In order for a miniature data acquisition chassis to be placed in any network, support for these INET standards is an important requirement.

In order to simplify the definition, installation and setup of the network it is also important that the miniature data acquisition chassis communicate with each other via Ethernet. In a typical flight test network a data acquisition chassis will acquire and packetize data, and forward those packets on to a recorder, a telemetry bridge or an on board processor. In modern flight test networks the telemetry bridge, recorder and processor may in fact be housed in one of the data acquisition chassis.

In an Ethernet network multiple nodes are connected via a network switch. The network switch can be a standalone box or a module that fits into the data acquisition chassis. While it is a necessity that a miniature acquisition chassis be able to house a switch module, in some configuration all of the slots in the chassis may be used for acquisition cards. One potential solution to this is to add daisy chaining capability to the chassis. In this scenario the controller card in the chassis would accept an Ethernet input from another chassis and combine the packets it receives from that Ethernet input with its own output packets for transmission upstream. By this method a number of chassis could be installed in tight spaces and connected together without the need for network switches or switch modules. Additionally given that the chassis is an independent network node, third party network equipment could also be daisy chained to the chassis in this way.

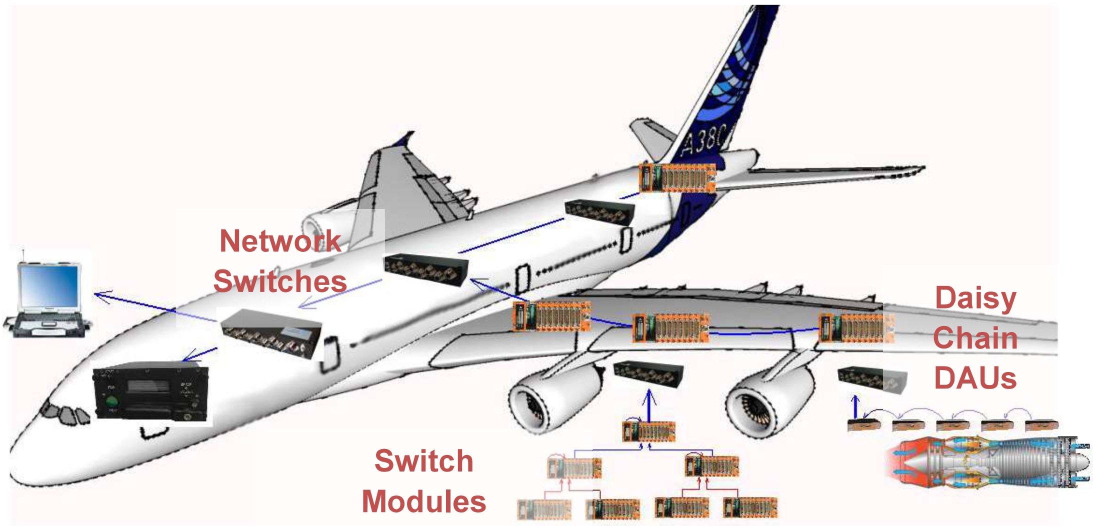

Figure 3: Network with network switches, module switches and daisy chained DAUs

6 CONCLUSION

The trend to move the data acquisition chassis closer to the sensor leads to many challenges for the design of a data acquisition chassis. With the use of a solid chassis approach many different sized data acquisition chassis can be created. This has the advantage that the same acquisition cards can be used in all chassis regardless of whether they are located in the cabin or remotely. However in some cases the small space envelopes available for the installation of the chassis lead to the requirement for a miniature chassis.

A miniature chassis will have similar requirements to the standard chassis in particular modularity and reliability. It has been proven that designing data acquisition chassis using FPGA based state machines produces extremely reliable data acquisition products. One complication of modularity is that there is a limit to how small a miniature modular chassis can be made. One potential solution to this is to locate the acquisition cards remotely from the chassis. This will allow data acquisition solutions to be fit into very small locations.

Locating the data acquisition chassis closer to the sensors can also lead to the chassis being placed in inhospitable places. Placing the chassis in high temperature zones can cause the components to reach temperatures outside of their specification. This can be a particular problem for miniature chassis where a large amount of electronics is squeezed into a small box. Building a chassis with remotely mounted modules may also serve to alleviate this problem. Fluid ingress is another challenge for modular chassis that are installed in locations which are exposed to the elements. However weather sealing can be accomplished using such technologies as form in place gaskets.

Finally it is important that a miniature chassis operates in a heterogeneous network with standard chassis from the same vendor and equipment from third parties. To ensure this, the chassis must be a full network node supporting open standards, including the soon to be published INET standards. In order to connect multiple miniature nodes to the network, it would be a significant advantage if the chassis had the built in capability to daisy chain other network nodes without needing a separate module. With these capabilities the remote miniature chassis would solve many of the challenges flight test engineers are currently facing.

REFERENCES

[1] A. Cooke, "History and Evolution of Metadata Standards for the FTI," in ITC, San Diego, 2014.

[2] IEEE, Precision clock synchronization protocol for networked measurement and control systems, IEEE Std. 1588, 2008.

[3] J. K. M. M. B. A. T Grace, "key components of the INET test article standard," in ITC, Las Vegas, 2009.

DOI 10.5162/etc2016/4.2

Multi-channel, robust measurement system for efficient flight testing

Kai Gilbert A. Author
imc Test & Measurement GmbH, Max-Planck-Str. 22b, 61381 Friedrichsdorf/Ts., Germany
kai.gilbert@imc-frankfurt.de

Abstract
With the increasing complexity of the latest types of aircraft, the requirements placed on today's flight test systems have also increased. A wide variety of signals and sensors, as well as an ever-increasing channel count from digital sources and aircraft buses, are acquired over multiple channels, monitored online and, ideally, synchronously stored in a common data sink. The constantly demanding time schedules coming from management require a particularly stabile and effective FTI system. In this case, it is a great advantage to be able to obtain all system components from a single source. For a solution to this challenge, imc Meßsysteme GmbH has put together a modular flight test system based on imc measurement systems and video technology. All acquired analog and digital values are stored in the aircraft and transmitted in parallel to the control station by PCM. Thus, at any given time, it is possible to view and evaluate the measurement data via imc STUDIO Monitor without having to land the aircraft. This saves time. Additionally, imc supports the instrumentation and commissioning when necessary with their own personnel resources to reach the goal faster.

Key words: flight test, data acquisition, telemetry, monitoring, robust measurement system

Intro

Before a new type of aircraft can be put into production, an extensive program for testing and certification must be passed. Performance testing, safety testing and low- and high-temperature tests are just a few of the requirements for certification (Certification flight tests).

High demands placed on data acquisition

For flight testing, prototype aircraft are equipped with comprehensive test flight instrumentation.

A variety of signals and sensors must be synchronously acquired. These include, for example:

- Strains
- Accelerations
- Temperatures
- Positions
- Pressures
- Voltages
- Displacements

In addition to analog sensors, these days a large amount of information communicated in digital form via buses like:

- ARINC
- ASCB-D
- CAN
- RS232, RS422, RS485
- Ethernet
- USB, etc.

In order to obtain visual information and cockpit displays parallel with the measurement data, synchronous video recordings from freely-positionable cameras are necessary.

In total, the test instrumentation in a single aircraft can range from a few hundred up to several thousand analog and digital measurement signals. All of these data are time-synchronously acquired in the aircraft and safely recorded in a central data pool. This saves from having subsequent combinations of different data sources. This results in time savings when supplying the measurement data for subsequent analyses.

Telemetric signal transmission

All test flights are typically coordinated and monitored by test engineers in a control room located back on the ground. To give them the capability to make the best possible assessment of the situation at any given time, telemetric transmission of selected measurement signals from the instrumented prototype aircraft to the control room is necessary. The transmitted data can then be monitored and saved online in the control room at the various monitor positions.

Modern flight test system

For such complex flight test instrumentations, the test and measurement specialists at imc Meßsysteme GmbH offer a modern solution concept. Thanks to its modular design, the imc flight test system can be optimally adapted to meet aircraft-specific tasks and flexibly expanded to meet future requirements as well.

The imc flight test system is based on:

1.) Modular imc measurement systems for all analog and digital data sources

2.) imc video technology with up to 8 cameras featuring individual resolution and frame rate settings

3.) Control PC with monitor

4.) Airworthy storage, network and server technology

5.) Telemetric signal transmission via PCM

Universal and modular measurement hardware

The foundation of the data acquisition is built with robust and airworthy imc measurement systems. With a modular design and universal measurement amplifier technology, a tailored layout is possible for capturing signals. Depending on the scope of the instrumentation, multiple measurement systems can be used and networked allowing thousands of channels to be synchronously acquired. The system can either be centrally installed in a 19” rack or spatially distributed throughout the aircraft. The measurement systems capture all analog and digital measurement values, as well as ARINC and ASCB-D field bus data. What is particularly helpful is that the measurement devices provide direct, real-time calculations. This delivers results during the running measurement and helps to reduce data down to the essentials.

Fig. 1. imc CRONOScompact modular measurement system

Flexible video technology

To be able to associate measurement data and flight information, time-synchronous video is necessary. For this, the video stream of the cockpit displays, as well as freely-positionable video cameras, are connected over a DVI matrix. This distributes the video information to monitors within the aircraft and to other high-performance PCs that can synchronously record the measurement data with the video data.

The heart of the test set-up

The testing is configured via a fanless, high-performance PC which serves as a control computer. Test engineers use this computer to transfer the configuration created in the office to the flight test system and make any adjustments when necessary. In addition to the configuration, the control computer also collects and centrally stores all of the measurement data from the different measurement systems. Simultaneously, the same measurement data stand available for online visualization on the monitors within the aircraft.

Fig. 2. Flight test system with monitor position in a test aircraft

Secure, central data storage

In the configuration software, the user decides where the data is to be stored.

- Internally on the measurement system’s CF card
- On the control PC

DOI 10.5162/etc2016/4.2

- On a robust NAS drive (MIL-STD-810E)
- Redundant measurement data storage

The NAS drive allows for one-handed operation of a removable storage medium which will enable a quick transfer of the measurement data to the control room. At the local ground station server, the transferred data can be immediately reproduced, evaluated and analyzed.

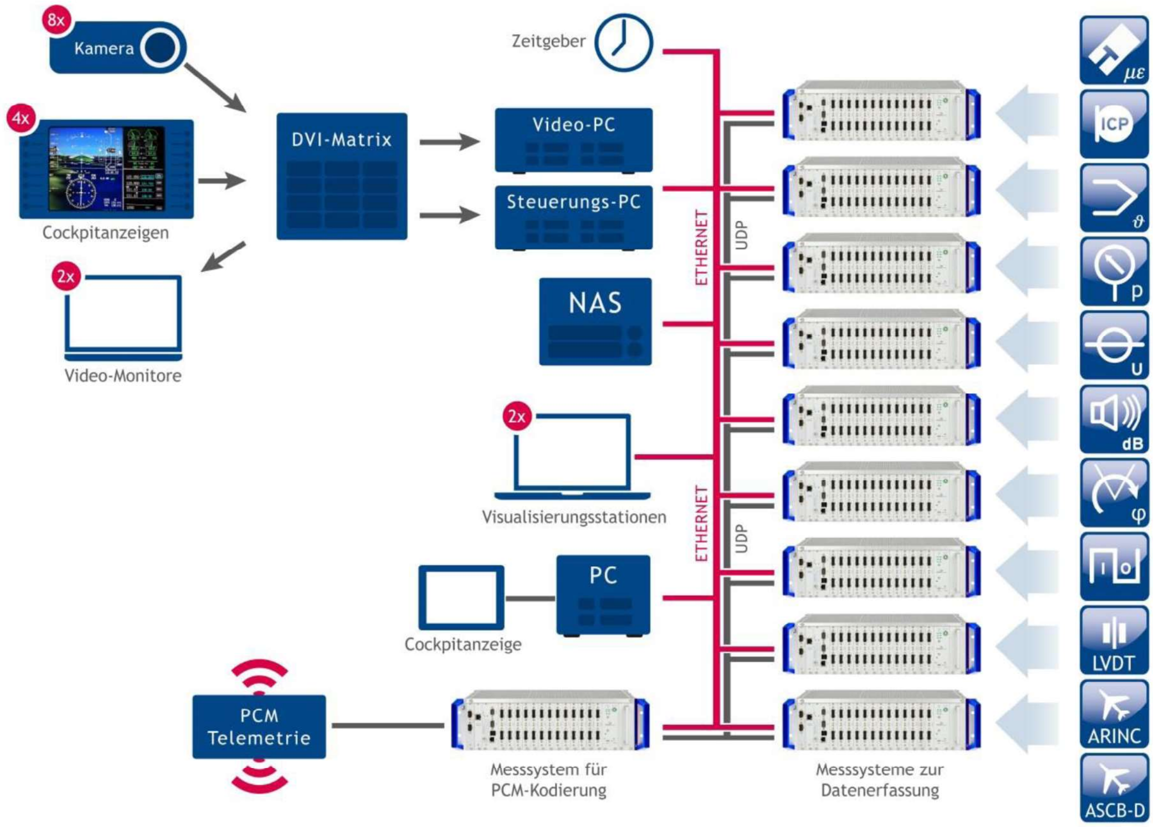

Fig. 3. imc flight test system design within an aircraft

Stabile power supply

To stabilize the power supply, the imc flight test system is equipped with a UPS system. This buffers temporary voltage drops and allows – depending on the batteries used – a self-sufficient operational time from 30 minutes up to several hours.

Telemetric signal transmission saves time

With a click of a mouse button, test engineers can select a telemetric transmission of all of the acquired signals within the aircraft. By means of PCM (pulse-code modulation), the selected measurement data will be transmitted online to the control center on the ground where they can be decoded, displayed and saved. This way, test engineers and technicians can already view and evaluate data and statuses online during the actual test flight. Of course, a real-time display of the measurement data is possible in the aircraft itself as well as in the control room – this flexibility is important to perform the testing in the most time-efficient manner as possible. Because the telemetric transmission is limited by your bandwidth, separate sampling rates can be configured on a channel-wise basis for the PCM transmission.

Comfortable software with flight-specific display elements

The complete operation and display of the measurement is carried out with imc STUDIO measurement software. It allows for convenient configuring of the test set-up from the office PC without being connected with the systems. In addition, it offers numerous possibilities for the visualization of the measurement data. For example, position data can be displayed on a moving map that literally moves in the curve window in relation to the position of the test aircraft.

With the imc Export Program, the user is able to carry out subsequent analyses of the measurement data with their own evaluation software. Alternatively, the powerful imc

FAMOS analysis software is also available. In addition to numerous display options and hundreds of ready-made analysis functions, it also offers automated data evaluations and provides a simple means of creating professional reports, thus increasing productivity.

Conclusion

Modern aircraft developments require increasingly complex testing within a tight timeframe. With the imc flight test system, test engineers have a proven and flexible solution available to them. All relevant measurement values from the flight test, such as that from sensors, aircraft buses, cockpit displays and video feeds, can be acquired synchronously from multiple channels and securely stored.

The comfortable software shortens configuration times and provides visualization and analysis at the push of a button. Furthermore, telemetric signal transmission allows more testing to be conducted in a shorter amount of time because the ground personnel can make direct assessments of the measurements without requiring the test aircraft to land between tests. This saves time and ensures productive test sequences without stopping.

imc Meßsysteme GmbH provides continued support to their customers with comprehensive services, such as with instrumentation, signal connections, commissioning or evaluations.

Lessons learned

Because of the multiple data sources and thousands of measurement channels, one of the greatest challenges turns out to be the startup time of the complete system.

In order to record all of the different data sources together in one data sink, it requires a lot of effort to safely boot up all of the components and have stabile operation with each other.

In the case of the imc flight test system, a configurable startup sequencer is used that guarantees an orderly startup of individual hardware components, thus ensuring a safe startup of the entire system.

As a further challenge, operation of the system is performed by various users who operate their individual measurement PCs differently. This leads to changes in software and firmware statuses that can cause problems upon startup of the system.

The solution to this is a fixed boot manager that resets all PCs upon startup to a defined starting configuration. This requires, however, that the boot time is extended by approx. 1 min 45 sec.

Since it is desired that all data sources are synchronously recorded, an external timecode interface is used which synchronizes all system components to a single time base. This process extends the startup time by an additional 2 minutes.

After the synchronization, the software configuration and the experiment are loaded into the connected hardware components and the system is prepared for startup. This process takes an additional 3 min 30 sec for all systems. Loading of the UMS data (digital data source with approx. 3000 channels) appeared to be the only outlier and significantly delayed the startup time of the overall system. This operation requires up to 8 minutes.

This puts the total startup time for the system at 12 minutes.

In conclusion, the following can be said: if startup times less than 5 minutes are required, then it will only be possible by sacrificing functionality.

For example, if synchronous video recording is omitted, then all of the measurement data can be locally saved in the imc measurement systems. Thus, additional measurement and storage PCs are obsolete. Such a configuration has the big advantage of being extremely stabile (imc standard software) and is ready to calculate within a short startup time of approx. 2 minutes. The disadvantage is that the data must be transferred after the measurement via a transfer program to an evaluation PC, or as an alternative, the flash cards in the measurement systems must be exchanged.

DOI 10.5162/etc2016/4.3

High Performance Multi-Vendor Network Data Acquisition Platform

Domingos Henrique Beolchi Rios
EMBRAER S.A. – Gavião Peixoto – SP - Brazil,
domingos.rios@embraer.com.br

Abstract:
As the aircrafts are becoming more complex, the amount of data to be captured and processed during the test flights increases a lot and that is what we saw in the past few years. This is a result of the increment on the number and diversity of aircraft buses and the need for more complex acquisition systems to face the requirements and the demand from engineering. This paper describes the architecture of one system that not only met these requirements but introduce new concepts such as data redundancy and multivendor support. The Acquisition System is 100% Network Based but also has one PCM output that is used during Telemetry. This paper also brings some solutions to problems like the high network bandwidth on board, the amount of data recorded during the flights and the manipulation of it on the ground after the flight to allow efficient post flight analysis. There are also additional challenges with the integration of equipment from multiple vendors and the real-time visualization both onboard and during Telemetry.

Key words: Network Data Acquisition, PCM, Real Time, Data Processing, Flight Test.

Introduction

We have being using PCM based acquisition systems from several years in many different aircrafts. Actually, we still have some of them operating and producing good results and data to be analyzed. The problem was that on some of the projects we had do acquire a large number of parameters (and consequently data) that has to be processed and stored during the flights. In order to properly handle all the requirements passed to us we decided to use an Ethernet base architecture, much more flexible and capable of accommodate many different data sources and large amount of data. We did this on a smooth way using the first project as a transition (PCM based with some Ethernet data) and finally got the full Ethernet on the second one (Ethernet Based with some PCM) [1]

Since this second one was bigger than the previous, we also took advantage from the weight savings on cable harness and the extra flexibility to accommodate analog data and many aircraft buses on the same system.

During the design and integration we faced several challenges, some of them are shared here.

Ehternet Based does not mean no PCM

We have a small PCM stream that is used only during Telemetry Sessions. It has less than 3% of all the data acquired and most of the parameters are under sampled on that transmission. This is another benefit of Ethernet acquisition: we can have the same data sampled with different rates without compromising the post flight analysis. This PCM stream has no use for us after the flight and is discarded.

DOI 10.5162/etc2016/4.3

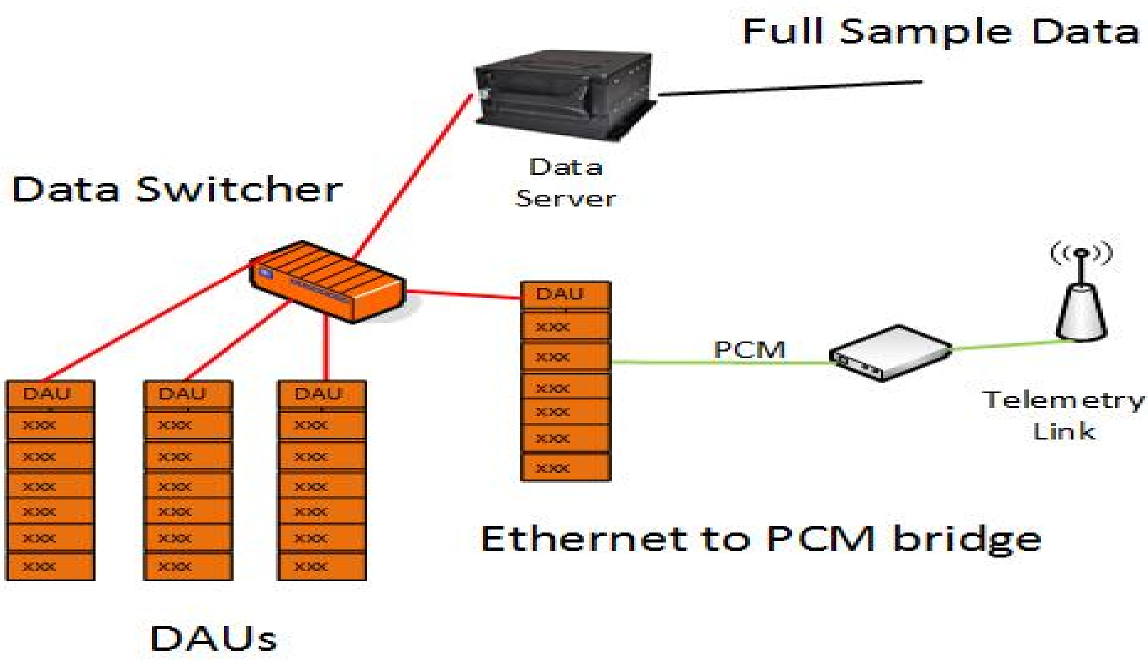

Fig. 1. PCM for Telemetry.

High Network Bandwidth

Ethernet is non-deterministic so we had to count on good acquisition timestamping, network traffic stability, zero packet loses and spare bandwidth to have a reliable system.

Added to this was the large number of parameters and aircraft buses required that caused high data rates on the acquisition network. To handle this we decided to physically segregate the data acquisition network from the other aircraft network traffic used during the flight (typically compressed video and Engineering Workstations). By doing this we end up with a network with relatively stable traffic during all the flight and spare bandwidth. The time synchronization was done by the standard IEEE-1588.

Another challenge derived from the high bandwidth was to find good Ethernet switchers because they are the heart of Ethernet based Acquisition Systems. The switchers must not only synchronize the time of all the acquisition units but also deliver every single package produced by them to the recorders and Data Servers on board with zero loses. Since the Data Acquisition Units are spread along the aircraft, we had to install many switchers on board distributed on layers to aggregate the traffic towards the recorders and servers.

DOI 10.5162/etc2016/4.3

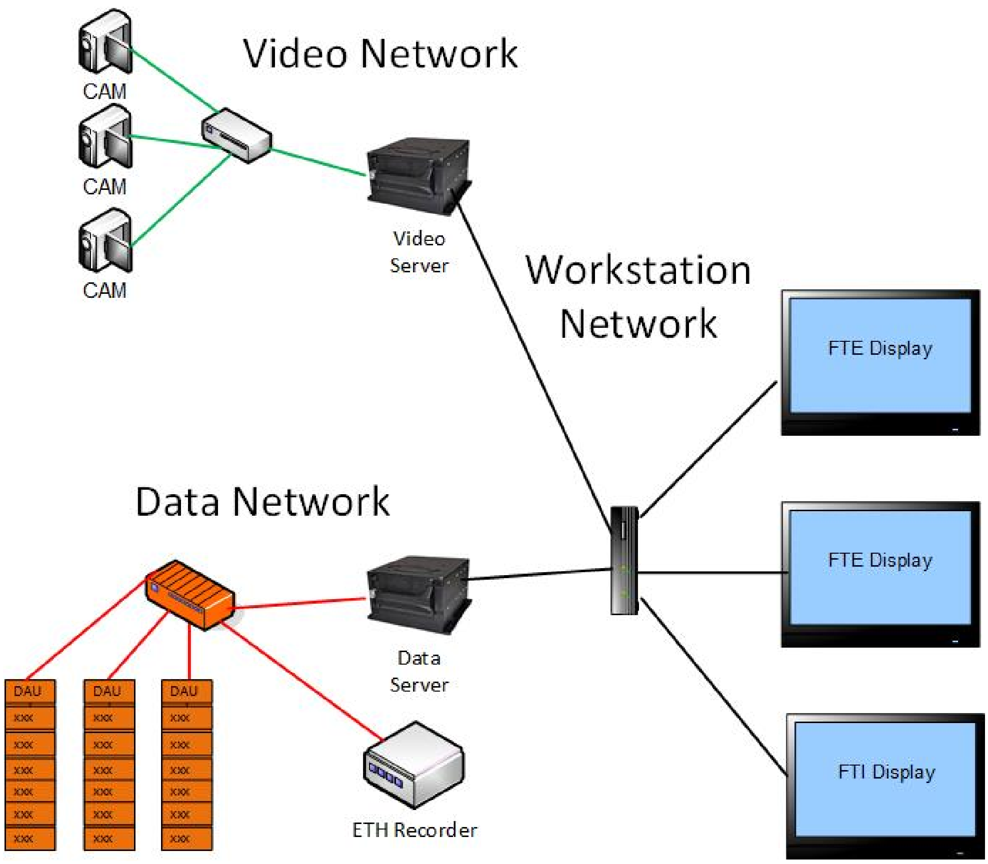

Fig. 2. Segregated Network Configuration.

Fault Tolerant

To improve the system reliability we designed a dual redundant network for acquisition and processing. If we have a failure on switcher, cable or server we don't lose the flight. Since the video acquisition was not essential on most of the flights we only have dual video servers an not the full network infrastructure as we have on Data Acquisition.

All the servers are also recorders so they have removable SSD modules to be collected after the flights. In order to have a Dissimilarity we added a third recorder that receives data from all the primary networks and just record them as a backup (no processing).

We also had to include a Redundancy removal layer on the Visualization Platform so it is transparent to the Engineer on board the source that is being used to receive the data.

DOI 10.5162/etc2016/4.3

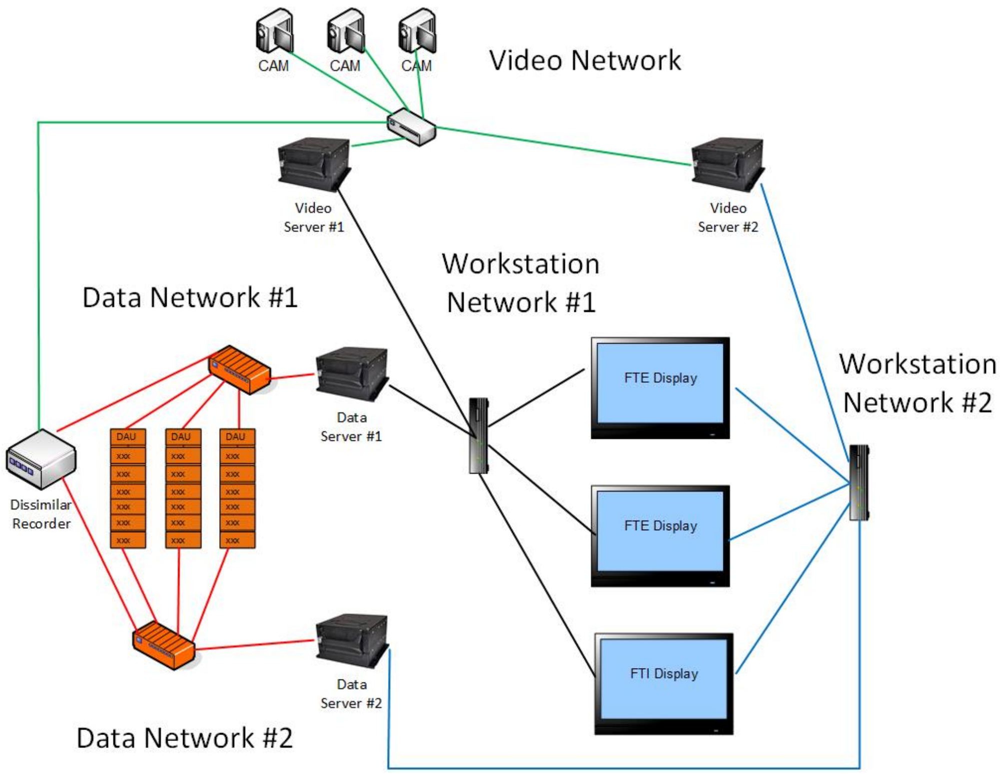

Fig. 3. Redundant Networks.

Amount of Data

With all the bandwidth and the redundancy installed, we end up with a huge amount of data being recorded after each flight. Even a single recording can have 1 Terabyte of information after certain test flights. To reduce the time spend to made the data available to be analyzed by the Engineering we have designed a way to not copy any data to fulfill the first requests just after the flight. To do this we insert the very same SSD module used on board into the Servers on the ground station. The actual copy and backup processes are done hours after the flight when the servers are not being used. Each flight uses 5 or 6 SSD modules, depending on the configuration.

We also have High Speed SSD modules with multiple access lines that allow us to read at 2GBytes/s. To reduce the amount of data recorded for historical purposes we store only the Raw Data (zero processed data stored) by using an on-demand data processing configuration.

DOI 10.5162/etc2016/4.3

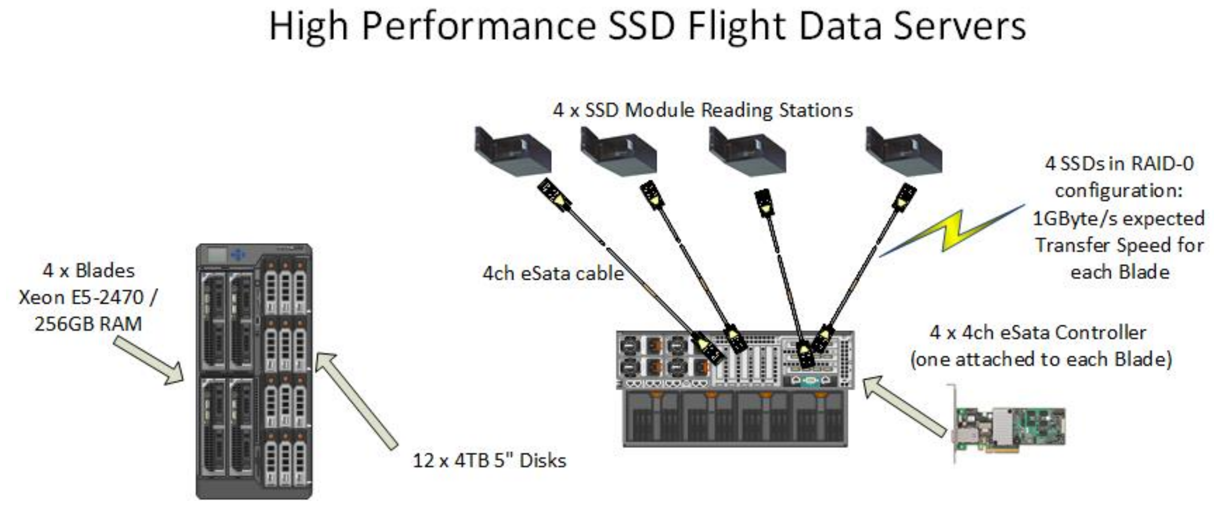

Fig. 4. Flight Data Servers.

Multiple Vendors

Not a single manufacturer had a solution to all of our requirements of data acquisition (like high data rates, optimized bus acquisition, recorders, switchers, etc.). So we had to design a system capable of receive data from multiple manufacturers and with different hardware platform. Everything must be converted to Ethernet first (usually with distinct protocols). After that, we collect all the sources in the main switcher and send the packages for recording and processing.

We decided to use a single protocol for the processed data (after RAW to EU conversion) and we had to write specific modules on the server to handle each different input protocol and convert the data to the same output format to be sent over the Workstation Network.

Integrate such a system is another big challenge because of the diversity of hardware, configuration programs and usually some particular view of the International Standards.

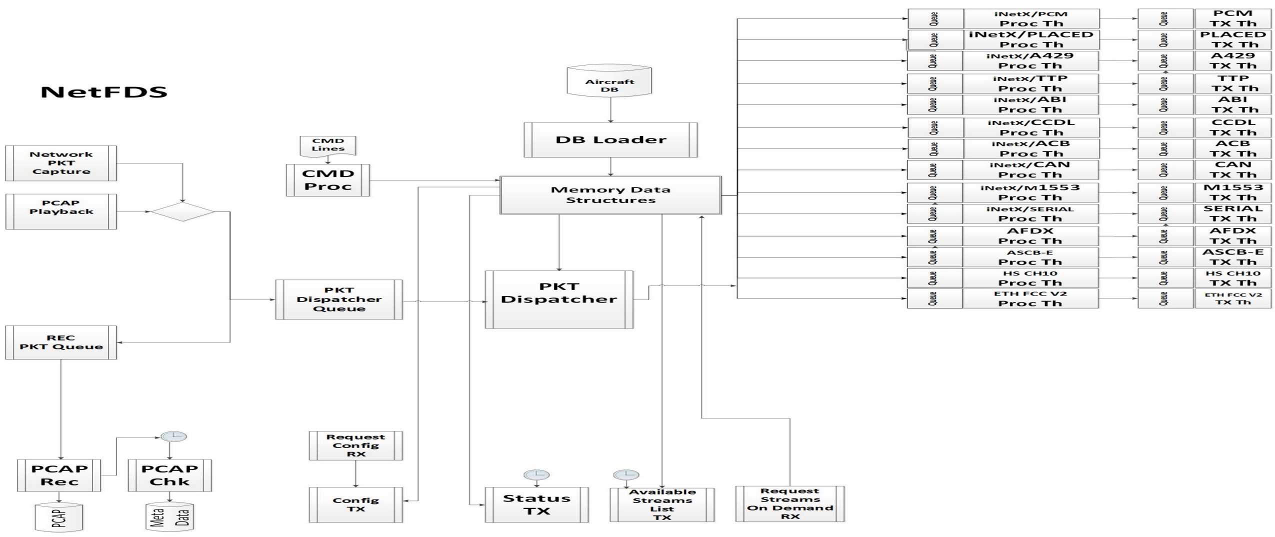

Fig. 5. Main Data Processor Software architecture.

Visualization Platform

The requirements for the Visualization Platform were not simple and due to the numbers involved, the job was not an easy one. The initial requirements include:

- High number of data sources (500+);

- High number of parameters (100K+);

- Ethernet bandwidth (300Mbps+);

- Redundancy (2 networks).

- Single platform onboard and during Telemetry sessions;

Custom displays (pilot, PIO)

Needless to say that we did not find a comercial tool that has all those requirements.

So we end up developing our own platform and we had to start from scratch because our previous versions were just for PCM systems.

- Electronic Flight Card Integration (Test Points, Procedures, Load Configuration changes, refueling);

- True Real-time display (all samples with coherency);

- Distinct time stamps for each data source;

- Integration with analysis tools (spreadsheets, Mathlab, 3rd party)

-

The software uses a common client interface that handles all network protocol and put the data in a shared memory to be used by client applications. The data can be also shared among other workstations over the network.

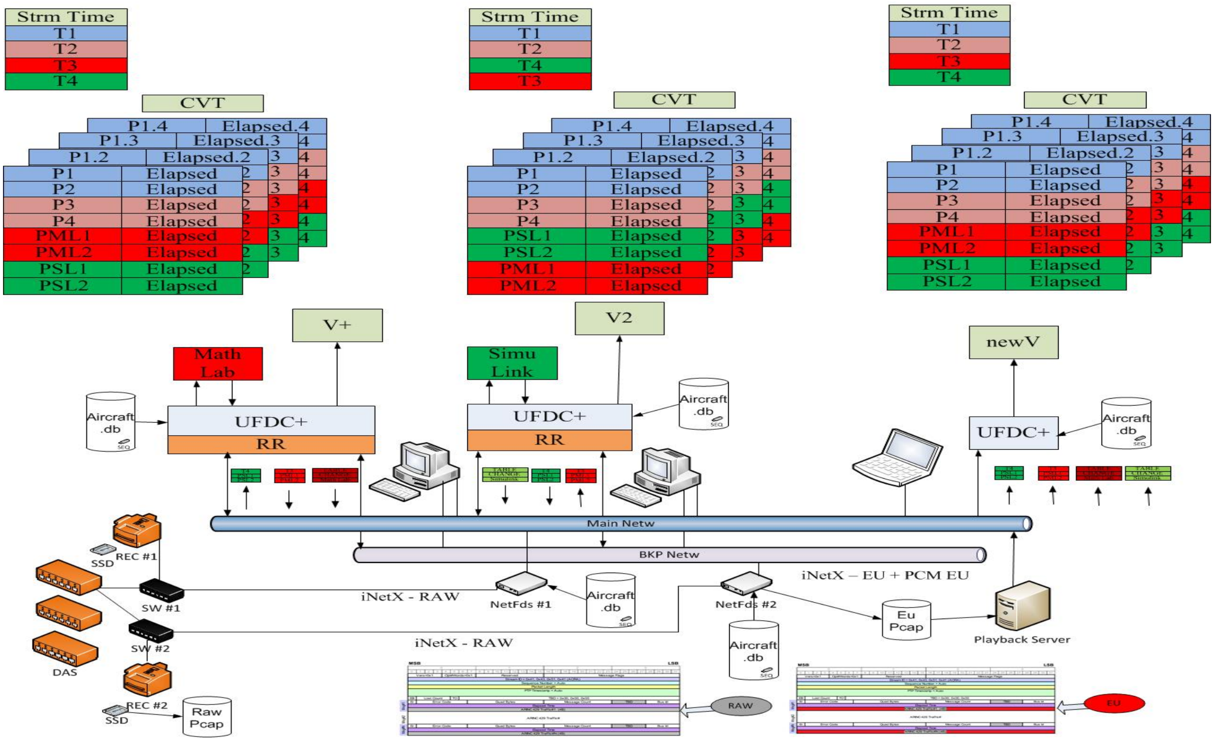

Fig. 6. Main Data Processor Software architecture.

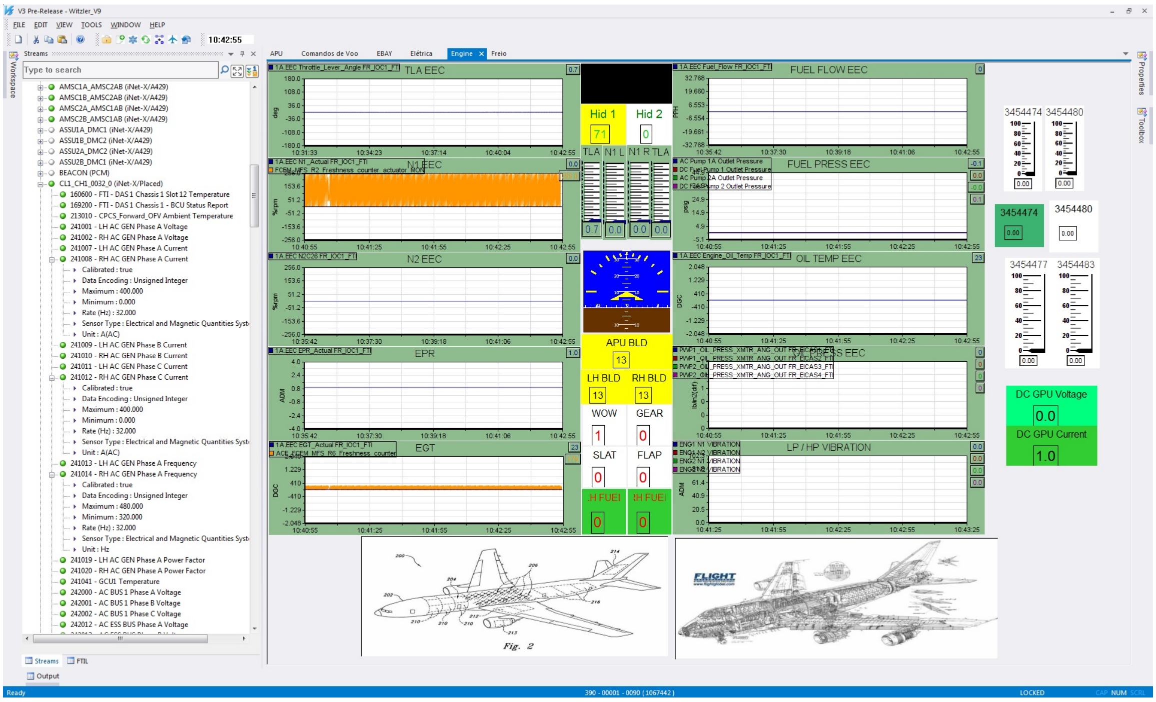

Fig. 7. Screen Sample of the Visualization Platform.

Conclusion

The System explained here is on its second generation so it has been improved (and increased) from its original configuration. It is being used by many aircrafts with very good results.

References

[1] Luiz Fernando de Souza, Domingos Henrique Beolchi Rios and Stephen Willis, 2012, “PCM to Ethernet: A Hybrid System Used to Certify the Next Generation of Data Transfer Technology”, Proceedings of the International Telemetry Conference 2012

DOI 10.5162/etc2016/4.6

The Research of Smart Ex-telemetry System of Launch Vechilce

Feng Tieshan[1], Li Daquan[1], Lan Kun[1]
1 Beijing institute of Astronautical Systems Engineering, Beijing, Fengtai Strict Beijing China,
fengtieshan1987@gmail.com
baiyou1987@163.com

Abstract

The article put forward a new idea to reduce the preparing time of launch vehicle. With the use of IP-based technology and artificial intelligence, every instrument in the launch vehicle can be connected with the high-speed and high-reliable data bus. Besides , the testing instruments on the launch pad will use the same protocol between the electronic instrument on board and off the board. In this way, a more simple testing process will be proposed which will reduce the preparing time and cut the cost of launching task. Many innovative details will be discussed in this paper. In Section I, practical issues for low-cost launching will be discussed in brief. In Section II, a general application scheme will be put forward to simplify the process of electronic design. Section III describes more details about the key technology to reduce the preparing time and launch cost. Section IV contains the models, results and analysis of the protocol simulation

Key words: launch cost, preparing time, IP-Based technology, Telemetry system, Simulation.

Introduction

The technology of launch vehicle stands for a country's ability of entering into the space autonomously. Since 1957, the first satellite is launched by the Soviet Union, the humans are pushing forward the technology of launching vehicle continuously. More than 500 lauches have been made to explore the outer space. In recent several modern locality conflicts, the military affairs have been revealed more and more important. At the same time, the weakness of the traditional space telemetry, test and control also restrict the application of launch vehicle. Besides when the natural disasters happens, the base stations of mobile phone are destroyed which makes troubles for rescuing. To sum up, it is important that reducing the launching time means a lot for a launch vehicle. For the war happens in future, because of the weakness of communication system of space-based, it is also important to enhancing the ability of rapidly-launching. Considering what is mentioned above, it is not hard to come to a conclusion that dropping down the cost , promoting the smart-test ability , realizing the low-cost and high-speed test is of significance for launch vehicles especially for the commercial launch vehicles.

Common architecture

The implement of smat-testing launching pad relies on the advanced electronic topology architecture and high-reliability transferring protocol. For this time, in the international aerospace launching application, ESA and NASA both take the TTE as the next generation high-speed data bus. This protocol is implemented based on AS6802 timing synchronization protocol, which is of great competing superiority. In conclude, the ability of networking and intelligentizing for launch vehicle has been the main developing stream. As while, the progress of networking technology also provide a new moment to implement the smart test of launching measuring system.

Different from the traditional measuring methods, in order to implement the fast testing system, the transferring protocol for the ground test and on-board test should be unified by one same protocol, which will increase the launching efficiency. Besides, the telemetry system also needs the ability of high reliability and expandable. However, the traditional networking transferring protocol and Time-trigged Ethernet can not provide the command-respond mechanism. As a result ,even the message can be transferred to the telemetry net through two different ways, we can not decide whether the destination node has received the message correctly. So we put forward a new application ,which will in use of the physical layer of Ethernet, while the other communication layers will referring to 1553B protocol. The topology of system can be seen in fig-1.

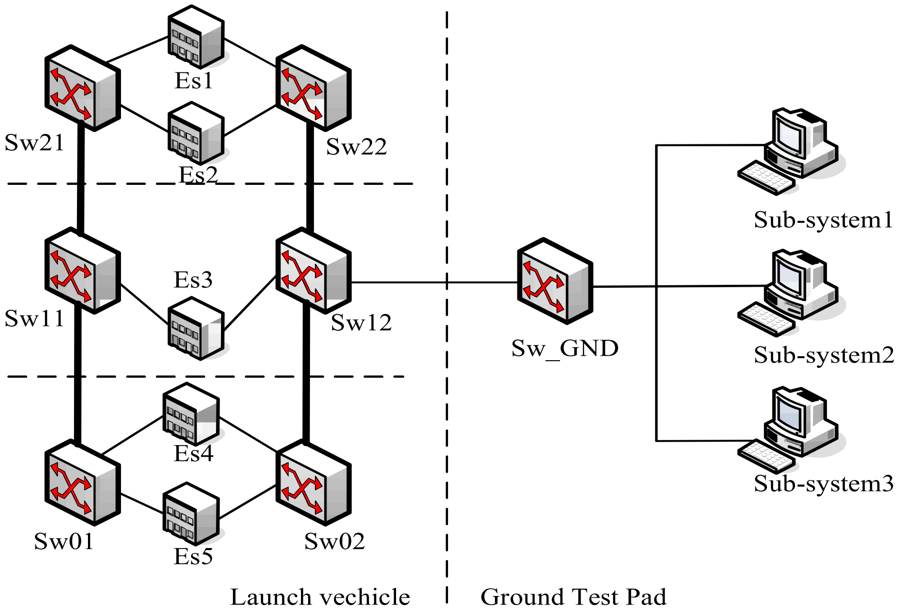

Fig 1 Testing Topology of Telemetry System

In Fig1, there are two parts for the testing topology of telemetry system. The first part is launch vehicle part, the other part is ground test pad. In launch vehicle part, there are two different electronic circuit board. For the first one is switch electronic board, which mainly swap the transferring message from the input port to the correct destination port according to the configuration table in local equipment. For the second one, every equipment on the network should set the appointed electronic board to achieve the network-communication function. The second part is Ground Test Pad. In this part, there are two kinds of equipment, the switch node and sub-system testing computer. The switch is used to send every message to specific node. While all the stations of different sub systems would be linked to the central switch node.

Traditionally, the telemetry community has used a time division method of packaging the data into link-level transmission data frames for transport over radio links. With the growth of the Internet, the transmission of the telemetry packets often looks like a computer to computer communications as more telecommunications are used for data acquisition and distribution. Data communication will occur over wireless and wired links as well as fiber optic links. The IP-Based Telemetry Network is optimized from the traditional Ethernet technology. The equipments in the system will be distributed with an unique IP address. Besides all the network equipments will also have a MAC address when they were manufactured. Depending on the real-time protocol (like IEEE 1588), the whole system will have a relatively accurate operational clock.

The IPTN communication profile is shown in Fig. 2.

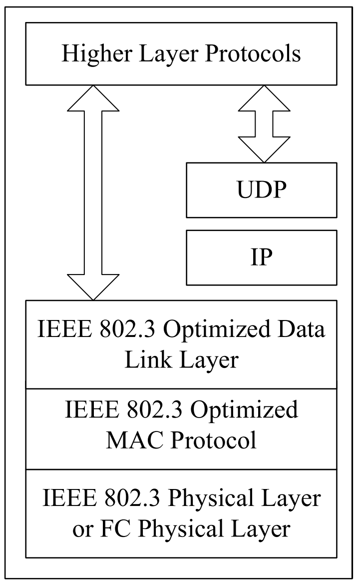

Fig.2. IPTN communication profile

In Fig 2, IEEE 802.3 Physical Layer has been used for references. In order to reduce the weight of electric cable and the influence of electronic interference.The fiber (References as FC0) is also taken into account. The Media Access Control Layer and the Data Link Layer are the most important Layers which determine many integrated performance such as error rate ,packet delay and so on.With regard to the IEEE 802.3 Protocol Data Unit, IPTN comprises three additional fields which have been allocated on the first five bytes of the ‘data’ field of the IEEE 802.3 original frame. In this way, the system could match the specific field to recognise the correct frame and discard the redundant frame.What’s more , as we do not destroy the original format of the IEEE 802.3 frame, the frames communicating in the network can also be transmitted in the industrial switchboard, which could unify the communicational protocols on board and ground. The highly mature UDP/IP services is invisible as well. The Internet Protocol sends or receives the network data of the net points. The IP is responsible for the fragmentation and re-assembly of blocks of messages. This is required when the amount of data needed to sent is greater than the maximum IP data payload of a single frame. The User Datagram Protocol (UDP) parses data from one or multiple applications to the lower network protocols. However the Transmit Control Protocol is most used in the Ethernet, the timing of the receipt is non-deterministic. As a result, UDP is preferable in the IPTN. The frame format is shown in Fig 3.

Preamble	Start of frame delimiter	MAC Destination	MAC Source	Tag	Length	Payload	CRC
7 octets	1 octet	6 octets	6 octets	4	2 octets	46~1500 octets	4 octets

Fig.3. IPTN Frame Format

Timing synchronization

The disadvantage of Ethernet, opposite to an astronautical application, is a non intrinsic determinism of its access method to the physical support. To improve the bandwidth and real-time speciality, people put forward many ideas to make the telemetry system a determinate one. In spite of increasing the bandwidth to avoid conflicts, many other ways have been raised to confirm the real-time speciality of the whole system.

IPTN, as a flexible and reliable system, has many ways to improve its electronic features. First, using the IEEE 802.3 PHY Layer to guarantee its 100/1000Mbps Ethernet communicating ports.Secondly, comprises three additional fields which have been allocated on the first five bytes of the ‘data’ field of the IEEE 802.3 original frame.These new data fields are used to manage the redundant frames and to distinguish different data types.

The transmission of the telemetry data from the payload segment to the user segment and the commands from the user to the payload are typical communications problems encountered in many settings. Synchronization is a key technology for telemetry system design. Based on the IEEE802.3 original frame, the synchronization information is also included in the improved packet structure. While the net is under operation, the network equipment will control the system clock and finish the synchronization of the crystal oscillators. The network message could be divided into two types.

1) Event message: a message with time stamp.When the message is delilvering in the network, the network equipment could calculate the point-to-point delay with the help of time information stored in the event message.
2) General message: Opposed to event message, the general message does not contain any time information, this kind of message is mainly used to build the master-slave relationships.

Three steps are followed to achieve the synchronization of the whole net.

1) Establishing the master clock. In order to supervise the different clocks of all the network equipments, there should be a precise system clock in the whole system. This precise system clock could be obtained from Beidou II or GPS. Besides it can also be acquired by the high-precision clock source.
2) Synchronize the frequency of different clocks. The master clock send the sync message to the slave one, in which message there is time information stamped the sending time. The slave point receives this message and record the receiving time. While the same slave point receives at least two messages continuously, according to the sending intervals between contiguous messages. The slave point could adjust its clock frequency to the master point. In this way, all the equipments in the network could work under the unitive frequency. The regulation of clock frequency shows in fig 4.

Synchronize the time of different clocks. The event messages are used in the process of clock synchronization. The detailed steps are as follows.

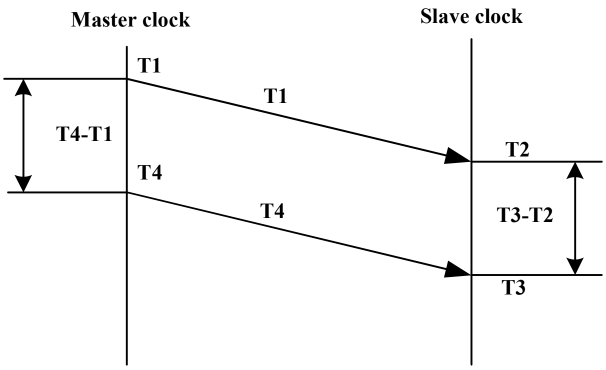

Fig.4. the Schematic diagram of frequency adjustment

1) The master clock send the sync message to the slave point, including the sending time T1;
2) The slave point records the receiving time T2;
3) The slave point returns the request messages to the master clock, and records the local sending time T3;
4) The master clock records the receiving time of request message T4. Then sending back the delay request message including the time T4 to the slave point;
5) The clock synchronization shows in the figure 5.

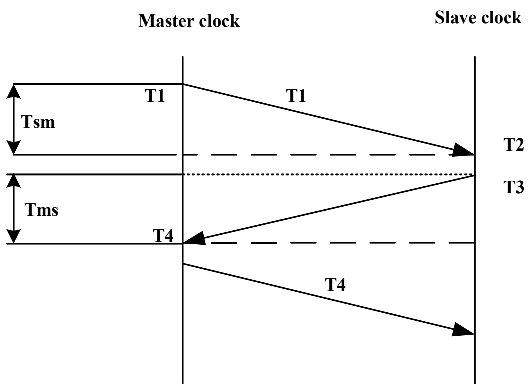

Fig.5. the Schematic diagram of timing adjustment

According to the four steps above, the slave clock could calculate the delay and off-time as follows.

Delay = [(T4 – T1) – (T3 – T2)]/2 [1]

Offtime = [(T2 – T1) – (T4 – T3)]/2 [2]

Depending on the route delay and off-time, the slave clock adjusts its clock to the master clock.

Data integration is a key function for telemetry syetem of launch vehicle. Compared with the traditional methods,the technology of net-based integration has its advantages in terms of reliability, data capacity, system intelligence, general duty and so on. In the launch vehicle data integration system, the configuration of the whole net is kernel, which decides some important designing targets, such as throughout capacity, packet loss probability and network delay. Considering the practical demanding, this article focuses on the configuration project of launch vehicle data integration system.

The appearance of virtual local area network tremendously promotes the development of real-time Ethernet. When the IPTN is working, there would be many virtual links flow into one equipment. In that case, this equipment must deal with these flows according to certain algorithm, which decides the performance of the whole network. In IPTN, the equipment implement a scheduler to manage the flows.The algorithm is mainly based on the Quality of Service (QoS). The scheduler would record the waiting time of every virtual links. According to the weight of links' priority, waiting time and the message length, the scheduler would send the proper link and update the weight of every items. The simulation will show the results of different scheduled algorithm.

The algorithm of scheduling

The algorithm of network frame scheduling has many mature methods, which is not available for launch vehicle. It is necessary to study the scheduling algorithm. Because the topology of network and end system are pre-settled, which results in a static network. Thanks to this special character, it is much easier for engineers to design the whole communication process of network. There are two different situations.

Directly-distributed schedule

The most important frame (we call it TimeStrict Frame,TSF) which needs to be transmitted at the very moment is scheduled as followed in Fig 6.

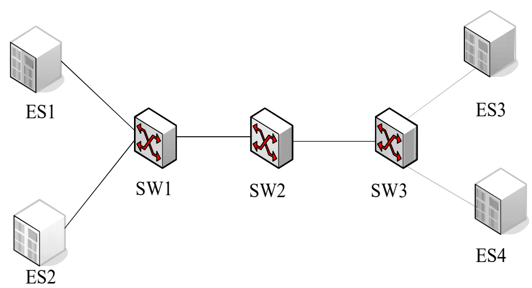

Fig.6. Directly-distributed schedule diagram

DOI 10.5162/etc2016/4.6

Sw1, Sw2 and Sw3 are three switches in the network. When these switches transmit frames, they only work as transparent equipments, which means that when the valid data are being transmitted through the network by ES (End System), the TSF would be discarded or conveyed transparently. In that case, time-strict frame would be transmitted at the very moment. For instance, when ES1 is designed to transmit the frames to ES3, ES1 would send the frame the SW1. SW1 receives this frame and swap this frame directly to SW2. SW2 and SW3 would do the same thing to transmit this frame coutinuously.

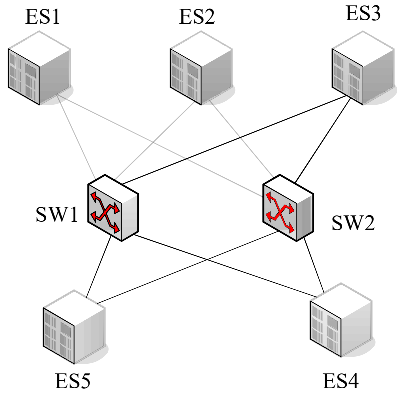

Fig.7. flowing frame in redundancy network

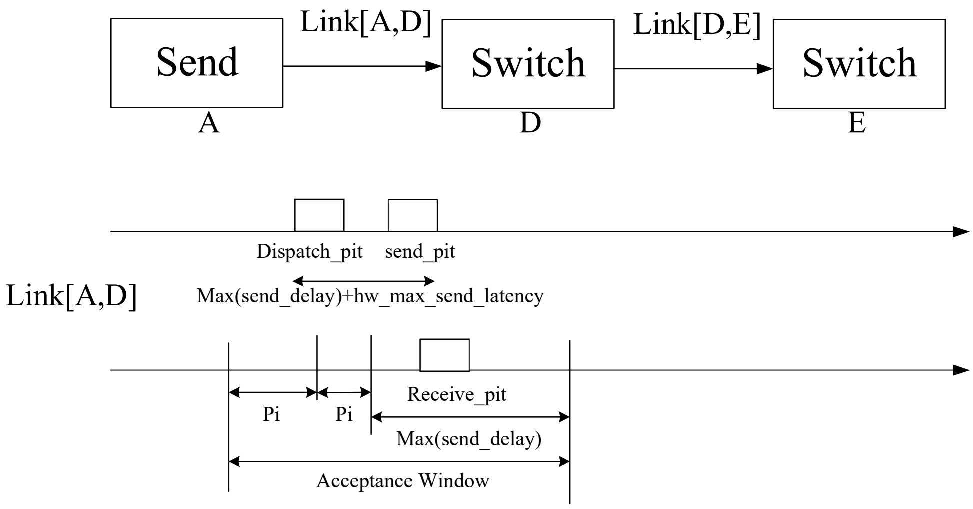

Fig.8 .Directly-distributed schedule diagram

Fig 7 shows a redundancy network. In this situation, when the ports of SW in the network is busy, the TS Frame would not be discarded. On the other hand, SW would store this frame, and puth them into the fifo, waiting for the free time to swap this frame again. The destination node would receive two frames from the source node and according to the specific judging rules, the destination node would discard one frame and receive the other. What`s more, when one frame is destroyed or lost in the net, the destination node would receive at least one frame.

Store-distributed schedule

In this part, we will directly get the algorithm. Firstly, we will define some definitions.

Dispatch_pit: the transferring time of the time-strict frame. This time is generated offline to trigger the dispatch of this kind of frame.

Send_pit: this moment refers to the transferring time of the first bit after the preamble.

Send_pit refers to the the scheduled moment at which time, just a new frame is being sent , resulting in postpone in net communication. Max(send_delay) stands for the maximum delay time between two different equipments. While hw_max_send_latency represents the settling time the circuit costs. So we can get:

$$\begin{aligned} send\_pit \in [&dispatch\_pit, dispatch\_pit \\ &+ \max(send\_delay) \\ &+ hw\_\max\_send\_latency] \end{aligned}$$

Receive_pit:
The receive_pit time represents the time the specific frame is being received.

$$receive\_pit = send\_pit + link\_latency$$

the models of the net equipment

The network equipment models are simulated with OPNET Modeler.There are two kinds of

DOI 10.5162/etc2016/4.6

models in the simulation, communicating point and switching point.
The communicating point in the network is shown in figure 9.

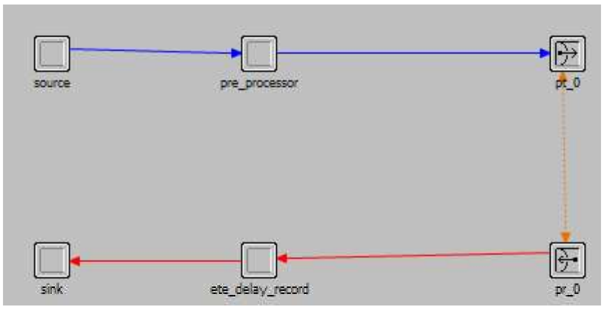

Fig.9. the model of communicating point

This node includes 6 parts. “Source” is used to generate the original data flow. “Pre-processor” is used to mark the timing stamp and assign the attributes for each virtual links. “pt_0” and “pr_0” is a mature function block to send and receive the network data. The results and synchronization is recorded by “Ete-delay-record” .At last, the data communicated in the network would flow into the “sink”.The sink extract the useful information and destroy the packet.
The switching point receives the data flows from other communicating points. The schematic diagram of switch point is shown in figure 10.

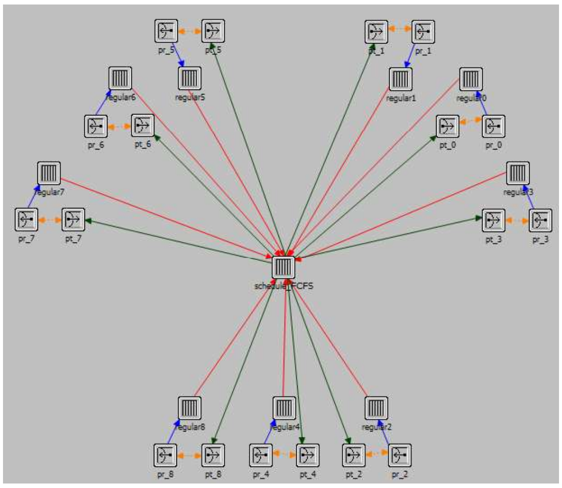

Fig.10. the model of switching point

Every switching point has 9 ports to communicate with other points. There are 4 sub-models in each switching node. The function of “pr” and “pt” is used to receive and send the network packet. “Regular” is used to realize the MAC protocol of the switching point. “Scheduler” is the most important sub-model in the switching node. This block will pick up the certain attributes of every data flows and send it out according to some certain algorithm, which has been introduced briefly.

3.2 **the test scenario**

In this section, we consider a work-conserving system shared by multiple input processes under different service disciplines. Within each source, FIFO is assumed. In order to compare different schedule algorithms, two scenarios are built to prove the correctness of the whole system.

3.2.1 **Scenario I**

In scenario I, eight communicating nodes(node1~node8), acted as data sources send network frames to node9 by routing switch node in the center.

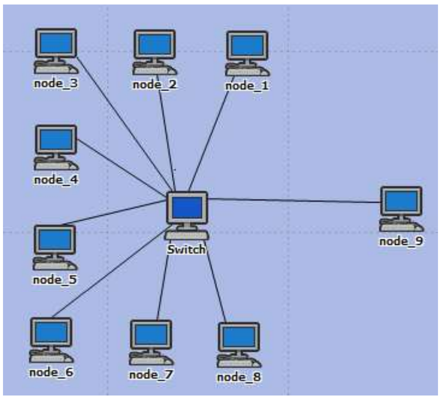

Fig.11. the topology of scenario I

In switch node, two different methods are used to testify the effects. One method is that every node in the network adopts the FIFO service discipline. The other one is that nodes in the network have strict priority. Assume that, if i<j, then the source I has a higher priority than the source j, which means that source j will not be served if there exists a workload from source I waiting for serving. Within the same source, FIFO is adopted. The results of the simulation would be shown in Fig 11.

3.2.2 **Scenario II**

In scenario II, an entire network would be built to check the correctness of the protocol. The topology of scenario II is showed in Fig12.

DOI 10.5162/etc2016/4.6

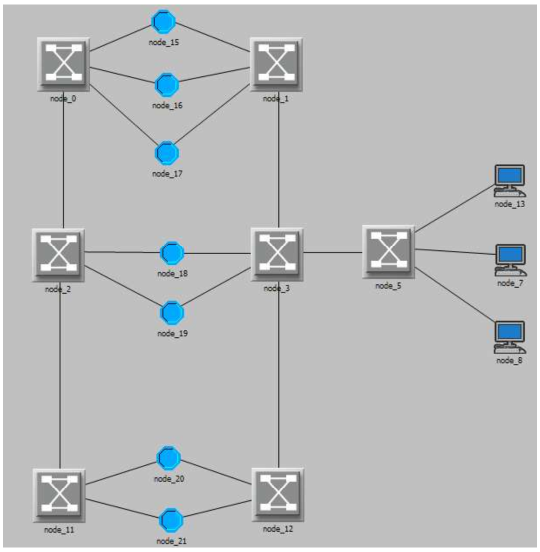

Fig.12. the topology of scenario II

In scenario II, the regular pattern of network nodes are listed in Table 1.

Table 1 Regular Pattern of Network Nodes

Identifier	Flows Type	Mean Value
Source1	Exponential	0.08
Source2	Exponential	0.08
Source3	Exponential	0.01
Source4	Exponential	0.01
Source5	Constant	0.08
Source6	Constant	0.08
Source7	Constant	0.08
Source8	Constant	0.08
Source9	Constant	0.01
Source10	Constant	0.01
Source11	Constant	0.01
Source12	Constant	0.01
Source13	Constant	0.01

Comparative Analysis of the two Scenarios

In the simulation, the flow admission control relies on the algorithms for scheduling. In scenario I, two approaches are applied to the same scenario. The results of three nodes are picked. The results are depicted in figure 13 and figure 15.

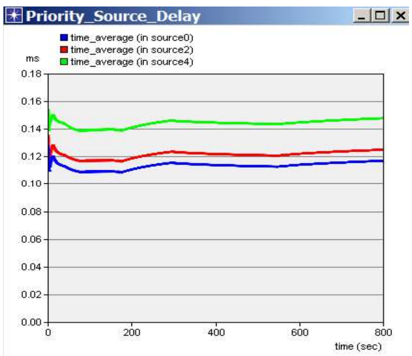

Fig.13. the results of FIFO schedule

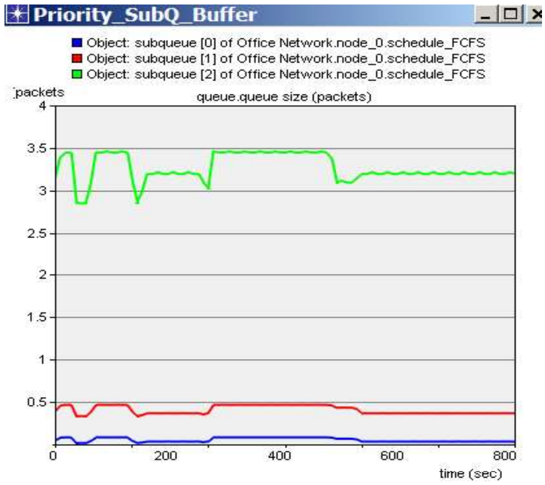

Fig.14 .the results of strict priority schedule

The correctness of the IPTN protocol is proved in scenario II. The result is showed in figure 15.

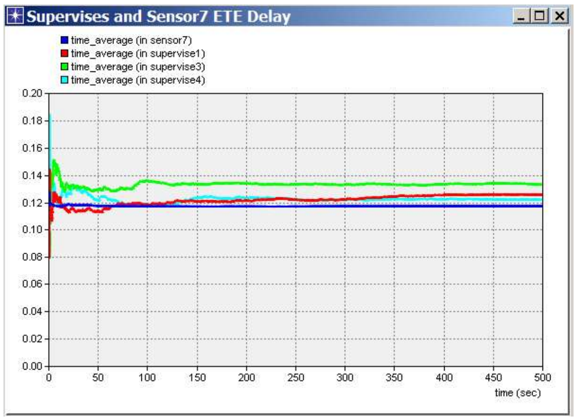

Fig.15. the topology of scenario I

The impact of the scheduling algorithm influences the real-time performance and the communicating process of the whole network. On these two scenarios, the trajectory approach shows two different trends, which implies the character of real-time. The full protocol stack is also proved in this simulation.

Conclusion

In order to reduce the preparing time for launching vehicle and decreasing the cost, the article put forward a new method to synthesize the on-board electronic system and on-ground test system. The traditional network communicating protocol can not meet the needs of real-time and high-reliability. Even some new real-time Ethernet protocol have settled these problems, the command frames transferring in the net can not be responded. The paper put forward a new method to make the equipments in the net communicate as 1553B-Based protocol. Besides, the equipments on the ground and the equipments on board can also be linked together. In this way, the interface between launch vehilce and ground can be simplified.

DOI 10.5162/etc2016/4.6

.

References

[1] International Reference Guide to Space Launch System, Steven J.Isakowity,AIAA;1991

[2] Van Allen Richard E, The future of Responsive Space [J]. A Summary of the results and papers from the 5th Responsive Space Conference,2007

[3] Ed Allen, William U. Integrated Ground Operations Demonstration Units Testing Plans and Status [R]. AIAA-2012-5247,2012

[4] Jain, R. and Routhier, S.A “Packet Trains: measurements and a new model for computer network traffic”. IEEE Journal on Selected Areas in Communications,1986. 4: 986-995

[5] Randy Black, Mitch Fletcher.“Next Generation Space Avionics: A Highly Reliable Layered System Implementation”, IEEE Communications Magazine. 2000, 38 (4)2004

DOI 10.5162/etc2016/5.1

Telemetry, Command and Control of UAs in the U.S. National Airspace

Presented By: Barry R. P. Jackson, Cahon Systems Inc.
RTCA SC228 Committee Member

1.1 Abstract

This presentation summarizes the current draft of the Minimum Operational Performance Standards (MOPS) generated by the Radio Technical Commission for Aeronautics (RTCA). The MOPS will be referenced by the FAA in its Technical Standard Order (TSO) to allow Unmanned Aircraft (UA) to fly in the U.S. National Airspace (NAS).

The TSO permits vendors to certify that their product meets the UA System (UAS) Control and Non-Payload Communication (CNPC) link standard, and if appropriate, the Detect And Avoid (DAA) standard. A TSO certified unit will simplify the certification process.

This presentation deals with the CNPC link only.

1.2 Introduction and History

The RTCA organization has supported the FAA for many years in developing DO-*xxx* type documents. From 2006-2012, the RTCA Special Committee (SC)-203 worked with the FAA to develop the standard to support UA flights within the NAS, including small UASs (sUASs).[1] Using this initial work, the (SC)-203 made a presentation to the International Telecommunications Union (ITU) for a spectrum allocation.

The ITU, at its 2009 meeting, agreed that a protected spectrum for CNPC needed to be allocated; see report ITU-R M.2171. Subsequently an allocation in L and C bands were sanctioned viz:

- L band 960 to 1164 MHz (may not be available for use in the U.S.A. due to a DoD concern with US Navy TACAN interference)
- C band 5030 – 5091 MHz

Because the original scope was too broad, (SC)-203 was disbanded and its effort was not completed. In 2013 the RTCA formed (SC)-228 with a narrower scope, building on the material developed under (SC)-203 and ITU-R M.2171, namely to develop the MOPS needed for non sUASs:

a) UAS DAA system [focus of Working Group (WG) 1]

[1] The limits placed on small UASs (drone systems) were initially described in the FAA's notice of proposed rulemaking (see the Federal Register, Volume 80; No.35; February 23, 2015) to add a new part 107 to Title 14 Code of Federal Regulations (14 CFR). This addition would "allow for routine civil operation of small UAS in the NAS and to provide safety rules for those operations".

DOI 10.5162/etc2016/5.1

b) UAS CNPC link (focus of WG 2).

Phase 1 of the MOPS being developed by (SC)-228 supports UA flights in the radio Line-Of-Sight (LOS) terrestrial environment. Phase 2 will cover non-LOS CNPC links. The CNPC link components and interfaces are shown within the rectangle in Figure 1 CNPC link major componentsFigure 1.

The CNPC link is one of several potential data links between any UA and the ground. An example of a non-CNPC link would be mission payload data. These links do not contain safety-of-flight information, and are outside the scope of this presentation.

The CNPC link carries all the data associated with controlling the safe flight of a UA including pilot to Air Traffic Control (ATC) audio communication.

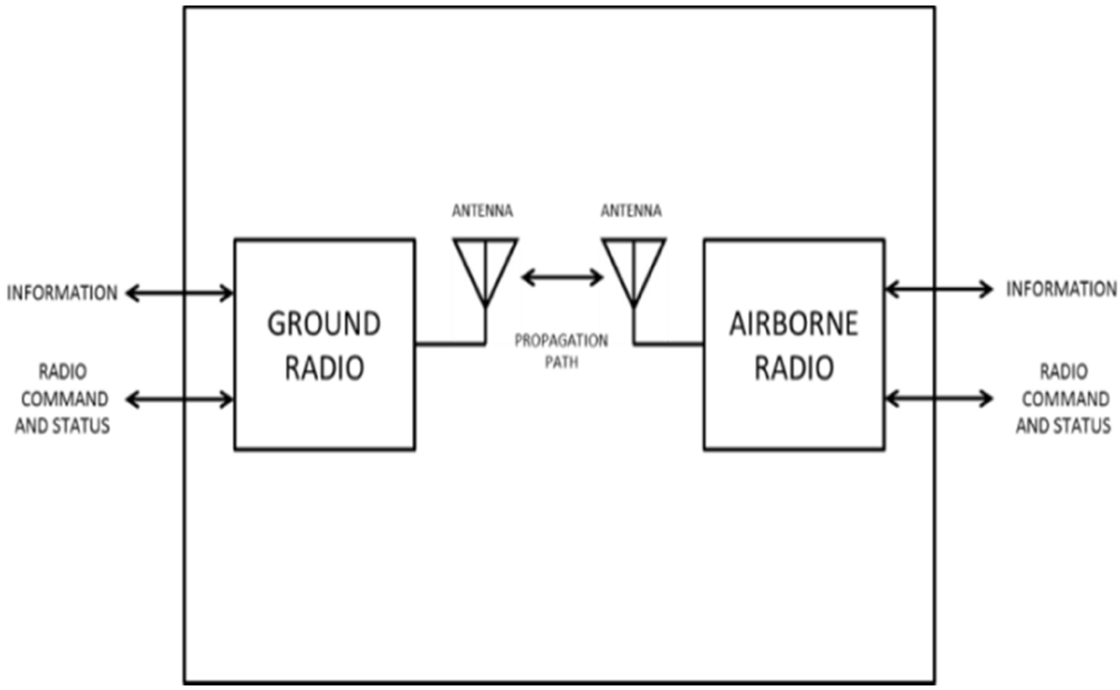

Figure 1 CNPC link major components

To confirm the authority of the MOPS, there will be a thorough validation process utilizing simulations and flight tests using CNPC link prototype airborne and ground radios and antennas. The MOPS will also include verification methods that can be used by radio designers to show compliance of their proposed radio and antenna designs with the MOPS.

The remainder of the presentation will give a brief overview of:

- Operational applications where the CNPC link could be used.
- Specific examples of UA operations.
- Needed information transfers.
- Translating UA operational scenarios into needed CNPC link features.
- System overview.

- Intended function.
- Anticipated growth of these CNPC link MOPS.
- Annotations and acknowledgements.

1.3 Operational Applications

This section reviews the operational aspects for UASs.

Overview of the Extent of UA Operational Scenarios

The MOPS developers recognize that there are many possible flight profiles that could be flown by UAs within or among the seven airspace classes defined by the FAA. To help explain the challenges in developing the CNPC link MOPS, three example UA flight paths within the airspace classes are shown in Figure 2.

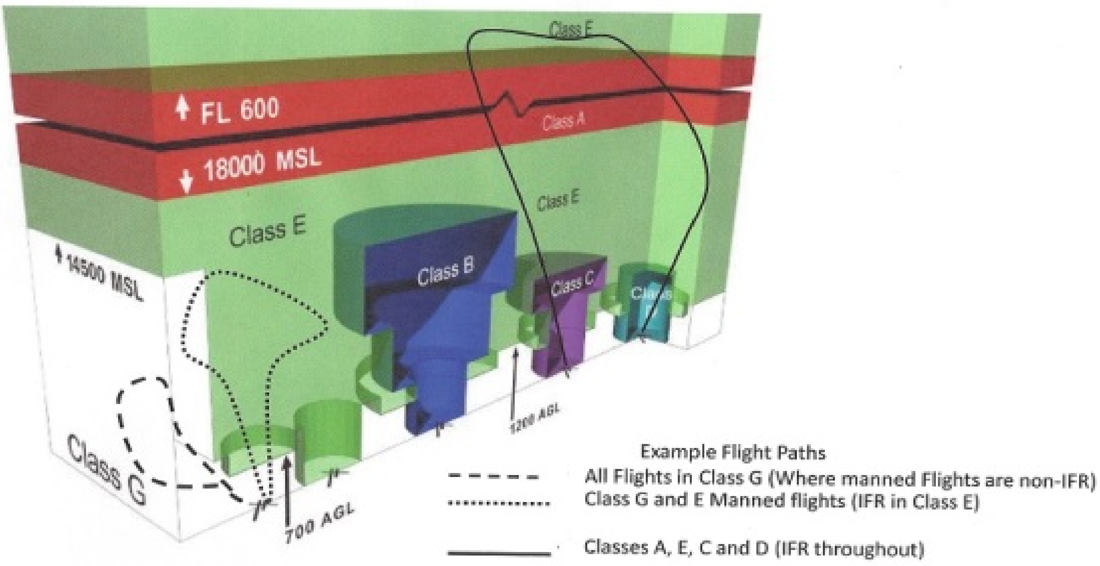

Figure 2 U.S. Airspace Classes with 3 examples of UA flight paths superimposed

The sizes of the UAs, their flight performance, and their avionics and sensor features range from simple to very complex. It is expected that a UA capable of flying within more congested airspace classes would be required to carry additional navigation and communication systems. The Ground Control Station (GCS) used by these UA pilots will be more complex than, for example, a GCS designed for a UA flying within class G airspace.

There are many possible flight paths, and associated types and amounts of information that may need to be sent to/from the pilot to promote safe flights.

There are also many different sizes of UAs coupled with a varying set of complexity of systems/sensors within the UAs and in GCS.

The MOPS is structured to identify standards that would be common to nearly all of the wide varieties of operational flights and types of UAs. When such commonality cannot be found, ranges of radio design characteristics that would support selected CNPC link features will be defined in the MOPS.

The current MOPS support flight operations similar to those shown in the dotted and dashed lines shown in Figure 2. This is defined as a point-to-point communication link.

The MOPS will be expanded to address flights where multiple UAs need to communicate with multiple ground terminals as they fly over extended ranges, i.e. flights similar to that shown by the solid line within Figure 2.

The MOPS describes the design characteristics for a set of equipment that multiple manufacturers could build and field. Those systems would be compatible in that they would not interfere with one another; however, they would not necessarily be interoperable.

In some scenarios, ground CNPC radio systems communicating with multiple UAs (whose CNPC airborne radios are manufactured by different companies) would need to have some degree of interoperability. At this time, there is insufficient data to specify the standards needed to achieve such interoperability.

1.4 Specific Examples of UA Operations

The flight profiles within the following four figures (Figure 3 through Figure 6) depict probable scenarios. The first two figures show examples of a flight path only within class G airspace. The other two are examples of flight paths classes G and E and classes A, E, C, and D from Figure 2.

Figure 3 shows a scenario that would be a near-term practical use of a UA flying in relatively remote areas, yet beyond the current proposed sUAS regulations. The UA is flying beyond the visual line-of-sight of the pilot but not within range of ATC radars. The CNPC link operational requirements include establishing a relay connection(s) that is within radio line-of-sight of the UA.

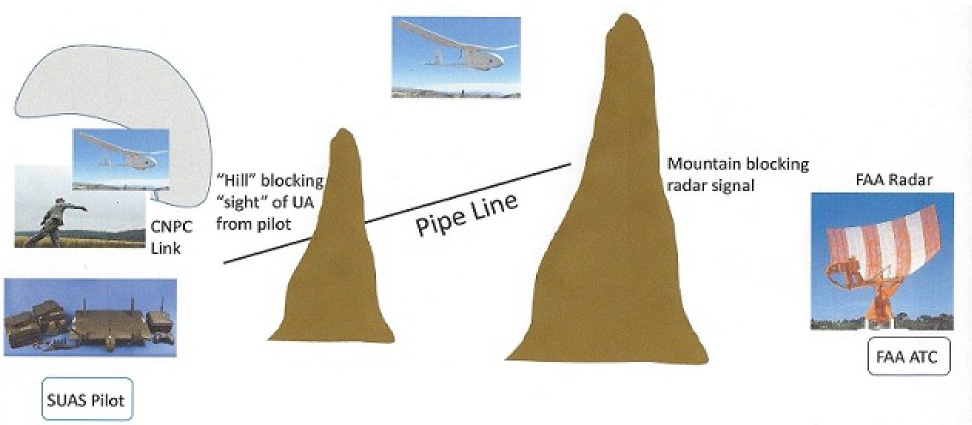

Figure 3 UA following a pipe line in mountains

Another potential operational scenario for sUAS operating outside of the current FAA sUAS regulations is shown in Figure 4; this shows multiple UAs flying in the same area conducting a package delivery or perhaps a video over-watch, all within an urban area. The key additional operational requirements for the CNPC link, beyond that of the above

DOI 10.5162/etc2016/5.1

example, are to safely handle signals coming to/from multiple UAs, the possible utilization of multiple third parties operating the ground terminal systems, and ensuring continuity of information transfers when transitioning between multiple CNPC link ground terminal system sites.

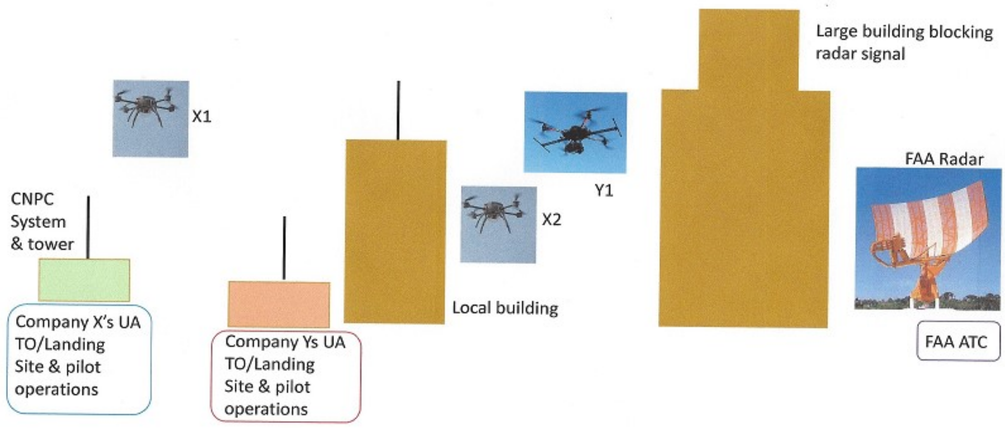

Figure 4 sUAs conducting operations in an urban environment

For flights within class E airspace, (see Figure 5) the CNPC link operational requirement is to ensure the link can carry additional information transfers. This is needed to support safe operation when flying in the class E airspace where many other aircraft are operating; some of those are flying under Visual Flight Rules (VFR) and others under Instrument Flight Rules (IFR). If there is just one UA flying near a ground terminal at any given period of time, then these MOPS would support this scenario. If there are more than one, then the manufacturer would need to develop their own solution (e.g. expanded standards) to address that scenario.

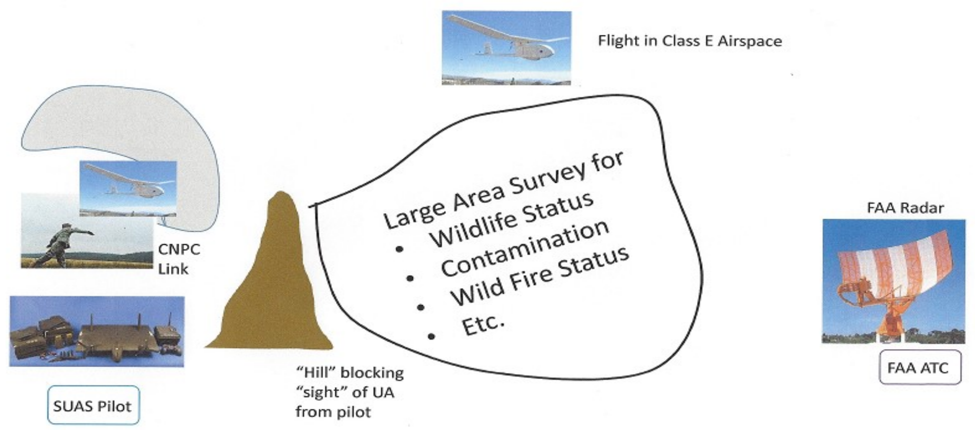

Figure 5 UAs flying in class G & E airspace

The most complex operational scenario is when UAs are flying in class C and D airspace and en route through classes A and E airspace (see Figure 6). The key additional CNPC link operational requirement is to ensure the link can carry any additional information transfers

DOI 10.5162/etc2016/5.1

needed to support safe operation when flying in the class A airspace and to communicate with approach/departure control and airport towers/ground control when within class C or D airspace. Since the MOPS does not explicitly support multiple UAs communication with one ground terminal, manufacturers would need to develop their own solutions to support this scenario.

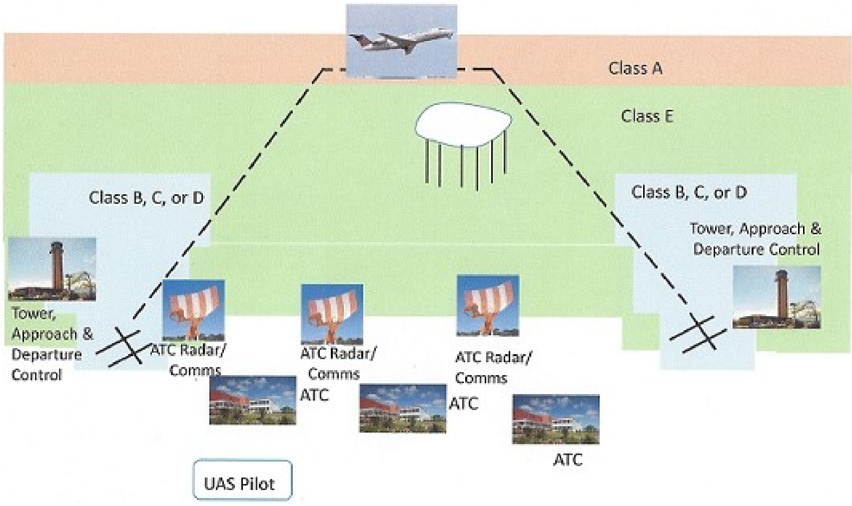

Figure 6 UAs flying in class A, E, C & D airspace matching those of most commercial airlines

1.5 Needed Information Transfers Specific Examples of UA Operations

With the wide range of flight scenarios, there is also a wide range of information transfers that would be needed during specific phases of the flight. During taxiing, takeoff, and landing the pilot would need to be in close contact with the tower, departure, and approach controllers. During taxi, takeoff, and landing, they may also need video from the UA's video camera(s) to keep the UA moving safely along the designated route. This video data sent via the CNPC link will need to be updated often, and need greater bandwidth as it is being sent. However video transmission may not be required throughout flight.

During normal flight, the pilot may need only periodic updates that all is "normal". As such, relatively little data would need to be sent (low bandwidth need), the update rate would be low, but would need to occur on a regular basis. During normal flights it is to be expected that the pilot would change some of the preset flight path guidance uploaded to the UA prior to takeoff, e.g. changing waypoints or altitudes to be flown. In this case, there would be an increase in the uplinked data to the UA. The data transmitted would be greater than during normal flight; the data would need to be updated often to confirm receipt and ensure the UA follows the new guidance.

However, in adverse weather conditions, when flights near other aircraft (when DAA actions may be required) or during emergency situations, the amount of data to be sent from the UA would increase. Video and/or weather data may be required to be sent to the pilot, and corresponding commands from the pilot to the UA. As such, a greater bandwidth would be needed, but this would not normally occur often during a flight.

A summary of these information transfers is displayed in Figure 7.

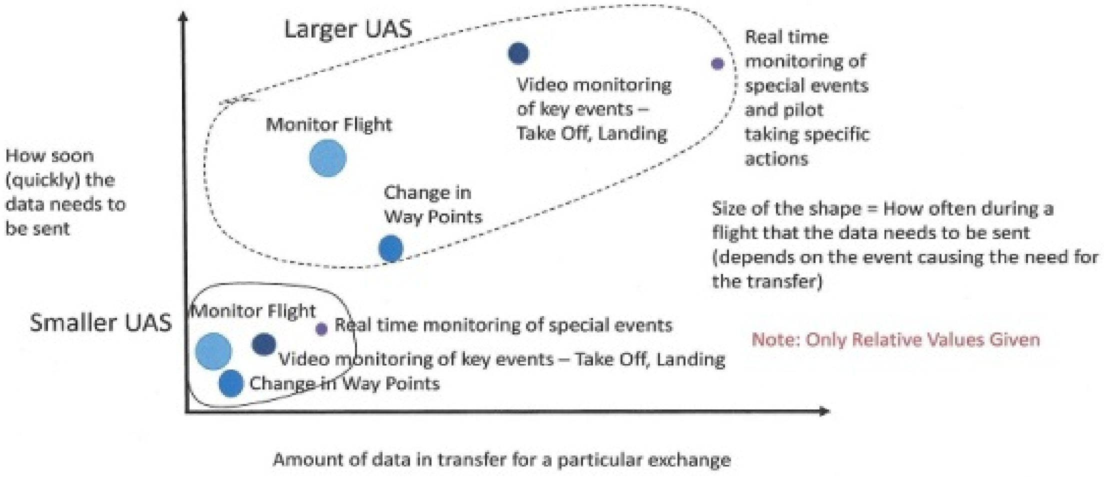

Figure 7 Relative Information Transfers that could be needed during UA flights in the NAS

1.6 Translating UA Operational Scenarios into Needed CNPC link Features

Once the operational requirements and the types of information transfers are determined, the next step is to define the features of the CNPC link so it can support such operations.

Note: only general descriptions of the key features are identified; the details of these and the specific design characteristics requirements will be in the final MOPS. The required features are:

- Support transfers of flight control information to/from pilot and UA, e.g. actual pilot control and monitoring of the UA's flight.
- Support for information transfers for such features as
  - UA location/navigation information, e.g. GPS, VOR, DME.
  - Detect And Avoid.
- Voice and data communications with airport towers, arrival and departure controlers, ATC, ATC radars, etc.
- Video images during taxiing, takeoff, landing, and emergencies.
- Weather information, e.g. data from a weather radar on the UA.
- Status information of key systems on the UA (to include the CNPC link airborne radio) and confirmation of changes to those systems.

- Data from selected backup/redundant systems on the UA.
- A Pilot is In Command (PIC). A Pilot is on the loop at all times. No autonomous flight is allowed.
- UA flights follow IFR requirements (FAA mandated if a flight is within the NAS). The CNPC link supports the needed information transfers for compliance.

In addition to the above, there are several features based on current FAA needs and regulations:

- The CNPC link airborne antenna(s) supports effective propagation to CNPC ground radios during all possible UA maneuvers.
- The CNPC airborne radio does not cause interference with other electronic systems on the UA (of particular concern is possible interference with transponders), in the area where the CNPC link ground terminal is located, or around other systems within the "radio horizon" of the CNPC link airborne antenna.
- Spectrum utilization needs to be both efficient and effective so it can *eventually support a large number of UAs operating in the same area simultaneously*.
- Sufficient spectrum is required to support any needed CNPC link redundancy to ensure the needed information transfers reach a satisfactory performance and safety level.
- The signal modulation selected must support changes in the bandwidth needed during normal UA flights, during emergency situations *and when multiple UAs are flying in the same general area*.
- The information sent over the CNPC link will be encrypted and authenticated to provide resistance to potential interference.

The current MOPS does not explicitly require the features italicized above; they may be addressed in a future development effort (Phase 1A MOPS).

1.7 System Overview

For successful UAS operations in the NAS, there are many systems beyond the scope of the CNPC link MOPS. A typical representation of these systems and the interfaces between those systems is illustrated in Figure 8. The key elements of the CNPC link are shown in solid lines and squares; systems outside the link are represented by dashed lines and squares.

Basic System

Within Figure 8, the systems outside the CNPC link MOPS include:

On the ground side:

- A distribution system to connect to and from the ground side of the CNPC link to the ground Flight and Radio Management System (FRMS).
- The FRMS to connect to and from the pilot's cockpit.

DOI 10.5162/etc2016/5.1

- A link from the pilot's cockpit to and from a Spectrum Authority (which assigns the frequencies that the CNPC link will use at various times and locations).
- A link from the pilot's cockpit (either directly and/or relayed through the UA) to ATC so flight clearances can be given and acknowledged.

On the air side:

- The airside of the CNPC link is connected to and from the aircraft's FRMS.
- The FRMS links to and from the various flight control, avionics, and other systems on the UA.

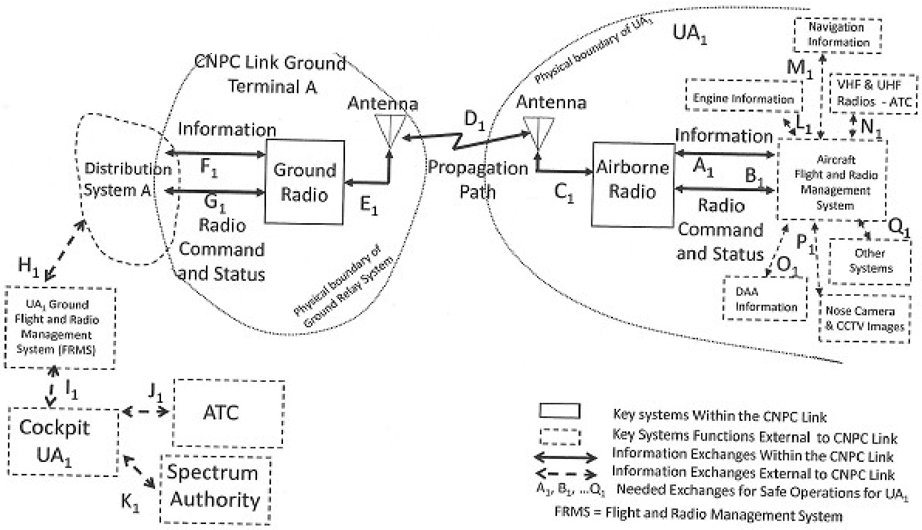

Figure 8 Basic Information transfers within & outside the CNPC link needed for safe UAS operations within the NAS

1.8 Intended Function

Basic CNPC link Functions

The MOPS describes the features and characteristics needed to achieve a point-to-point communication function for UAs flying in the NAS. There are additional features and characteristics that may be needed, but not included in this MOPS, to achieve multi-point communications when multiple UAs are seeking to communicate with a single ground terminal.

Depending on the intended operations, the CNPC link equipment and interfaces described will also support one or more of the following features of a point-to-point communication function:

- ATC voice and data relay
- DAA data exchange

- Weather radar data exchange
- Video data exchange

All of the equipment shall comply with the appropriate Federal Communications Commission (FCC) rules and International Civil Aviation Organization (ICAO) Remotely Piloted Aircraft Systems (RPAS) Standards. It will also provide a means to follow appropriate ATC procedures for UAs flying in the NAS.

Characteristics having defined values for all terrestrial CNPC links are listed in Table 1.

Table 1 Characteristics having defined values for all point to point CNPC links.

R-f	Frequency stability
Power rise time and fall times	Frequency quanta (smallest radio channel width)
Command and status interfaces	Output power and emission mask
Frequency bands to be used (L- and C-Bands)	Adjacent channel and spurious response rejection
Waveform structure [Time Division Duplex (TDD)]	Compatibility with other systems

In addition there are characteristics that are deemed to be manufacturer dependent, i.e., the manufacturer could select specific design characteristic values that best meet the radio manufactures chosen market sector and are given in Table 2.

Table 2 Characteristics having variable values for all point to point CNPC links.

Symbol rate	Receiver Sensitivity
Modulation Type	Frequency Capture Rate
Transmitter Output Power	Doppler Correction

Environmental Functions

Unless otherwise specified, the environmental conditions contained in RTCA DO-160G, (or later revision) will be used to establish the airborne equipment environmental standards criteria. The environmental conditions contained in RTCA DO-160G, and MIL-STD-810G, will be used to establish the ground equipment standards.

Assumptions

It is assumed that radio manufacturers have sufficient technical knowledge to understand the MOPS and experience to combine the various equipment described within the scope of the MOPS. With that background multiple venders should be able to manufacture the equipment. It is understood that the MOPS do not fully define all of the design characteristics but they are the minimum necessary for such developments.

1.9 Anticipated Growth

- As noted in several subsections, this MOPS does not include all of the design characteristics for the CNPC link to support multiple UAs communicating with just one ground terminal radio.
- For single ground CNPC radio systems to successfully communicate with multiple UAs whose CNPC airborne radios were manufactured by different companies, there needs to be some degree of interoperability between the ground radios and each airborne radio. Once sufficient information and knowledge is gained, and there is sufficient need for such a capability, the FAA could request the RTCA to develop such a MOPS.
- In addition, the SC-228 TOR already identifies the requirement to develop MOPS to support UA CNPC link communications via satellites. A separate MOPS development team will be required for that effort.

1.10 Annotations and acknowledgements

The current MOPS is in draft form and will be sent out for consultation; thus the foregoing is subject to change.

This presentation is a compilation of the original work by members of the RTCA SC228. The diagrams and some of the text are RTCA copyrighted and are used with their permission. The complete document will be available for purchase via the RTCA website (or at the address below) mid 2016 when the final document will be released.

RTCA, Inc.
1150 18th Street NW
Suite 910
Washington, DC 20036
(202) 833-9339

www.rtca.org

DOI 10.5162/etc2016/5.2

An IEEE 802.11 Based Telemetry System for Ultra Light Machines Flight Testing

Alberto Rolando, Luca Minichini, Federico Rossi
Department of Aerospace Science and Technology, Politecnico di Milano, Milano, Italy,
alberto.rolando@polimi.it

Abstract:
Initially conceived as the main research topic of a PhD, the *Mnemosine* Flight Test Instrumentation system designed and developed at Department of Aerospace Science and Technology of the Politecnico di Milano has been intensely used for more than one decade, in support of didactic activities, like the annual Student Flight Test Campaign within the MSc. Flight Testing course, as well as of research and third-party initiatives. The present paper presents the latest addition to *Mnemosine*: a telemetry link for real-time downloading and visualization of acquired data. With the objective to satisfy the very stringent budget constraints on one hand, and to maximise performance in terms of range and bandwidth on the other, the link has been developed starting from low cost, consumer-grade IEEE 802.11 components, that have been deeply tested and carefully tuned to adapt their performance to the particular application requirements. The proposed telemetry system is composed of an Airborne Station installed on the aircraft, a Ground Steerable Antenna Station, capable of aiming the high-gain directional antennae at the aircraft, a Meteo Station for acquiring air-related parameters at the airfield and a PC-based Ground Station running both the steerable antenna control software and the data processing and visualization software. Full details are given on the successful system test during the 11 Test Flights of the recent May 2015 Student Flight Test Campaign.

Key words: FTI, TELEMETRY, WIFI, IEEE 802.11, ULM.

Introduction

The Department of Aerospace Science and Technology of Politecnico di Milano (DSTA-Polimi) has a long-term established tradition in Flight Testing, dating back to 2004 when the development of *Mnemosine*, the in-house designed Flight Test Instrumentation (FTI) system tailor-made for the Department owned and operated TECNAM P92 Ultra-Light Machine (ULM), was started as the main topic of a PhD [1].

At DSTA-Polimi, Flight Testing activity is quite regularly carried out. For a start, it constitutes the core, and the pride, of the annual Student Flight Test Campaign (SFTC) within the MSc *Flight Testing* course [2]. In addition, a number of third party contracts has been stipulated over the years with Ultra Light Machines (ULMs) manufacturers for supporting the development and certification of their aircraft [3].

Since its initial introduction, *Mnemosine* FTI system has been continuously expanded and improved, mainly thanks to the contribution of a succession of MSc. Theses [4,5], and has so far successfully acquired data in more than 400 test flights.

The present paper describes the design, development and on field-testing of the latest addition to *Mnemosine* FTI: a telemetry system.

The Origin of a Telemetry System

From the very early day of operations, the desire of a telemetry system for *Mnemosine* FTI has emerged.

On one side, in fact, it has been experienced in a number of occasions that the possibility to monitor acquired parameters and quantities in real time could have saved time and increased mission effectiveness. Should, for example, a potentiometer cable be accidentally torn off by the Test Pilot (TP) or Flight Test Engineer (FTE) boarding the aircraft-as it did happen in one occasion-the early detection of the problem allowed by telemetry could have permitted to abort the test flight, fix the problem and then fly it in a very short time. Without telemetry, instead, on that particular occasion the test flight was entirely performed, the issue was detected only at data post-processing time, and the team was forced to reschedule the same test flight for the following day.

On the other side, having the possibility, via a telemetry link, to display in real time the acquired parameters would have a great benefit on the didactic effectiveness during the annual SFTC. For every day of activity of the campaign, in fact, students come to the airfield in groups, but only one at the time will fly, as the FTE in charge, his or her Flight Card. It is clear that the possibility, for the group on the ground, to follow the progress of each colleague’s test flight, and to cross check the real time data on a suitable Ground Station (GS) display with the Flight Card test points would have a very good impact on the quality of the overall Flight Test experience.

In order to properly start the activity that will eventually deliver the most appropriate telemetry system for the operating necessities of DSTA-Polimi Flight Testing activities, an initial investigation has yielded the following list of requirements:

- Low cost.
- Low power consumption
- Use of license-free band.
- Use of Commercial Off-The Shelf (COTS) hardware.
- Practical range in the order of 10 km.
- Sufficient bandwidth for transporting the whole acquired data (at the time in the order of 100 Kbps).

Although experiences and tests have been made with different available standards, like the 1.8 GHz Digital Enhanced Cordless Telephone (DECT) based Radio Frequency (RF) system [6] or the 2.4 GHz IEEE 802.15.4 Protocol [7], it gradually but clearly emerged that the most promising standard was IEEE 802.11, which is the base for the consumer Wi-Fi (Trademark of the Wi-Fi Alliance).

Driven by the overwhelming advance imposed by the consumer market, numerous and constantly increasing versions of IEEE 802.11 have been and are being standardised. In order to get in depth knowledge of the standard, a deep study of the 802.11n variant has been set as the subject of an MSc thesis [8].

Proposed Telemetry System Architecture

In order to satisfy all the cited requirements, the telemetry system has been designed split into four subsystems, as it can be seen in Figure 1:

- Airborne Station (AS).
- Ground Steerable Antenna Station (GSAS).
- Meteo Station (MS).
- Ground Station (GS).

As it can be noticed, two different wireless links are proposed.

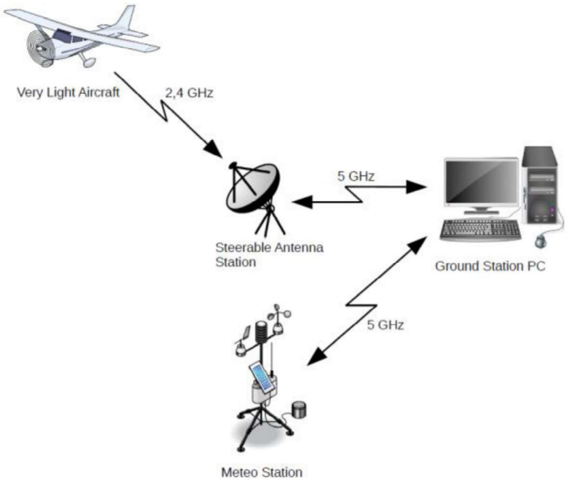

Figure 1: Proposed Telemetry System Architecture

The *Air RF Link* is dedicated to the communication between the aircraft and the ground. It has been assigned the operation on the 2.4 GHz band of IEEE 802.11n, mainly because the 5 GHz alternative would have potentially caused interference with radar systems.

The Ground RF Link operates on the 5 GHz band of IEEE 802.11n and is dedicated to the communication between GSAS, MS and GS. It permits the deployment of the GSAS and MS in the best position on the field, regardless of their distance from the GS.

A brief description of every subsystem is now given.

Airborne Station

The AS consist in a wireless board equipped with a 2.4 GHz wireless module, and is installed on board the aircraft. Communication with *Mnemosine* FTI system is through a wired Ethernet connection. The aircraft is equipped with two omnidirectional antennae installed on the lower aft part of the fuselage.

Ground Steerable Antenna Station

The task of the GSAS is to aim the antennae to the aircraft, to manage the communication on the AS on the Air RF Link and to relay it on the Ground RF Link.

GSAS is composed of different items: Antenna Steering Unit, Wireless units, GPS.

DOI 10.5162/etc2016/5.2

The Antenna Steering Unit permits to constantly aim the antennae at the aircraft, in order to maintain a constant quality Air RF Link with the AS. The steering system is controlled in Azimuth and Elevation angle thanks to a suitable dedicated unit. The set point is computed in real-time by the GS starting from the value of the aircraft coordinates and of the GSAS coordinates.

A dual-radio capable wireless board, equipped with dual wireless modules, manages and bridges all data traffic to and from Air RF link and Ground RF link.

The GPS module acquires GSAS position, in order to permit the GS to compute Azimuth and Elevation to aim at the aircraft.

Meteo Station

MS acquires air temperature and relative humidity, static pressure and wind (speed and intensity) data on the ground, to permit accurate post-flight data reduction and results validation. It permits accurate analysis of the acquired data and the definition of the aircraft performances during take-off and/or landing.

MS features a wireless board equipped with a 5 GHz wireless module in order to participate to the Ground RF Link.

Ground Station

The GS is equipped with a Personal Computer (PS) that runs three main tasks:

- Real time Azimuth and Elevation Computation
- Flight data display
- Flight and ground data recording

The first is performed starting from the knowledge of the position of the aircraft and of the GSAS, following the algorithm that will be described in the following sections.

For the flight data display, it has been integrated in the GS the software package developed for a previous work [7], with little adjustments and modifications to adapt it to the different platform characteristics.

Finally, all data passing through all networks has been recorded on the PC mass memory, in order to permit post-flight accurate analysis.

Telemetry System Hardware

A detailed description of the various hardware used for the system is given in the next sections.

Antenna Steering Unit

For steering ground antennae, a Moog QuickSet QPT-20 Positioner has been used.

Figure 2: Moog QuickSet QPT-20

It is a rugged and durable pan and tilt positioner designed for a wide variety of sensor positioning applications in harsh environments, and it can handle payloads up to 10.85 Nm.

Axes are actuated by means of a couple of brushed DC motors, while position feedback is given by means of a couple of potentiometers. Table 1 shows the main QPT-20 specifications.

Table 1: Pan and tilt positioner specifications

Parameter	Value
Load Capacity	10.85 Nm
Operating Voltage	24 VDC (± 4 VDC)
Pan-Axis Range	435° (± 217.5°)
Pan-Axis Speed	2° - 35°/sec
Tilt-Axis Range	180° (± 90°)
Tilt-Axis Speed	1.0° – 12°/sec
Operating Temperature	-15°C to 55°C
Feedback	Potentiometers (0.25° readout)
Repeatability	0.25°
Motor Type/Drive	DC Brush
Weight	6.48 Kg

Since, as it can be seen, the azimuth stroke is limited on one side, and the RF cables could not be tangled allowing unlimited rotations on the other, it has been necessary to identify the optimal strategy for azimuth reversing caused by an end-of-stroke situation.

Two different approaches were examined to deal with the issue: Complete Revolution Mode (CRM) and Half Revolution Mode plus Vertical Mirroring (HRM+VM).

DOI 10.5162/etc2016/5.2

In *Complete Revolution Mode* the antenna follows the aircraft till the limit stroke and then a 360° maximum speed azimuth rotation is imposed in the opposite direction in order to track again the target with no variation in the elevation angle.

In *Half Revolution Mode plus Vertical Mirroring* the antenna follows the aircraft till the limit stroke and then, unlike the previous case, at the same time a 180° azimuth rotation and a 180°-2α (where α is the current elevation angle) tilt rotation is performed. Both revolutions are performed, as before, at the maximum practical angular speed.

Figure 3: Antenna Steering Unit being tested at the lab.

The two approaches have been deeply analysed performing several tests on the actual hardware in the lab (Figure 3), and the resulting performance in terms of speed is shown in Table 2.

Table 2: Azimuth reversing timing

MODE	Starting elevation (deg)	Time (s)
CRM	n.a.	7.5 s
HRM+VM	10	10.7s
HRM+VM	20	9.2 s
HRM+VM	30	8.0 s

Analysing the reported data it is clearly visible that, if the starting elevation angle is smaller than 30°, CRM would be better because the re-engagement time is shorter than the other approach. Actually, HRM+VM is greatly penalized by the low maximum tilt-axis speed. Surprisingly, increasing the tilt motor power supply voltage the tilt performance doesn't increase.

If the starting elevation angle is greater than 30°, HRM+VM approach would be preferable for the reason stated above. Nevertheless this solution was discarded due to some considerations.

On one side, analysing data from all the previous flight test campaigns it has been discovered that the mean elevation angle of every flight was below 20°, mainly because of the limitations on the aircraft altitude imposed by the Air Traffic Control (ATC) regulations.

On the other, with this approach the tracking algorithm would be much more complicated.

Antennae

Many different types of antenna have been used in the system.

On board the aircraft a couple of WiMo 2.4-GHz Antenna Model 17009 have been installed on the lower aft part of the fuselage, as it can be noticed in Figure 6. Main specifications of such antenna are reported in Table 3.

Table 3: WiMo Model 17009 antenna specifications

Gain	2 dBi
Type	Omnidirectional
Polarisation	Vertical
Frequency range	2.4-2.5 GHz
Vertical beamwidth	65 deg
Horizontal beamwidth	360 deg

At the GSAS side, communication with the aircraft on the Air RF Link is managed via a couple of Calearo Directional Log-Periodic antennae, whose specifications are reported in Table 4.

Table 4: Calearo Log periodic antenna specifications.

Gain	11 dBi
Type	Directive
Polarisation	Vertical
Frequency range	1.7-2.5 GHz
Vertical beamwidth	46 deg
Horizontal beamwidth	58 deg

For the on-filed side of the 5 GHz Ground RF Link a couple of WiMo 5-GHz Antenna Model 18722.7 (see Table 5) have been used at both GSAS and MS side.

Table 5: WiMo Model 17009 antenna specifications

Gain	7 dBi
Type	Dipole
Polarisation	Vertical
Frequency range	5.1-5.8 GHz
Vertical beamwidth	40 deg
Horizontal beamwidth	360 deg

Finally, at the GS the 5 GHz Ground RF Link network is accessed via a pair of L-Com HG5817Y-NF (specifications in Table 6).

Table 6: L-Com HG5817Y-NF antenna specifications

Gain	16.5 dBi
Type	Yagi
Polarisation	Vertical
Frequency range	5.27-5.82 GHz
Vertical beamwidth	25 deg
Horizontal beamwidth	30 deg

Wireless boards & modules

For realising the whole 802.11x infrastructure a number of wireless boards and modules from Compex SG have been used. The main reason behind this decision is that Compex provides full support to OpenWRT on its products.

OpenWrt [9] is an embedded operating system based on the Linux kernel, primarily used on embedded devices to route network traffic, that is very actively supported by a large developers and users community. It has therefore been possible to develop a tailor made, custom compiled version of the board firmware that included all the settings and fine tweaks found in previous preliminary research [8] needed to optimise the performance of the standard Wi-Fi modules for the particular telemetry application.

Used Compex hardware included WPJ72 router board, WPJ342 wireless boards and WLE200NX wireless modules. Table 7 and Table 8 show the principal RF specifications of these.

Table 7:Compex WLE200NX specifications.

RF Chipset	Atheros AR9280
802.11 standards	a, b, g, n
MIMO channels	2x2
RF power (per chain)	16 dBm
Frequency Range	2.412 ~ 2.472 GHz, 5.180 ~ 5.825 GHz
Maximum data rate	300 Mbps

Table 8: Compex WPJ342 specifications.

RF Chipset	Atheros AR6236
802.11 standards	a, n
MIMO channels	2x2
RF power (per chain)	23 dBm
Frequency Range	5.180 ~ 5.825 GHz
Maximum data rate	300 Mbps

Telemetry System Software

Two different PC codes have been developed for managing the system, both in C++ using the Qt framework: the Antenna Steering Control software and the Data Visualisation software.

The *Antenna Steering Control* code is in charge of controlling the pan and tilt Azimuth and Elevation in order to correctly aim the antennae at the aircraft.

Required antenna azimuth and elevation values are computed starting from current Aircraft and GSAS position using well known formulae [10, 11].

A series of hardware in the loop simulations has been performed in the lab, feeding the algorithm with actual aircraft data acquired in previous Flight Test campaigns and speculating a reasonable GSAS position. Unfortunately, two main problems emerged.

First, GSAS was not able to track the target in the case of a low-altitude and high-speed flight above the station. This critical situation derived from the limited positioner motors speed performance. In order to deal with this problem, a Warning Index Mode (WIM), has been developed.

Additionally, as expected, during the 360° horizontal rotation, GSAS lost the target and re-engaged it after about 10 seconds. Obviously, during this amount of time, the changes its position so it has been necessary to develop a strategy to predict future aircraft position during Azimuth Reversal Manoeuvre.

Warning Index Mode

WIM has been introduced to enhance the positioner behaviour in case of a high-speed and low-altitude aircraft flyby above GSAS.

The limited Pan and Tilt motors performances didn't allow to track this type of overflight causing the target pointing loss. Since the positioner speed performance couldn't be increased, it has been introduced the Warning Index (WI) parameter that could alert the system about the issue mentioned above. By definition:

$$WI = \frac{V_{NE}\ [m/s]}{r_h\ \ [m]}$$

where

$$V_{NE} = \sqrt{V_N^2 + V_E^2}; \quad r_h = \sqrt{P_N^2 + P_E^2}$$

being

V_N, V_E= projected target speed in the north and east direction.

P_N, P_E = target position relative to the GSAS in the north and east direction.

As it can be noted, WI is directly proportional to the target speed projection in the horizontal plane (V_{NE}) and inversely proportional to the horizontal distance between the target and the tracking station (r_h).

Running multiple simulations it has been possible to identify 6.5 as a critical WI value. Above this limit, the GSAS motors were unable to track the target. In order to avoid this possibility, with WI greater than 6.5 the algorithm aims the antenna to the position that the aircraft will have in the following 5 seconds, obtained forward integrating the current aircraft position, capitalising the knowledge of the current aircraft velocity, using Adams-Bashforth (AB) Method [12]. The same method has been used to predict aircraft position during Azimuth Reversal Manoeuvres.

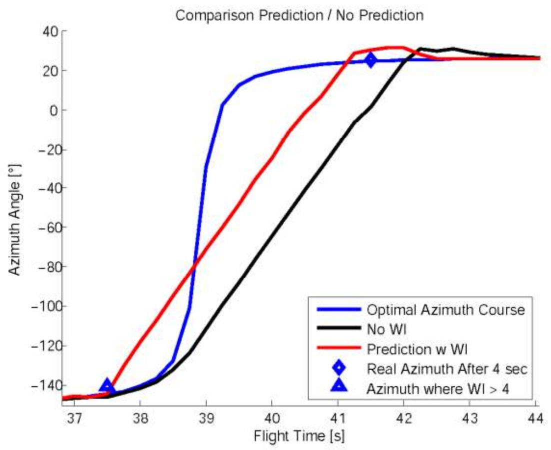

Figure 4: Performance of Warn Index Mode tracking

As it can be seen in Figure 4, the position prediction allows the GSAS to steer the antenna in advance in the direction of the predicted future position of the target. This way the overall pointing error is higher in the first part of the manoeuvre, but radically lower in the second, making the strategy effective. At the end of the 5 seconds the difference between the optimal azimuth and the predicted one is really low (few degrees). In the presented situation, without the position prediction the maximum error would have been of 160° (Figure 5), and since the antenna radiation pattern is about 46° wide, the Wi-Fi link between the aircraft and the GS would have been very likely lost.

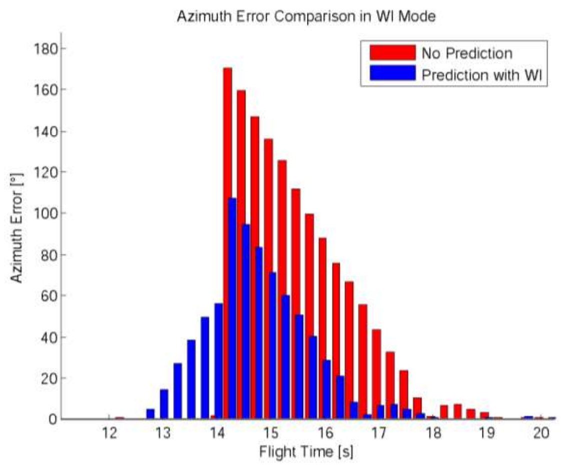

Figure 5: Azimuth error comparison

Field Tests

The developed Telemetry System field tests have been performed during the 2015 SFTC, that took place on the 23rd and 24th of May at Club Astra's airfield located in Mezzana Bigli (PV). The activity goal was to test and evaluate the telemetry system performances in a real-world operating scenario. The used aircraft was a Folder (I-9202), designed and built by Mezzana Bigli-based Nando Groppo S.r.l., equipped with *Mnemosine* FTI system, in its last Mk V version (Figure 6).

Figure 6: Nando Groppo Folder I-9202

A total of 11 Flights have been performed in the two days.

In Figure 7 it is visible the Steerable Antenna Station installed on its aluminium tripod. In the

DOI 10.5162/etc2016/5.2

foreground the plastic case containing all the electronics can be noted.

Figure 7: On-field deployed GSAS.

Figure 8 shows the MS with its sensors and antennae.

Figure 8: On-field deployed Meteo Station.

Following the enthusiastic first impression received at SFTC execution time, at its completion a through performance analysis has been carried out. It has been decided to use as GSAS "true" position its mean value observed during the whole test campaign, since the *static station* setting of the GSAS GPS.

In Figure 9 it's possible to take a look at the percentage of data that have not been picked up by the receiver due to link problems like:

- Out of range transmission.
- Warning Index Mode.
- Revolution Mode.
- Physical obstructions (like trees and buildings).

Test data from Flight No. 1, 2 and 8 are missing due to some technical problem.

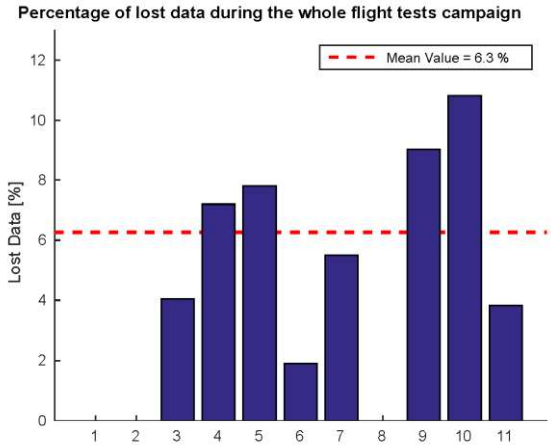

Figure 9: Percentage of lost data during the whole flight tests campaign

In Figure 10 and Figure 11 two statistics about the mean elevation angle and the mean distance when the aircraft signal was lost during each single flight are presented.

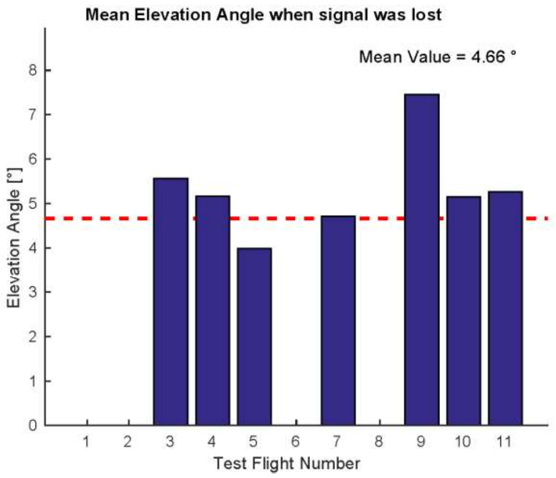

Figure 10: Mean Elevation Angle when signal was lost

Values are calculated neglecting the 360° azimuth mirroring phases. As it can be noticed, the sixth flight data are missing, given that no packets were lost during this flight apart those ones that were missed during the complete revolutions.

The mean elevation angle is rather low (4.66°) and this suggests that the dropouts in the connection were caused by physical obstructions (like trees and buildings) in the Line Of Sight.

Applying the specifications reported in each device datasheet to the Friis formula, a theoretical maximum radio range allowing a 6 dB margin was found to be 7 Km.

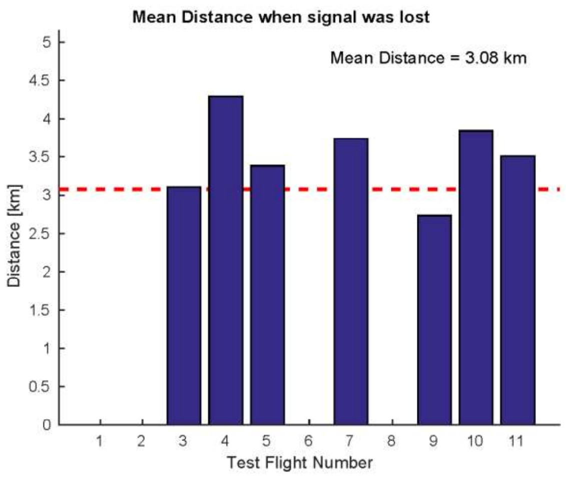

Figure 11: Mean Distance when signal was lost

Figure 12 presents the maximum distance reached by the aircraft in every flight of the campaign. The highest value was reached during the third flight with 6.13 Km.

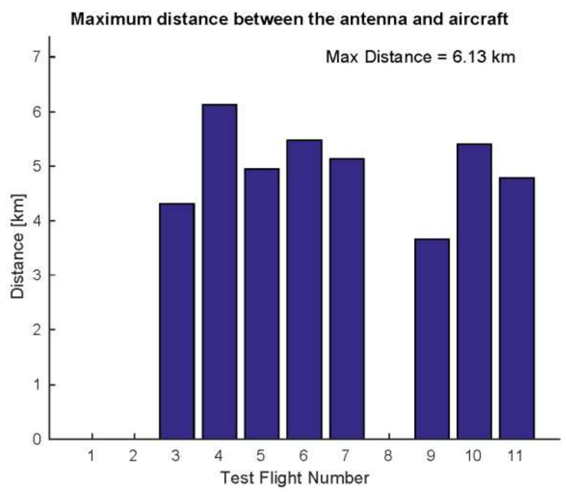

Figure 12: Maximum distance between the antenna and aircraft.

Hereafter all the data concerning the QPT-20 Elevation Motor Angles are reported and analysed (Figure 13). In the plot, GS set point determined using the Aircraft GPS position is drawn in red. Antenna Steering Unit feedback data acquired through the elevator motor internal potentiometer is drawn in blue. Correct value computed at post-flight phase by means of Matlab™ is drawn in black.

Analysing the data it can be seen that during the entire flight time, the GS Set point and the Antenna feedback have an evolution pretty much fitted compared to the Target Values.

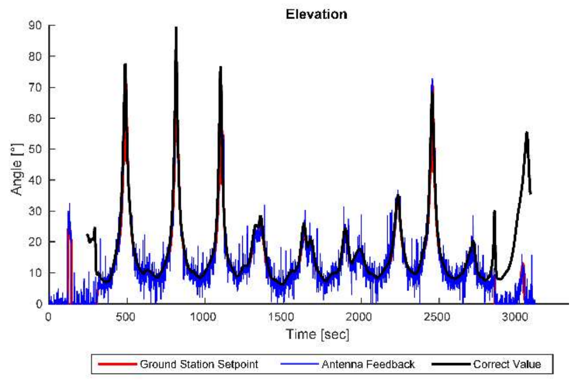

Figure 13: Elevation performance

Zooming in the previous diagram (Figure 14), three phenomena are clearly visible:

- An intense background noise affected the potentiometer feedback, despite the installation of an output 10-Hz low pass filter
- There is a slight difference (~ 2°) between the Target value and the GS set point probably caused by the position variation of the Meteo Station during the flight
- There is a slight delay caused by the sum of the signal acquisition, data elaboration and actuation time, so Antenna Steering Unit was always a bit *late* compared to the aircraft position.

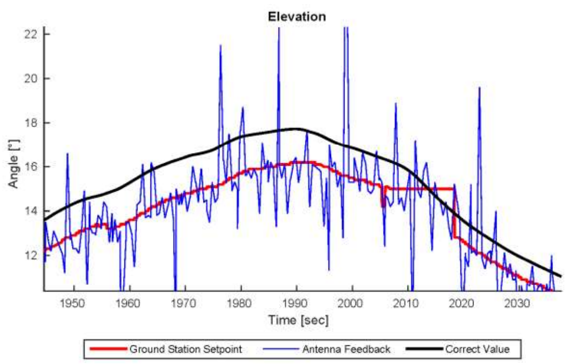

Figure 14: Detail of elevation performance

Figure 15 shows the difference between the GS Elevation set point and the Target Value; this discrepancy is called error. The mean value is 1.5 degrees, and the standard deviation is 1.23 degrees, which are quite remarkable results for the testing phase of the system.

DOI 10.5162/etc2016/5.2

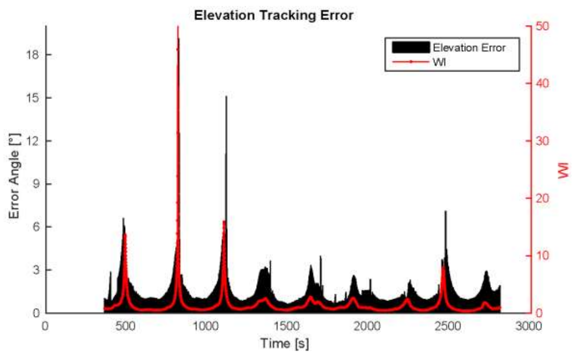

Figure 15: Elevation Tracking Error.

As far as azimuth is concerned, similar graphics are presented in Figure 16, Figure 17 and Figure 18. Like in the previous case, the behaviour of the system during the field test result is very close-fitting to the target data computed during the post-flight analysis.

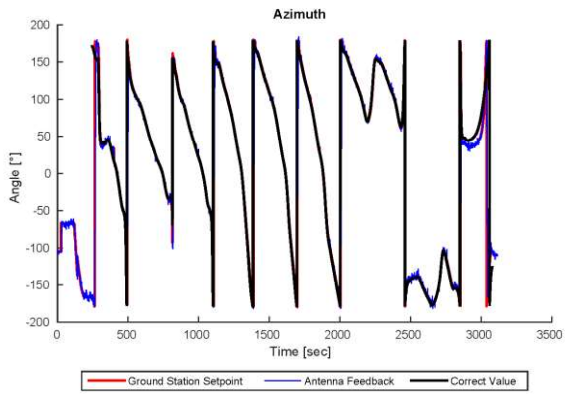

Figure 16: Azimuth performance

Differently from the elevation case, the background noise on the potentiometer feedback is more limited, so a better tracking performance has been obtained.

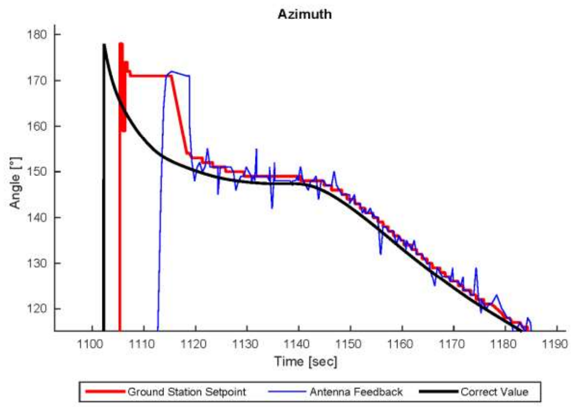

Figure 17: Detail of azimuth performance

As in the elevation case, Figure 18 shows the azimuth Antenna Tracking Error during the entire flight.

In this case too, the mean value and the standard deviation are small. However, differently from the elevation analysis, the error values that were greater than 330° were deleted since they represented the 360° Azimuth Reversal Manoeuvres.

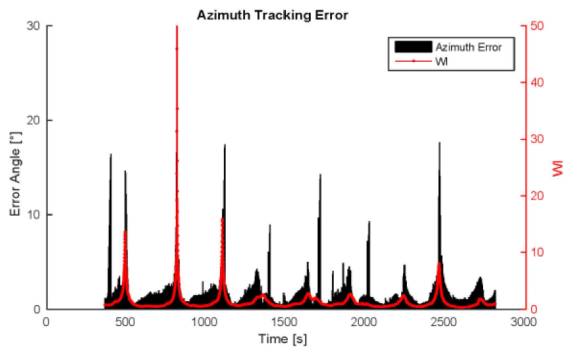

Figure 18: Azimuth Tracking Error

Conclusions and Future Developments

With the excellent performance observed during the on-field tests it can be said that the developed system satisfies the requirements and can be introduced as a standard capability for future campaigns.

The maximum reached radio link range was 6.13 Km against the theoretical 7 Km, and the few losses were identified as caused by obstructions (caused by buildings and vegetation) to the Line Of Sight between the Aircraft and GSAS.

As for the future developments, they may include:

- *GS LAN*: permit each student with a proper software installed on his or her PC to follow the progress of the flight.
- *Redundancy:* develop and deploy in different areas multiple GSAS, all interconnected to GS via the Internet by means of a Virtual Private Network.
- *Roving GSAS:* Mounting GSAS on a vehicle would permit to follow the aircraft moving on the ground, communicating with the GS over cellular phone data network.
- *Very high gain GSAS Antenna:* Having solved the remaining tracking error, a narrow beamwidth, high gain antenna can be used to extend the practical range.
- *Audio & Video Streaming:* Thanks to the TCP/IP convergence, it will be easy to add HD camera on board, connect it to the Ethernet network and get its signals all the way through the existing system
- *Two-way audio communication:* using a suitable audio-over-ip protocol it could

be possible to interface GS audio with the on-board Internal Communication System.

Acknowledgements

The authors would like to acknowledge the excellent support and the infectious enthusiasm provided by Professor Lorenzo Trainelli, responsible of the MSc Flight Testing course at DSTA-Polimi, Ing. Michele Riccobono () and Ing. Nando Groppo, owner, master and father of Ing. Nando Groppo S.r.l.

A special *grazie* to Ing. Filippo Covelli for his excellent preparatory work.

References

[1] A. Rolando, *Development of an Integrated Flight Test Instrumentation System for Ultra Light Machines,* Ph.D. Dissertation, Politecnico di Milano, Milano (2008)

[2] L. Trainelli, A. Rolando, G. Bonaita, P. Chimetto, *Experiences in Academic Flight Testing Education*, Aircraft Engineering and Aerospace Technology, Vol. 86, N. 1, p. 56-66 (2014); doi: 10.1108/AEAT-10-2012-0178

[3] L. Trainelli, A. Rolando, Reliable and Cost-Effective Flight Testing of Ultralight Aircraft, Journal of Aircraft, Vol. 48, N. 4, p. 1342-1350 (2011); doi: 10.2514/1.C031277

[4] T. Castelletti, *Design and development of the new generation of a flight test instrumentation system for ultra light machines,* MSc Thesis, Politecnico di Milano, Milano (2015)

[5] M. Grassi, *Design and implementation of flight test data processing software*, MSc Thesis, Politecnico di Milano, Milano (2015)

[6] A. Rolando, *A Telemetry Node for MNEMOSINE, a Flight Test Instrumentation System for Sport Aviation Aircraft*, Paper presented at 28th European Telemetry Conference (ETC 2008), New Munich Trade Fair Centre, Germany, p. 333-352 (2008)

[7] A. Rolando, C. Cardani, F. Rossi, *Academic Experiences with an 802.15.4 based telemetry system for UAV Applications*, Proceedings of the 34th European Telemetry and Test Conference (ETC 2014), Nuremberg, Germany, p. 82-87 (2014); doi: 10.5162/etc2014/5.1

[8] F. Covelli, *Design and optimization of an 802.11n based wireless link for Flight Test telemetry applications*, MSc Thesis, Politecnico di Milano, Milano (2013)

[9] http://www.openwrt.org, visited April 2016

[10] R. Burtch. A comparison of methods used in rectangular to geodetic coordinate transformations, ACSM Annual Conference and Technology Exhibition (2006), Orlando, FL, USA.

[11] G. H. Born, *Computation of azimuth and elevation*, http://ccar.colorado.edu/ASEN5070/handouts/Comp_of_Azimuth_Ele.ppt., visited May 2015

[12] A. Quarteroni, R. Sacco, F. Saleri, *Numerical Mathematics,* Springer Berlin Heidelberg, (2010)

DOI 10.5162/etc2016/5.3

Using LTE-networks for UAS-communication

Felix Maiwald and Axel Schulte
Institute of Flight Systems
Universität der Bundeswehr München (UBM)
85577 Neubiberg, GERMANY
{felix.maiwald, axel.schulte}@unibw.de

Abstract

This article discusses the usage of Long-Term Evolution (LTE) as IP-datalink for one or multiple micro unmanned aircraft systems (UAS). LTE offers robust coding schemes as well as very high sensitivity of receivers. In environments of highly limited transmit power, LTE therefore promises much better coverage in comparison to commercially applied UAS-datalinks like Wi-Fi or Lightbridge (DJI). Within this article, two commercial LTE-networks are evaluated and necessary IT-infrastructure for communication with UAS is specified. We also describe the integration of our multicopter-UAS into a commercial LTE-network. Thereby we developed a Linux-based tablet solution for guidance of our UAS via LTE. This includes the transmission of a live-video stream from our UAS to our tablet via LTE. In the contribution, we present the results of flight experiments we conducted at our testing site. The experiments show that guidance of small drones (including transmission of telemetry and sensor data) via public LTE infrastructure is feasible. Quantitative performance measurements will be presented in the paper. Future work comprises the setup of an own LTE-network and the guidance of multiple UAS via public LTE as well as via an own LTE-network.

Key words: UAS, LTE infrastructure, Live Video and Command Link

1. Introduction

In the recent years micro unmanned aircraft systems (UAS), commonly known as drones, found the way into public domain. These drones will be applied in civil, military and research applications, as well as leisure activities, policing, surveillance and security work (e.g. inspection of power lines). For this type of applications, there is the requirement to transmit large sensor data to the UAS operator. Analog data transmission is not capable to satisfy these requirements. The fixed video bandwidth and noise artifacts during flight phases with low signal strength prevent a high quality transmission of large sensor data frames.

Consequently noncommercial drones often use IP-based Datalinks like Wi-Fi (e.g. Parrot Bebob Drone) or proprietary Datalinks (e.g. DJI Lightbridge at 2.4 GHz ISM for video and 5 GHz for commands [1]) as communication link between pilot and the UAS. Using a Wi-Fi network seems to be interesting because of its low system price, low weight, and vendor independent availability. However, the legally permitted transmission power of Wi-Fi is limited by the federal network agencies (e.g. 100 mW EIRP for IEEE802.11n in Germany). The coverage of such data links is limited to direct environment only. Directional antennas with tracking functionality promise to increase the link coverage for single UAS but will violate the restrictions in transmission power due to antenna gain. Such antenna configuration also does not allow the simultaneous communication with multiple UASs.

The Institute of Flight Systems at the UBM investigates Manned-Unmanned Teaming Missions (MUM-T) where drones are guided from aboard a manned helicopter in a simulation setup. In another study, we also examine the support of infantry by drones in an urban scenario. The UAS carries at least one electro-optical sensor, which continuously delivers reconnaissance pictures. For both studies, real-time reconnaissance data (live video link) should be transmitted to the mobile ground station. The transmitted data also includes commands like further waypoints/routes and telemetry data such as current UAS-position and the status data. This information are necessary for the UAS-operator.

In this scenario, data transport from and to UAS should be realized via IP. Hence, the Institute of Flight Systems investigates on innovative IP-

DOI 10.5162/etc2016/5.3

based datalinks for communicating with UAS. The Long-Term Evolution (LTE) might be a pioneering technology for such datalinks as it offers robust coding schemes as well as very high sensitivity of receivers. In this article, we present a concept and first results when using a public LTE-network to transmit sensor data as well as commands between UAS and to the ground-based control station.

This paper is organized as follows. Section 2 describes the data-link for UAS, which has been formerly used at the UBM while Section 3 clarifies the lessons learned and requirements for a preferable UAS data-link. Section 4 assesses candidates for the data-link. Section 5 introduces a concept and basic evaluation of a data-link for UAS, which is based on commercial LTE-networks. Section 6 contains the evaluation of UAS-guidance in flight test via commercial LTE. Section 7 presents activities for set-up own LTE-network infrastructure at the Institute of Flight Systems.

2. Former work at the UBM

Before the UBM was investigating LTE technology, we used IEEE 802.11n-based data links for communicating between our fixed wing RC electric glider and the ground station (see Figure 1). The experimental set-up is described in [2]. Main results are recapped in the following. The glider is hand launched and equipped with a 1200 Watts electric propulsion system. The hull has been modified to accommodate an autopilot and a payload module containing two embedded computer boards. As a bridge data-link to the ground station we use a compact PCI Express 5GHz 802.11n module with +20 dBm transmit power and +5 dBm antenna.

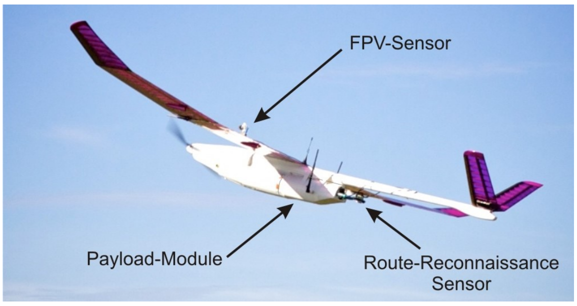

Figure 1: RC-Glider of UBM

The payload configuration consists of a video camera generating a 1080p stream @30 Hz MJPEG requiring a bandwidth of approximately 8 Mbit/s.

The ground station integrates 4 computers with two touchscreens and features a pan/tilt platform with two integrated 5 GHz directional antennas (16 dB gain) and 802.11n routers. For testing purpose only we set output power to +20 dBm. In our flight tests the radio link distance between ground station and glider ranged up to 550m.

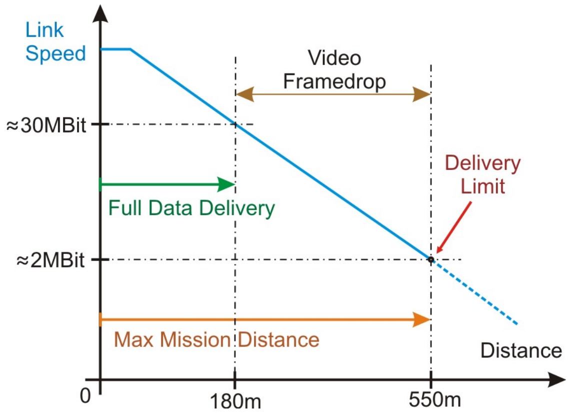

Figure 2: Approx. Maximum Mission Distance 5 GHz IEEE802.11n @ +20 dBm TX-Power (taken from [2])

The effective connection rate of the radio link depends on the distance between the UAS and the ground station, as well as the antenna orientation and the shadowing by the UAV itself (cf. Figure 2).

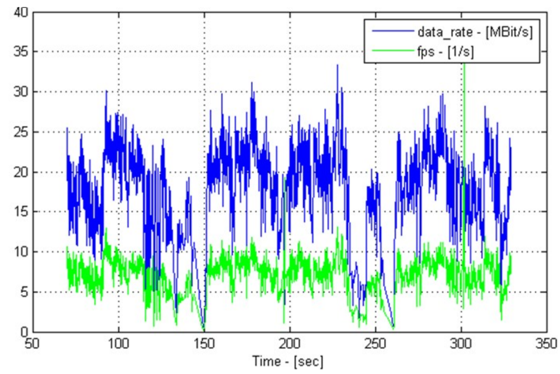

Figure 3: 802.11n TCP throughput (taken from [2])

Thus attitude changes during flight result in a fluctuating connection rate. Figure 3 shows the observed dependence qualitatively. Up to a distance of approximately 180m data streams could be delivered to ground station without losses. A variable delay of video frames of about 50…80ms is observed. This jitter of about 30ms is caused by requesting lost packets by the TCP protocol, which is acceptable and not disturbing. In distances between 180m and 550m, video streams responded to the worsening data connection with a frame drop, which led to a lower frame rate on the operator screen. At greater distances than approximately 550m, the effective connection speed dropped to less than 2Mbit/s. Here it was not possible to transfer the mission-critical high-resolution reconnaissance images to the ground control station.

The results allow the conclusion that – despite using directional antennas with 16 dB gain – the absolute maximum distance for a successful mission fulfilment based on IEE802.11n data-link is far below 550m.

3. Requirements for Data transmission

The previous trials revealed that TCP throughput using an IEEE802.11n data-link is convincing for slow moving platforms in close vicinity.

Our future activities consider data-links for moving UAS in wide area applications. We also extend the scenario with multiple UAS, which have to be connected via a data-link simultaneously.

The results of our findings are the base for specification of requirements for an UAS data-link. These requirements comprise the following topics:

a) *High Robustness and Reliability*

The air vehicles cruise with different speeds, up to 30m/s at maximum. This will result in rapidly changing receiving conditions (cf. multipath etc.). The data link should be robust being able to cope with those conditions.

b) *High Data rate*

The data-link is used for transmitting real-time reconnaissance data to the ground station. As a result the data-link should be broadband. Data should be transmitted with a minimum of 8 Mbit/s.

c) *Low latency*

The data-link may also be used for guiding the UAS via first person view (FPV) which requires low latency data transmission. A maximum of 80ms is acceptable for packet delay.

d) *High Coverage*

High coverage is mandatory not to lose the data connection – preferable sized 1 km radius from the start point at minimum. Data rate must not break down significantly in the edge of the cell.

e) *Short time for resynchronization in case of link lost*

If link lost occurs in spite of high coverage, the connection should be established again very quickly.

f) *Legality*

It has to be ensured that legal restrictions (i.e. allowed transmit power, license for frequency usage) must not be violated.

g) *Capable of Multi-UAS Scenario*

The UBM also investigates in scenarios, where several UAS will be located dynamically in an urban mission. The datalink should be able for simultaneously communication with several airborne entities, which are located at different positions.

4. Technical overview of candidates for a data-link

Consulting the above noted requirements, we consider the following three options as possible candidates for a data-link:

- Wi-Fi
- Commercial LTE provider
- Own LTE network

Technical assessment on Wi-Fi

At first we examine IEEE802.11n on fulfillment of the before noted and extended requirements.

IEEE802.11n is a wireless networking standard that uses multiple antennas to increase data rates. Theoretically, 802.11n networks can achieve up to 150 Mbit/s if there are no Bluetooth, microwave or other Wi-Fi emissions in the vicinity. It can be used in the 2.4 GHz or 5 GHz frequency bands and achieves short delays.

Due to German legal regulations of IEEE802.11n only very low transmission power is allowed. However, in a wide area scenario the likelihood of Wi-Fi packet loss will rise. TCP misinterprets packet loss as congestion – a dropdown in performance is likely to occur. Asadpour et al. [3] postulate that the automatic rate adaptation functionality of standard 802.11n chipsets cannot cope with the high mobility of UAS. Since Wi-Fi is released for generally use, interferences from other devices in the vicinity are to be expected. Hence, the stable coverage of 802.11n is quite limited – operations without directional antennas are not feasible. In case of using directional antennas the equivalent output power (EIRP) will go beyond existing legal regulations. The necessity of directional antennas makes scenarios with multi-UAS not feasible. The time for resynchronization (in case of link lost) cannot be measured exactly – but we assume a range of seconds from our observations.

Technical overview and assessment on LTE

With the introduction of LTE mobile technology it is possible to provide a mobile broadband access that has the potential to become a viable alternative to fixed broadband connection in terms of bandwidth and latency. The aim and design of the LTE system architecture (SAE)

DOI 10.5162/etc2016/5.3

and concepts are to efficiently support mass-market usage of any IP-based service.

LTE Rel. 8 fulfills the most notable of our requirements: To overcome the effect of frequency-selective fading due to multipath (known in other technologies like UMTS) LTE uses Orthogonal Frequency Division Multiplexing (OFDM) for the downlink. OFDM uses a large number of narrow sub-carriers for multi-carrier transmission. Data is transmitted over many (1200 per 20 MHz bandwidth) narrow band carriers of 180 KHz each instead of spreading one signal over the complete carrier bandwidth. Hence, LTE ensures higher robustness than other techniques like 802.11n, which uses 52 subcarriers only. In addition, LTE is specified for mobility up to 350 km/h and can therefore easily cope with our UAS-scenario.

The peak bit rate of LTE Rel. 8 yields up to 150 Mbit/s in the downlink and up to 50 Mbit/s in the uplink. Aggregation of two 20 MHz carriers facilitates up to 300 Mbit/s in downlink. Deutsche Telekom, a commercial network operator in Germany, has already rolled out this technology. In principle, roundtrip times of less than 10ms are possible. However, commercial LTE networks share the resources between all users in the LTE-cell. Prioritization and guaranteed minimum bandwidth are feasible in principle (cf. voice over LTE) but not offered for simple data transfer. Consequently, a specific minimum bitrate per user as well as a minimum roundtrip time cannot be guaranteed in today’s commercial LTE networks. If operating an own LTE-network, the allowed users and network load in the LTE-cell can be completely controlled.

The coverage of LTE depends on the band and the specific configuration (e.g. carrier frequency band, antenna tilt) as well as the maximum transmission power. This is true for commercial as well as own operated LTE networks. In principle, LTE is specified for cell sizes up to 100 km in diameter – with slight degradation after 30 km. To demonstrate the capability of LTE in air scenario we refer to [4] where the Deutsche Telekom and Airbus successfully tested LTE-based broadband services for passenger aircraft via “Direct-Air-to-Ground”. In practice, commercial LTE-cells achieve up to several kilometers in diameter. Consequently, link lost will be much less likely in comparison to Wi-Fi. In addition, the large-scaled coverage of LTE makes multi-UAS-scenarios possible.

The network operator and the German Federal Network Agency guarantee the legality of the commercial LTE-networks. Own operated LTE-network have to be authorized by the Federal Network Agency. At this point difficulties may arise from licensing available carrier frequencies from commercial network operators.

Figure 4 summarizes the requirements and fulfillment of assessed technologies for an UAS data-link. It comes clear that IEEE 802.11n does not satisfy our requirements. Therefore, we will evaluate LTE-based data-links as alternative solution. In the first step, commercial LTE-networks are examined here.

	WI-FI 802.11n	Commercial LTE network	Own LTE network
robustness	limited	very good	very good
data transfer rate	very good	depends on other subscriber in the cell	very good
latency	very good	depends on other subscriber in the cell	very good
coverage	limited w/o directional antenna and amplifier	depends on network operator	very good
time for re-syncronisation	limited	very good	very good
legality	limited (directional antenna mandatory)	very good	radio license mandatory
Multi-UAS-scenario	Not possible	very good	very good

Figure 4: Résumé of requirement assessment for data-link candidates

Overall LTE architecture

The main principles of the LTE-SAE architecture include a common anchor point and gateway (GW) node for all access technologies. This includes IP-based protocols on all interfaces and a minimum number of network nodes. Figure 5 shows a simplified view of the overall LTE architecture.

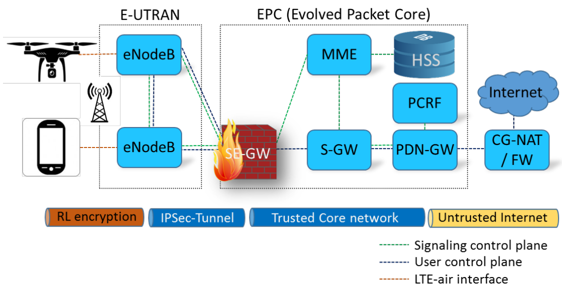

Figure 5: LTE-architecture in overview

The user equipment (UE), which is represented by our UAS as well as a ground station, are connected via encrypted radio link (RL encryption) to the LTE base station (eNodeB). Strong algorithms SNOW 3G / AES are used at this stage. The LTE eNodeB, which logically belongs to the E-UTRAN (evolved UMTS Terrestrial Radio Access), connects to the core networks’ Security Gateway (SE-GW) via an IKEv2/IPsec-Tunnel. The MME handles control signaling – for instance, for mobility. User data

DOI 10.5162/etc2016/5.3

is forwarded between base stations and gateway nodes over an IP-based transport infrastructure. The home subscriber server (HSS) stores configuration information (user specific entitlements) and the secret keys for simcard authentication, from where the keys for radio link encryption are derived.

The PDN gateway serves as a common anchor point for all access technologies, providing a stable IP point-of-presence for all users regardless of mobility within or between access technologies. The PDN-GW provides the access to the Internet where the PCRF (Policy and Charging Rules Function) controls connection parameters such as maximum bandwidth. A separate serving gateway (S-GW) is mandatory in roaming scenarios only. Otherwise, S-GW and PDN-GW functions are handled by the same network node.

5. Concept for UAS data-link based on commercial LTE-network

Due to limitations of available public IPv4-adresses, commercial LTE networks are configured to assign private IP-addresses to each UE most commonly. When analyzing the routes of IP-packets in these LTE networks we revealed that CG-NAT (carrier grade network access translation) is used twice for the packets. Consequently, services on UEs are not accessible from the internet and UEs are not able to communicate directly among each other. These restrictions preclude commercial LTE-networks as data-link for UAS at first.

We meet that challenges by building up own VPN-infrastructure (Virtual private Network). For this purpose, we configured a Linux-Ubuntu-server with openvpn. This server also manages the assignment of VPN-IP-addresses to UEs as well as routing between all connected UEs. As a consequence, all UEs are virtually located in the same network. Thereby, we overcome any restrictions in communication among each UEs and also relating to open ports. In addition, the communication is completely secured by strong encryption.

The logical packet flow using our VPN-infrastructure via commercial LTE-networks is shown in Figure 6.

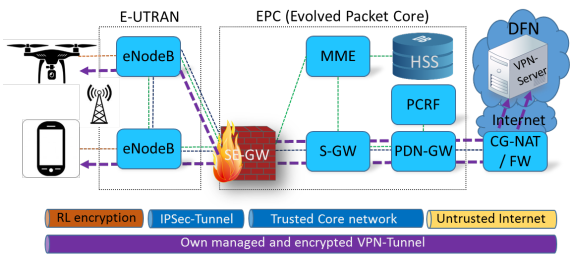

Figure 6: VPN-tunnel over public LTE-infrastructure

Each UE establishes an encrypted VPN-tunnel to our VPN-server at first. The VPN-server is located in the DFN (Deutsches Forschungsnetz) and thereby connected with 1Gbit/s to the internet. IP-packets are wrapped in the encrypted VPN-tunnel by each UE passing the eNodeB, Security Gateway, S-GW, PDN-GW and the Internet to the VPN-server. At the tunnel endpoint IP-packets are deciphered and routed to their destination. This may be another mobile UE or a cable-based device using an own VPN-tunnel.

Evaluating commercial LTE-networks

a) Basic LTE-network assessment at flight test area

Since our VPN-enhancement commercial LTE-networks might be beneficial as UAS data-link. First of all, we theoretically evaluated the E-UTRAN-Band coverage of commercial LTE-network operators at our desired flight test area (cf. Figure 7). The results are shown in Table 1.

Table 1: LTE-Coverage of commercial network operators at UBM flight test area

Operator	E-UTRAN-Band	Bandwidth [MHz]
Deut. Telekom	3, 20	20, 10
Vodafone-de	7, 20	20, 10
Telefónica	20	10
TelefónicaEplus	3	15

Based on the available carrier-bandwidth we expected highest data-rates in the networks of Deutsche Telekom and Vodafone – aggregating 30 MHz of bandwidth each. Consequently, these two networks will be examined in the following.

b) LTE-network performance test at flight test area

For the purpose of testing the performance of LTE-networks we measured the roundtrip time, up- and download rate to a server near Frankfurt for 6 different measure points at our flight test area (cf. Figure 7) on a weekday about noon.

Figure 7: Measure points at UBM flight test area

DOI 10.5162/etc2016/5.3

As test equipment we used a Samsung Galaxy G900FD, which is capable of LTE Cat. 4. LTE-Advanced is not supported. The Results of our measures can be found in the following Table 2.

To start with, our measures are representative at a specific location and time only. They are not generally valid for the tested network operators.

Table 2: Data rates for 2 network operators at measure points

Measure point	Round-trip [ms]	DL [Mbit/s]	UL [Mbit/s]
1 Telekom	52	32,9	10,3
1 Vodafone	76	7,2	0,5
2 Telekom	55	16,6	9,2
2 Vodafone	44	7	3,6
3 Telekom	52	20,3	10,5
3 Vodafone	48	7,7	4,4
4 Telekom	44	12,5	10,4
4 Vodafone	49	8,7	4,2
5 Telekom	48	9,2	10,6
5 Vodafone	53	12,4	5,5
6 Telekom	41	27	10
6 Vodafone	51	8	6

At our flight test area we revealed transfer rates between 9…32.9 Mbit/s in Downlink (mean: 19.75Mbit/s) and 9…10.6 Mbit/s in Uplink (mean: 10.1 Mbit/s) for the Deutsche Telekom. The Uplink suffered from contractual limitations.

Vodafone transfers between 7…12 Mbit/s in Downlink (mean: 8.5 Mbit/s) and 0.5…6 Mbit/s in Upload (mean: 4 Mbit/s).

Both network operators provide roundtrips in an acceptable range. To sum up, in our measures at the flight test area the Deutsche Telekom provided much better data rates than Vodafone. Using a Vodafone network did not fulfil our requirement (b). Hence, we only regarded Deutsche Telekom for all further tests.

c) Test of LTE-coverage in typical flight altitude

The next step comprised to prove evidence for LTE-coverage not only on ground level, but rather at typical flight altitude. This coverage mainly depends on the antenna tilt of the eNodeB. A typical flight altitude of our UAS is below 150 m AGL. Due to airspace regulations, altitudes above 150 m AGL are not allowed.

For this test (test setup depicted in Figure 8) we equipped an UAS with an LTE-modem (LG E975). The remote station (Laptop) on the ground was equipped with the Samsung G900FD as LTE-modem.

Both LTE-devices each built up a VPN-tunnel to our VPN-Server as already depicted in Figure 6. The VPN-IP-addresses are assigned to UEs by the VPN-server and ranged in the same logical network.

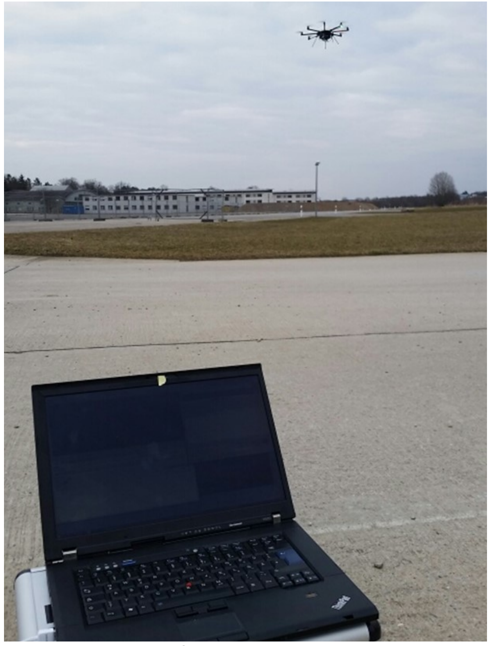

Figure 8: Test setup for evaluating the LTE-coverage in typical flight altitude at measure point 6

Our tests comprised measuring the roundtrip time as well as up- and download rate between these two devices (UE1, UE2) in the VPN. For measuring the roundtrip packets have to pass the route depicted in Figure 9.

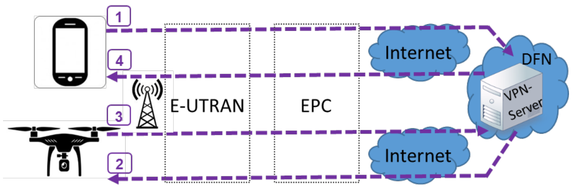

Figure 9: Network path for packet roundtrip

A safety pilot guided the UAS via a commercial remote control and thereby alternated the flight altitudes between 0...100 m above ground.

For measuring the relevant data, we used *iperf* in client- and server mode. The tests took place at flight test area (measure point 6 in Figure 7). This measure point was already used for our basic bandwidth tests.

Our measures (cf. Table 3) revealed a bandwidth between 12...15 Mbit/s in download and 7…12 Mbit/s in upload consistently in all examined flight altitudes. Despite the long network path through our VPN packet roundtrips are on an acceptable level.

To sum up, our measures provided proof for sufficient LTE coverage as well as sufficient performance of our VPN-Tunnel in typical flight altitudes at our flight test area.

Table 3: Data rates via LTE in typical flight altitudes of small UAS

Altitude AGL [m]	Round-trip [ms]	DL [Mbit/s]	UL [Mbit/s]
Ground 0m	75	15.9	7.7
73m	83	13.5	12.9
100m (1)	68	14.5	11.8
100m (2)	79	12.2	10.5

6. Evaluating UAS-guidance via commercial LTE-networks

In the previous chapter, a concept for an LTE-based data-link for UAS was provided. The concept has been realized by setup own IT-infrastructure. Basic tests of this data-link have been accomplished in the network of Deutsche Telekom. This chapter evaluates guiding an UAS via a commercial LTE-network. Thereby the LTE-datalink serves for:

- Live video data
- Command data (e.g. commanding routes and waypoints)
- Status data (e.g. position, altitude, conditions of battery)

UAS

Our UAS to be guided via LTE is based on an octocopter (cf. Figure 10). A navigational system (gps, glonass) is integrated to provide autopilot functions. The autopilot features dynamic position hold, auto start and waypoint functionality.

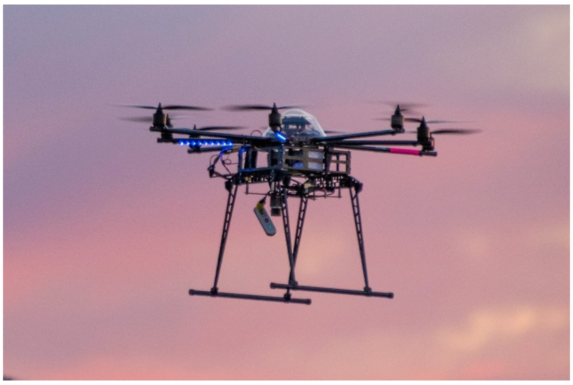

Figure 10: UAS integrated in commercial LTE-network

As payload we integrated a lightweight Armv7-Odroid XU4 microcomputer with Ubuntu 14.04. The data-link is established via a Cat. 4 LTE Modem (Huawei E-3276-150). Live video data is generated by an industrial 2 megapixel USB3.0 camera. The video data stream is compressed in real-time by AnyCom, a spread based interprocess communication architecture already used in the context of [2].

Electrical power is supplied by two 6s-LIPO-batteries with a capacity of 12000 mAh each. The total weight is just 6 kg – thereby making an airtime of 30 minutes possible.

UAS-guidance

UAS-guidance is realized by the use of a tablet-based computer. This approach enables a human machine interface (HMI) using multi-touch functionality. For this purpose we used a Microsoft Surface Pro 3 with a 30 cm display operating at Ubuntu 14.04. Input to HMI is realized either via a touch screen digitizer or a pen digitizer – each combined into a single layer.

The software application on the surface (cf. Figure 11) offers a window with live video and a second window for UAS guidance.

Figure 11: HMI for guidance of UAS based on tablet computer with touch-device

The desired position, altitude as well as routes are commanded on the base of aerial photo images in the background. Thereby, we expect slight operability and short training.

Test procedure

For this evaluation, both the UAS and the tablet computer connected to our VPN via LTE first. After starting the UAS by the safety pilot the authority is handed over to the UAS-operator and his tablet computer. Thereby the UAS is doing position hold waiting for command data instructions. Live video data as well as status data is continuously transmitted from the UAS to the tablet computer. During the tests, the UAS-operator did plan several routes and commanded the UAS to this routes. Figure 12 depicts guidance of the UAS during the flight experiment.

Figure 12: UAS-guidance by tablet computer via LTE

Results

The UAS successfully patrols on its commanded routes and waypoints. The maximum range tested was up to 500 m from the initial starting point (measure point 3). This was only due to legal constraints, which require eye sight to the UAS.

We noticed a smooth transmission of video data with a small delay via LTE. The quality of the video transmission was satisfactory. Eligible improvements in image quality could be realized via automatic image stabilization in the future. No link lost was observed.

7. First evaluation results of own LTE-network

In the previous chapter, we demonstrated the guidance of an UAS via commercial LTE-networks. In principle, this technique is sufficient to fulfill our requirements. However, commercial LTE is a shared medium between all subscribers in each of the cells. Thus without prioritization subscriber individual data-rates cannot be guaranteed.

The solution obviously offered here is to use own LTE infrastructure. Thereby, subscriber-management as well as bandwidth-management on the LTE-air interface is feasible. The UBM therefore investigates in the operation of own LTE infrastructure. This promising approach comprises building up an own EPC and an own eNodeB.

Such research activity is relevant for the German Armed Forces [5] as LTE may provide a military wideband data-link in the future – delivering lower latency, faster speeds and a more efficient architecture than the latest wireless military technologies. In this future scenario, a HALE-UAS (High Altitude Long Endurance) carries a LTE-based mobile hotspot to provide high-bandwidth communications for other UAS or ground troops in remote forward operating locations [6]. However, in our first LTE-trials, the LTE-nodes (eNodeB and EPC) both reside on a ground station.

Since commercial LTE equipment is designed for many thousands of subscribers and therefore cost intensive, we focused on small entry solutions. In the lower price segment, stand-alone solutions for a limited number of subscribers are offered integrating an eNodeB and an EPC in a single box. The signal generation is realized via software defined radio (SDR) and thus enables flexible operation in E-UTRAN-Bands.

Test equipment

For our LTE-trials, we used an Ettus B210 SDR (cf. Figure 13) as transceiver. This SDR is connected to a host computer through high-speed USB 3.0, which the host-based software uses to control the SDR hardware and transmit/receive data. The SDR covers a frequency range between 70 MHz to 6 GHz and provides the following subsystems: clock generation and synchronization, FPGA, ADCs, DACs, host processor interface, and power regulation. These are the basic components that are required for baseband processing of signals. A front-end daughterboard is used for analog operations such as up/down-conversion, filtering, and other signal conditioning.

Figure 13: ETTUS B210 SDR

We use amarisoft [7] as host-based software to control the SDR. Amarisoft features an eNodeB compliant to LTE rel.8 and offers standard S1 and GTP-U interfaces to the core network. The bandwidth and target E-UTRAN-band are fully configurable. The amarisoft core network (EPC) implements one MME with built-in SGW, PGW and HSS. It supports several eNodeBs with standard S1 interface. Hence our basic LTE-network consists of the B210, the amarisoft eNodeB and EPC which grant access to IP network.

Evaluation setup

We configured our basic LTE-network to operate at SISO 2.6 GHz and 20 MHz bandwidth. The radio license at 2.6 GHz was gratefully provided by Deutsche Telekom.

Figure 14: Basic LTE network integrated in a mobile ground station

For the evaluation we integrated our LTE-network into a mobile ground station (cf. Figure 14). A spectrum analyzer revealed an output power at the B210 at about -15 dBm. A +17 dBm amplifier (resulting output power +2 dBm) was applied for testing purposes.

The payload of our UAS and the laptop used for these tests is described in chapter 6.

Test procedure

The evaluation took place at flight test area (measure point 3 in Figure 7). In the first step, we measured the achieved LTE coverage with the power amplifier 1 m above ground level.

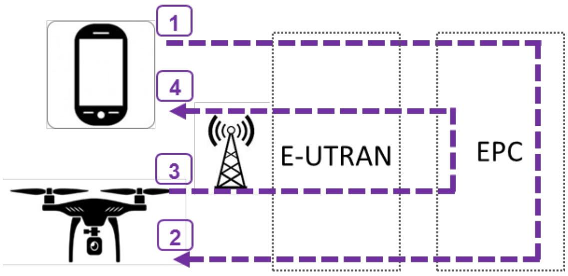

Figure 15: Network path for packet roundtrip with own LTE infrastructure

At the second step, the UAS and the Tablet are both connected via LTE. Live video streaming and data transfer tests are processed while the UAS is in flight 0…30 m above ground level. The network path in this experiment (cf. Figure 15) avoids any external nodes in the internet and is therefore a lot of shorter than before with the VPN-server.

Results

For evaluation of LTE coverage, we started from measure point 3 and increased the distance continuously. The signal itself was receivable up to a distance of 200 m. However data transfer was hardly possible in this configuration - we identified the power amplifier producing unsatisfactory linearity. As a result further tests were accomplished without power amplifier but limited transmit power (-15 dbm).

In the flight tests, we revealed data transfer rates with iperf at about 1 Mbit/s in uplink and downlink. The packet roundtrip time was acceptable between 70…80 ms. Streaming of video data was successful in principle but dropouts have been noticed. However, the coverage was very limited (below 30 m).

To sum up, IP data was transmitted between an UAS and a ground based laptop by using an own LTE eNodeB and own EPC. The limited coverage and unsatisfactory performance is mainly caused by the very limited transmit power of our Ettus-SDR. Antenna shadowing at our mobile ground station potentially affects the results, too. Further tests have to be accomplished with high-quality amplifiers.

8. Conclusion and Discussion:

This article focuses on the evaluation of IP-based data links for the communication between a ground station and UAS. We presented a concept for an UAS data link, which is based on commercial LTE networks. To eliminate limitations of commercial LTE networks, own IT-infrastructure has been established. The integration of an UAS and a handheld tablet solution into a commercial LTE Rel. 8 network has been demonstrated successfully.

As a result, commercial LTE networks are principally able to serve as an appropriate data link for UAS. Since LTE cells shares their bandwidth between the subscribed users, the practical data throughput of commercial LTE networks is far below the theoretical bandwidth. Our flight tests with mobile UAS revealed LTE as robust towards multipath propagation. This advantage bases upon the multi-carrier OFDM technology and its fast control algorithms.

Our experiments with LTE lead to the conclusion that best benefit is provided by operating own LTE-nodes and cells. However, using the frequency spectrum of a commercial network operator requires a radio-license. Consequently the German Armed Forces intend to acquire own LTE frequency spectrum in the future.

The tested LTE solutions from the low-cost market do not completely convince – further tests are necessary for using as a productive data link. The limited performance of our own LTE network is probably caused by the low transmission power and the suboptimal antenna position in the ground station. Nevertheless, we appraise LTE as a promising technology for future data links.

9. References

[1] Technical description DJI Lightbridge http://wiki.dji.com/en/index.php/DJI_Lightbridge

[2] F. Böhm, A. Schulte. Scalable COTS based data processing and distribution architecture for UAV technology demonstrators. European Telemetry and Test Conference etc2012. Munich, Germany. 12-14 June 2012.

[3] M. Asadpour, D. Giustiniano, K. A. Hummel, and S. Heimlicher, “Characterizing 802.11n aerial communication”, ANC 2013.

[4] Tweet: Breitbanddienste für Passagierflugzeuge über ein “LTE-Direct-Air-to-Ground”. https://www.telekom.com/medien/konzern/107624

[5] Tweet: Tetra-LTE-Pilotsystem von Airbus für die Bundeswehr. http://www.airbusgroup.com/int/en/news-media/press-releases/Airbus-Group/Financial_Communication/2014/12/20141204_airbus_defence_and_space_tetra_lte_bundeswehr/de_20141204_airbus_defence_and_space_tetra_lte_bundeswehr.html

[6] S. Malisuwan & W. Kaewphanuekrungsi. Ad Hoc UAV LTE Networks for Critical Communications. In International Journal of Computer Networking, Vol. 6(1), 2016, ISSN(E): 2278-9448

[7] Amarisoft: http://amarisoft.com/

DOI 10.5162/etc2016/5.4

Multi-Band (Ku, C, Wideband - Satcom, Narrowband Satcom) Telemetry Test System for UAV Application

Murat IMAY
Turkish Aerospace Ind, Inc. Ankara, Turkey
mimay@tai.com.tr, muratimay@gmail.com

ABSTRACT

"This paper describes the design, development, production of fully autonomous UAV data link test system. The ethernet based data link systems consist of Ku-Band, C-Band, Wideband-Satcom and Narrow-Band Satcom. Ground control station and all airborne hardware systems with simulation, monitoring capability that are be integrated into these telemetry test systems. Integration of GCS, Airborne hardware system and network based telemetry system with handover capability of UAV aircraft are also included in this paper.

These test system allows to user to simulate auto adjustable data link range with real data link equipment. Test automation software and auto adjustable data link range system are used to control the execution of tests and the comparison of actual outcomes with predicted outcomes.

Key words: UAV, Telemetry, Flight/Ground Test, Handover, LOS/BLOS.

INTRODUCTION of TAI UAV

Unmanned aerial vehicles (UAV) has been design and developed by Turkish Aerospace Industries to meet for customer requirements. Advanced Medium Altitude Long Endurance (MALE) class Unmanned Aerial System performs day and night, all-weather reconnaissance, target detection / identification and intelligence missions with its payloads, featuring autonomous flight capability including Automatic Take-off and Landing.

The platform is also equipped with a digital flight control system, electro-mechanical actuators, and flight control sensor systems such as GPS, pitot-static, air data computer, navigation sensor, transducers,temperature,pressure,displacement sensors, etc. Various tasks are distributed along flight management computers and auxiliary control boxes. All flight critical equipment is dual or triple redundant and emergency modes of operational scenarios are taken into consideration for fail safe design.

Fig. 1 Command and Control

UAV operations are supported by highly sophisticated ground control system with complete redundancy, developed by TAI. Whole mission segments of the air vehicle can be managed, monitored and controlled by a GCS. A pre-programmed mission plan can be loaded before the flight begins or can be altered during the flight. All the imagery stream of the payloads can be displayed and recorded in real time and

DOI 10.5162/etc2016/5.4

all the payloads can be controlled from the GCS.

Fig. 2 UAV and CS Real/SIM System

ATOLS allows the air vehicle to perform its operation without operator intervention, including the most critical phases which are landing and take-off.

TAI UAV has Radio Relay, electro-expulsive Ice Protection System, BLOS and LOS datalink with handover capability allowing operational security and ease.

HANDOVER

Flight distance of TAI UAV is more than Control Station (CS) telemetry LOS range. There is boundary to how far UAV can be controlled from a CS due to loss of line of sight or distortion of the data link signal due to distance away the UAV is from the CS. Before this happens control of the CS should be handed over to another CS.

TAI UAV requires not just for local tasks Line Of Sight (LOS) to its Control Station (CS) but for long distance flights) Beyond Line Of Sight (BLOS) and for endurance station keeping duties. In both cases the UAV will need to be handed over to another CS. In the first case the UAV is in another CS closer to the area the UAV is to carry out its task. In the second case the UAV will be flying for many hours in which case the UAV is handed over to another CS at different location.

Fig. 3 Handover BLOS Equipment Test System

There are three types of Handover for this UAV project, the first between CSs when the UAV is to be flown out of range of what can be flown by CS1 so the H/O is to CS2. The second type of H/O is between two LOS (Ku/C Band Datalink) in the same CS avoid one LOS data link failure, all datalink system is connected with each other via network so that any of datalink system can be selected by CS. The last one is satellite (BLOS wide/narrow Satcom) handover.

Handover process of UAV from one CS to another, there are some sophisticated steps of handover. In handing over the UAV between the CSs there can be hazards and unexpected problem therefore safety risks associated with the hazards must be eliminated on ground test before flight test.

Several critical test phases will be executed in these integration system with the importance of modeling and simulation of CS/UAV for ground and flight test.

Handover of TAI UAV occurs over a communication radio. Handover plan is based on transfer of control between two CS by switching transmitters on or off.

- CS verify they are using the same frequency of communication.
- Both CS verify critical flight control commands are on the same settings
- Receiving CS report readiness to initiate the transfer.

DOI 10.5162/etc2016/5.4

- Commanding CS acknowledges and report readiness to relinquish control.
- Commanding CS places its backup data link transmitter to OFF, Receiving CS places its backup data link transmitter transmitter to ON.
- Commanding CS places its primary data link transmitter to OFF, Receiving CS places its primary data link transmitter transmitter to ON.
- Receiving CS executes some maneuver (wing rock, heading change, etc.) in order to verify control

If handover is not accomplished, the first CS may assume the transfer has failed and turn its transmitter back or autopilot gets the control of UAV and it starts return to home state.

Aim of test for handover with real equipment is to identify the problems involved with the handover of a UAV between two control stations and provide mitigation to reduce the risk. In order to test all handover cases with real equipment, Architecture at Fig. 5 has been designed and produced. This system includes two air vehicle, 2 two ground station and two data link set, which are LOS and BLOS system. Simulation and monitoring system are also be included to simulate real environmental of flight.

Fig. 4 Handover LOS Equipment Test System

Using real RF equipment can be dangerous because of data link emitters in the test system environment due to hazards of electromagnetic radiation. A primary and back up data link for LOS(Ku-C)/BLOS(Wide-Narrow) are used in handover test system with attenuating the output power of RF equipment, connected air to ground via RF cable and monitoring the received signal strength. These test system provides the range and margin determined and also overturn event of a primary failure to secondary (or backup) data link. RF automatic attenuation equipment is used to simulate auto adjustable data link range with real data link equipment. Flight testing of range, loss of line of sight or distortion of the data link can be simulated with this equipment. Switching between real and simulation of LRU, data injection and equipment on/off is controlled by simulation system.

Handover test of different location of CS and same location is arranged by adjusting IP-based network domain setting.

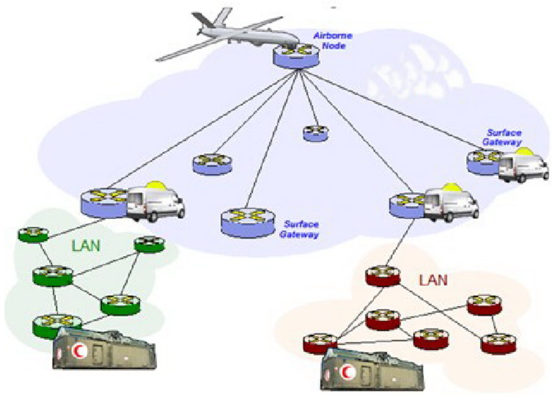

This network for a large number of GCS can be achieved, that provides a wide range of network by using the LAN and air vehicle as the communication node. This also provides an efficient network solution to backup of CS in case of a damage on the communication infrastructure due to earthquake, flood and etc.

DOI 10.5162/etc2016/5.4

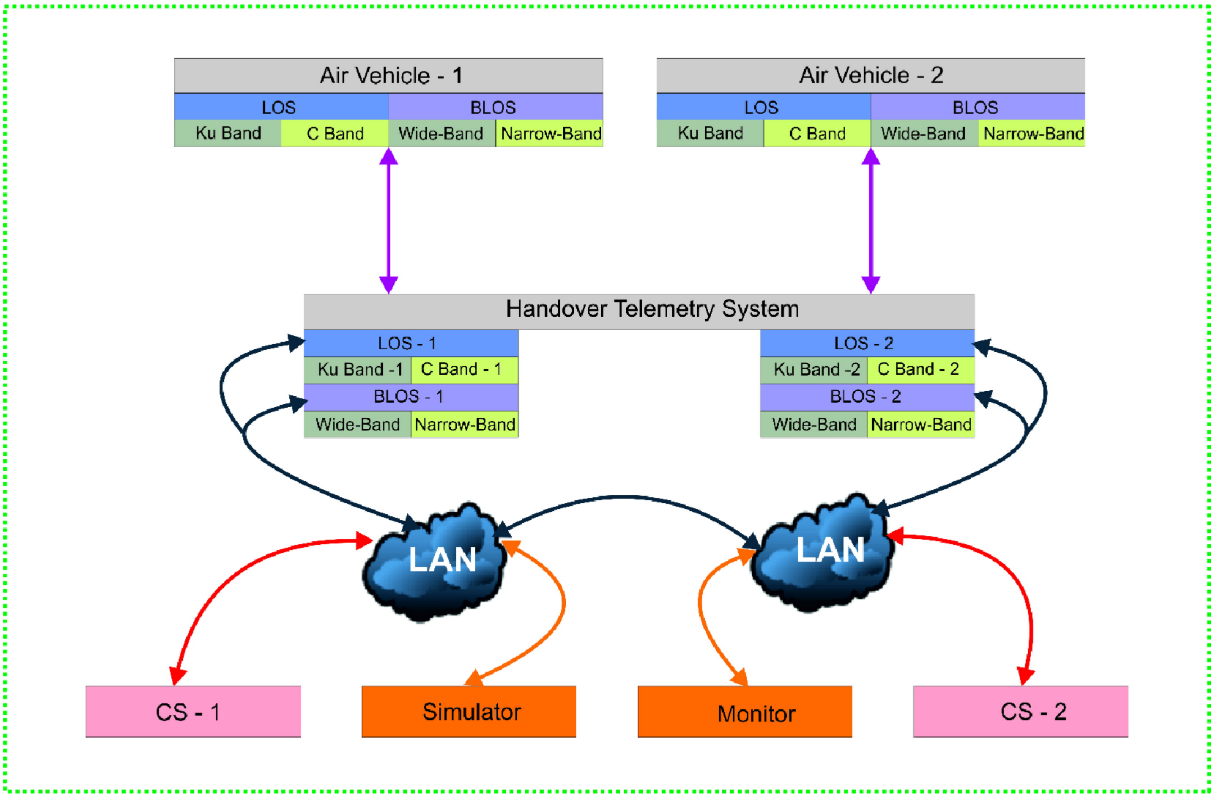

Fig. 5 Handover Architecture of TAI UAV

These test system allows us end-to-end integrated avionics and software integration, check-out, verification, and validation. This capability includes a Real-Time Environment for modeling of integration, simulation and relay interfaces system used for switching between simulation and real equipment.

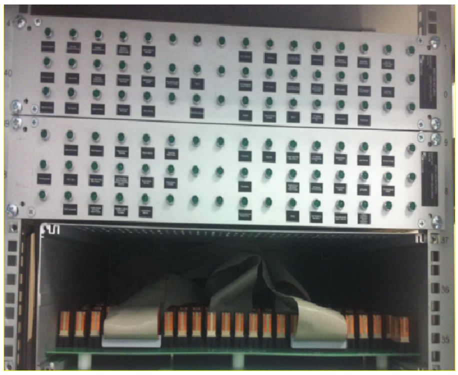

Fig. 6 Relay Panel of Handover System

Test of integration RF equipment with two CS and two air platform for handover is essential not only to reduce the risk of crash, but also to ensure that the system is technically ready for the flight testing.

These test system also allows us to understand behavior of LRU such as GPS navigation, air data computers, navigation computers, mission computers, and/or flight control computers.

This approach, using real/simulation equipment, has led to numerous advances in cost, reliability, and integration time savings. On the other hand, this approach comes with difficult problems when trying to verify functionality of RF system and UAV without flight test campaign. Because many of the functions requiring testing and verification during flight test. Without flight all environmental must be simulated by simulation and real equipment at the same time. These test system allows to inject all of the necessity data and reading all of them to comparison of actual outcomes with predicted outcomes. It also decreases the time and effort required to find out and fix problems by allowing isolation to the message including the error.

TEST AUTOMATION SOFTWARE

Special Test Automation Software has been designed and developed by TAI for execution automatically all test scenario. This software manages all real equipment and simulator for handover and also changing of RF signal strength during transmission for flight simulation of UAV. Automatic test software provides to increase the test case probability and reduce test engineer level tasking of TAI UAV project. Test engineer executes and monitors tests scenarios with this software, and provides data archiving for retrieval and analyses. This software electronically checks for air vehicle response corresponding to simulated or real data initiated at the CS/RF data link system. In some cases of UAV test can be needed inter-active test in order to simulate real environmental. The goal of automatic test software is successfully diagnosing all failure modes associated with the subsystems. In order to determine response and diagnose of whole system, these software allows inject any point of test flow numerous faults.

SUMMARY

Autonomous UAV data link test system, ground control station, airborne hardware systems with simulation, monitoring, handover capability of TAI UAV are mentioned in this paper. Performing hardware/software integration, architecture of handover and related issue are identified, and associated with handover test design of UAV is also presented.

REFERENCES

[1] STANAG 4586 Sec. 1-7-6 Edition No:3

[2] Cox, R. A. (2006). Multiple Aircraft Control Operational Utility Evaluation Final Report, HQ ACC Project 05-115A MD-1D, April 2006.

[3] TAI Design Documentation.

DOI 10.5162/etc2016/5.5

Usability of LTE for Transmitting Radar Data from DLR's Research Aircraft DO 228-212

Stefan V. Baumgartner[1], Daniel Rosigkeit, Anton Nottensteiner[1]
[1] German Aerospace Center (DLR), Microwaves and Radar Institute,
82234 Oberpfaffenhofen, Germany,
stefan.baumgartner@dlr.de

Abstract:
In the paper the usability of long term evolution (LTE) data transmission from an aircraft to the ground is investigated. Theoretical analyses and experimental measurements have been carried out by using a commercial low-cost LTE modem and the existing LTE base station infrastructure on ground. No hardware modifications were made. During the experiments the aircraft was operated in altitudes of approximately 1800 and 2800 m above ground. Over wide areas a stable LTE connection was achieved.

Key words: LTE, data transmission, aircraft, synthetic aperture radar (SAR), traffic management

Introduction

The DLR Microwaves and Radar Institute operates the multi-frequency and multi-channel synthetic aperture radar (SAR) sensor F-SAR [1], which is installed onboard a Dornier DO 228-212 research aircraft. Commonly, for most scientific remote sensing applications the raw radar data acquired with this sensor are processed to fully focused SAR images on ground after the aircraft has landed. For processing, the hard disks or solid state disks are removed from the aircraft and brought to the Institute's data processing facility.

Driven by DLR internal projects dedicated to traffic management for large scale events and disasters (e.g., the VABENE++ project [2]), a powerful onboard processor was developed during the past years. Processing of the radar data can now be carried out directly during the flight onboard the aircraft, parallel to data acquisition. The onboard processor has two main objectives:

- Extraction of relevant traffic information from the multi-channel radar data, preferably in real-time: this involves the detection of moving road vehicles and the estimation of their geographical positions, velocities and moving directions with high accuracy
- Generation of fully polarimetric high-resolution SAR images which can be used for disaster management (e.g., for infrastructure monitoring, for monitoring of flooded areas, etc.).

For traffic management and disaster monitoring it is essential, that the extracted traffic information (size of a few kByte) and the generated SAR images (size of dozens to hundreds of MBytes) are transferred to a server on ground immediately. For this task a data link is mandatory.

During some test flight campaigns a C-band microwave data link and an experimental optical laser communication link, developed by our colleagues from the DLR Communications and Navigation Institute, were successfully tested. These data links require a dedicated (mobile) ground station with an antenna or telescope which tracks the aircraft precisely. Both data link systems are quite complex, expensive and require some time and man power for setting up the (mobile) ground stations and for keeping them in operation.

One advantage, compared to conventional and even more expensive satellite communication links, is the achievable high data rate which is in the order of 10 Mbit/s for the microwave link and even larger for the optical link. However, under circumstances it might be difficult to install the ground station close to the event or disaster location within a small timeframe.

An alternative and low-cost data transmission technique, to our knowledge operationally not yet used for transmitting data from aircrafts, is long term evolution (LTE). In recent years several tests where made with LTE in fast moving vehicles. For instance, in a high speed Transrapid train moving with up to 430 km/h a stable LTE connection with data rates of 36 to 46 Mbit/s was achieved [3]. Also first airborne experiments with an Airbus A320 and some special not off-the-shelf ground stations, with antennas oriented to the sky, were very promising [4].

The hardware, integration, maintenance and operation costs for LTE are expected to be relatively low in comparison to a dedicated microwave link, which additionally require a dedicated ground station and a time and location dependent operation license.

For our radar-based traffic management applications we want to know whether the existing standard LTE infrastructure of the German Telekom can be used with a commercially available LTE modem for transmitting radar images and traffic data from our research aircraft DO 228-212 to the ground and internet.

In the following sections the considered LTE performance parameters, some simulation results and the measurement results acquired during an airborne experiment are presented and discussed.

LTE Performance Parameters

Important LTE performance parameters are the transmit (RX) and receive (RX) data rates, the signal-to-interference plus noise ratio (SINR), the received signal strength indicator (RSSI), the reference signal received power (RSRP), and the reference signal received quality (RSRQ) [6]. These parameters are mainly influenced by the transmit power of the LTE user equipment installed in the aircraft, the distance between the LTE base station and the aircraft, and the patterns and tilt angles of the antennas installed in the base stations on ground and in the aircraft.

The RSRP value represents the power contained in one LTE carrier of 15 kHz bandwidth. With the RSRP parameter different cells using the same carrier frequency can be compared in the LTE network and handover decisions can be made.

The RSRP and the closely related RSSI values alone can generally not be used for drawing final conclusions regarding the signal quality, since the influence of noise, intersymbol interferences (ISI) and other disturbing interferences are not reflected by these values. For assessing the signal quality more comprehensively, it is necessary to consider also the SINR and RSRQ values.

In Tab. 1 a classification of different RSRP, SINR and RSRQ values is made (see, e.g., [7]).

Tab. 1: Quality and usability of the LTE signal.

RSRP [dBm]	SINR [dB]	RSRQ [dB]	Receiving Quality	Signal Usability
>-70 to -79	>10	-3 to -5	very good level	VoIP, very high data rate
-80 to -89	6 to 10	-6 to -8	good level	high data rate
-90 to -100	0 to 5	-9 to -15	average level	half data rate
-101 to -110	<0	-16 to -20	poor signal	non stable connection

Tab. 1 suggests that a qualitative statement regarding receiving quality and usability of the LTE signal can be made if either the RSRP, the SINR or the RSRQ value is known.

Simulation

Before conducting any expensive flight experiments it is interesting to know, if at least theoretically a signal reception onboard the aircraft is possible and if the legally fixed and comparatively low TX power of the LTE user equipment is sufficient to transmit data successfully to the ground station.

For a very rough theoretical performance assessment it is sufficient to compute the expected RSRP values. The RSRP corresponds approximately to the received power P_{RX} in one channel which can be computed as

$$P_{\mathrm{RX}} = \frac{P_{\mathrm{TX}} \cdot G_{\mathrm{TX}} \cdot A_{\mathrm{RX}}}{4 \cdot \pi \cdot r^2 \cdot L} \quad (1)$$

where P_{TX} is the transmitted power in one channel, G_{TX} is the transmit antenna gain, A_{RX} is the effective area of the receiving antenna, r is the distance between the TX and RX antenna, and L are the losses.

The effective antenna area A_{RX} can also be expressed as a function of the elevation dependent RX antenna gain

$$A_{\mathrm{RX}} = \frac{\lambda^2 \cdot G_{\mathrm{RX}}(\theta_{\mathrm{el}})}{4 \cdot \pi} \quad (2)$$

where θ_{el} is the elevation angle of the antenna an λ is the wavelength of the signal.

Generally, the antenna main lobes of the LTE base stations are directed towards to the Earth with tilt angels between 0° and -10°. Therefore, the signals which will be received in the aircraft may originate from the side lobes and from reflections from the ground. For the theoretical analyses and simulations we have ignored potential reflections from the ground.

In Fig. 1 the power P_{RX} received at the base station is plotted for two different aircraft altitudes of 2000 m (in blue color) and 3000 m (black) above ground. Since the exact pattern of the base station antenna was not available, for simplification an ideally SINC shaped elevation antenna pattern without any tapering was considered in the simulation. For the antenna mounted at the aircraft an antenna gain of 0 dBi and a TX power P_{TX} of 200 mW (= 23 dBm) was assumed. With 0 dBi antenna gain also the equivalent intrinsic radiated power $EIRP = P_{\mathrm{TX}} \cdot G_{\mathrm{TX}}$ corresponds to the same value of 23 dBm, which is just the maximum EIRP allowed by law in Germany for LTE. For the simulation no additional losses were considered (i.e., $L = 0$ dB) and a RX antenna tilt angle of -10° was assumed.

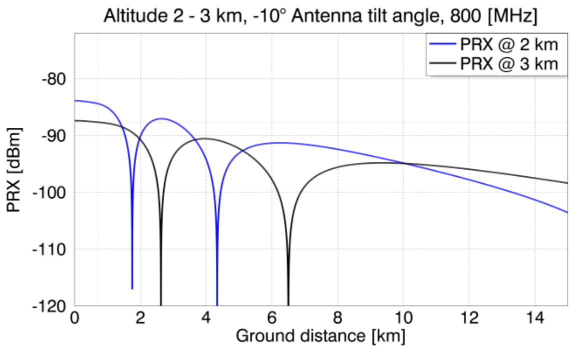

Fig. 1. Expected receive power P_{RX} as a function of ground distance for an aircraft altitude of 2 km (blue color) and 3 km (black) above ground.

By comparing the simulation results in Fig. 1 with the RSRP values listed in Tab. 1, at least an average receiving quality level with half data rate can be expected, since the RX power is larger than -100 dBm over a wide range. The antenna pattern notches in Fig. 1 are practically less relevant since we expect, as already mentioned, to receive also signals from ground reflections which might be much larger.

Experimental Results

The measurement flight was conducted at the end of October 2014. For the experiments a conventional FRITZ!Box 6842 LTE modem with the German Telekom as provider was used. The modem was provisionally installed in the right observation window of the DO 228-212, with a depression angle of approximately 40 degree (cf. Fig. 2 right). No external antennas were used.

Fig. 2. DLR's DO 228-212 research aircraft (left) and right observation window with provisionally installed LTE FRITZ!Box modem (right).

The LTE performance parameters measured by the FRITZ!Box were logged every two seconds. For logging we have written our own Python script which reads the measurement data directly from the FRITZ!Box's web interface. Additionally to the LTE parameters also the geographical positions of the aircraft were acquired using a conventional GPS tracker.

The flight tracks for carrying out the measurements were carefully planned taking into account the known positions of the LTE base stations on ground. Two laps in different altitudes of 2400 m and 3350 m above mean sea level have been flown (these altitudes correspond approximately to altitudes of 1800 and 2800 m above ground). The measured data corresponding to these altitudes have been spatially synchronized so that a direct LTE performance comparison of the different altitudes is possible.

The LTE base station may transmit simultaneously two signals with different polarizations. The FRITZ!Box has two internal antennas and each of these antennas can receive both transmitted signals. Thus, in total four received signals with different RSRP, SINR and RSRQ values are measured. When the FRITZ!Box is operated in the diversity mode, automatically the signal with the best quality is selected for data reception.

In Fig. 3 the measured maximum RSRP values are plotted (i.e., the maximum of the four RSRP values available at each measurement interval). Missing values indicate that the LTE connection was interrupted. Most of the valid RSRP values are within the -100 to -80 dBm interval. According to Tab. 1 this interval corresponds to an average to good receiving quality. The RSRP values at 2400 m altitude are generally better than at 3350 m.

DOI 10.5162/etc2016/5.5

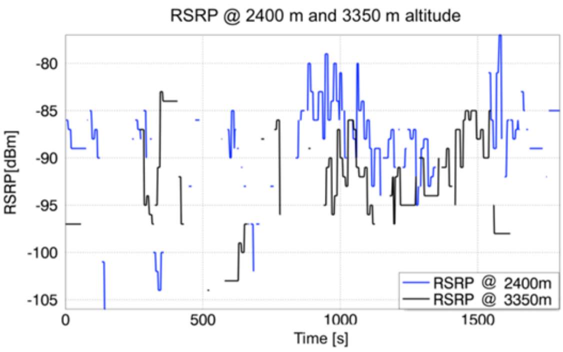

Fig. 3. Measured maximum RSRP values as a function of time for an aircraft altitude of 2400 m (blue) and 3350 m (black) above mean sea level.

The measured maximum RSRQ values are plotted in Fig. 4. They behave similar as the RSRP values: for the lower altitude of 2400 m higher values and, hence, a better LTE performance is observable. Many RSRQ values corresponding to 3350 m altitude are below -15 dB which indicates, according to Tab. 1, a poor signal quality and an unstable LTE connection. From this point of view it is recommended to choose the lower altitude for the envisaged traffic monitoring application.

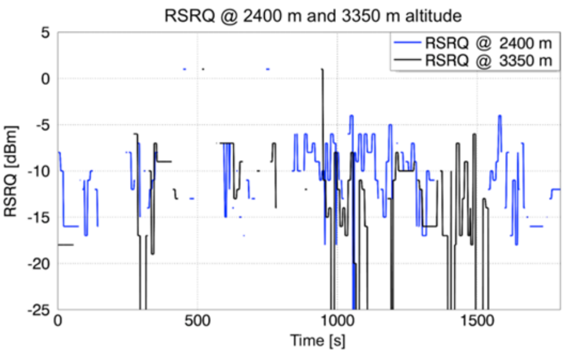

Fig. 4. Measured maximum RSRQ values as a function of time for an aircraft altitude of 2400 m (blue) and 3350 m (black) above mean sea level.

The measured maximum SINR values plotted in Fig. 5 are higher for the lower altitude (blue line). Values between 0 and 10 dB indicate an average to good receiving signal quality with half data rate (cf. Tab. 1). For values below 0 dB, as this is the case for a number of values corresponding to 3350 m altitude, only a poor signal quality and an unstable LTE connection can be achieved.

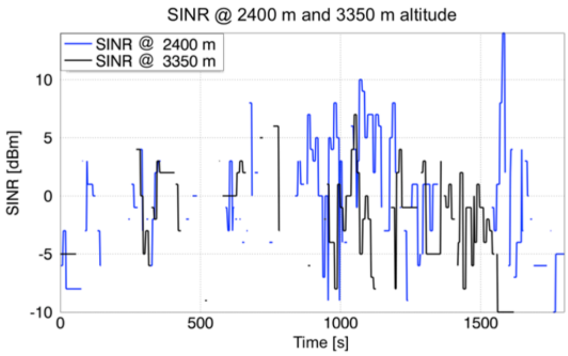

Fig. 5. Measured maximum SINR values as a function of time for an aircraft altitude of 2400 m (blue) and 3350 m (black) above mean sea level.

The FRITZ!Box is also able to measure the usable TX and RX data rates. The measured results for an altitude of 2400 m above mean sea level are depicted in Fig. 6.

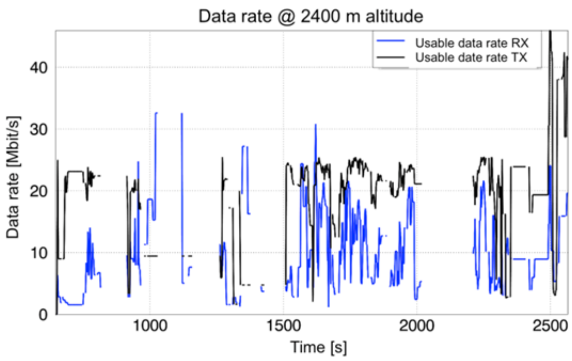

Fig. 6. Measured useable RX (blue) and TX (black) data rates as a function of time for an aircraft altitude of 2400 m above mean sea level.

Over wide regions the usable data rates are comparable with a home DSL connection. However, a strong fluctuation between approximately 2 and 20 MBit/s is observable for the RX case.

The usable TX data rate, which is more in important for our applications, since we want to transmit or “upload” SAR images and traffic data to the ground station, is over wide regions higher than 20 MBit/s.

Although the LTE connection was obviously unstable with several interruptions, it was possible to upload a larger SAR image (cf. Fig. 7) of 270 MByte size to the Dropbox cloud storage without any problems. After interrupts the LTE connection was successfully re-established and the data transfer automatically resumed.

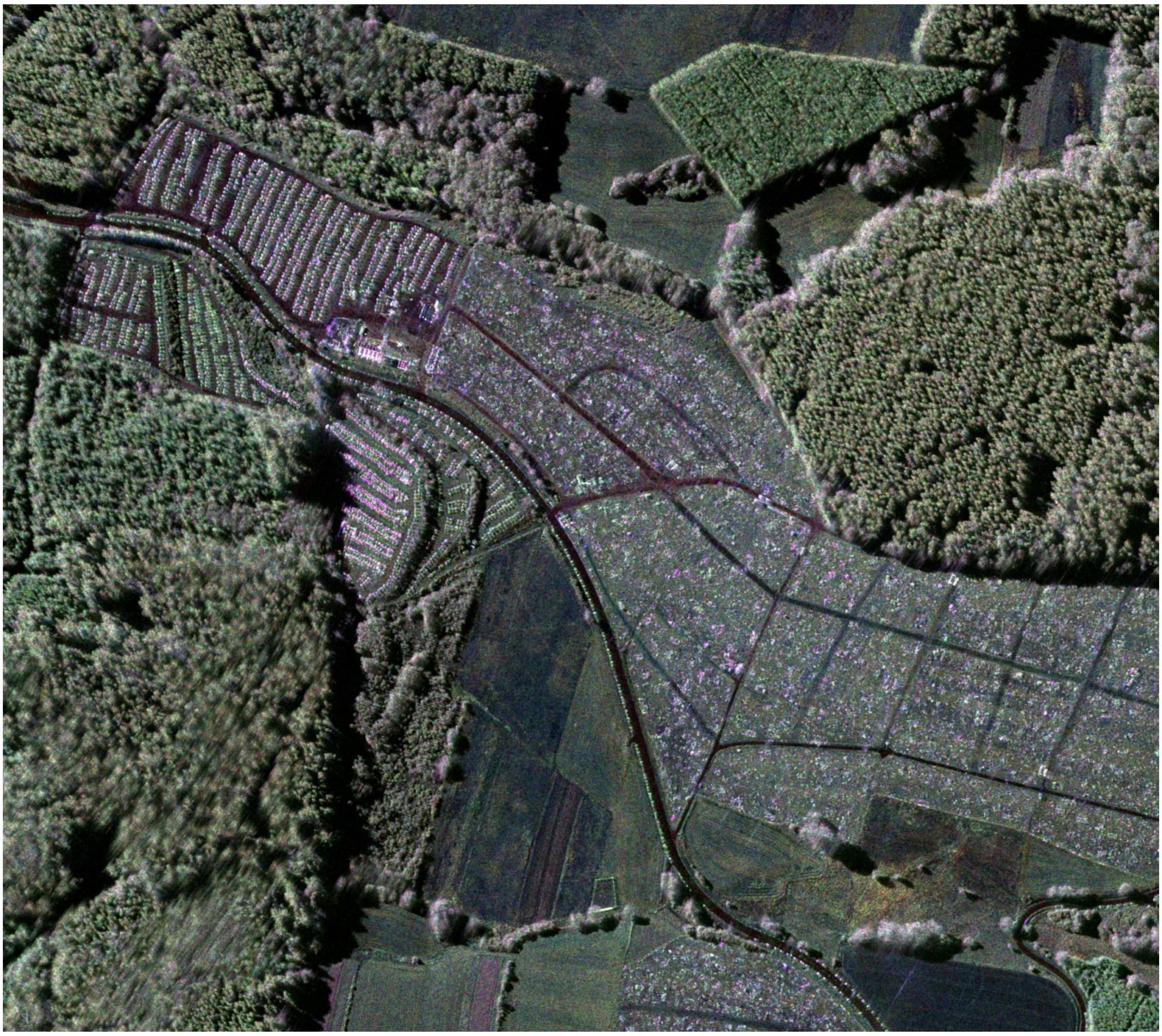

Fig. 7. Fully polarimetric high-resolution SAR image transferred via LTE. The SAR image was acquired four months before the LTE measurement flight during the "Rock am Ring 2014" open air festival. The image has a pixel size of 0.2 x 0.2 m and shows a 800 x 800 m area containing one of the festival's campsites (from the image center to the bottom right) and parking areas (top left). The colors in the SAR image appear due to different backscatter properties of the objects on the ground.

The transfer of the large SAR image took approximately 14 minutes, which results in an effective average TX data rate of 321 kByte/s. This effective data rate is assumed to be sufficiently high for the envisaged traffic management and disaster monitoring applications.

All measured LTE performance parameters were gelocated by synchronizing the GPS track with the measurements. Keyhole markup language (KML) data files were generated for visualizing the geocoded measurement results with Google Earth.

In Fig. 8 one can see in blue the whole flight track in 2400 and 3350 m altitude above mean sea level. The vertical colored lines, with a circle at the top, are the measured maximum RSRP values for a flight altitude of 3350 m. The length of the lines as well as the line and circle color represents the measured RSRP values. Green corresponds to a good signal (≥ -70 dBm) and red to poor signal strength (≤ -110 dBm).

The green pins are the known locations of the LTE base stations. They were found with the help of an online available net coverage map. Each LTE base station was visited prior to the flight to ensure that it really exists and to acquire important data for later evaluation, e.g., the eNodeB IDs of the stations. The colored circles around the base stations correspond to the broadcast radius on ground, where green is a radius of up to 6 km, yellow up to 9 and red up to 15 km. The aim of the flight track planning

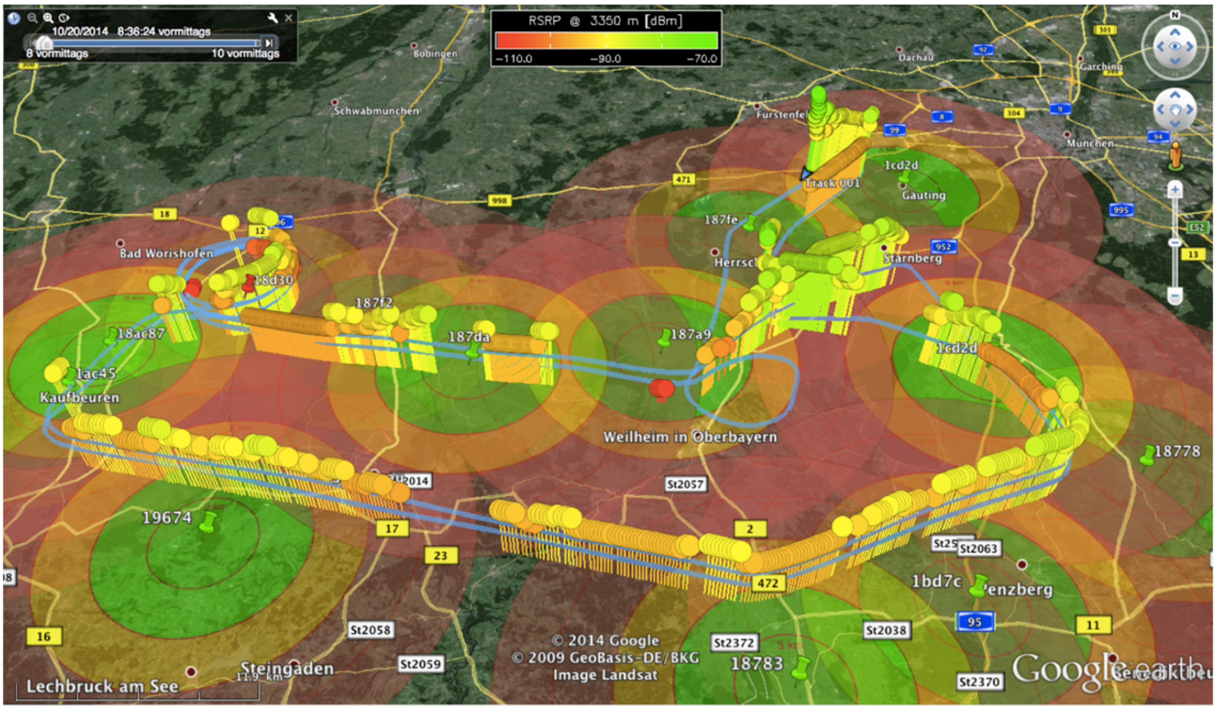

Fig. 8. Geocoded maximum measured RSRP values (colored circles with vertical lines) for 3350 m altitude above mean sea level. The blue lines represent the complete flight track at 3350 as well as at 2400 m altitude, the green pins represent the LTE base stations and the colored circles around the pins the distance.

was to ensure that the horizontal distance between the base station and the aircraft as far as possible is not larger than 10 km. According to Fig. 1 this would ensure that the RSRP values are larger than -95 dBm if the practically less relevant notches caused by the base station antenna pattern are neglected.

The gaps in the measured RSRP data shown in Fig. 8 occur mainly half way between two LTE base stations and directly above the base stations. This behavior was expected since the used FRITZ!Box modem has no omnidirectional but a directed antenna pattern pointing only to the right side with respect to the flight path with the mentioned depression angle of approximately 40°. For a fixed and approved integration of a LTE modem into the DO 228-212 research aircraft it is therefore recommended to use at least two external omnidirectional antennas mounted outside the aircraft at the bottom of the fuselage.

Conclusions and Recommendations

The simulation and measurements show that LTE for radar image and traffic data transmission in principle works in an aircraft flying at an altitude of 2000 to 3000 m above ground. Many of the measurement gaps, which correspond to a loss of LTE connection, could probably be avoided by using external omnidirectional antennas mounted outside the aircraft at the bottom of the fuselage. In this way negative shading effects caused by the aircraft fuselage and pointing errors of the internal antennas of the FRITZ!Box modem, which was provisionally mounted in the right observation window of the aircraft, can be avoided or at least strongly attenuated. Owing to the provisional experimental setup it was not possible to receive signals coming from the left side or directly from below the aircraft.

For an operational use it is also recommended to take into account the locations of the LTE base stations for the planning of the flight tracks. Especially for transferring large radar images with a size of hundreds of megabytes, the transmission time could be significantly decreased by a proper flight track selection. For the transmission of traffic data with a size of only a few KByte the maximum achievable data rates are of less importance. Here the objective is to keep the gaps where the LTE connection is interrupted as short as possible, so that real-time requirements can be fulfilled.

Furthermore, it is recommended to use data transmission software which supports automatic transmission pause and resume when the LTE connection is lost and re-established.

LTE seems to be a future-proof technology. The LTE infrastructure in Germany and Europe is constantly evolving. Inmarsat and Deutsche Telekom have created the European Aviation

Network (EAN) in the frame of a partnership. The goal of the EAN is that passengers in aircrafts flying European routes shall have access the high quality and high-speed broadband services [8]. Below altitudes of 10000 ft the internet connection is established via LTE, above 10000 ft via a satellite link. In the frame of the EAN the Deutsche Telekom will build and manage a new powerful mobile broadband network of approximately 300 LTE sites.

References

[1] A. Reigber, R. Scheiber, M. Jäger, P. Prats-Iraola, I. Hajnsek, T. Jagdhuber, K.P. Papathanassiou, M. Nannini, E. Aguilera, S. Baumgartner, R. Horn, A. Nottensteiner, and A. Moreira, Very-High Resolution Airborne Synthetic Aperture Radar Imaging: Signal Processing and Applications, *Proceedings of the IEEE*, 101 (3), 759-783 (2013); doi: 10.1109/JPROC.2012.2220511

[2] (2016) VABENE++ Traffic Management for Large Scale Events and Disasters [ONLINE]. Available: http://www.dlr.de/vabene/en

[3] (2016) Test LTE im Transrapid [ONLINE]. Available: http://www.silicon.de/41532605/test-lte-im-transrapid

[4] (2016) Telekom, Alcatel-Lucent und Airbus testen LTE im Flugzeug [ONLINE]. Available: http://www.areamobile.de/news/21185-telekom-alcatel-lucent-und-airbus-testen-lte-im-flugzeug

[5] S. V. Baumgartner, G. Krieger, Fast GMTI Algorithm For Traffic Monitoring Based On A Priori Knowledge, *IEEE Transactions and Geoscience and Remote Sensing*, 50 (11), 4626-4641 (2012); doi: 10.1109/TGRS.2012.2193133

[6] Martin Sauter , From GSM to LTE-Advanced: An Inroduction to Mobile Networks and Mobile Bordband, Wiley, 1st ed. (2011), ISBN 1118861957

[7] (2016) FTS: Was sind RSRP, RSRQ, RSSI und SINR? [ONLINE]. Available: http://blog.antennendiscount24.de/antennen/lte-antennen/lte-leistung

[8] (2016) European Aviation Network [ONLINE]. Available: http://www.inmarsat.com/european-aviation-network

DOI 10.5162/etc2016/5.6

Onboard Flight Termination System with Electronic Safe&Arm Mechanism: A Rapid Solution for High Velocity Flight Vehicles

Muhittin AKTAŞ[1], Celal ERTUĞRUL[2], Celalettin KARAKUŞ[2]
[1] Roketsan Missiles Inc., Ankara/TURKEY,
maktas@roketsan.com.tr
[2] Roketsan Missiles Inc., Ankara/TURKEY

Abstract:

Flight Termination System is a key element for range safety during flight tests of high velocity flight vehicles, like missiles, sounding rockets or launch vehicles. Range safety regulations require immediate termination of errant flight either by an RF flight termination signal from ground stations or by an onboard autonomous decision mechanism. On the other hand, tight schedules of related projects put engineers under pressure.

An Onboard Flight Termination System with Electronic Safe&Arm Mechanism developed by Roketsan and has completed three successful developmental flights. COTS products are used to shape the architecture of FTS which has been demonstrated to be a viable, reconfigurable and rapid solution for tight schedules of planned flight test activities. It was shown that FTS is capable of protecting life and property in event of an errant vehicle by terminating the flight. It is capable of replacing current human-in-the-loop systems or acting in parallel with them. FTS is configurable prior to flight with respect to mission specific rules set agreed upon by the range safety authority and the user to protect the public and assure mission success. This paper discusses the motivation for the project, describes the method of development and presents an overview of the architecture and the compatibility with RCC 319 standard.

Key words: Autonomous flight termination system, safe&arm, range safety, flight vehicle, missile.

Introduction and Purpose

Flight Termination System is a key element for range safety during flight tests of high velocity flight vehicles, like missiles, sounding rockets or launch vehicles. Range safety regulations require immediate termination of errant flight either by an RF flight termination signal from ground stations or by an onboard autonomous decision mechanism. On the other hand, tight schedules of related projects put engineers under pressure. For flight testing of a flight vehicle that can endanger public safety, a flight termination system is required. Engineers had less than 5 months to design, produce, test, and integration phases. In order to meet this urgent need Geliştirme Amaçlı Uçuş Sonlandırma Sistemi (eng. Developmental Flight Termination System) (GAUSS) project is kicked off, also it satisfied the need successfully.

By proposed GAUSS design, four different flight termination methods are realized reliably, three of them are autonomous; termination upon ground command, termination after predefined flight time elapsed, termination by loss of RF link with ground station and termination due to low voltage of batteries.

In this article, electronic parts including RF components that shape GAUSS architecture is provided with main technical parameters. Also operational sequence and working principles of GAUSS is explained. Finally applied tests for qualification and compatibility with RCC-319 standard are discussed.

System Architecture

GAUSS is composed of an antenna set, a receiver box, a decision unit and a battery pack. Onboard antenna set has three antennas those collect the RF signal of interest and deliver to receiver box. Receiver box includes two identical RF receivers for demodulating

DOI 10.5162/etc2016/5.6

commands sent from ground station and interface to the decision unit. Decision unit, as its name implies, determines if conditions for flight termination are occurred or not. Mainly, It interprets message delivered from receiver box, counts flight time, controls safe&arm switches according current status of flight, shapes the activation signal of pyrotechnics and forms telemetry data. Finally battery pack provides the power for electronic units and to activate pyrotechnics. All units of GAUSS designed fully redundant in order to meet 0.999 reliability requirement. Details of each unit are explained in related subsections. Functional architecture of GAUSS is shown below. (see Fig. 1).

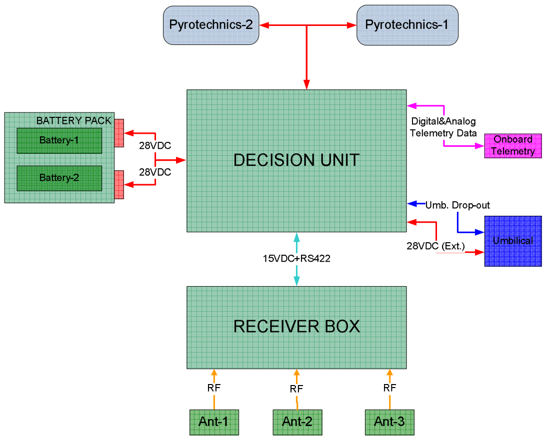

Fig. 1. GAUSS Architecture

Decision Unit

Decision Unit (DU) is responsible for managing flight termination system and acts as "brain" of it. Demodulated RF messages are delivered to and interpreted in DU. DU completes the actions commanded in messages received from Receiver Box. These actions include switching from external power to battery power, forcing start of the flight time and flight termination. It gives flight termination decision after predefined flight time elapses, RF link loss with ground station or low battery voltage. Dimensions of DU are 200 mm x 150 mm x 100 mm (Length x Width x Height) without mounting fixtures. 3D model of Decision Unit is shown below. (see Fig. 2)

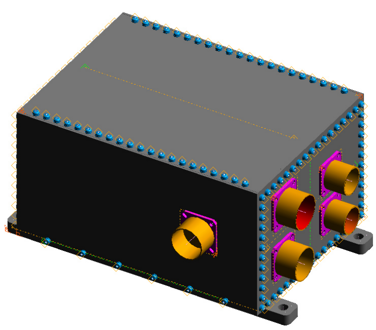

Fig. 2. 3D Model of Decision Unit

Decision unit consists of three electronic cards of two kinds, namely two Termination Control Cards and a Power Management & Telemetry Card. (see Fig. 3). Both cards are based on non-volatile FPGAs, that has 50K system gates, 1584 logic cells and 1M flash.

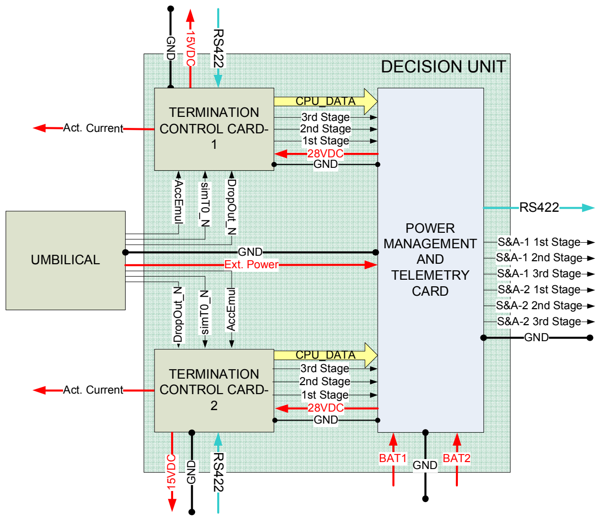

Fig. 3. Decision Unit Architecture

Power Management & Telemetry Card (PMTC) interfaces Decision Unit to External Power, supplying from ground station before flight and Battery Pack that used during flight. It provides capability of switching between external power and battery power when commanded. Possible noise on power line is filtered out by using Synqor's military grade, quarter brick passive filters and delivered to both PMTC's own and Termination Control Cards (TCC). Batteries voltages from two batteries are paralleled before distributing them to other components on this card. Battery voltages and currents draining from batteries are measured before paralleling using two industrial supervisor chips. PMTC also converts 28 VDC battery voltage to secondary voltages as its onboard FPGA and other components needs.

PMTC is responsible for packing and delivering telemetry data of GAUSS. Digital data from Termination Control Cards (TCC) and measured voltages/currents from supervisor chips are collected and digital telemetry frame are created by FPGA. On PMTC, all UART communications, including communication between PMTC and TCCs, Decision Unit and OTE is managed by FPGA via RS422 interface using MAX 490 chips. Additionally, PMTC converts analog telemetry signals to 10 V range and delivers them to OTE. Digital and analog telemetry data are shown below. (see Tab. 1)

DOI 10.5162/etc2016/5.6

Tab. 1: Telemetry Data

No	Data	Source
1	Battery Voltages	PMTC
2	Battery Currents	PMTC
3	Squib Test Results	TCC
4	Termination Flag	TCC
5	Drop-out Monitor	TCC
6	Mode	TCC
7	Station ID	TCC
8	RF Message	TCC
9	RF Error Count	TCC
10	FPGA Times	TCC
11	CPLD Times	TCC
12	IMU Supply Volt.	TCC
13	IMU Gyro Volt. X	TCC
14	IMU Gyro Volt. Y	TCC
15	IMU Gyro Volt. Z	TCC
16	IMU Acc. Volt. X	TCC
17	IMU Acc. Volt. Y	TCC
18	IMU Acc. Volt. Z	TCC
19	Arming Status.	TCC

Decision Unit has two identical TCCs. Each TCC works independently, i.e. each TCC gives power to different receivers and controls different pyrotechnics in order to prevent single point failure. TCC converts 28 VDC to secondary voltages as PMTC, it also produces 5 VDC for IMU chip on it and 15 VDC for RF Receiver. Again, same non-volatile FPGA is used on TCC in order to manage tasks including serial communications, timing and logic decisions.

TCCs have their own electronic safe & arm circuits on them. Each safe & arm circuit has three safety stages on it realized by twin redundant hard relays. First stage of relays is closed by a predetermined acceleration value in flight direction (1^{st} group in Fig. 4). Acceleration measurements in three-directions are made by single axis, 200 mV/g sensitive accelerometers. Here, it is good to note that first safety stage can be by-passed by emulated signals sent from umbilical or via RF commands. This option is added for ground testing of GAUSS. It also helps reliable flight termination action in case of projected acceleration is not measured by accelerometers because of erroneous launch or a failure in accelerometers.

Second stage is closed when safe separation time passes (3^{rd} group in Fig. 4). Safe separation time is the duration that test item is far enough from launching point not damage launch site and launching crew. From analyses of related flight vehicle and test range specifications, safe separation time is predefined as 5 seconds. Safe separation time is counted by FPGA.

Third stage is closed when termination command received, RF link loss exceeds predefined duration, completion of predefined flight time or low voltage of batteries (2^{nd} group in Fig. 4). Flight time is counted by both FPGA and CPLD's in order to increase reliability. Three low power CPLD's that can support internal clock frequency rates up to 300 MHz are used for this task. FPGA and CPLD's create totally 8 signals that each of them is enough to close third stage safety relays. Once closed, all relays are latched. After all safety stages are closed TCC shall deliver several Amperes of current for duration that guarantees reliable activation pyrotechnics. This is obtained by direct connection of the batteries and pyrotechnics after all safety relays are closed. Safety stages and default positions of relays before flight are shown below. Note that two poles of pyrotechnic devices are short circuited until safe separation time is elapsed. (see Fig. 4)

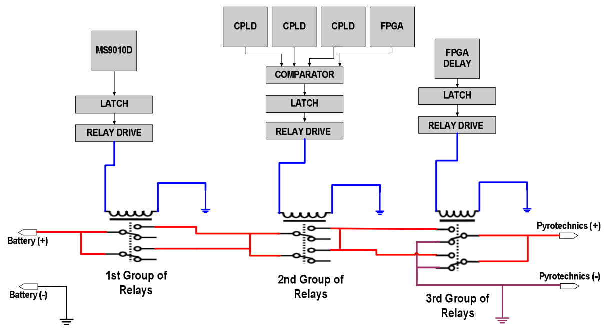

Fig. 4. Electronic Safe and Arm Device

Note that 3^{rd} group of relays that maintains second stage of safety (safe separation time) are the last circle of the activation chain. That's because of positive and negative poles of pyrotechnics line are intended to be in short circuit state until the flight vehicle is in a safe distance for launch site. After safe separation time elapses, these lines are switches to ready-to –activate position.

All parameters for controlling safety stages (magnitude and direction of acceleration, safe separation and flight times, RF link loss time for

DOI 10.5162/etc2016/5.6

flight termination) are programmable via JTAG interface of FPGA.

Both TCCs are equipped with, six degrees of freedom inertial sensor chips for experimental purposes. Acceleration and gyro measurements obtained from these chips are telemetered. This data is not used actively for onboard decision mechanisms. It has provided a comparable data with primary IMU of flight vehicle. In the future, this data also can be used for implementing onboard decision mechanisms to terminate flight by calculating instantaneous impact points.

Each TCC is capable of testing related pyrotechnic activation line's continuity. Test is realized by using FPGA.

Finally, telemetry data of each TCC (see Tab. 1) is packed by FPGA and sent to PMTC using RS 422 interface. Analog signal lines indicating statuses of safety stages are also delivered to PMTC.

Receiver Box

Receiver Box is used to receive and demodulate RF commands those are sent from ground station. RF signal collected by three antennas are delivered to Receiver Box. Inside receiver box, three antenna inputs are combined and then divided again to two identical receiver units using COTS combiner and divider units. They have maximum 0.3 dB insertion loss, minimum 19 dB isolation and maximum 1.35:1 VSWR.

Receiver units are also COTS airborne products that work at L band with nearly -80 dBm sensitivity, pricing around £16000 for each. Receiver sensitivity is selected according to link budget calculations using theoretical trajectory of flight vehicle that is to be tested. For reliable operation, 12 dB link margin is objected. Center frequency is programmable with 0.1 MHz steps. Bitrate of input signal is also programmable between 9600 and 115200 bps. Receivers are capable of outputting demodulated data via RS 422 interface. They are fed with 15 VDC supplied from DU. Interfaces and 3D model of Receiver box is shown below. (see Fig. 5 and Fig. 6) Dimensions of receiver box are 210 mm x 75 mm x 160 mm (Length x Width x Height) without mounting fixtures.

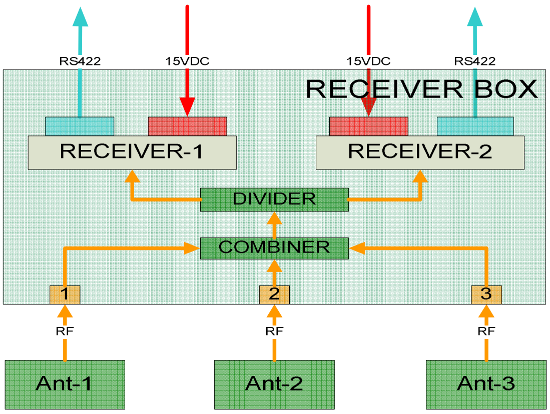

Fig. 5. Receiver Box Connection Diagram

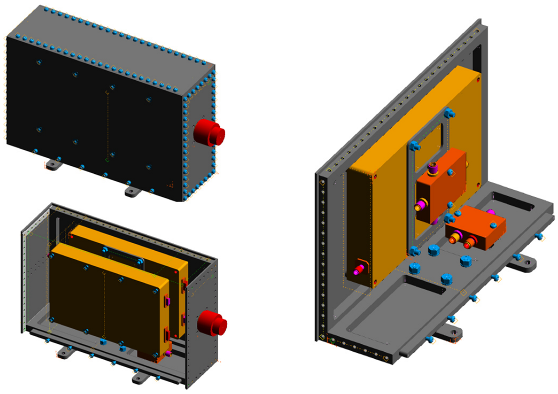

Fig. 6. 3D Model of Receiver Box

Antenna Set

Three antennas form onboard Antenna Set. Blade type antennas are used onboard antennas. (see Fig. 7)

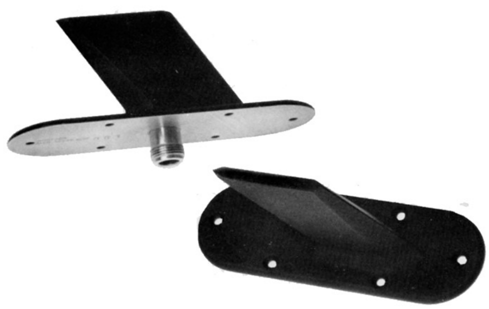

Fig. 7. Typical Blade Antenna

Blade antenna is about 40 mm height and 25 grams weight. These antennas are worse than conformal antennas by means of aerodynamics but performance/procurement duration was suitable for the project requirements so they are selected to use onboard. They have linear polarization and maximum 1.5:1 VSWR over operating band of RF receivers. Antennas are

DOI 10.5162/etc2016/5.6

connected to receiver box with SMA connectors.

Antenna has hemispherical pattern. It has omni-directional pattern in azimuth with 0 dBi gain. In elevation, it has minimum -5 dBi gain between 90° and -90° including 0° bore sight of the antenna. In order to shape an omnidirectional pattern around the flight vehicle three antennas are mounted with 120° separation between each other.

Battery Pack

Battery Pack includes two identical Li-ion batteries each can supply current for components of two channels with 150% margin under 30 Volts. Each battery weighs around 1.5 kg. In order to mount the battery to the flight vehicle a unique metallic fixture was used (see Fig. 8).

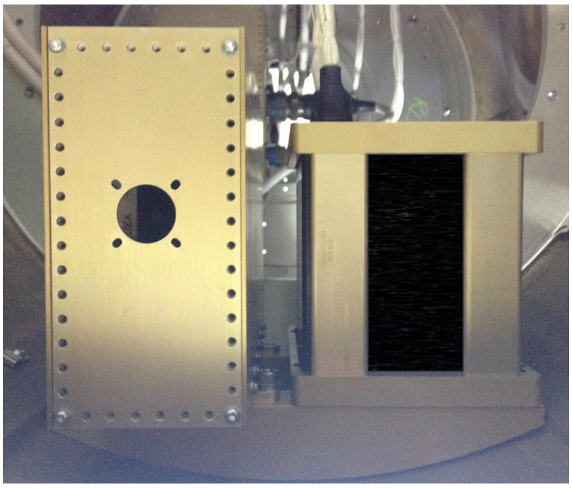

Fig. 8. Li-Ion Battery in Its Metallic Case with a Dummy Receiver Box mounted on Flight Vehicle

Operational Sequence

GAUSS has 5 different operating modes. After GAUSS is powered-on, it checks pyrotechnics lines continuity. If it is detected that two pyrotechnics are connected properly, GAUSS switches to "Idle Mode (IM)" and waits for RF commands. In parallel it starts to measure battery voltages, IMU outputs and send telemetry data automatically at each 10 ms. If pyrotechnics lines' continuity check is not passed GAUSS switches to "Emergency Stop Mode (ESM)". In ESM, power is switched to external power, all safety relays are switched to open state except the 3rd group. 3rd group relays are switched such position that positive and negative poles of pyrotechnics line are short circuit state in order to prevent an unintended activation of pyrotechnics. Flowchart of opening sequence of GAUSS is shown below (see Fig. 9).

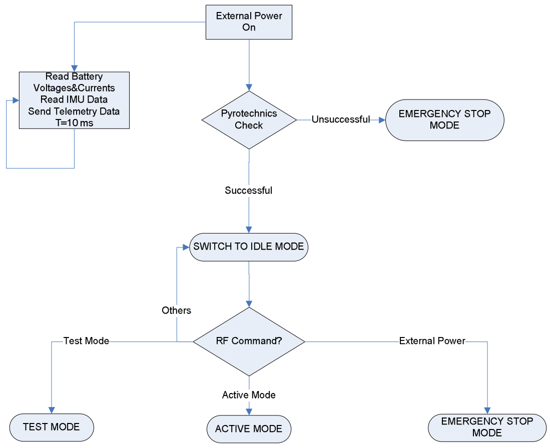

Fig. 9. Opening Sequence of GAUSS

In order to initiate launching sequence, GAUSS should be switched to "Active Mode (AM)". In AM, GAUSS waits for RF command to switch battery power. Eventually, it checks if flight is started, i.e. umbilical connector is still connected or not. In case of umbilical drop-out before Internal Power Command is received, GAUSS switches to ESM.

After Internal Power Command is received, GAUSS switches to Battery Power and starts to wait for umbilical drop-out. After umbilical drop-out sensed, GAUSS switches to "Flight Mode (FM)". After launch, it is expected that flight vehicle's movement shall cause 1st stage safety relays to close. In case of a failure in umbilical continuity check line, in accelerometers or an unexpected launch movement (e.g. lower acceleration values than expected) GAUSS can be switched to FM manually by an RF command, namely Flight Mode command. When this command is received, 1st stage of safety is by-passed and related relays are forced to close.

FPGAs and CPLDs start to count flight time with 10 ms resolution. This duration is also one processing cycle of GAUSS. In FM, predefined flight times for safe separation distance and termination are checked periodically in every cycle. After safe separation time is elapsed, 3rd group of relays are switched to activation state. Completion of predefined flight time causes termination action.

During normal flight, Flight Mode or Safe commands with frame counters in them are transmitted periodically from flight termination ground station. GAUSS checks for a new RF command at every cycle. If RF link between onboard unit and ground station is lost for a predefined duration GAUSS switches to "Termination Mode (TM)". Additionally, if RF Arm command is received in any portion of flight GAUSS also switches to TM. Only one

DOI 10.5162/etc2016/5.6

successful command is decided to be enough for starting termination action upon receiving Arm command to minimize potential hazard in risk, in case of a bad RF link. In order to prevent demodulation and decoding errors and receiving a "false alarm" Arm command, Arm command is selected to have maximum Hamming distance from other commands. Additionally, in every frame, command words are repeated and valid command is selected by voting.

In TM, safe separation duration is checked first. If it is already elapsed activating signal is delivered to pyrotechnics by closing 2nd group of relays for 300 ms. Activation signal is repeated to ensure success of flight termination in case of misfire. Operational flowchart of GAUSS during flight is shown below. (see Fig.10)

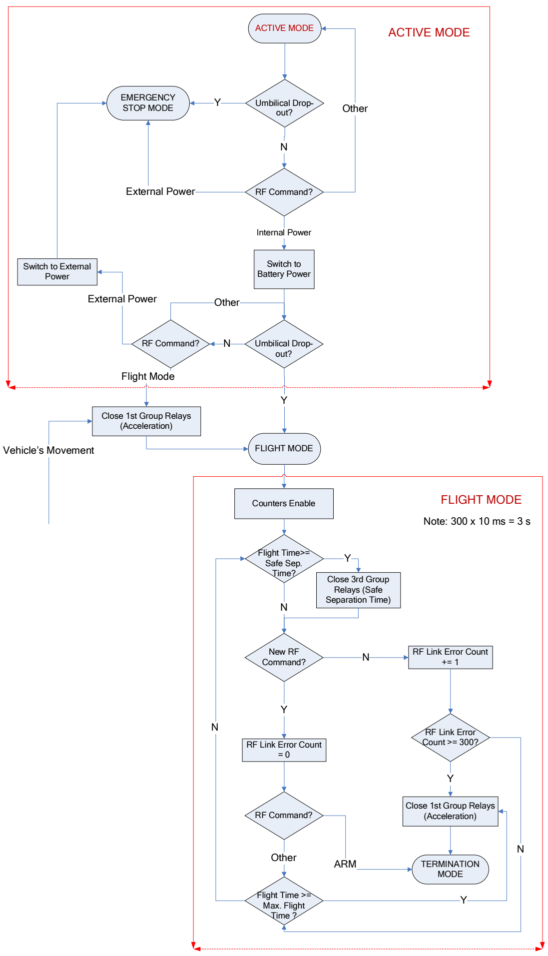

Fig. 10. Flight Sequence of GAUSS

Cabling and Harness

All signals of flight termination system are carried with redundant lines. Connectors and cables are selected among military grade components.

Environmental Requirements and Qualification

GAUSS is designed to operate in harsh environmental conditions, such as high temperature (up to 100°C in a couple of minutes), severe vibration (reaching 15 gRMS) and low pressure/high altitude (corresponding a few dozens of kilometers). Mechanical design, PCB design and component (avionic enclosure materials, electronic components, COTS products and harness components) selection is made according to these harsh environmental conditions. Fixtures those are used to integrate GAUSS to flight vehicle are designed not to amplify frequency modes of both flight vehicle and GAUSS. Also, a reliability analysis using dedicated software is conducted.

Operability under environmental conditions is verified through ground tests. Mainly, temperature, random vibration, acceleration and low pressure/high altitude tests are conducted to simulate flight environment. Additionally, in order to eliminate workmanship defects and faulty components during producing phase, environmental stress screening (ESS) tests are applied to every unit according to MIL-HDBK-344A. ESS also provides burn-in phase to electronic equipment; it helps to reach middle portion of the bathtub curve of product lifecycle-probability of failure (portion with least probability of failure) graph.

Ground Station

Ground Station of proposed design is composed of three main items which are RF Data Transmission System, directional antenna system, and a laptop-based control system. Two independent ground systems are used at different locations of test site for full redundancy.

Fig. 11. Typical Data Transmission System

The Data Transmission System which has maximum 40 W RF power output can be controlled remotely by an external computer via RS232 interface. This feature offers possibility of maintenance and easy update to the system. remotely. The FTS control software features a graphical user interface (GUI) that can be easily customized to suit different requirements. The control unit has a remote control interface which sends the required commands that can be selected from GUI.

Fig. 12 Typical Directional Antenna

COTS directional RHCP antenna is used as the ground antenna (see Fig.12). Because the tight schedule and need to provide a quick solution, antenna system does not include a tracking controller unit. In order to achieve high performance, optimal FTS ground system location is determined regarding the azimuth and elevation angle variation relative to the flight trajectory. Antenna beam widths and placements are selected according to worst case azimuth and elevation angles with respect to predefined trajectory.

RF Message Format

RF message of GAUSS consists of six blocks of the data including a frame synchronization word, ground station range ID number, transmission system ID number, counter for each command sent and Cylic Redundancy Check (CRC) block as shown below. (see Tab. 2.)

Message format is chosen to maintain safe operation and minimum processing effort. Time counter is used for determining the time of the link loss. The format and index of the message can be updated easily via GUI interface.

Tab. 2: Message Format

Frame Synch	Range ID	TX ID	Counter	Command	CRC

RF Link Margin

A radio propagation model (see Fig.14) and link analysis was conducted for the GAUSS. The RF link analysis includes path losses due to rain, fog, plume attenuation, other possible attenuation factors; ground system RF characteristics, onboard transmission characteristics and vehicle trajectory. The parameters used in the analysis are given below. (See Fig. 14 and Tab. 3). It is guaranteed to maintain 12 dB link margin in order to ensure reliable operation, attenuation values are exaggerated.

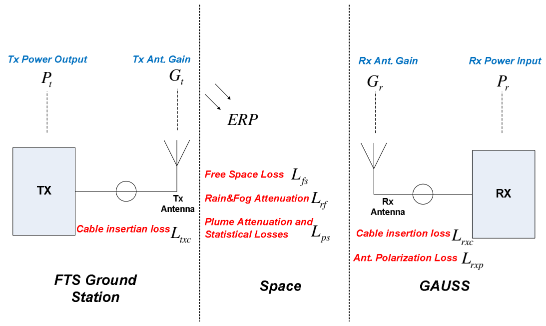

Fig. 14 Radio Propogation Model

Tab. 3: Parameters Used in RF Link Margin Calculation

S/N	Parameter
1	TX Output Power (P_t)
2	TX Cable Loss (L_{txc})
3	TX Antenna Gain (G_t)
4	ERP
5	Frequency (f)
6	Range (r)
7	Free Space Loss (L_{fs})
8	Plume Attenuation and Statistical Losses (L_{ps})
9	Rain and Fog Attenuation (L_{rf})
10	Total Loss in Space (L_{fs})
11	RX Antenna Gain (G_r)
12	RX Antenna Polarization Loss (L_{rxp})
13	RX Cable Loss (L_{rxc})
14	Received Power (P_r)
15	Receiver Sensitivity
16	Link Margin

Compatibility with RCC 319

During design phase of GAUSS, compatibility with basic requirements of RCC 319-10 (319-14 version was not released yet) is targeted, like redundancy of safety critical components that will affect desired termination action

(Termination Control Cards, batteries, receivers, cables and pyrotechnics), three stages of safety built-in-test capability and component derating criteria. On the other hand, some constraints restricted design team to stay incompatible with flight termination systems' international standard. Such requirements are frequency band, modulation technique or cross-strapping of fail-safe actions. [1].

Main difference between GAUSS design and RCC 319 is operating band and modulation technique. UHF band and frequency modulation of analog signals are proposed in standard. However, that is not compatible with standard yet useful and fastest solution to satisfy project needs are selected.

A fail-safe system shall generate Arm and Terminate outputs when it has been enabled and any specified fail-safe condition occurs [1]. Both loss-of-power and loss-of-command-link fail-safe measures are enabled in GAUSS design. In case of a failure in one of two redundant channels of flight termination system, in order to continue operation with fault-free channel, two channels should be cross-strapped with a termination inhibit logic. However, since design and testing phase of GAUSS is very short in time, cross-strapping of redundant channels is not implied. In order to maintain to continue the operation when one of batteries fails, powers of two batteries are paralleled in DU.

As ground antenna used in this project has no auto-track capability, a conservational approach for loss-of-command-link is executed. If one of two Termination Cards doesn't receive a new message from RF receivers for a predetermined time flight is terminated. Continuing the flight with one receiver is not considered as a reliable operation. Implying cross-strapping logic proposed in RCC 319 shall maintain true fail-safe measure.

Another incompatibility with RCC 319 is; RCC requires flight termination receivers' to have -107 dBm guaranteed sensitivity at least. However, due to tight schedule of project, purchasable COTS receiver-transmitter couple that can provide safe link margin in test scenario with shortest lead time is preferred.

Summary

GAUSS is proposed and demonstrated successfully in flight tests as a maybe not cost efficient but saving-the-day solution. It satisfies key requirements of RCC-319 standard. It is hoped that this design shall maintain a baseline for a flight termination system that is fully compatible with range safe community's requirements. Improving and adding more intelligence to autonomous functions, truly implementing fail-safe inhibits and more reliable radio links are taken as future design goals.

References

[1] Range Commanders Council, Range Safety Group, *Document 319-10 Flight Termination Systems Commonality Standard*

[2] Department of Defense, Military Handbook, *MIL-HDBK-344A Environmental Stress Screening of Electronic Equipment. doi: 16 August 1993*

DOI 10.5162/etc2016/6.1

Merging of Flight Test Data within the UMAT TDS

Tjorven Gerhard[1], Tobias Paul[1]
[1] ESG Elektroniksystem- und Logistik GmbH, Fürstenfeldbruck, Germany
tobias.paul@esg.de

Abstract:
In close cooperation with Bundeswehr, ESG has modified an *UMS Skeldar R-350* UAS to offer a testbed for in flight evaluation of payload and avionics. This testbed is called *Unmanned Mission Avionics Test Helicopter* (UMAT). In order to provide a complete test environment, a truck based laboratory enhances monitoring, control, and recording capabilities. It is called Flexible Mobile Ground Control Station (FlexMobGCS). In this paper we present the UMAT Test Data System (TDS) which is a modular, digital and powerful system for capturing, recording, transmitting, analysing and archiving of test data during flight test operations with the UMAT. The TDS is used to evaluate experimental equipment during flight tests like avionics or mission management functions as well as human machine interactions. The TDS consists of an air segment within the UMAT, a data link and the ground segment within the FlexMobGCS. In this paper the focus lies on the challenges of the TDS ground segment and its integration into the TDS air segment.

Key words: testbed, unmanned aircraft, avionics, recording

Introduction

The UMAT [1], [2] is based on the R-350 VTOL Remotely Piloted Air System (RPAS) of UMS Skeldar, see Fig. 1. The R-350 has a rotor diameter of 3.5 m and a maximum take-off weight of 145 kg including a payload weight of 38 kg. The maximum flight duration is estimated with 3.5+ h at a maximum speed of 120 km/h. Due to the fact that the base systems is part of a continuous development, the flight envelope might vary in future.

Fig. 1. UMAT

To provide a test helicopter, modifications to the purchased R-350 have been made. With these modifications, experimental equipment can be tested either mounted on a nose payload bay carrier or within a cassette which is mounted in the R-350s main payload bay. Both, nose payload bay carrier and the cassette are mechanically and electrically decoupled from the R-350. In addition, the R-350 is protected by a firewall like equipment toward erroneous signals submitted by the experimental equipment. Those extensions allow the flight testing of not certified / qualified experimental equipment.

The capabilities of the UMAT focus on four areas:

1. Evaluation of performance capabilities of alternative COTS (commercial of the shelf) mission avionics
2. Risk reduction during development, e.g. by bringing rapid prototypes into flight test
3. Examination of new mission concepts like MUM-T [3] (Manned-Unmanned Teaming) or SAAFu [4] (Sense & Avoid Assistance Function for the UAS Operator)
4. Examination of certification topics and operating procedures

Within those areas ESG performs the integration, performs or supports the steps: flight test planning, execution of the flight tests, and data analysis.

The available state-of-the-art experimental Mission Management Computer – based on an open Integrated Modular Avionics (IMA) [5], [6] architecture – supports the development and analysis of mission management functions, that will boost the autonomy of future UAS. As a

DOI 10.5162/etc2016/6.1

tactical-UAS-sized system the UMAT is ideally suited to support the demonstration of operational concepts for military and civil VTOL-UAS applications.

The Flexible Mobile Ground Control Station (FlexMobGCS, see Fig. 2) consists of the workstations for the pilot in command (PIC) and the Payload Operator (PO) in the front, including redundant mission computers and flight safety management computers. Additionally the FlexMobGCS includes two flight test engineer workstations in the forward section. The rear section holds the flight test observation area where the flight test can be monitored by customers, see Fig. 3. This rear section can also be converted to a maintenance and assembling area for the UMAT. In addition this rear part is used to transport the UMAT to the flight test area.

Fig. 2. FlexMobGCS with generator

Fig. 3. FlexMobGCS interior

The Test Data System

The UMAT Test Data System (TDS) is a modular system which enables the flight test engineer to perform a live analysis during the flight test as well as after the flight. With the TDS, the system state and flight state data of the UAS are captured as well as data of the permanent test equipment including Human-Machine-Interactions (HMI) and the variable flight test equipment that may differ for every flight test. To be able to address all these areas, a digital and powerful system for capturing, recording, transmitting, analysing, and archiving of test data during flight test operations with the UMAT is needed, see Fig. 4. Some test data is captured and recorded on board the UMAT or sent down to the ground control station via the TDS data link whereas other test data is captured in the ground control station. Each relevant data source in the UMAT and the FlexMobGCS is captured. The captured data is then transmitted to recording devices and to analysis software. After the flight test, they can be transmitted to a data server for further processing or archiving.

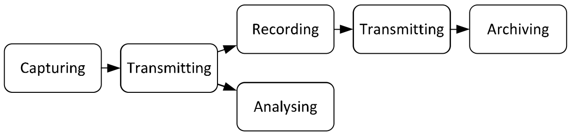

Fig. 4. TDS functions

The test data system consists of three segments:

- the air segment which includes the capturing and recording of data in the UMAT,
- the data link which sends the test data from the UMAT live to the FlexMobGCS, and
- the ground segment which includes all data sources in the FlexMobGCS as well as the analysis software and the archiving capabilities.

For the air segment of the test data system, several commercial solutions were available using manned test flight equipment. In general, a test data system for manned aircrafts can also be used for the UMAT if size and weight are within the payload capabilities. Using a test data system for a manned aircraft has the advantage of choosing complete and mature solutions. The requirements for the TDS of the air segment include: reliability, rugged design, and weather resistant. Some of the available solutions were: PowerDNA from United Electronics Industries, HiDANplus from RTD Embedded Technologies, KAM-500 from ACRA CONTROL, and MiniR 700 from AMPEX. For the UMAT we chose the KAM-500 from ACRA Control as the TDS air segment because it is reliable, offers many different sensors for the air segment and analysis software is available.

Regarding the required high capacity test data link, commercial state of the art solutions were available also. These solutions include but are not limited to: Condor UAV RF Tranceiver from Sabtech, Airborne Transmitter and Receiver from Emhiser, X-5000-REC from Smartronix, and Digital Data Link from NSM Surveillance. We chose the NSM Surveillance data link.

The ground segment of the UMATs test data system had to be integrated into the analysis software of the air segment, so that data from the ground segment can be analysed together with data from the air segment. The data sources in the FlexMobGCS are mostly COTS components and require modification to be compatible with the test data system of the air segment. As a result there are no state of the art solutions for the ground segment available. Instead customized solutions had to be found. The following data sources and sensors in the FlexMobGCS have to be addressed by the ground segment of the test data system:

- **Weather station:** A weather station is installed outside the GCS to capture among other things temperature, air pressure, wind speed and direction.
- **GCS internal temperatures:** Additionally the temperature inside the GCS is captured.
- **Cameras:** Several cameras are mounted in and outside the FlexMobGCS to monitor the interior of the GCS, the landing site and to track the UMAT during flight.
- **Data links:** Furthermore the network communication of the data links is monitored. There are three different data links in the FlexMobGCS:
    - the command and control (C2) data link,
    - the video data link for the camera mounted on the UMAT and
    - the TDS data link.
- **Network communication:** Additionally the network communication of the PIC and PO workstations including the mission computers, the flight safety management computers and the ground data terminals is captured.
- **HMI:** For the analysis of human machine interactions and human factors the input of the PIC and Po via keyboard, mouse or rotary switches into the mission and flight safety management computers has to be captured as well as the monitor screens of these computers. Head movement and movement of PIC and PO are also information that are captured for analysing human machine interaction and human factors.
- **Intercom system:** Another data source that has to be addressed is the intercom system in GCS.

As a result many different signals have to be captured including USB, serial, Ethernet, DVI and analogue signals.

Faced Challenges

In the following section, the challenges und solutions of the TDS for the ground segment as well as the challenges resulting from the integration into the analysis software of the air segment are presented. The TDS for the ground segment has to handle challenges like:

1. Time synchronization of the air and ground segment
2. Integration of the ground data sources into the analysis software of the air segment
3. Expandability of the ground system for future experimental equipment which is unknown today
4. Different data types have to be captured and processed ranging from huge video data or audio data to high frequency numerical data.
5. Controlling a distributed system.

Both the systems in the FlexMobGCS and the UMAT are time synchronized with GPS so that data is perfectly synchronized when it is captured. The analysis software runs in the GCS so that the data from the GCS is nearly instantly in the analysis software. The data from the UMAT has to be send down to the GCS via the TDS data link and thereby arriving at the analysis software delayed. As a result, the data of the ground and the air segment is no longer synchronized which poses a problem for the analysis software because it can only cope with time synchronized data where $t_2 = t_3$ is satisfied in Fig. 5. The only solution is to resynchronize the data by either artificially delaying the data from the ground segment or by overriding the timestamp of the air data in the ground segment and sending the air data as well as the value of the time delay to the analysis software.

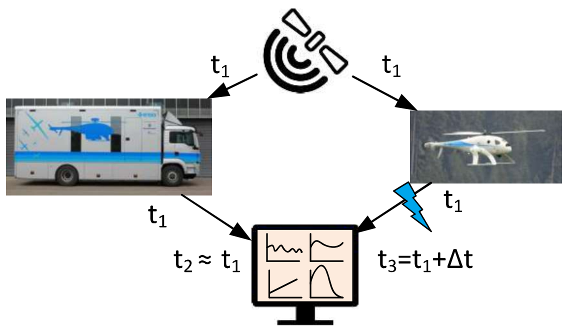

Fig. 5. Time synchronization of the ground and air segment

To integrate the ground segment into the air segment the data of the ground segment has to be analysed with the analysis software of the air segment. The analysis software provides an interface for numerical data. This Ethernet interface accepts numerical data in the proprietary IENA format. The data sources in the ground control station that generate numerical data provide different interfaces ranging from proprietary Ethernet over serial to USB interfaces. In order to convert the data into the IENA format for each data source, a customized software module is implemented to convert the data. If necessary, a hardware capturing device is connected to the data source so that the customized software can access the data. The data is then forwarded to the analysis software as well as a recording software module as shown in Fig. 6.

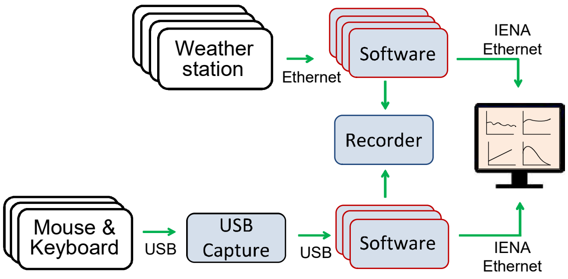

Fig. 6. Integration of numerical data

For the multimedia data sources in the ground segment like the intercom, the computer screens, and the cameras, a different solution is needed. Due to the huge data sizes of the multimedia data, the analysis software of the air segment is not suited for the analysis of this data. As a result, a second analysis software optimized for multimedia data is implemented. Both analysis software have to be synchronized to enable the flight test engineer to analyse numerical and multimedia data together. This means that an interface between the air segment analysis software and the multimedia analysis software has to be implemented so that the multimedia analysis software can be controlled by the analysis software of the air segment.

The test data system has a modular design to prepare the system for future expansion due to new experimental equipment in the air segment or the ground segment. New experimental equipment in the air segment can either be integrated for on-board capturing and recording into the sensor suite of the test data system of the air segment (KAM-500) or the data of the new experimental equipment can be sent to the ground segment for capturing and recording in the ground segment. For capturing and recording of new experimental equipment in the ground segment, where the data source itself can either be in the air segment or in the ground segment, the modular TDS can be expanded by writing a new customized software module for the new data source and adding if necessary a capturing device as depicted in Fig. 6.

With the architecture in Fig. 6, sources with different data types can be realized in the Test Data System. If huge data sizes occur, which are the cases when capturing high resolution video or DVI data, the capturing device has to be able to handle them by reducing the frequency and thus not capturing every frame and by compressing the video using standard algorithms like the H.264.

The ground segment of the test data system is a highly distributed system where hardware capturing modules are distributed throughout the FlexMobGCS and where the customized software modules are running on different computers and servers, see Fig. 7. The flight test engineer has a dedicated workstation from which he can control all hardware and software components of the test data system. We have implemented a control software for the TDS which provides the flight test engineer with a graphical user interface to control the TDS ground segment. Using this software, the flight test engineer can

1. Configure all hardware and software components
2. Start and stop all TDS functions on the hardware components
3. Transfer all recorded data from every hardware to a data server
4. Shutdown all hardware components

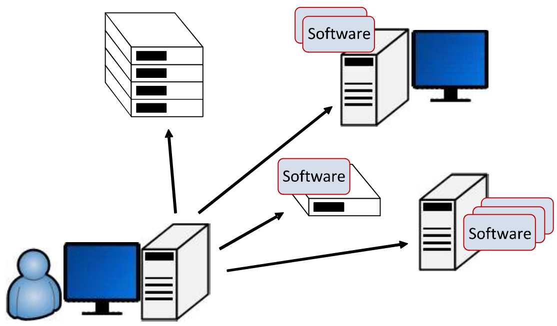

Fig. 7. The distributed system

Conclusion

A test data system for an unmanned aircraft system consists of three segments:

- the air segment,
- the data link, and
- the ground segment.

All three segments are integrated in the test data system and function as one system. The test data system is used to analyse the flight test. Therefore it has to capture, record, transmit, analyse, and archive the test data. For the air segment solutions from the manned test aviation can be integrated in the unmanned aircraft and for the data link segment available digital data links can be used.

There is no commercial of the shelf solution available regarding the ground segment because the COTS components of the ground control station cannot easily be integrated with the aircraft components of the air segment. For this integration to work customized software for each data source in the ground segment has to be implemented to convert the data. The following challenges have to be addressed when integration ground and air segment: the time synchronization of air and ground segment, the integration of test data from ground and air segment into one analysis software, the expandability of the system for future experimental equipment that is unknown today, the management of different data sources and different data formats and the control of the distributed system by the flight test engineer. In this paper solutions for these challenges are presented.

References

[1] H.-W. Schulz, Certification Process for a VTOL-UAS Experimental System, *26th International UAV Systems Conference*, Bristol / UK, 2011.

[2] H.-W. Schulz, The Unmanned Mission Avionics Test Helicopter - A flexible and versatile VTOL-UAS Experimental System, *International Archives of the Photogrammetry, Remote Sensing and Spatial Information Science*, Zürich / CH, 2011.

[3] T. Paul und E. Brämer, Operational Considerations for Teaming Manned and Unmanned Helicopter, *2012 International Conference on Unmanned Aircraft Systems*, Philadelphia / USA, 2012.

[4] O. Horz, Integration of Military Unmanned Aircraft Systems Into German Airspace & Sense and Avoid Assistant, *DGLR Symposium 2013: Workshop "UAV Autonomie" - Automatisierung unbemannter Luftfahrzeuge*, München, 2013.

[5] E. Brämer, IMA - Integrierte Modulare Avionik, *Spektrum - Magazin der ESG Elektroniksystem- und Logistik-GmbH*, pp. 6-7, Oktober 2010.

[6] M. Gangkofer, IMA³, *Spektrum - Magazin der ESG Elektroniksystem- und Logistik-GmbH*, pp. 5-6, Juli 2012.

DOI 10.5162/etc2016/6.2

Mini Mobile Telemetry System Application

Serdar ÇORA[1], Mahmut Kürşad ARPACIOĞLU[1], Hakan ESER[1]
[1] TAI - Turkish Aerospace Industries, Inc., Fethiye Mahallesi, Havacilik Bulvari No: 17, 06980 Kazan-ANKARA / TURKEY,
scora@tai.com.tr, mkarpacioglu@tai.com.tr, heser@tai.com.tr

Abstract:

Mini Mobile Telemetry System is a ruggedized pc with three screens which the receiver board, the decommutator board and the GPS time generator board has placed in. Customized panels are used for RF, GPS signal inputs and serial data outputs for the flexible operational usage of the system. Various types of antennas are used for different operational scenarios.
Mini Mobile Telemetry System which is designed and configured for special needs of TAI Turkish Aerospace Industries Inc., serves for three main purposes.
The first purpose of the system is to serve such a portable telemetry station which one person could transport, install and operate on field easily. System could support up to three flight test engineers with customized displays which could be enough for a low risk test flight without occupying huge telemetry ground station.
The second purpose of the system is to have the chance for to be fixed in a mid-size A/C such a flying test bed. The real time visualization of data which is gathered from the vehicle under test during a flight test is possible. There will be no problem about the target range in reasonable ranges and LOS on the A/C that chase the vehicle under test with proper antenna installation.
The third purpose of the system is to serve such a flying relay station for scenarios that LOS or range limits between ground station and vehicle under test could not be achieved. Such maneuvers performed at low altitude or out of range for receiving antenna on ground could be examples.

Key words: Telemetry, Mobile, Flying Test Bed, Flight Test, Instrumentation.

System Description

Mini Mobile Telemetry System is a ruggedized pc with three displays which the receiver board, the decommutator board and the GPS time code generator board has placed in. Customized panels are used for RF, GPS signal inputs and serial data input/outputs for flexible operational usage of the system.

Fig. 1. Mini Mobile Telemetry System

Aim for Designing such a System

Main purpose for such a design is to have the ability of using a telemetry system for flight tests under flexible conditions. Mini Mobile Telemetry System could be used on ground and on air for so many test scenarios which could be performed in close ranges on ground and onboard. The range of the relay operation purposes is limited with the capabilities of the telemetry system on ground. IRIG-106 standards were considered during system design and operation.

System Components

A ruggedized pc is used to assemble the system components. Main consideration was to be able to use multiple displays and to meet the system components power requirements.

A dual channel receiver board is chosen which has the proper sensitivity and dynamic range levels. A Decommutator Board is chosen which is compatible with the FTI data acquisition units. A GPS Time Code Generator board is used to generate the IRIG-B time code which has to be inserted to decommutator board so gathered data packets will be marked with the precise time tag. Real Time Data Analysis Software is used to monitor the flight test parameters in real time. In-house designed gauges and displays are used in Test Monitoring Displays.

The Interconnection Panel is designed to establish and operate required antenna and other signal connections easily. The interconnection panel protects the neat connectors and cable assemblies on pci boards.

Figure 2 The Interconnection Panel

The Interconnection Panel also has the input and output signal connections for the decommutator board. Low loss adapters have been chosen which supports the certain frequency band for the application.

Instrumented Aircraft

The Mini Mobile Telemetry System has been used on flight tests of Turkish Primary and Basic Trainer, 'HURKUS' Project. The project has two prototype aircrafts and both of them are instrumented for flight test purposes. Telemetry transmitters are placed onboard for real time data acquisition in telemetry ground stations.

Figure 3 Turkish Primary and Basic Trainer, 'HURKUS'

Antenna locations on prototype aircrafts were decided after the propagation of antennas were analyzed via a software. The software uses the antenna specific information that are supplied by the manufacturer. A 3D model of the platform which antennas placed on used to simulate the radiation patterns and power levels due to distance of the receiver antenna.

Images of the analysis which have performed are given below. The horizontal bar graph indicates the power level between -240 dBm to -10dBm.

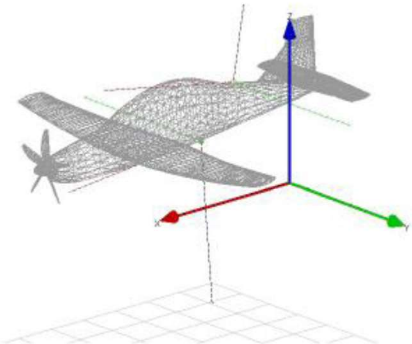

Figure 4 Antenna Placement on HURKUS Aircraft

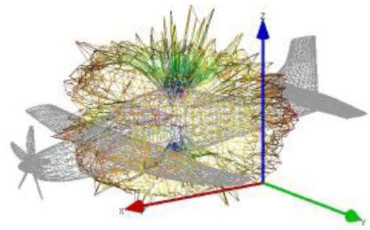

Figure 5 Farezone Analysis

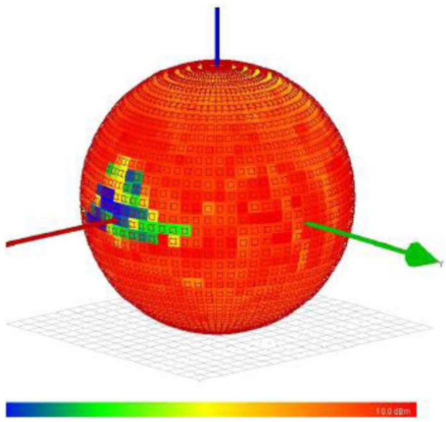

Figure 6 Total Power Analysis

System Operation Scenarios

First option for the system is to serve on ground for up to three flight test engineers during close range flight tests. The system has been operated during Turkish Primary and Basic

Trainer, ‘HURKUS’ Project flight test campaign. The comments of flight test engineers for the Mini Mobile Telemetry system was ‘satisfactory’. A VHF radio was used by the lead flight test engineer to communicate with the test pilot. Each flight test engineer used one ‘test specific designed’ display to follow the requested parameters during flight tests. Some sample display figures are given below.

Figure 7 Test Monitoring Screen # 1

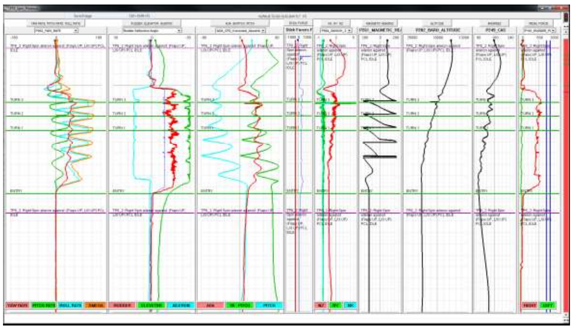

Figure 8 Test Monitoring Screen # 2

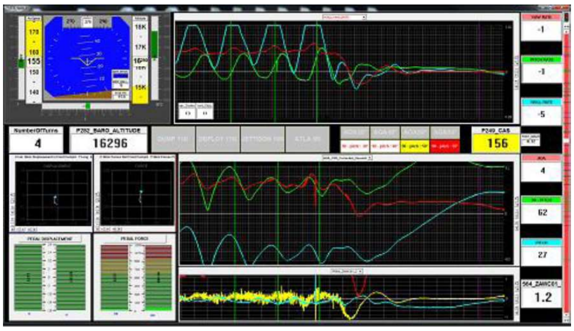

Figure 9 Test Monitoring Screen # 3

For flight test operations conducted on ground, Mini Mobile Telemetry System could be placed anywhere on ground within the limitations of line of sight and range. One GPS antenna and Two receiving (omni-directional | LHCP, RHCP) antennas are used with LNAs mounted on tripods on ground. Antenna connections were made using the interconnection panel.

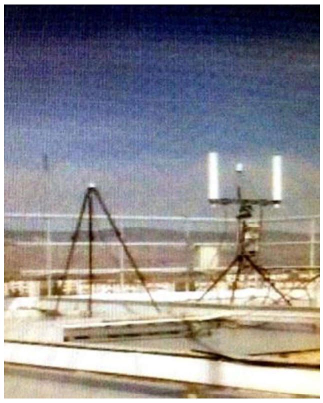

Figure 10 Receiving Antennas (LHCP & RHCP) and GPS Antenna

Figure 11 Receiving Antennas (LHCP & RHCP)

Figure 12 Mini Mobile Telemetry System

Figure 13 Mini Mobile Telemetry System in Operation

DOI 10.5162/etc2016/6.2

The system architecture for on ground operations is given below.

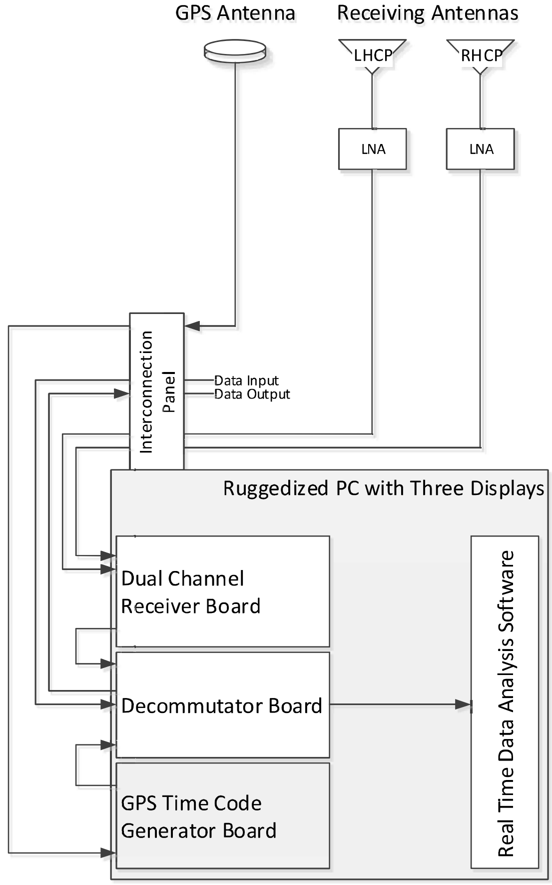

Figure 14 Mini Mobile Telemetry System – On Ground Configuration Architecture

According to calculations, the expectation was to reach 26km operational range in line of sight. It has was seen that the system could operate up to 30 km without data loss.

Second option for the system is to serve onboard in a flying test bed. A Grumman S-2E/T model A/C has been using as a flying test bed in Turkish Aerospace Industries Inc. For this scenario four receiving antennas (circular polarization) with LNAs planned to be fixed on the A/C for real time data gathering. Antenna placement is planned to be mounted to the top of the front and rear fuselage and to the bottom of the front and rear fuselage. Antenna placement is shown on the figure below.

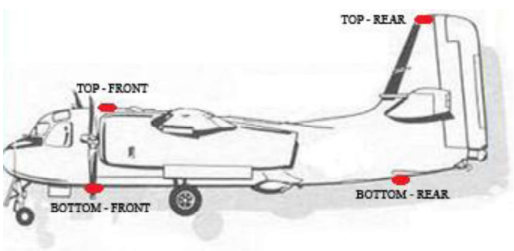

Figure 15 Receiving Antenna Placement

Figure 16 S2E/T – Flying Test Bed

RF switches are chosen to navigate the input signals to the receiver. All signal cables are chosen in low loss specifications and all cables are chosen manufactured of aluminum based materials to use the advantage of low weight and minimum bend radius. The system architecture for on board configuration is given below.

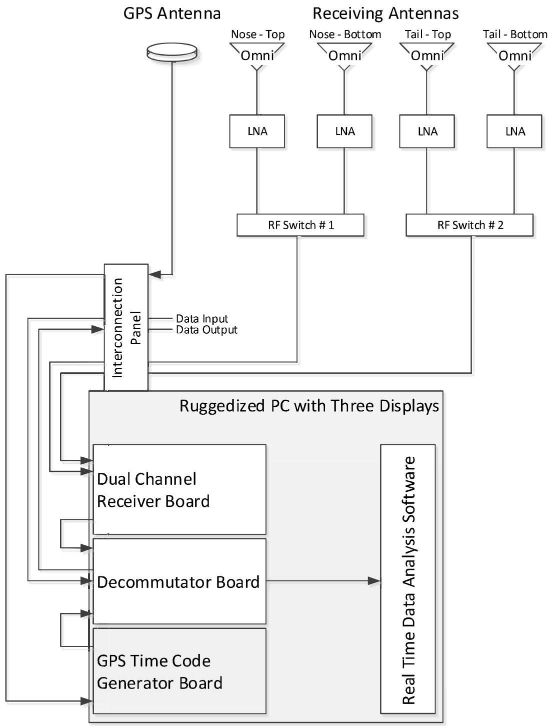

Figure 17 Mini Mobile Telemetry System – On Board Configuration Architecture

On board configuration allows flight test engineers to monitor the data flow of the A/C under test from the chase A/C (flying test bed). For the second option, three flight test engineers will be able to monitor the flight test parameters.

It has been evaluated that this configuration could be useful during long distance ferry flights that stationary telemetry systems range limits are exceeded.

DOI 10.5162/etc2016/6.2

Third option for the system is to serve as a flying relay station in the flying test bed. For this scenario two transmitting antennas will be mounted on the A/C additional to four receiving antennas described in second option.

Antenna placement and propagation analysis is shown below. The horizontal bar graph indicates the power level between -240 dBm to -13dBm.

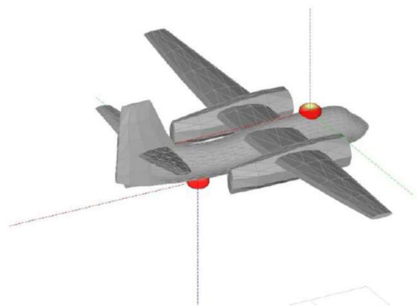

Figure 18 Receiving Antenna Placement on S2-E/T Aircraft

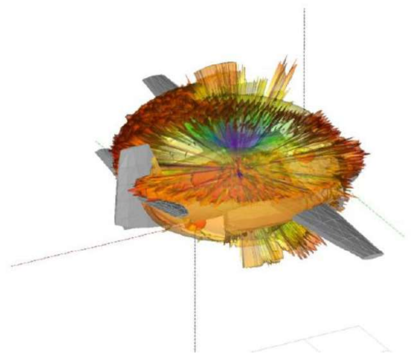

Figure 19 Farezone Analysis

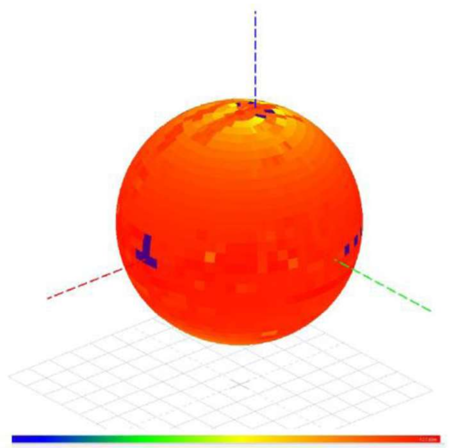

Figure 20 Total Power Analysis

For this option, the antenna of telemetry ground station will be tracing the chase A/C which is the flying test bed instead of tracing the A/C under test. Using the flying test bed as a relay station will allow the telemetry ground station to keep gathering data during flight tests which are performed out of line of sight such low altitude maneuvers.

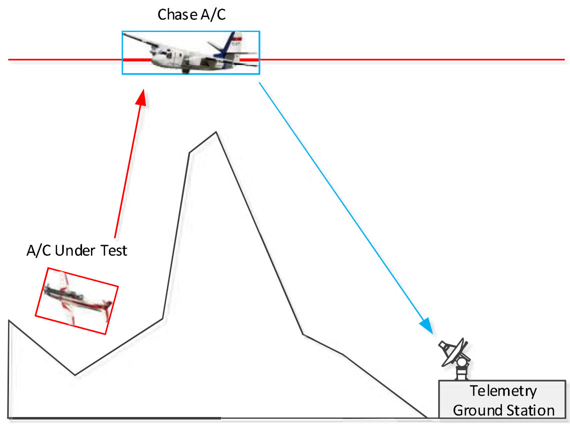

Figure 21 Flying Relay Station Figure

The system architecture for the flying relay station configuration is given below.

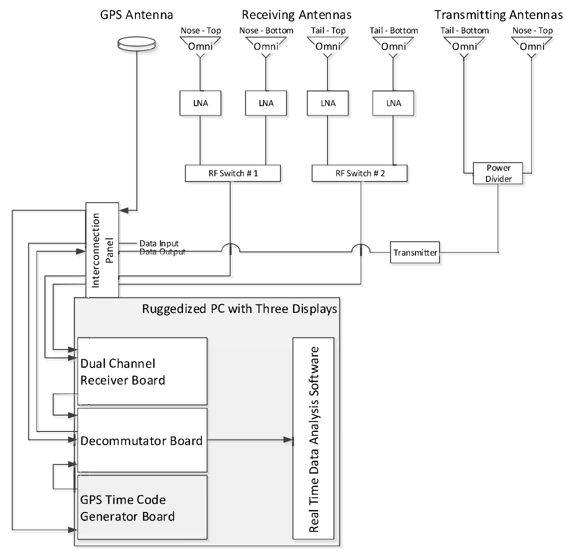

Figure 22 Mini Mobile Telemetry System – Flying Relay Station Configuration Architecture

It has been stated that Mini Mobile Telemetry System is a perfect alternative of huge ground stations due to its operational flexibility for mainly three different flight test operations. The first one is the flight tests which could be performed at close range and could be managed up to three flight test engineers on ground. The second one is the onboard configuration which could be used during long range flight tests or ferry flights so parameters gathered from the A/C under test could be monitored in the chase A/C. The third one is the flying relay station configuration which transfers the gathered data packets from the A/C under test to Telemetry Ground Station.

DOI 10.5162/etc2016/6.4

A Study on Implementation of Network Based Telemetry System Using Retransmission

Sooyeol Im, Chiho Hwang, Hwansuk Lee, Inho Choi
Agency for Defense Development, Korea,
syim@add.re.kr

Abstract:
In recent years, a network based telemetry system has received a great attention as the upcoming telemetry paradigm. This paper considers a network based telemetry system with one master telemetry and two slave telemetries. The master telemetry merges data from each slave telemetry and own measured data, and the merged data is transmitted to the ground receiving station. If there exist some errors in data from the salve telemetry, the master telemetry requests retransmission to corresponding slave telemetry. In this paper, we propose a retransmission algorithm applied to implementing the network based telemetry system. Simulation results demonstrate that the proposed retransmission algorithm improves the performance of the wireless communication between the master and slave telemetries.

Key words: Telemetry System, Retransmission, Additive White Gaussian Noise, Bit Error Rate, Frame Error Rate

Introduction

The newly developed flight vehicles should confirm the stability and suitability of the design parameters by analyzing the flight test results. The telemetry system, in the flight test for the performance evaluation of the flight vehicle, acquires data from sensors attached to the flight vehicle and status of subsystems, and transmits the measured data to the ground receiving station via wireless communications [1]. The standardization of the telemetry system is actively in progress by Range Commanders Council (RCC) and Inter Range Instrumentation Group (IRIG) [2].

In recent years, a network based telemetry system has received a great attention as the upcoming telemetry paradigm due to the applicability to the group of flight vehicles [3], [4]. In the formation of group of flight vehicles, each flight vehicle has its own on-board telemetry, and the on-board telemetries and ground receiving station are networked via wireless communications. Integrated Network Enhanced Telemetry (iNET) project of Central Test and Evaluation Investment Program (CTEIP) is actively on defining the concept and requirements of the system, defining the network and communication protocol, incorporating standardized technologies [5], [6].

In the flight test of the group of flight vehicles, each telemetry has been allocated frequency band separately using frequency division multiplexing (FDM). In such a telemetry system, in accordance with the number of flight vehicles, there should be multiple frequency bands and multiple wireless receiving system in the ground receiving station.

This paper considers a network based telemetry system with multiple on-board telemetries. One on-board telemetry (master telemetry) receives data from multiple on-board telemetries (slave telemetries) acquiring its own measured data. Slave telemetries transmit the measured data to the master telemetry in turn using time division multiplexing (TDM) over one frequency band. The master telemetry merges the data from slave telemetries and its own data, and the merged data is transmitted to the ground receiving station. In such a network, the retransmission scheme is applied to the telemetry system via the bidirectional communication link between the master and slave telemetries, and we propose a retransmission algorithm determining which slave telemetry retransmits which error-frame. Simulation results demonstrate that the proposed retransmission algorithm improves the performance of bit error rate (BER) and frame error rate (FER) between the master and slave telemetries.

DOI 10.5162/etc2016/6.4

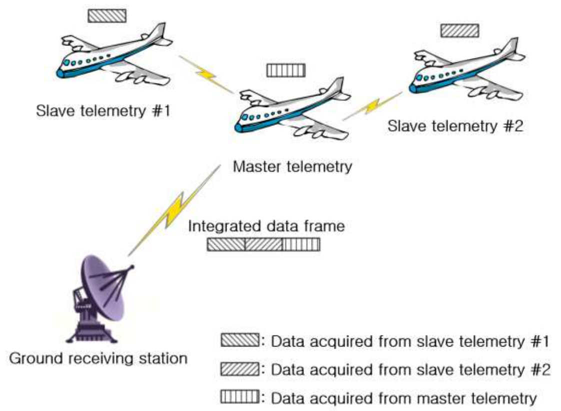

Fig. 1. Network based telemetry system.

The remainder of this paper is organized as follows. In Section II, we introduce the system model applied in this paper. Details of the proposed retransmission algorithm are given in Section III. In Section IV, some simulation results are provided to demonstrate the performance of the proposed retransmission algorithm. Finally, this paper is concluded in Section V.

System Model

This paper considers a network based telemetry system with one master telemetry and two slave telemetries as shown in Fig. 1. Each slave telemetry acquires and transmits the measured data to the master telemetry. The master telemetry merges and transmits the data from slave telemetries and its own data to the ground receiving station.

The master telemetry and two slave telemetries take a data transmission using TDM. One cycle of the data transmission is shown in Fig. 2. The master telemetry broadcasts the data request command in each cycle. Each salve telemetry, received the data request command from the master telemetry, transmits the acquired data to the master telemetry at a predefined time. In such a procedure, each slave telemetry transmits the data measured at the same time. In case that there are some errors in the data received by the master telemetry, the master telemetry inserts the retransmission request into the data request command. The slave telemetry, received the data request command containing the retransmission request, retransmits the corresponding data frame to the master telemetry. The number of retransmission within one cycle is defined in accordance with the circumstance of the telemetry system such as wireless communication bandwidth, the amount of data acquired by the slave telemetry.

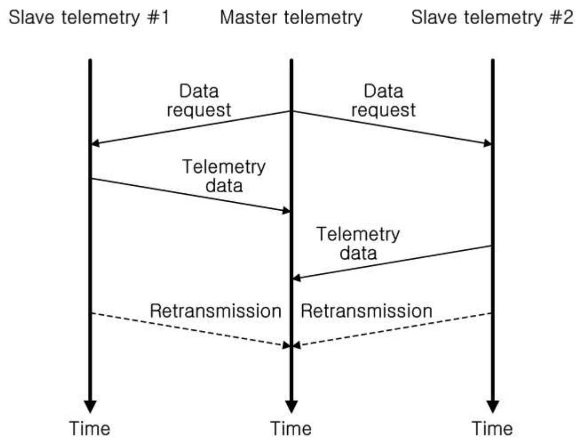

Fig. 2. Data transmission between the master telemetry and slave telemetries in the network based telemetry system.

Retransmission Algorithm

In this section, we explain the retransmission algorithm for data retransmission of the slave telemetry in the network based telemetry system. Since one of two slave telemetries retransmits the measured data in a cycle, it is necessary to determine which slave telemetry retransmits the data in corresponding cycle.

The master telemetry executes the retransmission algorithm and inserts the result of the retransmission algorithm into the data request command in corresponding cycle. For the retransmission algorithm execution, in this paper, it is assumed that the master telemetry has two status registers about the data received from each slave telemetry. The bits of the status register are shifted when receiving the data frame from the slave telemetry, and the corresponding bit of the corresponding status register is set in accordance of the result of error detection such Cyclic redundancy code (CRC). If there exists error in the received data, the corresponding bit of the corresponding status register is set to 1. Otherwise, the corresponding bit is set to 0. The length of the status register is determined in accordance with the size of the memory of the slave telemetries due to the number of data frames stored in the memory of slave telemetries depends on the length of the status register.

The flowchart of the retransmission algorithm executed at the master telemetry is shown in Fig. 3. By choosing the slave telemetry with larger status register value, let the slave telemetry with older error-frame preferentially retransmits the corresponding frame. The retransmission algorithm proposed in this paper allows N-times consecutive retransmission using RetriLock variable. In case that a slave

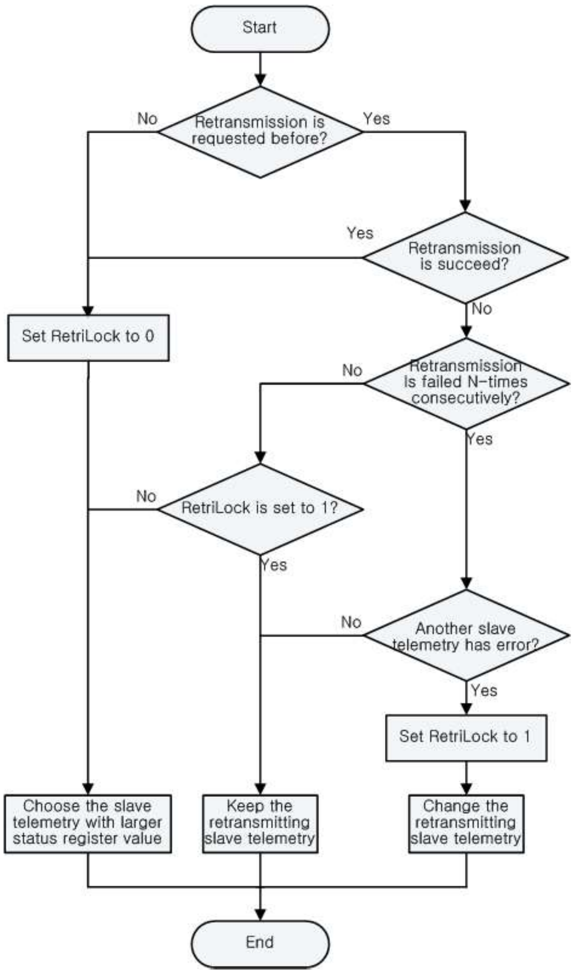

Fig. 3. Flowchart of retransmission algorithm.

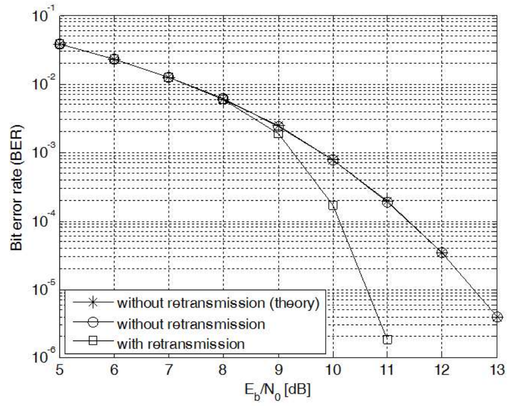

Fig. 4. Comparison of BER performance of FSK modulation with/without retransmission over AWGN channel.

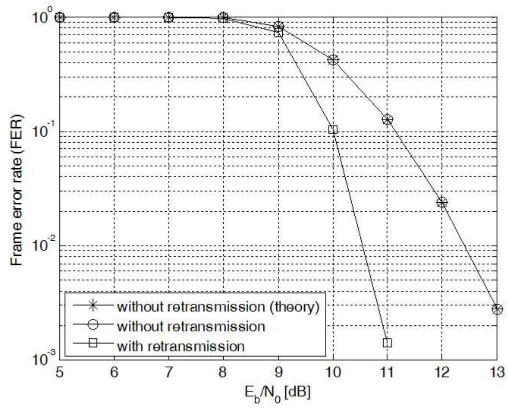

Fig. 5. Comparison of FER performance of FSK modulation with/without retransmission over AWGN channel.

telemetry fails retransmission N-times consecutively, RetriLock is set to 1, and the retransmitting slave telemetry is changed in the next cycle. As a result of the retransmission algorithm, the master telemetry inserts the information about which slave telemetry retransmits which data frame, using the status register value, into the data request command.

Performance Evaluation

In this section, some simulation results are provided to demonstrate the proposed retransmission algorithm. We consider the network based telemetry system that two slave telemetries transmit each acquired data and one master telemetry receives the data. Each slave telemetry modulates the acquired data using frequency shift keying (FSK). For the sake of simplicity, it is assumed that the wireless channel between the master and slave telemetries is modeled as Additive White Gaussian Noise (AWGN) channel, and the data frame is retransmitted once a cycle. It is further assumed that the length of the status register is 16 bits, and the length of the data frame is 88 bytes.

We change the retransmitting slave telemetry in case that the corresponding slave telemetry fails the retransmission twice consecutively.

Fig. 4 presents the BER performance of FSK modulation over AWGN channel. For performance comparison, the BER performance of the FSK without retransmission over AWGN is plotted. The result can be represented using Q-function as follows [7]:

$$\begin{aligned} P_b &= Q\left(\sqrt{\frac{E_b}{N_0}}\right) \\ &= \frac{1}{\sqrt{2\pi}}\int_{\sqrt{\frac{E_b}{N_0}}}^{\infty} \exp\left(-\frac{x^2}{2}\right)dx. \end{aligned} \tag{1}$$

In the range of low E_b/N_0, as shown if Fig. 4, the retransmission algorithm does not influence the BER performance. In the simulation environment of this paper, the retransmission algorithm enhances the BER performance in the range of $E_b / N_0 \geq 8\text{dB}$, and the influence of the retransmission algorithm gets higher with increasing E_b / N_0. In general, reliable communication can be achieved at 10^{-5} of BER [8], [9], and the proposed retransmission algorithm obtains 2dB of E_b / N_0 gain at 10^{-5} of BER compared to the conventional scheme without retransmission.

Fig. 5 presents the FER performance of FSK modulation over AWGN channel. For performance comparison, the FER performance of the FSK without retransmission over AWGN is plotted. Since we assumed that the length of the data frame is 88 bytes (i.e., 704 bits), theoretical FER can be represented by the Q-function, using eq. (1), as follows:

$$\begin{aligned} P_f &= 1-\left(1-P_b\right)^{704} \\ &= 1-\left(1-Q\left(\sqrt{\frac{E_b}{N_0}}\right)\right)^{704} \\ &= 1-\left(1-\frac{1}{\sqrt{2\pi}}\int_{\sqrt{\frac{E_b}{N_0}}}^{\infty}\exp\left(-\frac{x^2}{2}\right)dx\right)^{704}. \end{aligned} \tag{2}$$

In the range of low E_b / N_0, like the result of BER in Fig. 4, the retransmission algorithm does not influence the FER performance. With increasing E_b / N_0, however, the influence of the retransmission algorithm gets higher. In the range of $E_b / N_0 \geq 9.5\text{dB}$ (i.e., BER is less than $1/704 \approx 1.42\times10^{-3}$), deterministically, there exist data frames without error due to none of bits within one frame has error. In the statistical simulation results of this paper, in the range of $E_b / N_0 \geq 8\text{dB}$ (i.e., BER is less than 6×10^{-3}), there exist data frames without error, and the influence of the retransmission algorithms arises.

Conclusion

This paper studied the implementation of the network based telemetry system with one master telemetry and two slave telemetries. In such a scenario, the retransmission algorithm is applied to the telemetry system to enable the retransmission of the error-frame via the bidirectional communication link. To this end, we proposed the retransmission algorithm determining which slave telemetry retransmits to the master telemetry. Simulation results demonstrated that the proposed retransmission algorithm enhances the performance of the BER and FER over AWGN channel compared to the results without retransmission.

By extending our work, the proposed retransmission algorithm can be generalized for the case that there exist multiple slave telemetries (i.e., not two slave telemetries, but N-slave telemetries), and more realistic wireless channel model (e.g., Rayleigh, Rician channel model) can be applied in evaluating and analyzing the performance of the proposed retransmission algorithm. Furthermore, mathematical derivation of the BER and FER can be obtained in a given channel model, and the theoretical results can be compared with the statistical simulation results.

References

[1] F. Garden, R. Jedlicka, and R. Henry, *Telemetry Systems Engineering*, Artech House, 2002.

[2] RCC, *Telemetry Standards*, IRIG Standard, 106-15, July 2015.

[3] S. Kim, S. Cho, S. Cho, and C. Park, “Development of operation network system and processor in the loop simulation for swarm of small UAVs,” *J. Inst. Contr. Robot. Syst.*, vol. 18, no. 5, pp. 433-438, May 2012.

[4] S. Kim and Y. Kim, “Behavioral decentralized optimum controller design for UAV formation flight,” *J. of The Korean Society for Aeronautical & Space Sciences*, vol. 36, no. 6, pp. 565-573, June 2008.

[5] T. Grace, J. Kenney, M. Moodie, and B. Abbot, “Key components of the iNET test article standard,” in *Proc. Int. Telemetering Conf.*, pp. 1-10, 2009.

[6] B. Abbot, M. Moodie, T. Newton, and T. Grace, “iNET system design concepts,” in *Proc. Int. Telemetering Conf.*, pp. 1-9, 2011.

[7] S. Haykin, *Digital Communications*, John Wiley & Sons, 1988.

[8] D. Costello, J. Hagenauer, H. Imai, and S. Wicker, “Applications of error-control coding,” *IEEE Trans. Inform. Theory*, vol. 44, no. 6, pp. 2531-2560, Oct. 2988.

[9] J. Proakis, *Digital Communications*, McGraw-Hill, 2000.

DOI 10.5162/etc2016/7.2

"Telemetry Band C & S Capabilities Integrated for Test Range Activities"

Attendant:
Antonio Javier Mesa Fortún
Authors: Antonio Mesa Fortún, Neves Seoane Vieira, Ana Corrales Sierra.
E-mails: mesafaj@inta.es, seoanevn@inta.es, corralessa@inta.es

Phone: +34 959 208 813
Mobile: +34 690 170 939
Centro de Experimentación de "El Arenosillo" (CEDEA)

INTA
National Institute for Aerospace Technology
Ctra. San Juan del Puerto Matalascañas (A494) Km.34
21130 Mazagón-Huelva. Spain.

INTA as Governmental Center and Public Research Establishment specialized in the aerospace field; it is in charge of 2 important roles in Spain. Certification accoding to Regulation for Defense Airworthiness Royal Decrete 866/2015 and test means for aeronautical programs declared as "defense strategic".

"El Arenosillo" test range (INTA/CEDEA) has been for fifty years the Official test Range for Spanish Ministry of Defense, in order to support all development, certification and qualification programs for Military and Civil Aircrafts. Manned & unmanned aircrafts and their systems integration. INTA has been supporting as Government Furnished Facilities (GFF´s) tests for Certification, Qualification and Development flight test activities.

According to the needs that have been requested by Industry and Government, INTA/CEDEA had implemented a new autotracking system for Band C and S in 2015. In a very short time (only 15 minutes), it is possible to swap from one band to the other with a modular structure. It means to save costs in order to complaint all types of exercises. Additionally, this new autotracking capability has been fully integrated at INTA/CEDEA. It means that it coexists with 3 RADAR´s systems and 4 optronic systems. It lets to coordinate and optimize test activities sharing information from one system to the rest.

Aim of current abstract is to show the way this telemetry system has been integrated coexisting with additional system and providing its own test information for tracking capabilities as main data source to slave rest of sensors. In addition, when this new system is working in slave mode in order to catch aerial vehicle and provide telemetry data for flight test activities.

Key words: "Auto-tracking", "test range instrumentation", "unmanned vehicles", "certification airworthiness tests" and "Band S & C".

DOI 10.5162/etc2016/7.2

1. Introduction.

National Institute for Aerospace Technology (INTA), founded in 1942, is a public research establishment attached to Spanish Ministry of Defence (MoD), hence, a governmental organization. Which is under direct Government decisions from State Secretary of Defense.

INTA activites on research trascend the scope of military applications to benefit, through new developments and applications, the most varied areas of activity. Currently, INTA personnel is based in technologists and researchers of the highest level in their areas of competence, while equipping itself with major infrastructures in the form of installations, facilities and laboratories for research, development, measurement and testing, all of them, pioneers in Europe and frequently used by national and international organizations.

INTA carries through its research activities in a highly cooperative environment, in collaboration with other partners in many international programs, participating also in most of international aeronautic and space forums. This interantionalization of activities is one of the most significative features of INTA. Summarizing INTA profile in figures, human resources working in INTA and its associated sites consist of more than 1.600 people with facilities situated at several different locations in Spain, each one with a definite purpose.

Aim of current paper in to show the way telemetry capabilities have been integrated at one of its test centers, Arenosillo Test Range (INTA/CEDEA), recently in 2015. These facilities located in the south of Spain, have been supporting activities for aeronautical Military and Civil Aircrafts, certification for solar energy systems and atmospheric studies. In fact, since 1962 supporting Research & Development (R&D) processes for any kind of activities, specially Aeronautical and Scientific programs can be counted among their main activities.

INTA/CEDEA is considered one of the most capable Test Ranges in Europe to support tests for Certification, Qualification and Research & Development activities. Manned and unmanned Aeronautical and ground systems can be validated and tested at its facilities. Additionally, training activities for National and Foreign military corps are one of the most relevant activities. National, foreign, governmental and industrial organizations have been performing experimental activities at INTA/CEDEA facilities since 1962. It means that taking into account this wide catalogue of possibilities, it is necessary to be supported by a high-specialized instrumentation.

INTA/CEDEA added values are based on three important pillars:

- Wide safety test area.
- High specialized instrumentation.
- Stable & suitable weather conditions for test activities.

INTA/CEDEA, joined to Centro de Investigación Aerotransportada de Rozas (INTA/CIAR), second INTA Test Centre in north of Spain, is involved in an ambitious expansion program to increase operational capabilities, specially focused in Unmanned Aerial Vehicles (UAVs). This new concept for next future will be supported by new instrumentation capabilities, specially increasing telemetry possibilities. It has been designed as an expansion from current INTA/CEDEA (Experimental Test Center) experience and capabilities. Based on it, some main ways have been implemented to define its main strategy. Ambitious expansion projects based on 40 years experience on the following activities:

- Certification/Qualification activities to integrate systems on aerial platforms.
- Operations of aerial unmanned vehicles and its improvement designs.
- Trayectographic systems.
- Supporting industries and National & Foreign Government forces.

2. INTA/CEDEA Autotracking Telemetry Capabilities.

Taking into account current needs to manage data, it was decided to integrate a new Band C auto-tracking system antenna at INTA/CEDEA test range instrumentation systems. However, it was decide to keep also Band S capabilities. Compromise solution decided has been to install a new system with both capabilities, taking into account that autotracking was not previously available at Test Range facilities for Band S. It was supported to integrate.

The solution decided was a 1.8m parabolic S&C Band Tracking System. It is installed at a high performance pedestal with a processor to manage its behaviour linked via fiber optic to the

Antenna Control Unit (ACU) located in the telemetry control room.

System consists of the following major elements:

- A high-performance pedestal driven by one brushless motor per axis. An Elevation over Azimuth pedestal design.
- A 1.8m carbon fiber parabolic reflector.
- 2 feeds: 1 S-Band tracking feed and 1 C-Band. Both tracking feeds with common backend.
- 1 Digital high-performance servo controllers closing the motor control loop.
- A real-time pedestal controller located at the servo enclosure at the pedestal.
- Fiber Optic Ethernet link between the pedestal and the ACU.

This system, previously described, is not INTA design. It has been provided by an external supplier.

Figure 1. Antenna instalation at CEDEA Test Range Facilities.

This system has following innovation concepts from typical telemetry equipment:

- To reduce S & C Band feed. It is designed with a common backend, permanently mounted on the antenna, that includes the amplifiers and the hybrid, to generate the right handed circular polarization (RHCP) & left handed circular polarization (LHCP).
- It means that antena user has the capability to install 2 different radomes that can be easily interchanged to meet the specific mission band of operation: S or C Band. It takes onbly 15 minutes.
  - This enables to minimize feed's cross section, minimize the Radio Frequency (RF) switching and thus increase the resulting G/T.
  - Reduce the filter complexity by requiring a simple but efficient narrow bandpass filter thus reducing the filter loss which in turn increases the overall G/T.
  - Feed RF output is provided on a fiber optic interface.
    - A transceiver that digitizes the RF signal in a manner suitable for Fiber Optic transport.
    - The transceiver has the added feature of giving the option to the user to re-generate the RF in the control room in the original band (S or C) or to an intermediate band (from C to S-Band or C- to L-Band for example) or to IF (70 MHz, 100MHz,…). This means that S-Band receivers can work with the C-Band feed. Furthermore, since the output can also be produced at IF (70MHz) there is no need for any receivers.

The pedestal includes a one brushless motor drive per axis design complemented with digital absolute angle encoders position feedback for each axis (typically from Heidenhain Corp.). The Elevation motor and feed are cable-wrapped to the Azimuth axis.

3. Advantage of a modular feed.

Feed design takes a competitive ventage than most conventional telemetry tracking feeds. Nomally, for an efficient dualband feed design, in order to get both added capability, impacts on more filtering, more RF components and a bigger housing. Final consequence means a reduction for the overall efficiency of the feed. To circumvent this limitation a modular feed solution has been adopted by supplier. This design splits the band dependent components and the band independent components. By doing so, a

common backend includes the Low Noise Amplifier (LNAs) and hybrids. Band independent components, as well as the motor for the nutating horn of the front end. The backend is permanently fixed to the antenna by the spars and feed ring. Individual front ends, one per band, configures final structure. These will be mounted on to the backend with the help of self-locating push-on coaxial RF connections and a quick release clamp.
This innovative approach allows to minimize the RF losses as fewer RF components are required and more efficient RF filtering can happen. Due to the effincy to design/acquire a high Q narrow bandpass filter with very low loss than incorporate a complex multiple bandpass filter. As conclusion, this modular approach reduces the size (length & cross-section) and weight of the feed. It reduces also the RF blockage. All this put together means that for the same reflector size the resulting G/T increases considerably.

This feed modular approach has the following advantages:

- Cost reduction for both capabilities at only 1 equipment. Cheaper to produce two band specific feeds than an all encompassing feed.
- Increased RF efficiency: less RF components, targeted filtering, size reduction.
- Better filtering of unwanted signals
- Backend structure is permanently fixed to the antenna. From operational point of view it takes the advantage that no need to realign the RF when changing front redomes.

4. INTA/CEDEA equipment instrumentation.

From instrumentation point of view, INTA/CEDEA is able to support multiple test scenarios due to its flexible structure, based on a redundant instrumentation system. A net of sensors implemented by optronic systems, RADAR´s, IR cameras, telemetry (described previously), and tracking systems are able to accommodate for each test scenario, fulfilling multiple test requirements as: some aerial platforms, some targets (aerial and maritime) and whatever system to check, qualify or certify. Mentioned structure can accommodate, for test requirements, trying to optimize all involves means, with a main aim: "to support and secure each operation test in a safe way".


Figure 2. RADAR Tracking at INTA/CEDEA.

In addition, mentioned structure is able to track and to link data between whatever aerial vehicles, instrumentation and aerial/ground development equipment. It means that INTA/CEDEA is able to support test for aerial vehicles, targets, aerial and ground systems and command unmanned aerial, ground and maritime systems. All systems at the same time or stand alone for each one.

A consequence and added value provided by this instrumentation structure drives to following opportunities:

- To manage in advance "Test Procedure and scheduled Programme" accommodating test means for each requirement, in a flexible way.
- To reschedule in real time, once test has begun, and accommodate to changes based on on-going test results.
- To evaluate in real time data information by telemetry.

Functional principle for all these equipments are based:

- For optronic systems: infrared (IR) & optical (OT) contrast. Also RADAR doppler (RDP).
- For tradicional monopulse tracking RADAR sytems.

Architecture instrumentation net is done by:

DOI 10.5162/etc2016/7.2

- 4 optronic platforms with IR, OT & RDP payloads.
- 3 Tracking RADARs.
- 1 Telemetry antenna for S & C Bands.

Figure 3. Optronic System at INTA/CEDEA Test Range.

5. Telemetry contribution to Test Range instrumentation.

Taking into account this instrumentation scenario, new telemetry system has been integrated taking into account information from rest of systems, (optronic and RADAR´s). It means that:

- For a high speed aerial platform. Optronic systems are able to catch from the beginning of its movement. Its high performance in terms of speed and high instrumentation payload weight (up to 1.000kg).
- For slow flying systems, all instruments (optronic, RADARs and Telemetry) are able to catch from the beginning.

From operational point of view, this architecture is able to slave rest of systems to a master equipment. In real time, is possible to update this configuration. It lets in case that for example, master loses its tracking, to recover swapping master-slave configuration. All systems are able to work according to this philosophy, including new telemetry system. In fact, contribution from this new equipment has increased test range reliability from tracking point of view.

Master equipment provide its relative polar coordinates from its own position. All of them are geo-reference located. Polar coordinates are provide by their own azimuth and elevation angles. Additionally range is provided and fix the aerial vehicle. This information, combined with its geo-reference position, is managed in order to provide the new relative position between slave equipment and system to track.

Information from telemetry system has 1 advantage. GPS position is possible to receive from aerial vehicle. It means that is possible to cross check this information and pedestal angular position. GPS position is used also to feed tracking data net. New telemetry system contribution has 1 disadvantage: only radial information is possible to extract from its pedestal. However for near vehicles is not a constraint. For aerial platforms coming far away, this radial information is so important. In these conditions, only telemetry system is able to track. GPS information allows to slave all tracking devices based on these kind of data. In case that no GPS is available, this radial information let to focus in "waiting position" all the systems. Once its functional principle is able to catch, device will be working in tracking mode if it is needed.

This configuration is described in figure 2.

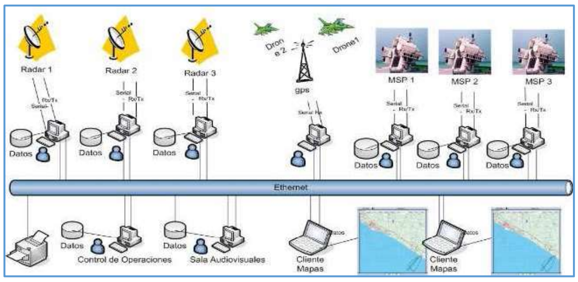

Figure 4. INTA/CEDEA tracking data management.

6. Telemetry antenna integration at test range infrastructure.

As it has been mentioned, antenna has implemented and ACU to manage different control options. There are six different operational modes: manual, search, stand by, tracking, acquire and slave. For last one is possible to get the information from: Ethernet, Serial and P-Track.

This same philosophy has been implemented for all equipment's: RADAR´s, optronic and for sure telemetry. It is possible also to charge an expected simulation trajectory. In case that tracking will be loose, it will operate in order to recover vehicle auto-tracking.

To integrate autotracking anetnna at Test Range instrumentation is necessary a new application at the ACU. It lets to know the field of the frame that sends all sensors to the control station. Once realized the application, thereby it enslaves ACU, therefore if the ACU lost the

DOI 10.5162/etc2016/7.2

target, thanks to this new application, operator can know the position of the target and to get again auto tracking capabilities. Due to its high tracking range capability, telemetry antena is able to provide, as commented, GPS data and radial tracking information. Normally this last topic has more added value.

Following milestones describes the process to integrate at Test Range Control Center (TRCC). TRCCS is responsible of coordination, monitoring and recording whatever operational mission being conducted at the center. A data acquisition system is in charge to collect a set of physical signals and to digitizalize. This set of information is processed and it drives data transmision between all and each of the sensors forming the test center: RADAR´s, Optronic and Telemetry. It lets different devices the capacity to interactuate among themselves.

The TRCCS communicates with the sensors through coded frames bi-phase PCM signal synchronised. Thank the advance of new technology, benefiting from the Ethernet network and developed in the majority of teams. The Ethernet network has a transmission capacity of information, speed and reliability. The servers, where the positions of the aerial vehicles are received, is recorded in the system and is able to send the position of a sensor to all other sensors.

Current application can receive up to five mobile vehicle positions at the same time. In the new system also will be necessary software implementing that the operator is able to pass the position to any sensor regardless of your manual or automatic monitoring.

In order to keep the antenna in slave mode, new application for ACU, need to know protocol information that arrives to it. Information passed is (X, Y, Z), absolute coordinates gotten from relative coordinates from each sensor and its own georeferenced sensor location. ACU is responsible for adapting the frame X, Y, Z, such that the antenna can recognize the vehicle position.

7. Conclusions.

According to the acquisition of a new telemetry system for INTA/CEDEA Test Range, its tracking capabilities has been increased. INTA/CEDEA has been traditionally a trajectography center, with all its devices, RADARs and Optronic integrated at a Ethernet data system communication, working between sensors communications at a swapping Master & Slave mode.

This new antenna for Band S & C has been integrated in order to keep this operational protocol between sensors in real time.
In order to reduce costs and keep performances for both Bands, a system based on a modular feed has been implemented.

It lets Arenosillo Test Range to increase its tracking capabilities, but also its particular flexible structure. It means that these devices have the added value to be able to adapt for multiple flight test scenarios.

Figure 5. Tiger HAD for Certification and Qualification Tests at INTA/CEDEA.

8. References.

[1]. Arenosillo test Range configuration. A. Mesa. National Institute for Aerospace Technology. INTA-2014.

[2]. Modular solution band for Band S & C. Creative Digital Systems Integration, INC. L. Gravel. February 2015.

[3]. Copyright © 2016 INTA-A. Mesa, N. Seoane, A. Corrales.

DOI 10.5162/etc2016/7.3

Novel 11 m S-/X-/K-Band Remote Sensing Ground Station Antenna

Gerbert Lagerweij
VERTEX ANTENNENTECHNIK GmbH
Baumstr. 46 - 50, 47198 Duisburg/Germany,
glagerweij@vertexant.de

ABSTRACT

Modern geospatial techniques enable the provision of up-to-date imagery to the public through the media and internet. Improvements to earth monitoring satellites, such as SAR, and the very high resolution data received from these satellites, result in very large data files or a wide band pipe required for the transmission to the receiving earth stations. These large bandwidths cannot be provided by the regular allocated slot in X-Band. The only way to increase the bandwidth of the downlink is the exploitation of K-Band (25.5–27 GHz).

Vertex Antennentechnik (VA) has developed a triband full motion Antenna System with 11.5 meter diameter which incorporates S-, X- and K-Band. In conventional multiband Antennas, it is difficult to optimize Antenna parameters such as aperture efficiency and sidelobe performance in all three bands simultaneously. This paper discusses some advantages and design considerations and highlights the overall performance of a novel triband Antenna system for Remote Sensing (RS) applications which has been commissioned in 2016.

Key words: Reflector Antennas, Remote Sensing, Ground Station, S-/X-/K-Band, Monopulse tracking.

INCREASING BANDWIDTH REQUIREMENTS

Remote Sensing applications within the domain of natural hazards and disasters have become extremely important. In order to monitor actual weather or earth surface conditions in near real time, visual High Resolution images are required by national emergency services. This results in very large data files or wide band pipes for the transmission to the receiving earth stations. These large bandwidths cannot be provided by the regular allocated slot in X-Band (7.8 - 8.5 GHz) even when both polarization are exploited.

UTILIZATION OF K-BAND FOR RS

The remedy for this limited bandwidth is to utilize K-Band (25.5–27 GHz) which includes 2.5 GHz of continuous bandwidth in each polarization. This natural development is similar to the exploitation of Ka–Band in commercial satellite communication which started a decade ago.
For newly planned ground stations, the TM/TC chains will mostly remain in S-Band (Rx=2200-2300 / Tx=2025-2120MHz) whereas high speed data are down linked in X- or K–Band. In addition to the TM/TC transmit and receive chains in S-Band, the Antenna System requires autotrack, hence the feed system of the Antenna supports monopulse tracking in all three bands in order to precisely track the LEO or MEO spacecraft with an accuracy of a few tenths of a millidegrees. Simultaneous tracking in S and K-Band enables to utilize these large Antennas for acquisition aid support.

K-BAND READY

It is expected that in the near future operators of RS ground stations will require an upgrade from S-/X-Band to S-/K-Band or even S-/X-/K-Band.
In order enable to upgrade an existing S-/X-Band Antenna to S-/K- or S-/X-/K-Band, the mechanical properties of the Antenna are required to meet stringent requirements for mechanical stiffness, pointing error and reflector surface accuracy.
In addition, the Servo & Drive system should be able to support precise monopulse tracking as the tracking accuracy requirements for K-Band are much more stringent compared to X-Band.
VA delivers full motion Antennas which are suitable for K-Band operations, as various analyses are conducted

DOI 10.5162/etc2016/7.3

during the design phase such as wind,- temperature,- gravity changes, pointing and tracking accuracies. Internal design optimization routines and tools result in a very rigid mechanical structure which is required to comply with the K-Band requirements.

These Antennas are inherently “K-Band Ready”.

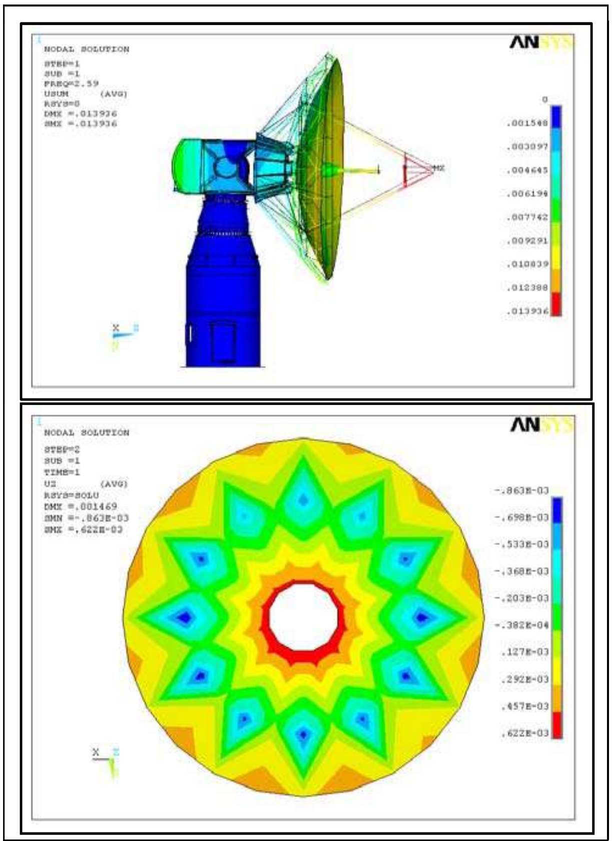

Figure 1. Examples of structural analyses

A VA Antenna initially equipped for S-/X-Band operation can be converted into S-/X-/K-Band by changing only the feed system and LNA`s; no further improvements or upgrades of the mechanics or Servo & Drive system or top the reflective surface are required.

FEED SYSTEM DESIGN

The feed system has a coaxial architecture. It comprises an optimized junction for S- and X-band with TE11-Mode (sum) / TEM-mode (difference) and a conventional K-Band waveguide network with a TE21 tracking coupler. The X-Band network has been integrated as waveguide solution. An integrated waveguide to coax transition in S-Band leads to a compact and highly integrated coaxial S-Band network solution.

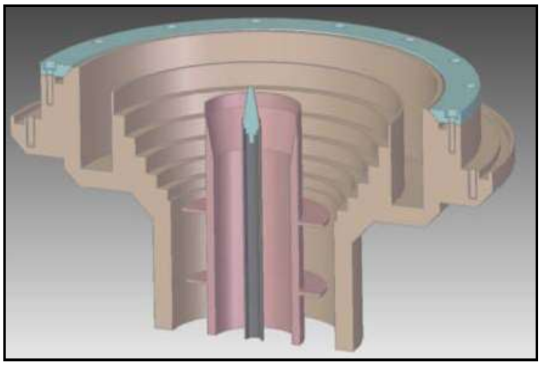

Figure 2. Coaxial S-/X-/K-Band Horn structure

The feed components such as the diplexers, OMT`s and monopulse couplers are housed inside the feed cone. The S-Band diplexers are folded in order to keep the physical length as small as possible. The feed system incorporates S-Band 2Tx/2Rx plus MP port; X-Band 2Rx plus MP port, K-Band 2Rx plus 2MP ports in total 12 ports.

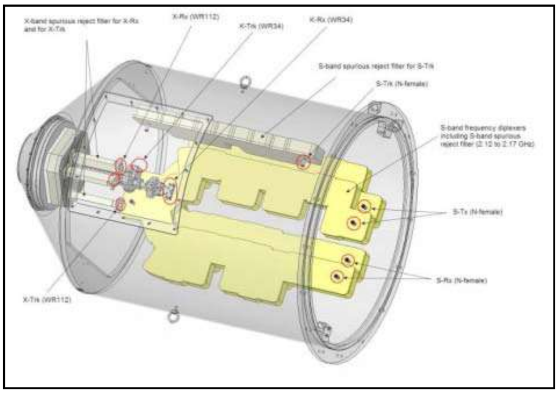

Figure 3. S/X/K-Band Feed System with 12 ports

Fig. 2 and 3 are shown with courtesy of Mirad microwave AG.

ANTENNA GEOMETRY

The geometry of the Antenna System utilizes a ring focus design which allows for a very compact arrangement of the radiating horn and subreflector. Another advantage of a ring focus design is that the Antenna can simultaneously achieve high efficiency values in all three bands.

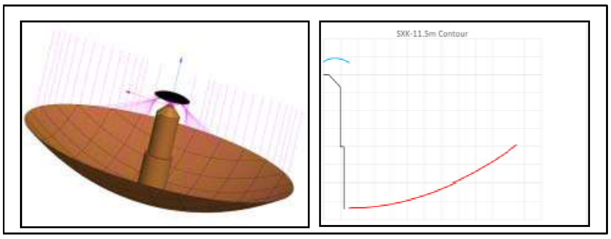

Figure 4. Ring focus geometry and shaping

DOI 10.5162/etc2016/7.3

MEASURED RF - PERFORMANCE

Due to the fact that the performance of the Antenna can be modeled and optimized in all three bands individually without compromising each other, the Antenna efficiency in all three bands is quite high. The measured results of the 11.5 meter tri-band Antenna System are depicted in the next table.

- RX Frequency	2.200	2.300			8.025	8.400	25.500	27.500	GHz
- TX Frequency			2.025	2.110					GHz
Antenna Gain at Feed output	45.8	46.1	45.2	45.2	57.7	58.0	66.5	67.1	dBi
Figure of Merit (G/T)	23.5	24.2			37.2	37.3	41.9	42.5	dB/K

Table 1. Measured RF values of 11.5 m S-/X-/K-Band Antenna System

The Receive patterns in X-Band for the sum and delta signals have been measured with a beacon of a geostationary satellite which was outside of the receive band hence the dynamic range of the measurement was poor.

All patterns in show excellent symmetry and the sidelobes are well below the 29-25log (theta) envelope. Some examples of pattern measurements are depicted here:

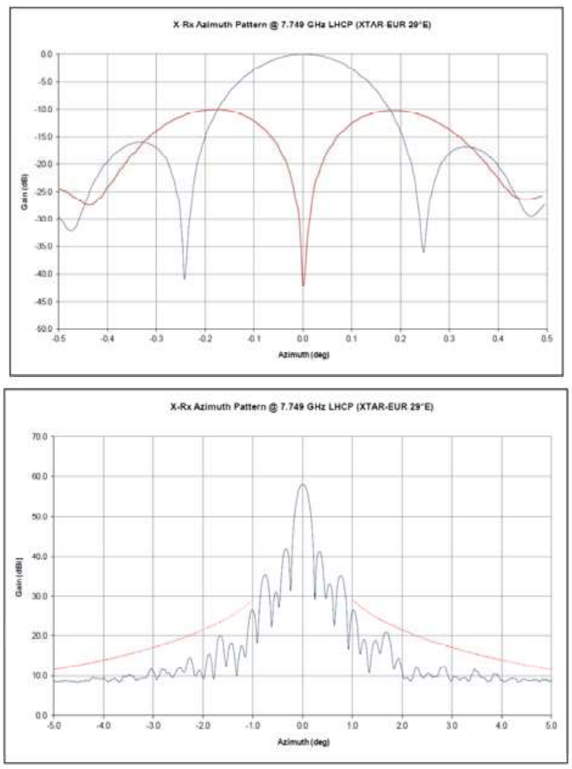

Figure 5. Some Antenna patterns

Figure 6. 11.5 m S-/X-/K-Band Antenna System installed and ready for operation

DOI 10.5162/etc2016/8.1

Instrumentation for Outer Measurements in Aeronautical Applications

Alain LAURENT, Technical manager at LMSM
LMSM 42 avenue Paul Cézanne 13090 Aix-en-Provence, France
lamesuresurmesure@orange.fr

Abstract:

Measuring a lot of in flow wall parameters (more than thousands like pressure, acoustic, temperature, vibration…) needs to set up sensors on the outer airframe skin where temperature is as low as -40°c (-40°F), flow Mach number as high as 0.92 and dynamic pressure as high as 320 hPa. The installation has to avoid any disturbance of both the flow and the measured signals.

But setting up sensors and connecting them to a data acquisition system which has to be powered is very time consuming. For a flight test, a lot of data had to be extracted in order to analyze them. LMSM has developed a system for solving such challenge by sticking the whole system (power, acquisition system, control system and wireless downloading). Thanks to its CaptiFlex™ technology, tested by DGA EV in flight (www.captiflex.fr), it avoids any hole into the airframe and it allows different kinds of sensors to be housed in a same CaptiFlex™ device.

Our paper will detail a new autonomous power and wireless system for taking highly resolution pictures of a commercial Aircraft leading edge during long term experimentation (14 months)

The system operates at flight temperature (-40°C up to 70°C) and includes a power supply, a micro-camera, control system and software, and a CaptiFlex™ architecture allowing the system to be to stick down the outer skin of an aircraft.

The system is very fast to install and cuts the costs not only in workshop but also for the program by getting more flight parameter values at the same time.

Thanks to Clean Sky and Airbus collaboration and thanks to Captronic support, LMSM has achieved the requirements of this very innovative solution which is now a product adaptable to other applications.

Key words: Autonomous energetic system, Micro-Camera, flight test instrumentation, HD photo, system plug and play.

Introduction:

The dream of the instrumentation staff is to have a “plug & play” system fast to install and easy to maintain.

The dream of test engineers is to collect the more measured parameters as possible and to exploit them just after the end of the flight.

The dream of the pilot is not to be disturbed by the flight test instrumentation and so having one which is thin and as light as possible.

The dream of program manager is to minimize test costs and test duration.

Are these dreams compatible? Yesterday the answer was No, but by now the answer is Yes.

With conventional technology, if you want to set up sensors on the outer skin of a wing, you need sensors (highly cost), and inboard data acquisition system, a power source from the aircraft, and a lot of time and workload both for design (where and how wires go through the aircraft) and installation. During this last phase, aircraft is under a hangar and does not fly and so it has no productivity.

In order to cut the flight test costs and their duration, we propose a “plug & play” system which is stuck on the outer skin of the aircraft and includes an autonomous power system able to meet the power need, an acquisition system for collecting data, a control system software for saving measurements with wireless data transfer capabilities capable of downloading measurement data in few minutes.

Many configurations exist to take up such a challenge as, for instance, those illustrated by the following bloc diagrams:

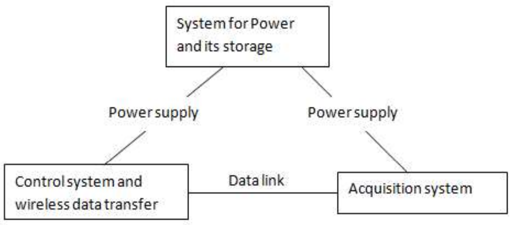

Exemple of bloc diagram 1

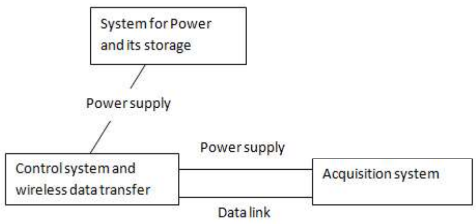

Exemple of bloc diagram 2

The Clean Sky project implements one of these architectures and provides an autonomous micro camera system intended to be mounted on the outer skin of a commercial aircraft. The project was supported by the European Clean Sky program and the French Captronic organization.

Clean Sky topic: “Camera development for in-service monitoring of leading-edge contamination”:

The Clean Sky Smart Fixed Wing Aircraft Integrated Technology Demonstrator (SFWA-ITD) consortium is interested in understanding the typical level of contamination and minor damage to a wing leading-edge in operational service.

Ideally this would include improved information about the rate of insect or other contamination and its currently unknown dependence on altitude, climatic zones, seasons and environment as well as the cleaning impact of flight through rain, or clouds and any impact of WIPS (Wing Ice Protection System) operation.

In this call of proposals topic, one has to develop a compact and autonomously working camera system suitable to record the contamination on the wing leading-edge. The camera system will be installed on a short-range or long range aircraft at a position to view a section of the wing leading-edge. The system will be used to perform camera recordings during regular operational flights.

One has to develop an autonomous high resolution micro camera system for the installation on an in-service aircraft that can view a section of the wing leading-edge (either a fixed leading-edge or the leading-edge of retracted slats). To ensure an adequate field of view it is proposed to install the camera in a fairing at the fuselage or pylon.

The camera system should include the following components: camera, power system, memory and control system, mount for all components, aerodynamic fairing to cover the complete camera system.

One has to ensure installation of the camera system and fairing during an overnight check without the necessity of permanent changes to the aircraft structure.

The selection of the camera equipment will be under the consideration of typical operating conditions during the flight.

The viewing area should be about 500 mm span by 250 mm chord and the span wise location should be defined to suit the camera choice and installation.

One has to provide the camera and ensure camera view to be of suitable quality to be able to capture insect contaminations within the recordings. A minimum spatial resolution of about 4 px/mm will be needed as typical insect residues have the size of about 1 mm in lateral direction.

One has to provide recording equipment that operates fully autonomously without external power source for the expected number of days away from the home base or until down loading of data is practically possible. System ensures that recording equipment take pictures every 10-60 seconds during climb-out and descent and every 15 minutes during cruise.

System has to record altitude for each image (e.g. GPS sensor) and ensure allocation of altitude data to the recorded images. Time (GMT) and date to be inserted on the images.

System has to ensure easy access to data storage (e.g. wireless data reading to avoid necessity of camera access).

The certification of this micro camera system is due by the “Airbus Deutschland” Topic Manager.

Further requirements during the development

During the development the system was further improved so as to meet the following requirements:

- The viewing area was increased to 800 mm/1000 mm span which is about twice the initial requirement.
- Pictures have also to be taken during the takeoff and landing phases, every ten seconds.
- The aircraft can be an A320 and its slats are extended during takeoff and landing phases.
- There are about 5 flights a day and about 100 pictures are to be taken during each flight. Data downloading must be performed only every two days.
- The camera must be arranged on the fuselage at 4 m from the middle of the leading edge.
- Monitoring will be performed during 14 months except December and January months.

The A320 flight domain temperature is between -38°C and +45°C, the cruise Mach number is M0.78, the cruise speed goes up to 220 m/s, the cruise altitude is 33 000’ and pressure varies from 250 hPa to 1500 hPa.

These updates led to:

- A three times greater viewing area and the same increase in picture volume, and their consequences on the allocated data storage and power required for the wireless data transfer.
- Improvement of the camera in order to achieve the high spatial resolution required.

and to take up the following challenges:

- Designing a power system working at low temperature (about -40°C) and at low pressure (250 hPa) for supplying enough power for two days.
- Identifying automatically flight and ground phases that are not known by the system. For instance the landing phase begins respectively at 3010’ before landing in Marseille-Marignane arrival and 4400’ before landing in Zurich.
- Providing high picture resolution at 4 m.

- Adapting the CaptiFlex™ technology to the micro camera system. CaptiFlex™ is a technology allowing sensors to be installed on the outer skin of airframe.

Project management:

The technical project was organized in 4 Work Packages:

- Camera and control system
- Power system
- Integration into CaptiFlex™
- Aircraft installation

The development time was 18 months.

Results

The architecture of developed system is shown in bloc diagram 2 and has a separate power supply coupled to the control system which includes the micro camera as well as the acquisition system.

Camera

To meet the different requirements, the chosen camera has the following specifications:

- Retina sensor with 1.1 µm pixel dimension
- High quality 6-lens, f/2.2 and a 26 mm focal length
- Total thickness of about 10 mm and low weight
- Low-power camera
- Shooting time less than 5 seconds.

So, due to the 25° leading edge swept angle and greater area view, the spatial resolution is comprised between 3 Px/mm and more than 4 px/mm. Each picture has at least a 3MB volume.

Control system

Work at an external temperature of -40°C.

It includes Wi-Fi, a GPS and other sensors such as accelerometers.

A 32 GB memory allows to record about 10 500 pictures, with a 21 days autonomy.

During a Paris Orly-Marseille commercial flight, the system took pictures according to the following scheme: one picture every 10 s during take-off and landing, one picture every minute during climb out, no picture during cruise and one picture every two minutes during descent. During its cruise, the aircraft's altitude decreased a little down to the 30 000' limits (which is the beginning of the descent phase) and afterwards increased a lit bit over 30 000'; that is why on the following graph, pictures were taken during the end of cruise phase.

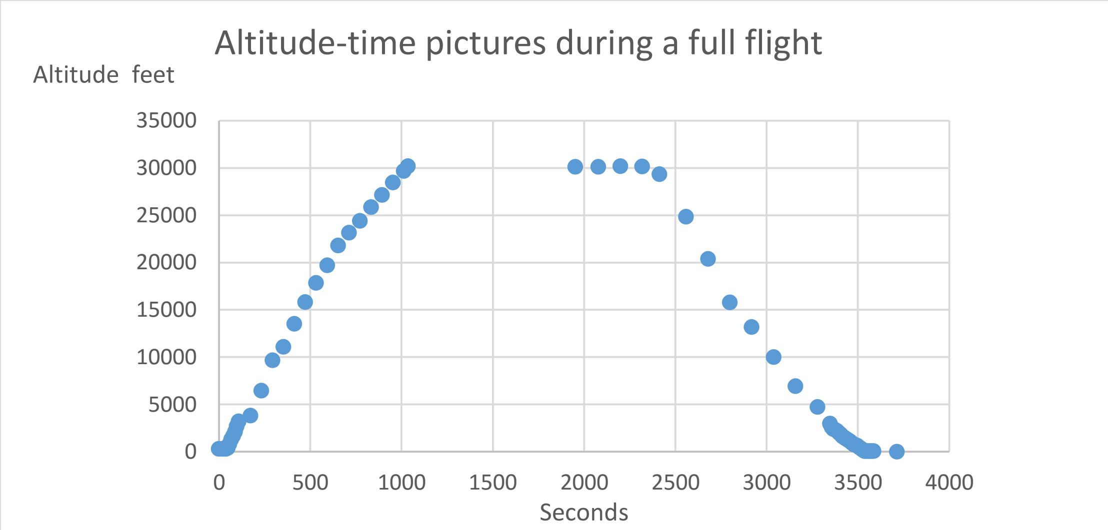

During this flight, mean power consumptions are:

Phase	Power consumption (W)
Taxi out	0.8
Take off	1.6
Climb out	0.9
Cruise	0.9
Descent	0.9
Landing	1.6
Taxi in	0.8
Parking	0.7

But some functions of the micro camera system demands power peaks from about 6W up to 20 W.

Wireless transfer:

For downloading pictures Wi-Fi is used. Test for downloading 85 pictures of about 1MB each with an ADSL link shows a transfer rate of about 700 kb/s. But for downloading 1000 pictures of 3MB each, it is insufficient.

So, the choice is to get fibre optics as internet link with a real speed of 50 Mbps at least as internet flow. Afterwards, the bottle neck is the real Wi-Fi flow. Such a solution allows transferring the two day picture records in less than about 10 minutes.

Power system:

- operates at -40°C and under low pressure such as 250 hPa
- Supplies high power peak when needed.

Integration into CaptiFlex™:

In order to match with easy installation on Aircraft and A320 flight domain constrains (temperature [-38°C ; +45°C], M0.78, FL350, [250 hPa ; 1500 hPa]), the CaptiFlex™ technology was used. It provides support sheet with adhesive tape and tapered edge on its boundaries, cavities to set up sensors and/or electronics and covers to close cavities.

Mechanical and thermal and pressure stresses were testing during flight test up to M0.92 and FL400 and dynamic pressure 320 hPa. In addition, long term lab-tests were successfully performed with a cycle of 3 h simulated flight during more than 300 cycles.

Vibration lab-tests were successfully performed under the French military GAM EG 13 standard which is equivalent to the DO 160 standard.

CaptiFlex™ EMI lab-tests and light protection were also performed under NF 17025 standard.

Installation on aircraft:

Topic Manager has the responsibilities of Certification process and installation of the micro camera system on aircraft; LMSM gives only installation procedures and will deliver technical assistance for its installation.

For the first installation of the system on a DGA EV Alpha-Jet aircraft, the duration for setting up 10 sensors was about 2 hours. Such a time matches with the installation time requirement during an overnight check.

In a few words, the installation procedure begins by mounting the system on the aircraft outer airframe.

Then, energy storage is charged and afterwards control system software is powered on.

Finally, every cover is set up on its own cavity and a waterproofing around it is performed.

Intellectual properties:

Following to Clean Sky rules (grant agreement), Foreground shall be the property of the beneficiary carrying out the work generating that foreground. So LMSM is the only owner of these technologies. As soon as the authorisation to disclose their content is granted, detail specifications of the system will be available on our website www.le-captiflex.fr.

The research leading to these results has received funding from the European Union's Seven Framework Programme (FP7/2007-20013) for the Clean Sky Joint Technology initiative under grant agreement project number 641577.

NDA were signed with Captronic and our subcontractors.

Summary:

LMSM has developed the required innovative Clean Sky micro camera system to be installed on the outer skin of an A320 fuselage. The system includes a compact and autonomous micro camera for taking high quality pictures for long periods up to 14 months with enough power; a memory and a control system; and an aerodynamic housing. An automatic control system software identifies the flight and ground phases and their corresponding picture rates. An automatic wireless transfer process with high data transfer rate is also provided, which needs only few minutes to download 3 GB of data. The system also offers a reduced installation time without permanent changes to the aircraft structure. The system also meets the Topic Manager requirements in order to achieve the SFWA-ITD aims.

Thanks to the new technologies and solutions implemented during the development of the system, the “stick and measure” concept is now a reality. LMSM products are available and thanks to its know-how and design methodology they can be adapted to various other configurations or applications.

DOI 10.5162/etc2016/8.2

Wireless Data Acquisition in Flight Test Networks

Diarmuid Collins
Curtiss-Wright
Corporation
Dublin, Ireland

ABSTRACT

The use of wireless data networks is ubiquitous in the consumer world. They have gained significant traction due to advantages afforded by the lack of wires. These same advantages can prove valuable in Flight Test for data acquisition. Sensor nodes are ideal candidates for low bandwidth wireless networks. Located in remote, hard to reach and hostile environments, wirelessly acquiring data from such sensor can solve a number of existing issues for FTI engineers. Implementing such wireless communication introduces a number of challenges such as guaranteeing reliable transfer of the sensor data and time synchronization of the remote nodes. This paper addresses wireless sensor acquisition, the associated challenges and discusses approaches and solutions to these problems.

Keywords: WSN, Wireless Sensor Networks, LXRS, Wireless LAN

1 INTRODUCTION

Flight Test Instrumentation (FTI) systems extensively utilize wired networking technologies because they are a proven technology; however, in a number of scenarios wired networks present significant shortcomings. Most of these shortcomings, ironically, relate to the unavoidable fact that the networks involve wires.

One of the most significant of these limitations is accessibility, in a number of scenarios it is simply not possible to route a wire to a remote sensor thereby making acquisition impossible. Another limitation is weight. As networks increase in size and complexity, the weight of the wires contributes to a significant proportion of the total weight of the acquisition system. Additionally, the inflexibility of a wired network is another aspect which limits the utility of such a system and can significantly increase the cost of testing.

Wireless networks alleviate many of these issues. The ability of the wireless network to easily and quickly change its topology and augment an already installed network is a significant advantage that wireless brings. This paper will examine these issues and will propose solutions based on wireless technology. In particular, solutions involving wireless sensor networks will be addressed.

2 WIRELESS DATA ACQUISITION SCENARIOS

There are a number of specific use cases that can be considered for wireless data acquisition. Addressing these scenarios can help to identify the particular requirements for each scenario and therefore help in selecting the most suitable technology. The following are a list of uses cases identified in FTI

2.1 USE CASES

1. Wireless Sensors: Remote sensors gather measurements and the data is transmitted to a wireless data acquisition user module that allows the measurements to be transmitted on the wired network
2. Point-to-point Wireless Data Acquisition: Data acquired from various sensors and busses is acquired in a wireless remote DAU. The acquired data is then transmitted wirelessly to a receiving wireless DAU.
3. Wireless Bridge. Two wired Ethernet networks can be bridged using a wireless link. This allows two networks which may be physically impossible to connect, be bridged using a wireless link.
4. Wireless Access Point: Multiple remote wireless RDAUS can associate with an Access Point and transmit the acquired data wirelessly to the access point. An access point is typically a router and a wireless bridge in the one unit. This unit also allows wireless clients such as real time analysis PCs connect to the FTI network.
5. Wireless Data Mining: A PC with a wireless network card can connect to the FTI network to mine the data recorded from the acquisition system.
6. Telemetry: A long-range Ethernet link to the ground to allow part of the acquired data be transmitted to the ground as well as commands sent to the FTI network.

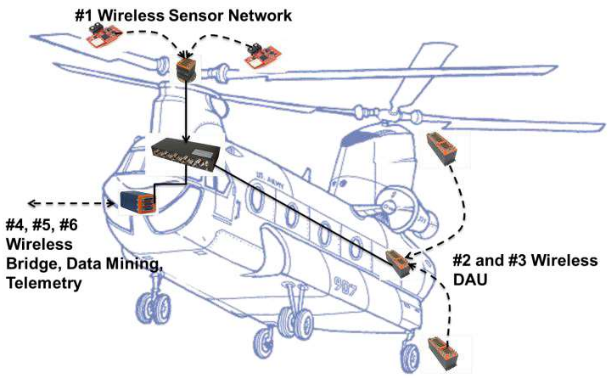

Figure 1 Wireless Acquisition Scenarios

2.2 FTI SPECIFIC CHALLENGES

Wireless networks in commercial spaces have already addressed a number of the issues which wireless communications systems encounter. Network contention is primary among these. Many protocols use a Carrier Sense Multiple Access with Collision Avoidance (CSMA/AC) schemes as a channel access method. This mechanism introduces packet latency, packet loss and a reduction in the transmit determinism and still may suffer collisions due to the hidden terminal problem or simultaneous transmission. These are all undesirable factors in FTI networks, where guaranteed delivery of packets, is a strict requirement. As a result, mechanisms to mitigate against packet loss should be accounted for in FTI wireless networks.

The variability in the packet delay through the network has a significant impact on time synchronization mechanisms such as Precision Time Protocol (PTP) [1]. PTP is a widely used time synchronization mechanism in FTI networks, allowing remote data acquisition units to be synchronized accurately to a common time source. In replacing wired links with wireless connections, the time synchronization of remote DAUs need to be maintained or replaced with equivalent schemes.

DOI 10.5162/etc2016/8.2

3 WIRELESS TECHNOLOGIES

There are a number of wireless standards that are currently in use in the commercial world. To match the FTI scenarios previously identified to wireless standards, it's important to compare these standards, identifying advantages and disadvantages.

3.1 WIRELESS LAN

IEEE 802.11 is a set of standards that operate primarily in the 2.4GHz and 5GHz bands. This standard is commonly known as Wi-Fi, and widely used in the office and at home. There are a number of protocols defined using this standard, currently the most widely used being 802.11g and 802.11n. The key features are briefly summarized here

	802.11b	***802.11g***	***802.11n***	***802.11ac***
Release	1999	2003	2009	2014
Frequency (GHz)	2.4	2.4	2.4/5	5
Max Data Rate (Mbit/s)	11	54	150	1000+
Modulation	DSSS	DSSS, OFDM	OFDM	OFDM
Range (LOS m)	100	100	250	

Figure 2 Wi-Fi Standards

The key features that Wi-Fi brings are relatively high data rates and wide adoption in the commercial world. The data rates approach or exceed 100Base-T Ethernet rates, making it suitable for scenarios where significant data is transmitted such as a Wireless Network bridging and Wireless Access Points. However with such data rates, come significant power requirements. A single chip WLAN module could easily draw up to 1000mW when transmitting at 802.11g data rates. [2] For devices line-powered this could be acceptable but for battery powered devices which need to remain autonomous, this is quite high power consumption. For wireless sensor networks, the combination of high data rates and high power consumption is not ideal.

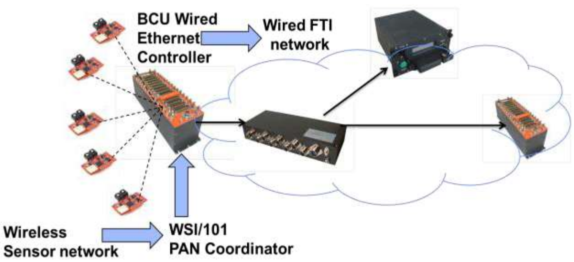

Figure 3 Zigbee Acquisition Module

3.2 ZIGBEE

Zigbee is a networking standard generally used for low data rate, home automation and industrial control applications such as lighting control. It is based on the IEEE 802.15.4 radio standard and supports applications that require periodic short data transfers up to 250kbit/s over distances to 75m. The standard provides for low end-to-end latency and is a

DOI 10.5162/etc2016/8.2

relatively mature standard. However there are still a number of shortcomings in the standard that has been explored in previous papers and experimental developments. [3] Contention when accessing the network has a significant impact on the aggregate data rate. Time synchronization of the remote Zigbee nodes is also not part of the standard, whereas accurate timestamping of wireless samples in FTI is crucial. Zigbee provides a very interesting option for Wireless Sensor Networks while not having the complete answer.

3.3 BLUETOOTH

Bluetooth is another wireless standard for use over short distances. It's was originally standardized as IEEE 802.15.1 but is now maintained by the Bluetooth SIG. Data is transmitted using a Time Division mechanism which makes is suitable for FTI wireless sensor networks. Bluetooth is generally considered a short-range communication protocol which is typically less than 10 meters. However the radio uses a frequency-hopping spread spectrum mechanism, which can complicate regulatory compliance in a tightly regulated environment on a plane.

3.4 ANT+

ANT is a proprietary wireless technology developed by Dynastream Innovations. It's a targeted at low data rates using a TDM system in the 2.4GHz spectrum. The data rates supported are quite low (~20kbps) which limit the application area.

4 WIRELESS SENSOR NETWORKS

A Wireless Sensor Network (WSN) is network of spatially distributed sensors that monitor physical or environmental conditions such as temperature, pressure, strain, etc. These wireless sensors transmit the acquired data to an acquisition system. Wireless sensors are typically small with ultra-low power requirements running on batteries or utilizing energy harvesting schemes.

The ease of installation of wireless sensor networks brings advantages to debug or temporary installs. The install time for a wireless sensor network is quicker than a wired network. Furthermore, modification of an existing sensor network is significantly quicker than modification of wired installs. This has been demonstrated in a Cabin Comfort install on the A350 MSN2. [4]

4.1 DATA SOURCES

Typically sensors are sampling analog data sources with varying profiles of data rates.

- Acceleration. Typical accelerometers contain multiple channels to measure on three planes of motion. Sampling rates vary but can reach rates of kHz. As a result they can be quite demanding on bandwidth.
- Temperature. In many scenarios, temperature changes are relatively slow allowing low sampling rates.
- Strain. Similar to accelerometers, strain measurements range from very low sampling rates measure in samples per hour to hundreds of Hz.

In many of these measurements the acquisition systems follow a similar approach. The data is sampled, some signal conditioning is performed

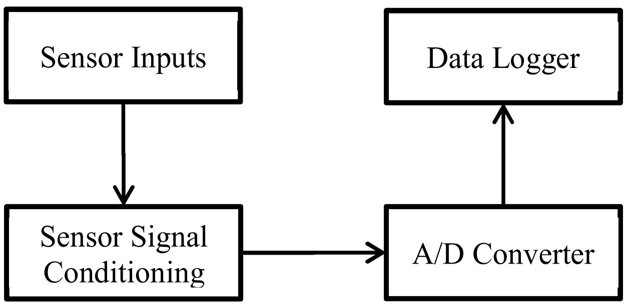

Figure 4 Signal Acquisition

DOI 10.5162/etc2016/8.2

and the resulting data is logged. The signal conditioning can vary between applications and installations so should be programmable.

4.2 LXRS

As previously mentioned there are a number of wireless protocols that can be used for wireless sensor networks, however many come with limitations. An alternate approach is to use a proprietary wireless protocol that specifically addresses these limitations. LXRS is a wireless communication protocol which is designed for (but not limited to) the IEEE 802.15.4 communication standard. LXRS describes a method for guaranteed data delivery, mitigation of channel contention, and measurement synchronization. All of which, are essential features of a wireless measurement system..

4.2.1 Medium Access Control

Data transfer using the LXRS protocol follows a Time Division Multiplexed (TDM) approach. The bandwidth on the network is divided into time slots. Each sensor node on the network is programmed to transmit only during the assigned time slot. Multiple time slots can be assigned to a node to meet the aggregate data rate requirements of the node. This approach removes the impact of collisions to the data transfer, increasing the determinism and network throughput while significantly reducing the number of retransmits.

4.2.2 Time Synchronization

In FTI networks, the accuracy of timestamping of analog samples is a key requirement. The ability to synchronize and align samples taken from a wireless sensor with samples from standard wired sensors is crucial in the analysis of the acquired data. To achieve this on the wireless sensor network, the LXRS protocol supports time synchronization accuracy of ±32 microseconds. Upon startup, all sensor nodes within the network synchronize their sampling intervals to a broadcast beacon signal from the wireless gateway. The wireless sensors use high precision real-time clocks to maintain time stability between beacon re-synchronizations which occur every 20 seconds. In a setup where the Wireless gateway is integrated into a wired Ethernet network, the source time could eventually come from a PTP grandmaster.

4.2.3 Data Integrity

While implementing a TDM based data transfer mechanism reduces packet collisions between wireless nodes, due to the nature of wireless networks, elimination of all packet loss is still a significant challenge. The channel environment itself posts a number of challenges which a communication system needs to overcome. Specifically, due to a changing environment with multiple transmission paths, the wireless signal can suffer serious degradation which varies over time. Sensors can be moved or physical obstructions can temporarily interfere with transmit and receive paths. Temporary radio interference from other transmission sources may also cause packet loss.

LXRS includes a mechanism for overcoming the packet loss due to these temporary interference scenarios. Packets which are successfully received by the wireless gateway are acknowledged in a handshaking mechanism. Each wireless sensor contains some non-volatile memory in which the wireless samples are stored. Packets that are not acknowledged remain within NVM on the node and are scheduled for retransmission at later time. The time-stamping of the sample is also recorded so that the timestamp matches the sampling time and not the transmit time, meaning that the timing fidelity of the measurement is maintained despite being buffered.

4.2.4 Extended Range

WSN which been designed to utilize LXRS have also been designed to support a larger transmit range. The transmit range is a function of the transmit power and the nature of the environment. In a line of sight application the range is between 1.5 km and 2 km depending on the regulatory requirements. In more confined and congested environments the effective range is reduced. Additionally, in harsh RF environments characterized by severe frequency selective fading, the increased transmit power serves to increase the reliability of the RF link by increasing the link budget.

4.3 POWER CONSUMPTION AND SENSOR AUTONOMY

The ideal wireless sensor will consume no power, allowing the sensor to remain installed with no power source or requirement to change batteries. However for the sensor to measure, process or transmit, some power will be consumed. Minimizing this power consumption will extend the time between either replacement of the battery or recharging of the battery.

The operation of the wireless sensor can be split into three distinct modes of operation

- Logging and processing of sensed data. Typically 5mW.
- Wireless transmission of sensed data. Typically 45 mW.
- Sleeping between data samples. Typically 0.02mW [5]

To maximize battery life of the remote sensor each mode of operation should be optimized. However it is clear from the figures that limiting the wireless transmission operations would have the largest impact on the battery life. By locally logging the sensed data in the wireless sensor and then transmitting a burst of samples would be a more efficient use of the battery rather than transmitting each sample. LXRS supports such a mechanism [6].

Judiciously configuring the remote sensor to sample at the minimum rate needed to meet the measurement requirement would be the next approach in maximizing battery life. With two orders of magnitude between sleep mode and logging of data, it is clear that only sampling data at the minimum required rate will maximize battery life.

4.3.1 Energy Harvesting

While the ideal wireless sensor consuming no power is not achievable, an alternate solution is to use an energy harvesting mechanism on the sensor. This would provide for a fully autonomous sensor, removing the requirement for battery replacement or recharging. However the efficacy of such a device is highly depended on the amount of non-electrical energy (vibration, thermal gradients, cyclical strain, etc…) found within the environment. Each harvester requires a significant level of customization to operate within specific scenarios.

Due to the power consumption of the measurement and transmission system, this facility is best suited to low sampling rate measurements like strain or temperature. At 10Hz it has been shown than power consumption of a wireless sensor node can be implemented at 90µW [7]. This level of power can be satisfied by piezoelectric energy harvesters or photovoltaic sources.

Higher samples rates have been achieved in a number of applications including monitoring the loads on pitch-links continuously at 128 Hz [8] and rotor system vibration periodically at 4 kHz. [9]

4.4 INTEGRATION IN ACQUISITION SYSTEMS

The Wireless Sensor Network, once acquiring data from remote sensors, needs to be integrated into the same acquisition system as all the wired sensors, forming a homogeneous network.

This includes:

- Programming the WSN using standard network protocols such as TFTP and SNMP.
- Transmitting acquired data using the same packet formats, for example IENA or iNet-X.
- Time synchronization using PTP or NTP.

With modern open standards such as XidML [10], it is possible to store information on how data is acquired, processed and transmitted in an FTI network. When used in combination with configuration software such as DASStudio [11], it is possible to configure and acquire data from WSN, just as easily as from wired sensors.

Once recorded, the source of parameters, whether wired or wireless, is transparent to the FTI engineer analyzing the results. This makes it even easier to move between wired and wireless sensors.

5 CONCLUSION

It is trivial to imagine a number of scenarios in which wireless technology can solve existing FTI problems or make existing solutions more flexible, efficient and cheaper. However the introduction of wireless technologies will not be without its challenges. In Wireless Sensor Networks, reliable transmission of acquired data and time synchronization issues present challenges which can be addressed using wireless standards such as LXRS. Integration of such protocols into existing network infrastructure is possible by using acquisition modules like the Curtiss-Wright KAM-500 module, the KAM/WSI/104. The gains that wireless sensor networks promise provide an attractive goal for the move to wireless.

6 REFERENCES

[1] N. Cranley and D. Corry, "Analysis and Application Scenarios for Telemetry Data

Transmission and Synchronization over Wireless LAN," in *ITC*, 2008.

[2] Redpine, "RS9110-N-11-03 802.11abgn WLAN Module Data Sheet," 2012. [Online]. Available: http://www.redpinesignals.com/pdfs/RS9110-N-11-03/RS9110-N-11-03_Module_DataSheet_v1.31.pdf.

[3] N. Cranley, "Experimental Investigation of Wireless Technologies for Data Acquisition," *ITC.*

[4] J. Galibert, A. Plo and S. Garay, "Cabin Comfort Flight Tests Installation," *ETTC,* 2015.

[5] S. Arms, C. Townsend, J. Galbreath and A. Newhard, "Wireless Strain Sensing Networks," in *European Workshop on Structural Health Monitoring*, Munich, 2004.

[6] LORD MicroStrain, "LXRS Data Communications Protocol," 9 July 2013. [Online]. Available: http://files.microstrain.com/Wireless-Sensor-Networks-LXRS-Data-Communication-Protocol.pdf.

[7] Microstrain, "Power Management for Energy Harvesting Wireless Sensors," 2005.

[8] S. Arms, "Tracking Pitch Link Dynamic Loads with Energy Harvesting Wireless Sensors," 2007. [Online]. Available: http://www.microstrain.com/sites/default/files/applications/files/Wireless-Energy-Harvesting-Pitch-Link-Load-Monitoring.pdf..

[9] D. Wells, "Development of a Helicopter On-Rotor HUM System Powered by Vibration Energy Harvesting," *40th European Rotor Forum (ERF2014),* 2014.

[10] "XidML," [Online]. Available: http://www.xidml.org/.

[11] Curtiss-Wright, "DAS Studio 3," 2015. [Online]. Available: http://www.cwc-ae.com/product/das-studio-3.

DOI 10.5162/etc2016/8.3

Ariane 5 Space Launcher Vehicle Equipment Bay Wireless Sensor Network Telemetry Subsystem with Smart Sensors

Hendra Kesuma[1], Johannes Sebald[2], Tejas Ahobala[1], Steffen Paul[1]
[1] Institute of Electrodynamics and Microelectronics,
(ITEM) University of Bremen, Germany
{kesuma, steffen.paul}@me.uni-bremen.de, tejas.ahobala@gmail.com
[2] Engineering Upper Stage Avionics,
Airbus Defence & Space Bremen, Germany
johannes.sebald@airbus.com

Abstract:
In this work we show the design and implementation of an efficient telemetry subsystem for Wireless Sensor Networks inside the Vehicle Equipment Bay (VEB) of the ARIANE 5. The telemetry subsystem is utilizing infrared data communication and consists of various smart sensor chips such as temperature sensor, humidity sensor, visible light intensity sensor, infrared light sensor, acceleration sensor, air pressure sensor and 10 bit analog to digital (ADC) input for analog sensors. The heart of the telemetry subsystem is a microcontroller for controlling the smart sensors and power management. The Multi Layer Insulation (MLI) that covers part of the VEB and the strong requirements to minimize the electromagnetic interference inside the launcher made infrared data communication preferable over classical RF narrow band communication. Other factors like low complexity of the infrared system compared to UWB systems are also taken in consideration. The data received by an Access Point (AP) is processed before being forwarded to a Data Concentrator.

Key words: Smart Sensor, Avionic Gateway, Wireless Sensor Network, Infrared, Multi Layer Insulation, ARIANE 5 and Launcher.

I. Introduction

The main part of this work is done to be used by a project called Reliable Sensor Network (RSN) in the frame of European Agency's Program called Future Launchers Preparatory Program (FLPP) [1,7] that maintains long term independent access in space technology and increases European competitiveness in the worldwide space launcher market.

The telemetry subsystems is combined with wireless technologies such as Ultra-wide Band and Infrared. Commercial components are used in combination for the space electronics to build the subsystems. This is intended to shorten development time and cost which is the part of the progressive restructuring European launcher industries [2]. However radiation sensitivity has to be accessed for COTS components, depending on required reliability figures and expected radiation effects.

In order to miniaturize sensor system, some sensors are replaced with commercial components.

The usage of the sensors on the Ariane 5 are categorized as following: (1) to provide information about the behavior of the rocket when flying, (2) to identify anomalies in the operation when flying, (3) to secure the position of the rocket when flying, (4) to measure the characteristics of the rocket when flying, (5) to measure the levels of environment inside the fairing, and (6) to provide a coherence and standardization of the equipment [3].

The main focus of this work is developing a telemetry subsystem for application inside the Ariane 5 Vehicle Equipment Bay (VEB) [4] that houses a significant part of the vehicle avionics and is partly covered by Multi Layer Insulation MLI [5] (see fig. 1).

DOI 10.5162/etc2016/8.3

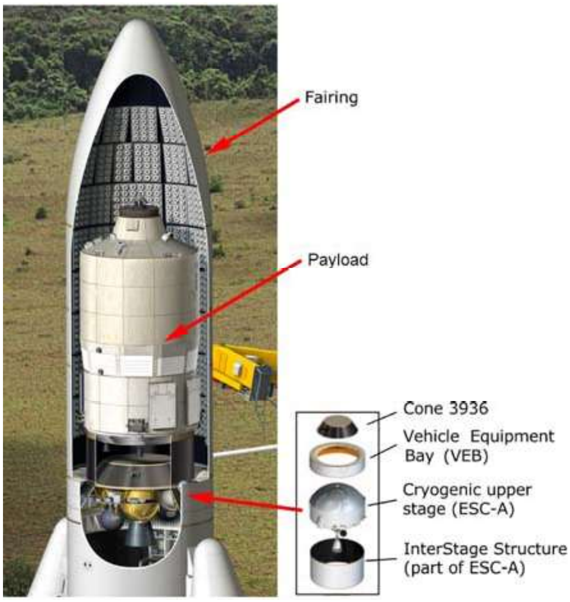

Fig. 1: The ARIANE 5 upper stage that mainly consists of Fairing, Payload and Vehicle Equipment Bay (VEB) [6].

The telemetry subsystem is developed as part of the Reliable Sensor Network (RSN) that consists of Avionic Network Gateway, Data Concentrator, Infrared Access Point, Infrared Sensor Network, Ultra-wide Band Access Point, UWB Sensor Network, Smart Sensors and some wired analog sensors as shown in figure 2 [7].

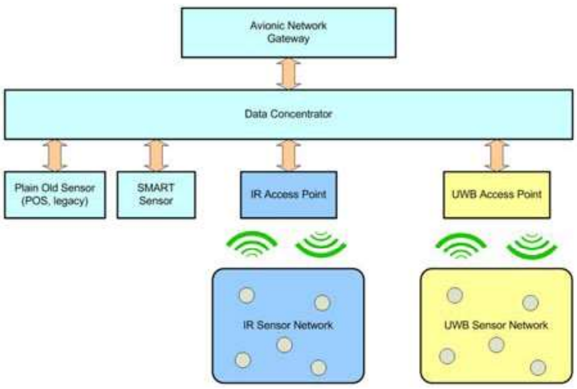

Fig. 2: The telemetry subsystems that are part of the Reliable Sensor Network within the VEB [7].

The main goal in this project is to achieve a reliable wireless sensor system design. As reference the following measurements have been foreseen:

- Air pressure /temperature measurement
- 3-axis Acceleration measurement
- Infrared/visible light intensity measurement
- Air humidity measurement

The architecture, hardware and measurement results are described as follow:

II. Sensor Node Description

The telemetry sub system consists of mainly Access Point and sensor nodes. In this section the sensor node will be described in more details started with its architecture, the smart sensors attached on it and at the end is its hardware description.

A. Sensor Node Architecture

The architecture of the telemetry subsystem on the wireless sensor node is described in figure 3.

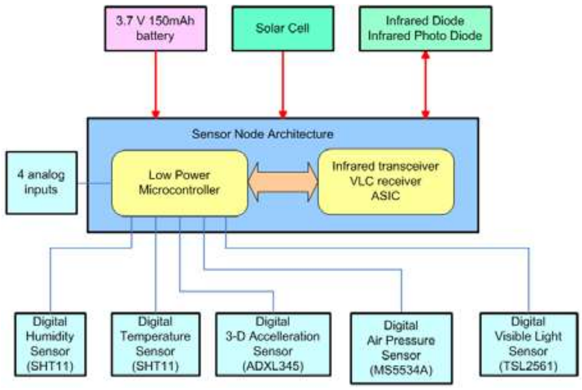

Fig. 3: Architecture of the sensor node.

The sensor node architecture consists of three main parts. The sensing part is built by a low power microcontroller connected with so called "smart" digital sensors. It also provides four analogue inputs to accommodate this kind of sensors as well. The transmission part is constructed with an self-designed ASIC, infrared transceiver and solar cell for Visible Light Communication (VLC)/energy harvesting. The power management part is supplied by a 3.7V/150mAh lithium battery and charged with a 6 V solar cell.

B. Smart Sensors Overview

There are four different kind of smart sensors tested to build the telemetry sensor node as shown in figure 4. They are a humidity and temperature sensor [8], an infrared and visible light sensor [9], a relative air pressure sensor [10] and a 3-axis accelerometer [11].

DOI 10.5162/etc2016/8.3

Fig. 4: The smart sensors overview for building the telemetry subsystems on the wireless sensor node.

C. Sensor Node Hardware description

The realization of the sensor node architecture that is built with commercial components and a self designed ASIC is shown in figure 5. The infrared transceiver are placed surrounding the ASIC to increase the signal coverage and the smart sensors are located on the left and right side of the ASIC.

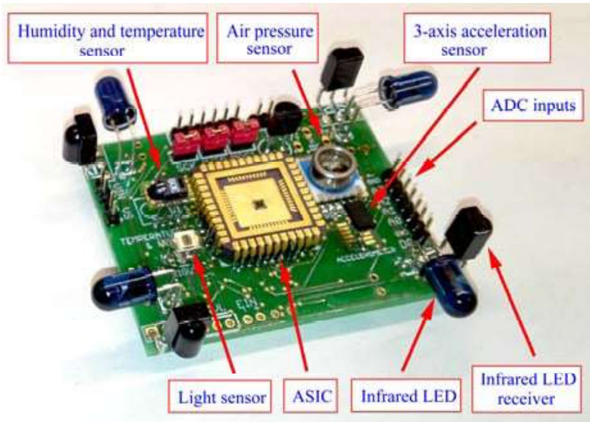

Fig. 5: The sensor node hardware description.

The casing for the sensor node that is designed with the solar cell holder is shown in figure 6. The solar cell is placed to face the incoming light that provides energy to charge the battery and carries information to initiate telemetry measurement on the sensor node.

III. Smart Sensor Measurement

The smart sensors are tested and measured to investigate their operational behaviour compared to the datasheet from the manufacturer. The discussion of the and measurement and results of each sensor are presented in the following sections.

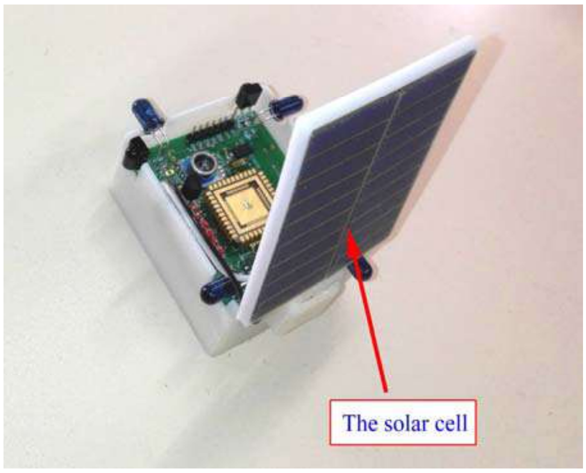

Fig. 6: The sensor node's casing with the solar cell installed.

A. Acceleration Sensor ADXL345

The 3-axis accelerometer has a maximum measurement range of ± 16 g. With only 40 µA current consumption and typical voltage supply of 3.3 V, it reaches a resolution of 4mg/LSB with 13-bits output data for each axis. The sensor measures static acceleration of gravity, dynamic acceleration from movement/shocks and is able to measure inclination changes up to 1° [11]. The time it takes to perform 3-axis measurement is about 1.61 ms as shown in the measurement, see figure 7.

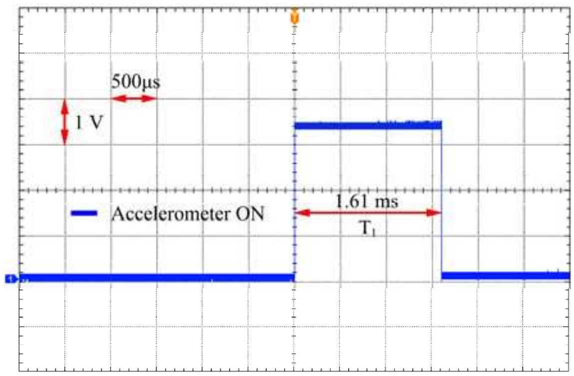

Fig. 7: The accelerometer sensor active period measurement.

In the so called the burst measurement mode the sensor takes 168 ms for 100 measurement samples. These samples are required for analysing the vibration / shock spectrum of events during flight. Figure 8 shows the active period measurement for 100 data samples.

DOI 10.5162/etc2016/8.3

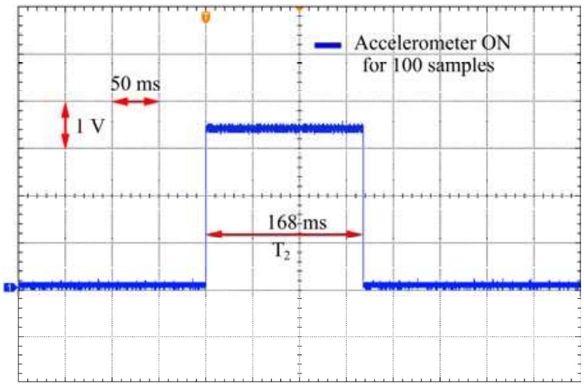

Fig. 8: The accelerometer sensor active period measurement for 100 data samples.

B. Light Sensor TSL2561

The TSL2561 converts light intensity to digital signal output providing the digital data stream via I^{2}C bus. The light sensor consists of a visible light 640 nm and a 940 nm infrared photo diode. The 16 bits data output of the sensor allows measurement up to 40,000 LUX. The current consumption during active mode is 0.6 mA with a typical voltage supply of 3.3 V [9]. During the mission, the infrared light sensor can be used to detect heat sources in the vacuum. The time it takes to perform light intensity measurement is about 32 ms as shown in the measurement, see figure 9.

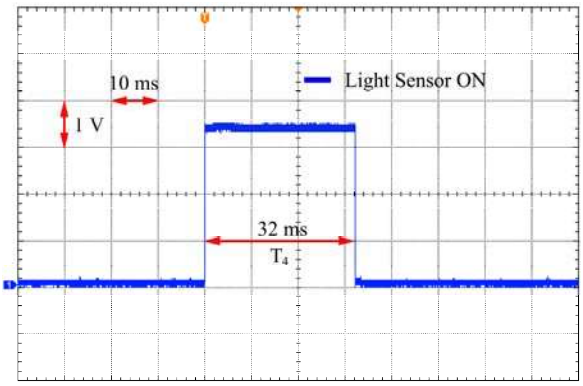

Fig. 9: The light sensor active period measurement.

C. Air Pressure Sensor MS5534A

The air pressure sensor MS5534A works with piezoresistive pressure sensing elements. The changes of the air pressure bends the membrane of the sensor, hence the values of the resistors on the membrane vary and can be measured by the electronic circuit embedded inside the sensor housing. The pressure range is 300 to 1100 mBar for this sensor. The current consumption during measurement is 1 mA at a typical supply voltage of 3.3 V. The relative air pressure sensor also incorporates a temperature sensor for linearity error correction. This correction increases the measurement accuracy to less than 1 mBar in the temperature range of 10°C to 60°C [10]. The time it takes to perform relative air pressure measurement is about 71.6 ms and is shown in the measurement, see figure 10.

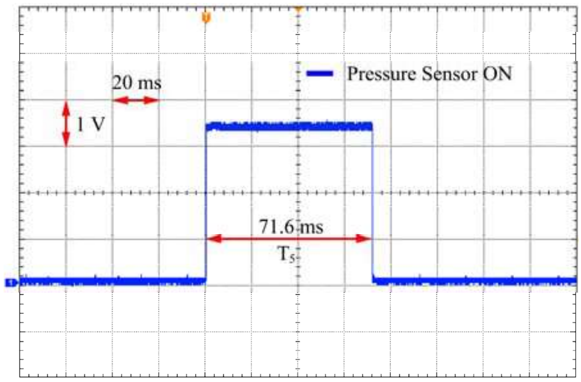

Fig. 10: The relative air pressure sensor active period measurement.

D. Humidity Sensor SHT11

The air humidity sensor SHT11 is using capacitive sensor elements for measuring the relative air humidity. A band-gap temperature sensor is embedded for a temperature compensation calculation process of the humidity data. The accuracy of the humidity measurement is ± 3%. Typical current consumption is 1 mA at 3.3 V [8]. The time it takes to perform relative humidity and temperature measurement is about 1.401 second as shown in the measurement, see figure 11.

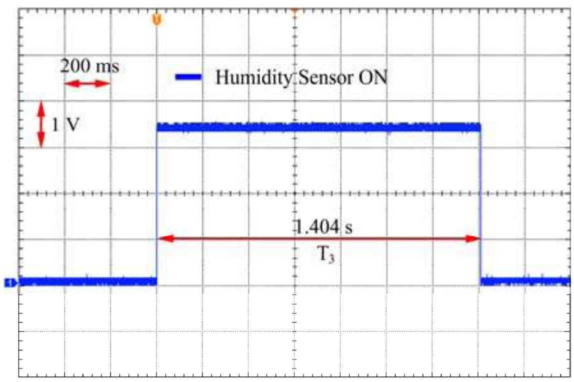

Fig. 11: The relative air humidity sensor active period measurement.

The measurement time up to 1.4 second is due to the internal measurement principle of the SHT11. The heater is turned on for the capacitive sensor calibration and it determines the humidity measurement time.

IV. Telemetry Measurement

The telemetry subsystem measurement requires Access Points that consist of Visible Light Communication LEDs and Infrared (IR) transceiver units. The description of the measurement is presented in the following section.

A. VLC and Infrared Access Point

The VLC consists of 3 high power LEDs and is controlled by a series of drivers to send the information to the solar cells of the sensor nodes. The IR transceiver at the Access Point then receives the measurement result transmitted by the sensor node. The Access Points are also able to communicate with the sensor node through infrared transmitter if the VLC is not available. Figure 12 shows the VLC and Infrared Access Point hardware.

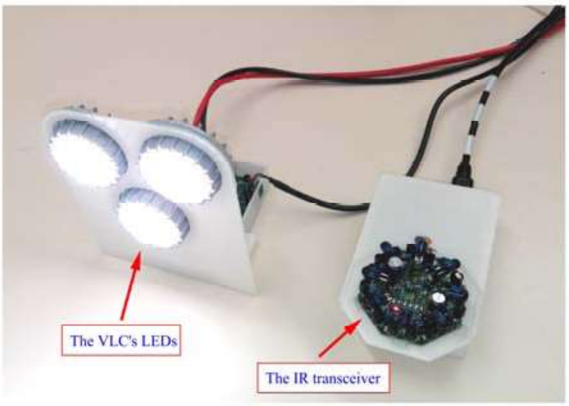

Fig. 12: The VLC and Infrared transceiver hardware.

B. Telemetry Subsystems Experiment with MLI

The telemetry subsystem experiment shown in figure 13 is utilizing the Multi Layer Insulation (MLI) to reflect the energy and information transmitted by the Access Point. The sensor node with its solar cell is placed facing a MLI surface that is covering on the experiment wall. A barrier is placed between the sensor node and the access point to prevent Line of Sight communication for the infrared and visible light.

The VLC is supplied with 0.13A and 21.7 V from a DC power supply. The goal of the experiment is to test the diffuse non line of sight visible/infrared propagation with the help of MLI reflection inside the Ariane 5 VEB [12].

The telemetry subsystem measurement sequence at the sensor node is shown in figure 14. The first sequence M_1 is to perform 3-axis acceleration measurement with 100 data samples. The second sequence M_2 is for measuring the infrared light and visible light intensity. The air pressure measurement with temperature compensation is done at M_3. The last sequence M_4 is performing a relative air humidity measurement. The total time it takes to perform the measurement cycle is 1.684 second.

The power consumption for M_1 is 132 µW, M_2 is 1.98 mW, M_3 + M_4 is 3.3 mW. The communication between the Sensor Node and Access Point is shown for the VLC and Infrared signal paths, see figure 13.

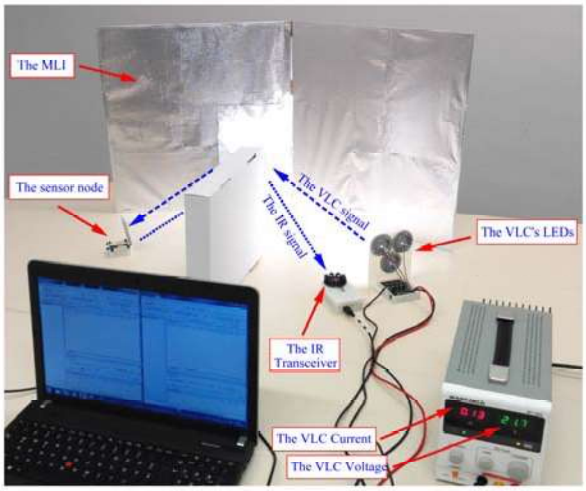

Fig. 13: The telemetry subsystems experiment setup with MLI.

The results from the measurement show that the Access Point VLC can manage to provide energy and send commands to activate the Sensor Node with the help of its solar cell. After receiving the commands the Sensor Node is able to complete the measurement sequences and send the measurement results back via infrared communication to the Access Point.

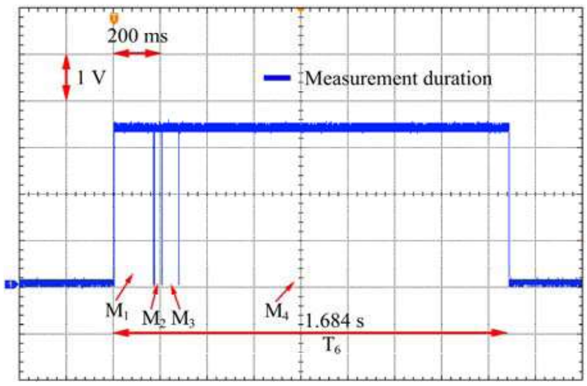

Fig. 14: The telemetry subsystems measurement sequences with the smart sensors.

V. Conclusion

The concept of telemetry subsystems with the smart sensors that is part of the Reliable Sensor Network in Ariane 5 VEB has been realized and investigated. The important results are:

- The smart sensors that measure five different physical quantities (temperature, humidity, light, pressure, acceleration) are successfully integrated in and tested within the Sensor Node.
- Each smart sensor with its required measurement period is verified by the measurement results. The 3-axis acceleration sensors requires the smallest amount of measurement time of 1.6 ms.
- The telemetry communication system can be operated in NLOS configuration using reflection at MLI for VLC and Infrared for the communication between access point and Sensor Node.
- The power consumption of maximum 3.3 mW for the sensor node measurement of all sensors is remarkable lower that the power consumption of the standalone analogue sensors used today.

Further development is planned for more compact Sensor Node size and measurement inside a flight representative VEB by the end of this year.

References

[1] *European Space Agency, “Space Engineering & Technology”, 4th January 2016.*

[2] *European Space Agency, “Next-Generation Launchers”, 9th October 2008.*

[3] *M. Trojaola, "Sensors and systems in space: Ariane 5", Fagor Sensores, Avenida de Alava s/n, 20550 Aretxabaleta, Guipuzcoa Spain, 2002. doi:10.1016/0924-4247(93)80040-N*

[4] *"The VEB for Ariane 5G's third and Last qualification flight," ESA/CNES/Arianespace, Id 209081, 2004.*

[5] *"Multi Layer Insulation Films for Aerospace," DUNMORE Corporation, 2015.*

[6] *Eduard Perez, "Ariane, 5 User's Manual," European Space Agency, Revision 1, pp. 1-271, 2011.*

[7] *H. J. Besstermueller, J. Sebald, V., H.-J. Borchers, M. Schneider, H. Luttmann, V.Schmid, "Wireless-Sensor Networks in Space Technology Demonstration on ISS", 12. Dresdner Sensor-Symposium 2015, DOI 10.5162/12dss2015/7.3*

[8] *Sensorion AG, The Sensor Company, “Humidity and Temperature Sensor IC, SHT1x”, version 5, December 2011.*

[9] *Texas Advanced Optoelectronic Solution, “Light-to-Digital Cnnverter, TSL2560”, TAOS059N, March 2009.*

[10] *Intersema, AMSYS GmbH, “Barometer Module, MS5534A” ECN 510, October 2002.*

[11] *Analog Devices, “3-axis Digital Accelerometer, ADXL345”, Revision 0, 2009.*

[12] *Fritz R. Gfeller, and Urs Bapst, "Wireless In-House Data Communication via Diffuse Infrared Radiation," Proceedings of the IEEE, vol. 67, No. 11, pp. 1474-1486, November 1979.*

DOI 10.5162/etc2016/9.1

Remote monitoring and sophisticated analysis of status data from power generators

Martin Bussas, Philipp Baum
TROUT GmbH, Parkstr.28, 34119 Kassel, Germany
m.bussas@trout-gmbh.de

Abstract

Selected power generator data, which is exchanged via CAN bus or MODBUS, is picked from the data bus by a Programmable Logical Controller PLC. Together with position data, which is provided by a separate GPS module, it is sent via Uniform Data Protocol UDP using a modem and the Global System for Mobile Communications GSM to a dedicated internet server. On the internet server, the received data is analyzed and stored in a database management system.

The content of the database is processed by a web server and can be accessed user-dependently and password-protected with any browser on personal computers, tablets or smartphones. The layout of the display automatically adjusts to the display capabilities of the terminal. In addition, static data of the device such as operating instructions and spare parts lists can be viewed.

The position data of the device is used for a geographical representation of the power supply on google maps. In addition, if the power supply is a mobile generator, a major change of the position may be used to generate a theft alarm via e-mail or text message.

Key words: PLC, GSM, GPS, power generator

Remote Monitoring and Statistical Evaluation Overview

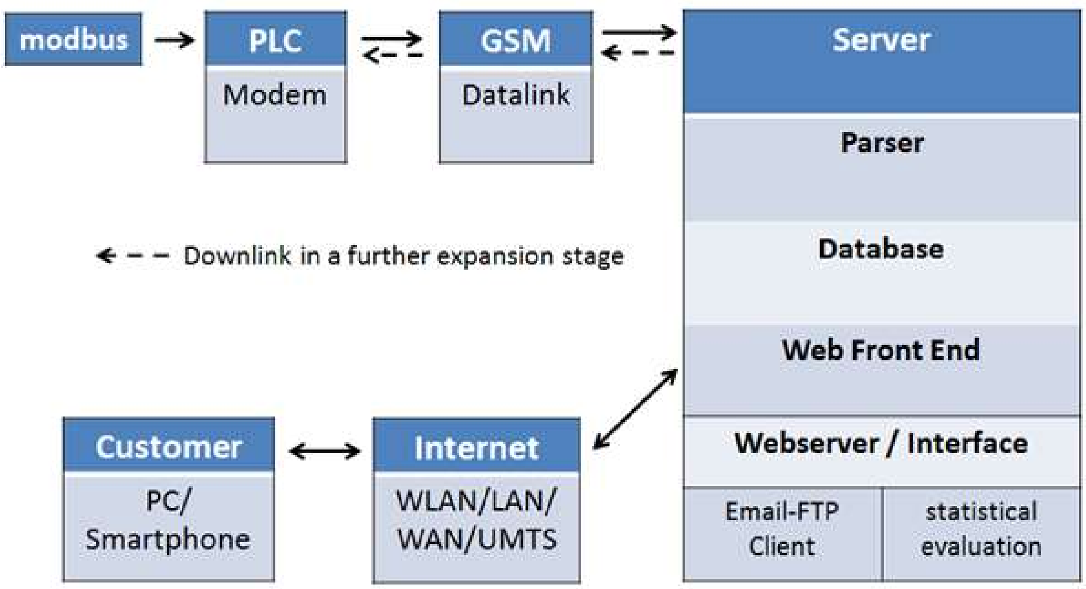

Fig.1. System Structure

Processing of message and operating data

The power generator transports the requested operating MOD/CANBUS data to the transmission unit which combines the operating data with further parameters (date, time, position) and creates a data package which is sent to the server.

The power generators are either independent generators (diesel generators, PV plants), power distributors or stores that are integrated into the grid. The data collection corresponds to the respective type.

Web portal

After logging in with user data and password, all power generators that are assigned to the user and stored in the server's database are displayed. The display arrangement depends on the resolution of the user device.

The button 'Parameter' displays a more detailed view and the user can access the operating data.

Operating modes

Examples of different operating modes of power generators follow:

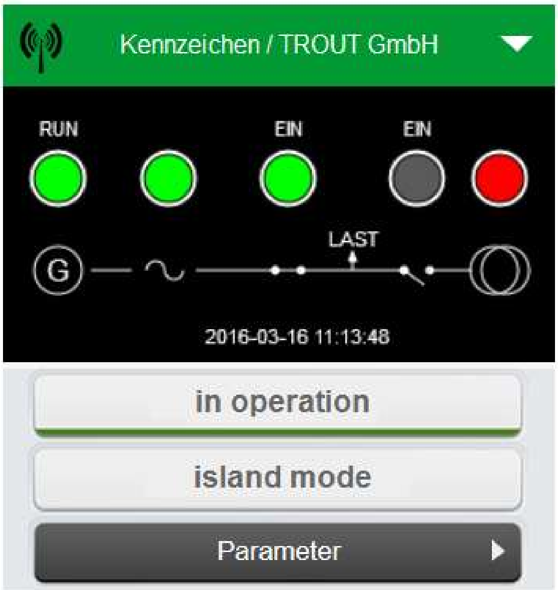

Fig.2.0. Power generator on, grid not available and not connected.

Figure 2.0 shows a fully functional generator in island mode. This means that the generator has no connection to the power grid. As an indication, the switch on the right hand side of LAST (power consumer) is open. The switch on the left hand side of LAST is closed, which means that LAST is supplied with energy by the power generator.

A generator which is out of operation is shown in figure 2.1.

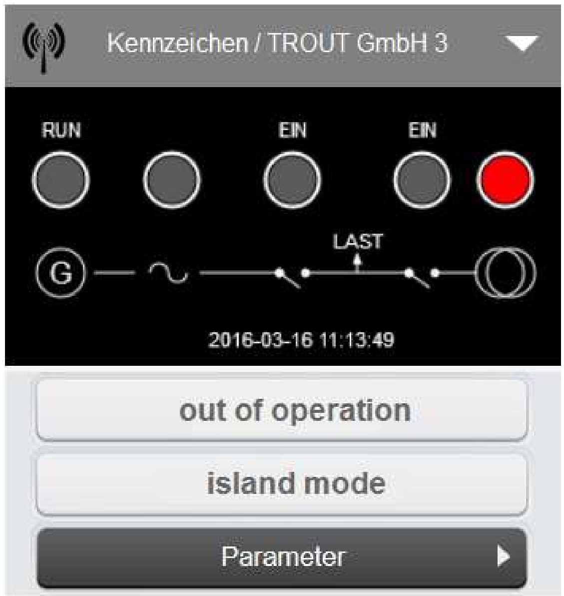

Fig.2.1. Power generator off, grid not available and not connected.

Figure 2.2 shows a generator which is in an unknown state because the data link is broken, which is indicated by the crossed antenna symbol on the upper left. LAST is supplied by the grid. The last data set, before the connection was broken, was transferred at 10:44 on the 26th January, which is displayed on the bottom of the black rectangle.

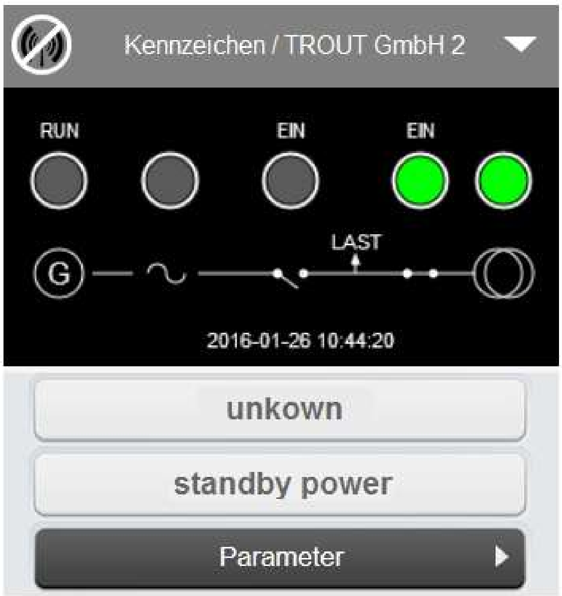

Fig.2.2. No data transfer from power generator, grid available and connected.

DOI 10.5162/etc2016/9.1

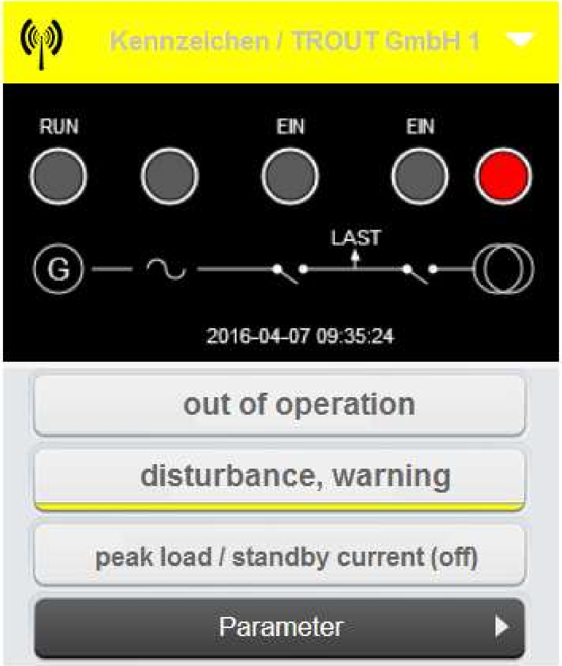

Fig.2.3. Disturbance message and warning from power generator.

A yellow marking indicates that the generator is sending warnings (see figure 2.3). The disturbances reach from problems such as 'fuel level is low' to minor malfunction of the generator.

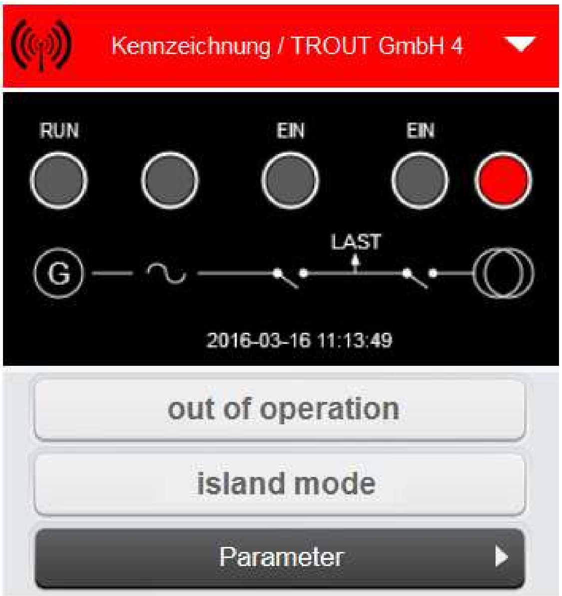

Fig.2.4. Malfunction of power generator, error message sent.

If the generator has a major problem, the marking turns red (see figure 2.4.). The service technician is informed via e-mail or text message. The message is repeated every 24 hours until the cause of the malfunction status is eliminated.

Integration of a GPS module

The power generator's position can be monitored with an integrated GPS module. Logging on to the monitoring portal, the user can invoke a geographical overview of his power generators. The power generator is visualised on a digital map with a colored marker depending on the condition, and a label. If the power generator is moved from its assigned position, a displacement message may be sent.

Fig.3. Visualisation of geographic position on a digital map.

Customised adjustment according to customer requirements

The application offers configuration of the user interface according to the customer requirements including optical adjustments such as background or company logo, as well as menu adaptation.

As the server receives many parameters from the power generator at any time, the user may want to display a selection only. Therefore it is possible to create a personal template. The selected parameters are then displayed in a customised list. Figure 4 shows an example.

Parameter	
Generator voltage [V]:	396
Generator frequency [Hz]:	50,9
Mains voltage [V]:	396
Main frequency [Hz]:	50,9
Power factor [cos φ]	1,00
Fuel level [%]:	29
Residual term [h]:	5
Motor temperature [°C]:	79
Next maintenance [d]:	48

Fig. 4. Customised parameter list.

Advanced administration of remote monitoring customers

Manufacturers or distributers of power generators may offer their customers remote monitoring as an additional service. The manufacturer or distributer receives administrator right for user administration in order to add users and assign power generators to them. In the following the users customise the handling of the operating data themselves.

Statistical evaluation of the operating data

The module for statistical evaluation creates a collection of selected operating data using the historical data of the power generator from the database on the server (work, fuel consumption, oil pressure). The data collection can be displayed graphically in many different views.

For instance, the generator's work may be shown over a period of time. Furthermore, different operating data can be combined in one diagram, to examine potential dependences such as work and fuel consumption.

The module for statistical evaluation further offers to the user the output of specific profitability factors of the power generators, such as running costs and efficiency. If a previously set value range is not achieved, the application will display and send a warning message.

Plots

Figure 5 shows power together with fuel level of a power generator. The fuel fillings and daily consumption can easily be seen. Due to measurement inaccuracies, time intervals occur during which the fuel level stays on one level, unaffected by operation. Similarly, disturbances emerge that interrupt the even curve progression (see fig. 5: 18:00 to 22:00). [1][2]

These irregularities complicate the statistical processing and subsequent evaluation of the operating data. The application addresses this problem and compensates potential disturbances by catching such artefacts with integrated filters. Fig. 6 shows the effect of one such filter.

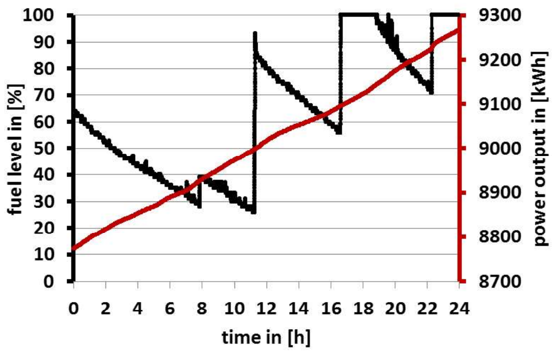

Fig.5. Power and fuel vs. time

After being processed by the filter, the data is analysed more specifically together with the technical parameters of the power generator.

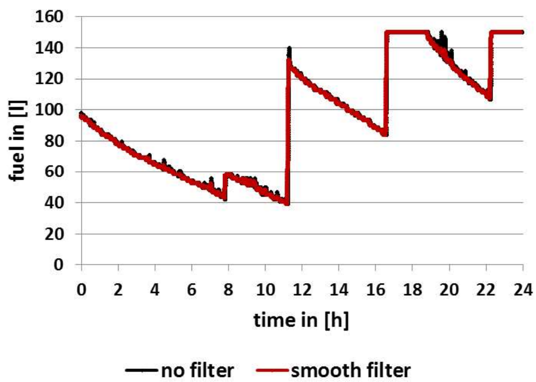

Fig.6. Filter options

A straightforward example is fuel consumption per kilowatt hour. The application calculates the values and displays them graphically for the user (see Figure 7).

DOI 10.5162/etc2016/9.1

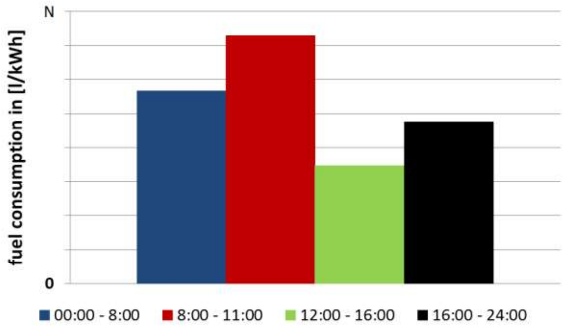

Fig.7. Fuel consumption per kilowatt hour.

The module for statistical evaluation compares the operating data with manufacturer specifications and generates a protocol of deviations. Over longer periods of time, for example, decreasing efficiency or increasing fuel consumption can be observed.

The module detects trends and may send messages to the manufacturer, distributer or service technician.

In addition, the operating cost may be calculated. This includes variable costs, such as fuel price, and fixed costs such as rent, depletion and maintenance.

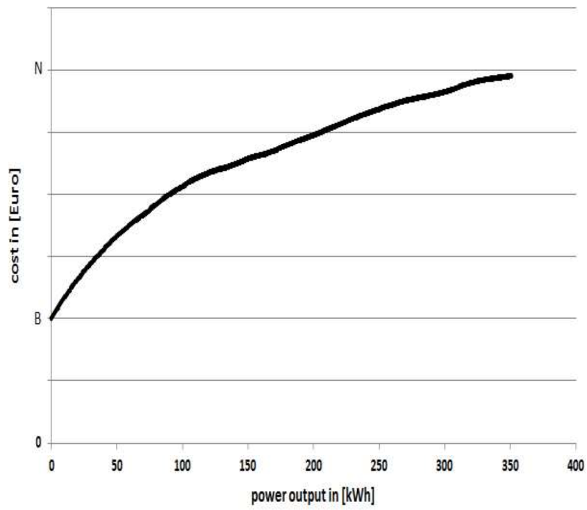

Fig.8. Cost per kilowatt hour and day.

The user is free to combine any single parameters with each other. As the example in figure 9 shows.

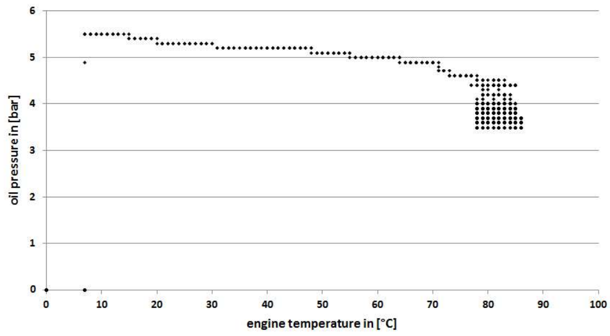

Fig.9. Oil pressure vs. motor temperature.

The module for statistical evaluation uses collected operating data, manufacturer specifications and the recorded malfunctions. It can calculate the probability for further malfunctions and issues recommendations for variable maintenance intervals.

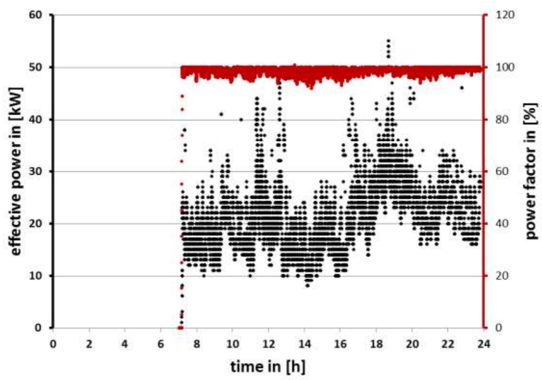

Fig.10. Effective power and power factor over a period of time

In addition to the previously described applications for power generators, these methods can equally be applied to power stores and distributors.

An additional application can calculate predictions on the expected life span of the power stores. If these are below the expected value, the operator can adjust the power store's utilisation to increase the life span.

Provided with additional sensor data, the application can create time-dependent distribution patterns for power distributors, from which the users' and departments' consumption pattern can be derived. Further improvements are to be developed.

References

[1] http://wiki.infowiss.net/Datenanalyse

[2] Werner A. Stahel, Statistische Datenanalyse, Eine Einführung für Naturwissenschaftler, 3. Auflage, p33ff

DOI 10.5162/etc2016/9.3

A Frame-Based Combining Method for Telemetry Data

Alparslan ARASAN[1], Celal ERTUĞRUL[2]
[1]Roketsan Missiles Inc., Ankara/TURKEY
alparslan.arasan@roketsan.com.tr
[2]Roketsan Missiles Inc., Ankara/TURKEY

Abstract:
Ground stations in multiple receiver telemetry systems receive flight data independently in different locations. In these systems, flight data from different sources should be selected in the most accurate combination. There has been word-based telemetry data combining methods in the literature. These methods select each word in telemetry frame independently. In this paper we introduce a frame-based selection method, considering that errors in telemetry systems affect many words in a frame at once. The method we introduce selects all the words in a frame from one source. We compare the effectiveness of the two combining methods using real flight data and demonstrate the superiority of our method.

Key words: flight data processing, data combining, multiple receiver telemetry, post-process, flight test

Introduction

Telemetry systems are used in launch vehicles, missiles and unmanned air vehicles to gather flight information regarding the vehicle such as position and velocity, and to gather scientific data such as temperature, pressure and vibration in order to use in flight analyses [1]. In telemetry systems, data that is collected from sensors and electronic equipment is modulated and transmitted from on-board antennas. In the ground station, telemetry data is received, demodulated and recorded to be analyzed later in the post-process. In cases where flight trajectory goes out of the coverage area of the ground station, more than one ground station at different locations should be used in order to cover the entire flight trajectory and to establish a telemetry link without communication loss.

In multiple receiver telemetry systems each ground station record telemetry data independently. Thus, telemetry data from different ground stations should be selected in the most accurate combination. Combining methods can be divided into two categories regarding when the process is applied: pre-detection combining methods that combine telemetry data in the RF level, post-detection combining methods that selects the strongest signal in the digital level. Pre-detection methods use weighting factor system by assigning a gain to each ground station and averaging according to the gain factors. The gain factors can be assigned according to the Automatic Gain Control (AGC) values of the receivers [2] or simple averaging can be applied by assigning the same gain factor to each ground station. Urech suggests a pre-detection combining method by assigning gain factors according to the Signal to Noise Ratio (SNR) of the telemetry signals [3]. In order to realize pre-detection combining method, a network that can collect real-time data of each ground station into one place should be established between ground stations. The network should handle synchronization problems in real time where the distance between ground stations is large. In addition to that, mobile telemetry ground stations make it difficult to use network infrastructure of the area. Therefore, pre-detection combining method is generally used in applications where ground stations / antennas are close to each other. Furthermore, there are Commercial of the Shelf (COTS) products that combine different telemetry signals to improve signal quality by using spatial diversity.

It is more practical to use post-detection methods where the distance between ground stations is large. There has been word-based post-detection telemetry data combining methods in the literature. Wilson proposed a word-based data combining method that uses correlation between successive samples [4]. Since most of the telemetry data is expected not to change radically between successive samples, the combining method selects the station that gives the least difference. In this

DOI 10.5162/etc2016/9.3

study, Wilson's method is improved by performing combining frame-based instead of word-based.

Combining Methods

In order to improve the combining method efficiency, a pre-knowledge about the telemetry link or ground stations should be used as a priori. SNR values of the telemetry signals or AGC values of the ground stations can be used as a priori. In this paper, correlation between successive samples, and the information that errors in telemetry links tend to last longer than a word are used as a priori.

A typical telemetry data is composed of avionic information such as current, voltage and software mode indicator, and sensor data such as temperature, acceleration, vibration and pressure. These data ordinarily have high autocorrelation function output. For example a temperature sensor that measures air temperature is supposed to give output that does not involve high peaks. Therefore if large difference in the temperature output is observed in telemetry data it is accepted as an error. In addition to that, oversampled sensor outputs increase correlation between successive samples. Moreover, some of the data in the telemetry frame remain constant through the flight for reasons such as bit-synchronization and frame-synchronization. Therefore, changes in such constant words indicate errors. For the very reason, there should only be small differences between successive samples. Hence, Minimum Mean Square Error (MMSE) between successive samples can be used as the selection criteria.

Let N be the number of ground station and Φ_1, Φ_2, ..., Φ_N be telemetry data series. Then $\Phi_i(f, w)$ denotes the w.th word of f.th frame belonging to station i. At first, mod of the word is selected as follows:

$$Q(f, w) = mod(\ \Phi_1(f, w), \Phi_2(f, w), \ldots , \Phi_N(f, w)\ ) \quad (1)$$

$$q(f, w) = Q(f, w) \quad (2)$$

$Q(f, w)$ denotes the mod of the word and $q(f, w)$ denotes the selected word. If there is only one mod for the word, the word obtained from eq. (1) is selected as indicated in eq. (2). In the case that there are multiple mods of the word, another method should be used. For example, if 3 out of 4 ground stations have the same word, then the predominant word can be selected. However, in the event of 2 stations have same word and other 2 stations have another word, stations give 2 mods and another method should be applied. In such cases word-based selection methods based on MMSE are used in the literature. The method takes into account that telemetry data does not vary in a large extend between successive samples and selects the word from the station that gives the least MMSE. Word-based method employs the selection to each word independently.

In this paper, the selection method is implemented as frame-based. Different from the word-based method, the proposed algorithm selects all the words in a frame from only one ground station. In order to clarify differences of the two methods, word-based method in the literature is reviewed and the proposed frame-based method is analyzed.

Word-Based Method

The method Wilson suggests selects each word in a frame independently. Let d_m be the distance of a word to its neighboring samples, the method applies each mod obtained from eq. (1) to eq. (3).

$$q(f, w) = \underset{m}{\arg min}\{\ d_m\colon \mathrm{m} \in Q(f, w)\ \} \quad (3)$$

Distance of a word to its neighboring samples is calculated as follows:

$$d_m = [\Phi_m(f, w) - \Phi_m(f\text{-}1, w)]^2 + [\Phi_m(f, w) - \Phi_m(f+1, w)]^2 \quad (4)$$

For each ground station, distances obtained from eq. (4) are compared as indicated in eq. (3), and the word whose station has minimum distance is selected. Word-based method can select each word in a frame from different stations. For example,

$$q(f, w\text{-}1), q(f, w), q(f, w+1)$$

word series can be selected as

$$\Phi_2(f, w\text{-}1), \Phi_1(f, w), \Phi_2(f, w+1).$$

On the contrary, frame-based method selects each word in a frame from only one station. Considering the previous example, the word series

$$q(f, w\text{-}1), q(f, w), q(f, w+1)$$

should be selected as

$$\Phi_1(f, w\text{-}1), \Phi_1(f, w), \Phi_1(f, w+1)$$

or

$$\Phi_2(f, w\text{-}1), \Phi_2(f, w), \Phi_2(f, w+1).$$

Frame-Based Method

Proposed frame-based method calculates distances of the words to their neighboring samples in a same way as word-based method applies using eq. (4). Then, cumulative distance of the frame for each station is calculated as in eq. (5).

$$q(f,\, w) = \underset{m}{\arg\min}\{\, \textstyle\sum_k d_m\text{: m} \in Q(f,\, w) \,\} \qquad (5)$$

The station that produces the minimum cumulative distance is selected for all of the words in the considered frame.

The motivation behind the cumulative distance approach is that if an error occurs in a frame, probability of another error occurring in the same frame is high. This is because error sources in the telemetry links do not consist of only Gaussian noise. Error sources such as multipath fading and synchronization loss cause multiple word errors in the frame. Since such error causes are commonly observed in telemetry systems, it can be used as a priori in the combining method to increase performance.

Flight Test Results

In order to demonstrate efficiency, both of the methods are implemented on 6 different flight test data. In the analysis, errors are detected by Cyclic Redundancy Check (CRC) codes of the frames.

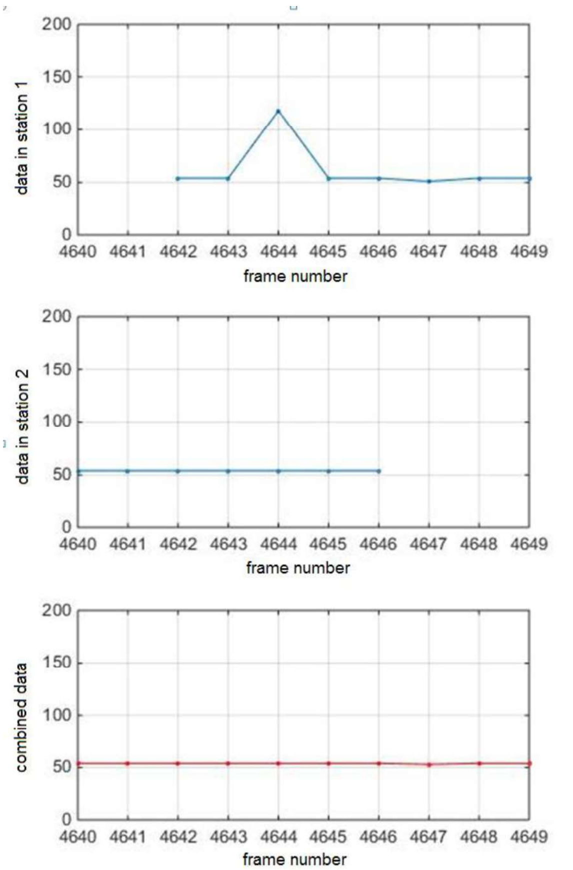

Fig.1: Temperature sensor output in two ground stations and word-based combining method output

Figure 1 illustrates a temperature sensor output for several frames in 2 stations and also word-based combining method output. As the figure shows, 2 stations have different values for temperature data in 4644. frame. Therefore a selection method should be applied to the word, either word-based or frame-based. If the word-based selection method is used, d_m for the stations is calculated from eq. (4) as follows:

Station1: $(54\text{-}118)^2 + (54\text{-}118)^2 = 8192$

Station2: $(54\text{-}54)^2 + (54\text{-}54)^2 = 0$

As a result, station that gives the minimum distance, second station, should be selected. However, for the frame-based selection method, all of the words in the frame should be considered. For the words that two stations do not agree on in the 4644. frame, d_m should be calculated and cumulative distance should be compared for 2 stations.

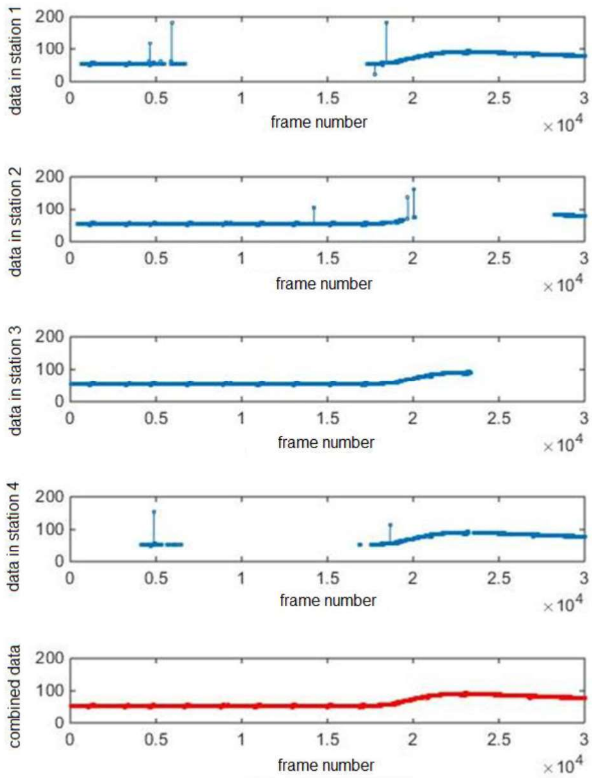

Fig.2: Temperature sensor output throughout the flight in 4 stations and frame-based combining method output

Figure 2 demonstrates a temperature sensor output throughout the flight in 4 stations and final data after frame-based combining method is applied. Since the ground stations do not cover the entire flight trajectory, telemetry link loss occurs occasionally. In addition to that, errors take place in individual stations. However in the combined data, a smooth and continuous sensor data is obtained.

Flight data from 4 ground stations that are located at 4 different locations are collected and combined with both word-based according to eq. (3) and frame-based according to eq. (5). Since the combining methods are post-processes, processing time is not considered in this study.

For all of the 6 flight tests the same frame format is used (e.g. frame length, synchronization word, CRC equation). Error occasion in the frame is checked by CRC code and number of frames that contains errors is calculated for each flight test. Frame Error Rate (FER), the ratio of errored frame to total number of frames, is used as criteria for the comparison of methods.

Tab.1: Frame error rates of combining methods

Flight Test No	**Word-Based FER (%)**	**Frame-Based FER (%)**
Test-1	5.5×10^{-3}	1.7×10^{-3}
Test-2	10^{-2}	3.7×10^{-3}
Test-3	1.3×10^{-2}	4.7×10^{-3}
Test-4	4×10^{-3}	8.1×10^{-4}
Test-5	2.4×10^{-2}	4.8×10^{-3}
Test-6	10^{-2}	2.2×10^{-3}

In all flight tests the proposed frame-based combining method produces better performance, resulting in 2.7 to 5.1 times lower frame error rates. It is turn out that the proposed frame-based combining method is a strong data combining method candidate for multiple receiver telemetry systems.

Conclusions

In this study, data combining methods that are used in telemetry applications are investigated and a new frame-based method is proposed instead of the word-based combining methods in the literature, considering that errors in telemetry systems affect many words in a frame at once. The two methods are compared using real flight data, and the results demonstrate the superiority of the proposed method.

References

[1] F: Carden, R. Jedlicka, and R. Henry, *Telemetry System Engineering*, Artech House, 2-5, 2002

[2] Graham, Richard A., Jr. *"An Examination of Spatial Diversity Combining Using Commercial Off the Shelf Equipment in Missile Telemetry", ITC International Telemetering Conference Proceedings,* 2014

[3] J. M. Urech, *"Processed Data Combination for Telemetry Improvement-DSS62", JPL Technical Report 32-1526, Vol.II,* 1971

[4] Michael J. Wilson, *"Combining and Filtering Telemetry Data", Army Research Laboratory,* ARL-TR-3143. 2004